Investigation of the hippocampus in aging and Alzheimer's disease progression using multimodal MRI techniques

Aurélie Bussy, MSc

A thesis submitted to McGill University in partial fulfillment of the requirements of the degree of Doctor of Philosophy

Integrated Program in Neuroscience

Departments of Psychiatry, Neurology and Neurosurgery

McGill University, Montreal

August 9, 2023

Abstract

Across the globe, most nations are facing challenges posed by longer life expectancy resulting in the increased proportion of elderly citizens and prevalence of neurodegenerative disorders such as Alzheimer's disease (AD). Susceptibility to AD may be attributed to immutable factors (sex, ethnicity, genetics) or modifiable risk factors (education, physical activity, body weight, hypertension, smoking). The hippocampus is a key brain region involved in learning, memory, and spatial navigation which has been studied in relation to different diseases. However, the relationship between hippocampal morphometry and microstructure in age-related and AD-related brain modifications remains largely unexplored.

In **Chapter 3**, the impact of magnetic resonance imaging (MRI) acquisition-type on age-related volumetric relationships of the hippocampus and its subfields was examined. To better understand the conflicting conclusions in the literature, two commonly used acquisitions (standard isotropic T1-weighted (T1w) and anisotropic T2-weighted (T2w) slab scans), and a recently developed scan (T2w high-resolution isotropic) were analyzed. It was found that using different types of scans resulted in significantly different volume estimates and volumetric age-relationships. Slab volume estimates were consistently lower and showed important age trajectory differences compared to the other two scans. Accounting for methodological differences, cornus ammonis (CA) 1 showed the highest volume preservation in aging while CA2CA3 was the most impacted. This project challenges the conventional preference for slab images in capturing age-related hippocampal volume changes and highlights the need to consider alternative imaging sequences for more accurate assessments of

hippocampal trajectories.

In **Chapter 4**, the hippocampal morphometric age-related variation was investigated using vertex-wise surface area (SA) and displacement measures. An antero-posterior effect for SA and a medial-lateral effect for displacement were discovered, indicating that aging principally affected the SA of the posterior hippocampus and caused an increase in hippocampal curvature. The shape of the hippocampus was also examined in relation to other known factors involved in age-related decline, including sex, cognition, apolipoprotein $\epsilon 4$ allele (APOE-$\epsilon 4$ allele) mutation, and education. The findings suggest that as people age, the hippocampus becomes more curved, which could explain why age-related changes could be better captured by isotropic scans.

In **Chapter 5**, we investigated non-invasive microstructural metrics across the AD disease spectrum, ranging from healthy aging individuals to those with frank onset of AD. While amyloid and tau are the main pathological hallmarks of AD, the disease is multifactorial and involves other microstructural changes such as myelin deterioration and inflammation-induced increase in iron. In this project, we used quantitative MRI (qMRI), a non-invasive technique that can estimate myelin and iron content in the brain with T1 and T2* metrics respectively. A matrix decomposition technique was employed to derive joint signatures of covariance across morphometric and microstructural measures in the cortex and hippocampus. Partial least squares was used to link hippocampal and cortical metrics to medical, lifestyle, and cognitive information. Our findings suggest that decreased cortical thickness (CT) and SA in the cortex and higher T1 and T2* in the hippocampus were associated with past smoking consumption, high blood pressure and cholesterol, lower cognitive scores, and higher anxiety. Further, this pattern was significantly related to higher age and AD progression suggesting that hippocampal qMRI metrics could be valuable and sensitive non-invasive tools for investigating AD.

Altogether, this thesis used various imaging techniques and statistical analysis to comprehensively investigate multiple dimensions of age and disease-related brain alterations.

Résumé

À travers le monde, la plupart des nations font face à des défis posés par l'allongement de l'espérance de vie, entraînant un vieillissement de la population ainsi qu'une augmentation de la prévalence de troubles neurodégénératifs tels que la maladie d'Alzheimer (MA). La susceptibilité à la MA peut être attribuée à des facteurs immuables (sexe, ethnicité, génétique) ou à des facteurs de risque modifiables (éducation, activité physique, hypertension, tabagisme). L'hippocampe est une région clé du cerveau impliquée dans l'apprentissage et la mémoire qui a été étudiée dans de nombreuses maladies. Cependant, la relation entre la morphométrie et la microstructure de l'hippocampe dans les modifications cérébrales liées à l'âge et à la MA reste largement inexplorée. Dans le **Chapitre 3**, l'impact du type d'acquisition d'imagerie par résonance magnétique (IRM) sur les relations volumétriques liées à l'âge de l'hippocampe et de ses sous-régions a été examiné. Pour mieux comprendre les conclusions contradictoires dans la littérature, deux acquisitions standards (isotropiques pondérées en T1 (T1w) et slabs anisotropiques pondérées en T2 (T2w)) ainsi qu'une acquisition récemment développée (T2w isotropique haute résolution) ont été analysées. Il a été constaté que l'utilisation de différents types d'acquisitions entraînait des estimations de volume et des relations volumétriques liées à l'âge significativement différentes. Les estimations de volume en slab étaient systématiquement plus faibles et ont montré des différences importantes de trajectoire liées à l'âge par rapport aux deux autres acquisitions. Ce projet remet ainsi en question la préférence pour les images en slab pour capturer les changements de volume de l'hippocampe liés à l'âge. Dans le **Chapitre 4**, la variation morphométrique liée à

l'âge de l'hippocampe a été étudiée en utilisant des mesures de surface et de déplacement. Les résultats ont montré que le vieillissement affectait principalement la surface de l'hippocampe postérieur et entraînait une augmentation de la courbure de l'hippocampe. La forme de l'hippocampe a également été examinée en relation avec d'autres facteurs tels que le sexe, la cognition, la mutation apolipoprotéine E4 et l'éducation. Les résultats suggèrent que lorsque les gens vieillissent, l'hippocampe devient plus courbe, ce qui pourrait expliquer pourquoi les changements liés à l'âge pourraient être mieux capturés par des scans isotropiques. Dans le **Chapitre 5**, nous avons étudié des mesures microstructurales non invasives à travers le spectre de la MA. La MA est multifactorielle et entraîne des changements microstructuraux tels que la détérioration de la myéline et l'augmentation de la teneur en fer induite par l'inflammation. Dans ce projet, nous avons utilisé l'IRM quantitative (IRMq), une technique qui peut estimer la teneur en myéline et en fer dans le cerveau, avec les mesures T1 et T2* respectivement. Nous avons employé une technique de décomposition de la matrice pour dériver des signatures conjointes de covariance des mesures morphométriques et microstructurales du cortex et de l'hippocampe. Les mesures hippocampiques et corticales ont été liées aux informations médicales, de mode de vie et cognitives. Les résultats suggèrent que l'amincissement cortical et la diminution de la surface corticale, ainsi qu'une augmentation de T1 et T2* dans l'hippocampe, étaient associés à une consommation antérieure de tabac, une hypertension artérielle, un taux élevé de cholestérol, des scores cognitifs bas et une anxiété élevée. De plus, ce schéma était significativement lié à un âge avancé et à une progression de la MA, suggérant que les mesures IRMq de l'hippocampe pourraient être des outils non invasifs précieux et sensibles pour étudier la MA. Dans l'ensemble, cette thèse a utilisé différentes techniques d'imagerie et d'analyses statistiques pour étudier de manière exhaustive les multiples dimensions des altérations cérébrales liées à l'âge et à la MA.

Acknowledgments

My doctoral thesis is a reflection of my growth as a scientist throughout my academic journey. This progress is largely attributable to the invaluable mentorship of several inspiring scientists who have contributed significantly to my development. First and foremost, I wish to express my sincere gratitude to my PhD supervisor, **Dr. Mallar Chakravarty**. Your support and guidance have been instrumental in my academic journey. I am immensely grateful for the freedom and independence you provided me to pursue my research interests, and for the countless opportunities you gave me to present my work and develop my research interests. I am also indebted for helping me improve my critical thinking, writing, and presentation skills. Whether it was during professional events like conferences and lab meetings or more casual settings such as lab gatherings or delightful dinners, I have always appreciated the discussions we had together.

My doctoral degree would not have been possible without the invaluable assistance of numerous exceptional researchers. First, I am immensely grateful to **Dr. Gabriel Devenyi** for your great research abilities and for tirelessly helping me debug problems countless times. Your responsiveness and efficiency in providing assistance were truly a privilege to have. Additionally, your critical feedback and challenging insights were instrumental in sharpening my attention to detail. I am grateful to my committee members, **Dr. Sylvia Villeneuve** and **Dr. Christine Tardif**, for your constructive feedback and support during my progress presentations. Additionally, I thank my collaborators, **Dr. Simon Ducharme** and **Dr. Nathan Spreng**, for trusting me with our projects and for your generosity in sharing

data and collaborative spirit. Thank you to the **Alzheimer Society**, **Healthy Brain for Healthy life** and **Québec Bio-Imaging Network** for your fundings which have been instrumental for my thesis.

I want to express my deep gratitude to my cobralab colleagues for creating such an exceptional work environment. Your diverse perspectives, brilliant insights, and lively personalities made our lab meetings the highlight of my weeks. I want to give special thanks to my dearest friend and brilliant colleague, **Lani Cupo**. Your exceptional research skills and unique perspective have had an immeasurable impact on my work. I consider it a privilege to have grown alongside you and forged a lasting friendship throughout our doctoral studies. Our discussions, both philosophical and scientific, were enlightening and stimulating, and I will always cherish the memories of our invaluable "debriefs". To **Swapna Premasiri**, I am also so grateful that my phD brought me to meet you. Swapna, you are probably the kindest person I know, and I am so happy that we started our PhD on the same day. You became family over the years and while we went through a lot together, I am grateful for each step of the way. You can not imagine how happy I am to see you flourish now. To **Nadia Blostein**, thank you for being a lively and loving friend who always reminds me to take time to laugh and relax with friends. I am excited to see where life takes you and to watch you thrive in your next experiences. To my former lab colleague and friend, **Dr Eric Plitman**, thank you for your instrumental help during my first year of PhD, you have been such a patient, kind and fun teacher. Our discussions, debriefs and teasing were so precious, our office has never become as fun as it was in 2019, thank you for these great memories. You also are an inspiration of exceptional accomplishments and of never letting go of your dreams and ambition. To **Dr Raihaan Patel**, thank you for your help and for always being so generous. Rai, you made the lab a better place thanks to your great advice and insights. To **Dr Elisa Guma**, thank you for being such a happy and kind colleague with whom I really enjoyed sharing drinks and great discussions. Finally, I want to express my happiness in seeing **Olivier Parent** pursue my research theme at the lab. It was a pleasure to watch

you grow into a great PhD student, and I look forward to seeing you at conferences in the future. To all other lab members that I consider my friends, **Gabriel Desrosiers-Gregoire**, **Mila Urosevic**, **Justine Ziolkowski**, **Dr Yohan Yee**, **Dr Jérémie Fouquet**, thank you for having been such great teammates.

Last but certainly not least, I would like to thank my family and friends. To my parents, thank you for everything, I would not have achieved that without the exceptional education and unconditional love you gave me during my life. **Maman**, tu as toujours été un exemple de gentillesse et de générosité, j'espère devenir un jour aussi bienveillante que toi. **Papa**, tu es un exemple de réussite, mais aussi de modestie, merci pour les valeurs que tu nous as transmises. À vous deux, merci pour vos sacrifices, vos encouragements, et votre amour, je vous en serais éternellement reconnaissante. To my siblings, **Simon** and **Lola**, I am so grateful, you have been amazing role models for me since childhood. Simon, merci d'être un frère extraordinaire qui a contribué à façonner ma personnalité, mon humour, mon esprit critique et mon ambition. Te voir exceller dans ta carrière et devenir toi-même un chercheur accompli, a certainement été une source d'inspiration pour moi, m'encourageant à suivre ce chemin. Lola, ton épanouissement dans ta carrière, ta vie de couple et maintenant dans ton rôle de mère est sans aucun doute une grande source d'inspiration pour moi. Au reste de ma famille, tantes, oncles, cousins et cousines je vous remercie de m'avoir apporté une communauté nécessaire qui m'a aidé à m'épanouir depuis l'enfance. Par dessus tout, je tiens à remercier mon grand-père, qui a toujours été un exemple de positivité et de bienvaillance, ainsi que ma grand-mère à qui je pense avec tendresse.

To my dear friends **Andrea** and **Bruno**, I am incredibly grateful that our paths crossed thanks to our wonderful dogs. Votre amitié, nos randonnées, campings et soirées m'ont certainement aidé à profiter et à décompresser durant ces deux dernières années de thèse. Merci à **Pola** d'avoir égayé nos balades quotidiennes avec sa folie et ses bêtises.

Thank you to my beloved furry companions who have brought so much joy and comfort to my life. Merci à **Bibou**, mon petit cochon adoré qui m'a accompagné durant mes débuts

de thèse et qui m'a apporté beaucoup de joie et d'amour. Merci à **Panda**, mon chien policier incroyable qui me comble d'amour depuis toutes ces années. Ta présence constante m'a rappelé l'importance de vivre chaque journée avec intensité et de savourer les petits bonheurs de la vie lors de nos moments passés ensemble.

And finally, to the most important person in my life, thank you to **John Tassi**, my soulmate and bestfriend. Merci mon chat pour ton amour, merci pour les sacrifices que tu as fait pour être à mes côtés et de m'avoir suivi encore et encore au fil de mes études. Merci d'être une personne extraordinaire, inspirante et tellement passionnée. Te voir devenir la personne que tu es aujourd'hui a été un privilège, je suis tellement fière de toi. Personne n'a jamais autant cru en moi que toi, et tes encouragements pour que je devienne 'chaton présidente' ont été tellement essentiels à ma réussite. Toi seul peut me redonner le sourire si facilement grâce à ta bonne humeur inégalable et tes chansons rigolotes. Je t'aime tellement, merci.

Contents

Glossary

α flip angle. 40, 131, 188

$B1^+$ radio frequency transmit field. 210, 211

$B1^-$ radio frequency receive field. 210

Aβ β-amyloid peptide. 24, 29, 30, 31, 34, 182, 206, 209, 250

Aβ40 40-amino acid form of Aβ. 30

Aβ42 42-amino acid form of Aβ. 30

AD Alzheimer's disease. iii, iv, xlv, 2, 5, 6, 8, 9, 24, 25, 26, 29, 30, 31, 32, 33, 34, 35, 36, 37, 63, 74, 88, 97, 128, 130, 149, 153, 180, 181, 182, 183, 184, 185, 195, 198, 199, 200, 203, 204, 205, 206, 207, 208, 209, 210, 211, 212, 239, 240, 241, 243, 244, 246, 249, 250, 251, 252

ADB Alzheimer's Disease Biomarker. xxxiv, xxxv, xxxvi, 68, 71, 73, 97, 111, 130, 131, 133, 185

ADNI Alzheimer's Disease Neuroimaging Initiative. 67, 68, 69, 73, 76, 78, 85, 91, 97, 107, 108, 111, 131

aHPC anterior hippocampus. 20

AIC Akaike information criterion. 62, 73, 77, 78, 81, 136, 139, 140, 141, 142, 144, 145, 152, 155, 157, 161, 162, 163

Apo-E apolipoprotein E. 30, 34

APOE-ϵ4 allele apolipoprotein ϵ4 allele. iv, xlv, 9, 74, 75, 88, 126, 130, 131, 132, 137, 138, 146, 150, 155, 160, 182, 193, 194, 201, 202, 206, 220, 222, 224, 241, 243, 246

APP amyloid precursor protein. 29, 30, 34

ASHS Automatic segmentation of hippocampal subfields. 57, 78, 87, 93, 110, 244

BBB blood-brain barrier. 30, 206

BEaST Brain Extraction based on nonlocal Segmentation Technique. 133

BP blood pressure. 199, 201, 205, 241, 244, 252

BSR bootstrap ratio. 139, 141, 158, 159, 164, 165, 201, 221, 223

CA cornus ammonis. iii, 15, 61, 63, 127, 128

CA2CA3 combined CA2 and CA3. 71, 73, 78, 80, 81, 82, 83, 84, 85, 86, 87, 94, 95, 133, 147, 153

CA4DG combined CA4 and dentate gyrus. 71, 73, 76, 78, 80, 81, 82, 84, 85, 86, 87, 133, 140, 153

Cam-CAN Cambridge Centre for Ageing and Neuroscience. 68, 69, 97, 111, 139, 145, 146

CNR contrast to noise ratio. 76, 77, 85, 89, 90, 94, 108

CNS central nervous system. 12, 14, 31

CSF cerebrospinal fluid. 12, 31, 46, 54, 251

CT cortical thickness. iv, 21, 28, 149, 181, 189, 191, 192, 193, 197, 198, 199, 200, 203, 204, 215, 218, 241, 247, 248

DBM deformation based morphometry. 58, 190, 191

DG dentate gyrus. 15, 16, 17, 18, 19, 20, 64, 78, 151, 152, 153

DTI diffusion tensor imaging. 14, 22

EC entorhinal cortex. 15, 16, 17, 18, 19, 23, 33, 152, 153, 246

EOAD early onset Alzheimer's disease. 34

EPI echo-planar imaging. 37

FA fractional anisotropy. 22, 29

FAMHX cognitively healthy individuals with a parental AD-history. 185, 194, 198, 199, 200, 202, 203, 204

FDR false-discovery rate. 137, 150, 162, 163, 194, 200

FOV field-of-view. 67, 72, 89, 99, 100, 188, 189

GM grey matter. 11, 18, 20, 21, 25, 27, 28, 45, 46, 54, 62, 63, 71, 73, 74, 75, 77, 78, 81, 83, 84, 88, 90, 105, 133, 134, 137, 184, 189, 248

GRAPPA GeneRalized Autocalibrating Partial Parallel Acquisition. 131, 188

HA Healthy Aging. 68, 73, 76, 85, 97, 108, 111, 130, 131, 133

HC healthy controls. 33, 185, 195, 198, 199, 200, 202, 203, 204, 208

HIPS HIPpocampus subfield Segmentation. 58, 77, 85, 86, 93, 95, 109, 244

ICC Intraclass correlation coefficient. 76, 85, 87

ICV intracranial volume. xxix, 73, 74, 75, 77, 78, 79, 80, 81, 83, 84, 87, 89, 102, 103, 104, 105, 109, 110, 140

J relative Jacobian. 190, 191, 192, 193, 198, 199, 200, 218, 241

lmer linear mixed-effect model. 62, 73, 77, 78, 136, 137

LOAD late onset Alzheimer's disease. 34

LV latent variable. 137, 138, 139, 141, 143, 144, 158, 159, 164, 165, 193, 194, 199, 201, 221, 223

MAGeT Multiple Automatically Generated Templates. 57, 62, 71, 72, 77, 78, 85, 86, 87, 92, 93, 95, 101, 109, 110, 127, 133, 134, 240, 244, 245

MB mammillary bodies. 18, 19, 64, 71, 74, 81, 82, 84, 87, 94, 95, 105

MCI mild cognitive impairment. 33, 35, 36, 37, 97, 185, 195, 199, 200, 202, 204, 205

MD mean diffusivity. 22, 28, 29, 250

MMSE mini mental state examination. 36, 37, 97, 98, 131, 132, 137, 138, 140, 155, 160, 205

MNI Montreal Neurological Institute. 70, 133

MoCA Montreal cognitive assessment. 36, 37, 187

MP2RAGE magnetization prepared 2 rapid acquisition by gradient echo. 188, 192, 210, 247

MPM multi-parameter mapping. 22, 247

MPRAGE magnetization prepared rapid acquisition by gradient echo. 62, 66, 67, 68, 69, 70, 99, 131, 139, 210

MR magnetic resonance. 21, 37, 48, 49, 61, 69, 70, 130, 208, 239, 242

MRI magnetic resonance imaging. iii, xlv, 7, 8, 15, 22, 34, 37, 43, 44, 45, 46, 48, 51, 52, 54, 56, 57, 61, 64, 65, 68, 69, 70, 73, 76, 91, 92, 93, 98, 128, 131, 132, 133, 139, 180, 181, 183, 185, 187, 203, 208, 239, 241, 242, 244, 247, 248, 249, 250, 251

MS multiple sclerosis. 46

MT magnetization transfer. 211, 248, 249

MTL medial temporal lobe. 15, 32, 33, 35

MTR magnetization transfer ratio. 204, 248

MWF myelin water fraction. 248, 249

NFT neurofibrillary tangles. 29, 32, 35, 209

NMF non-negative matrix factorization. 191, 193, 194, 195, 198, 200, 217, 243

NMR nuclear magnetic resonance. 37

NODDI neurite orientation dispersion and density imaging. 22

PaS parasubiculum. 18

PD proton density. 45, 189, 211, 250

PET positron emission tomography. 8, 31, 37, 209, 210, 211, 250, 251

pHPC posterior hippocampus. 20

PLS partial least square. xlv, 126, 127, 131, 137, 138, 139, 141, 143, 144, 148, 150, 158, 159, 164, 165, 193, 194, 199, 202, 222, 224

PREVENT-AD Pre-symptomatic Evaluation of Experimental or Novel Treatments for Alzheimer Disease. xxxvi, 185

ProS prosubiculum. 18

PSEN1 presenilin 1. 34

PSEN2 presenilin 2. 34

PSub presubiculum. 18

ptau hyperphosphorylated microtubule associated protein tau. 24, 29, 182, 250

PVE partial volume effect. 94

QC quality control. 68, 70, 71, 73, 90, 91, 92, 131, 132, 135, 156, 185, 186, 187, 188, 189, 244

qMRI quantitative MRI. iv, 9, 22, 45, 46, 180, 181, 183, 184, 185, 203, 207, 211, 241, 247, 248, 250, 251

QSM quantitative susceptibility mapping. 248, 250

RBANS repeatable battery for the assessment of neuropsychological status. 131, 132, 137, 138, 140, 143, 144, 155, 160, 187

RF radiofrequency. 39, 44, 45, 46, 49, 183

ROI region-of-interest. 72, 90, 134

SA surface area. iv, 21, 126, 127, 134, 135, 137, 138, 140, 142, 143, 144, 145, 146, 147, 148, 149, 150, 151, 152, 154, 158, 162, 164, 189, 191, 192, 193, 197, 198, 199, 200, 203, 204, 218, 240, 241, 245, 248

SCI subjective cognitive impairment. 35

SNR signal to noise ratio. 94

SRLM stratum radiatum, lacunosum and moleculare. 15, 23, 61, 62, 63, 71, 74, 80, 81, 82, 83, 84, 85, 88, 89, 90, 94, 103, 104, 105, 133, 140

T1w T1-weighted. iii, 8, 15, 44, 45, 50, 51, 57, 61, 62, 65, 66, 67, 69, 70, 71, 72, 75, 76, 77, 82, 84, 85, 86, 87, 90, 91, 94, 95, 96, 99, 105, 106, 107, 108, 131, 133, 154, 188, 189, 190, 191, 192, 204, 239, 240, 244, 245

T2w T2-weighted. iii, 9, 15, 45, 50, 57, 61, 62, 65, 66, 67, 68, 69, 70, 71, 75, 76, 82, 84, 85, 86, 87, 90, 91, 95, 96, 99, 105, 106, 107, 108, 133, 154, 204, 239, 240, 242, 245

TE echo time. 44, 45, 50, 99, 100, 131, 188, 189

TI inversion time. 99, 131, 188

TR repetition time. 44, 45, 50, 99, 100, 131, 188

TSE turbo spin echo. 62, 66, 67, 68, 69, 70

WM white matter. 8, 11, 14, 18, 21, 22, 27, 28, 29, 45, 46, 54, 61, 62, 64, 66, 71, 73, 74, 75, 76, 77, 81, 83, 84, 87, 88, 89, 90, 96, 105, 107, 189, 205, 211, 248, 250, 251

WMH white matter hyperintensities. 29, 251

List of Figures

List of Tables

Contributions

Contributions of author

The original work in this thesis spans **Chapters 3, 4,** and **5**. For each of these manuscripts, I led the experimental design, data processing, statistical analyses, and interpretation under the guidance and supervision of Dr. M Mallar Chakravarty. I wrote the first draft of these manuscripts and incorporated revisions from co-authors and peer reviewers. Each study features a number of co-authors whose contributions were integral and invaluable to the completion of this work. Their contributions are demarcated below:

Chapter 3: **Aurélie Bussy**, Eric Plitman, Raihaan Patel, Stephanie Tullo, Alyssa Salaciak, Saashi A. Bedford, Sarah Farzin, Marie-Lise Béland, Vanessa Valiquette, Christina Kazazian, Christine L. Tardif, Gabriel A. Devenyi, M. Mallar Chakravarty. *Hippocampal subfield volumes across the healthy lifespan and the effects of MR sequence on estimates.* NeuroImage, February 2021. https://doi.org/10.1016/j.neuroimage.2021.117931

- Eric Plitman : provided guidance in the conceptualization and in the image processing
- Raihaan Patel : provided methodological and statistical support
- Stephanie Tullo, Alyssa Salaciak, Saashi A. Bedford, Sarah Farzin, Marie-Lise Beland, Vanessa Valiquette and Christina Kazazian : all participated in the data collection of the Alzheimer's Disease Biomarker (ADB) dataset and in the data curation

- Christine L. Tardif : provided expertise in the ADB imaging protocol development
- Gabriel A. Devenyi : provided technical support to perform the image processing and the formal statistical analysis
- M. Mallar Chakravarty : supervised the study and provided guidance in conceptualization of the study, interpretations of results, and writing of the manuscript
- All authors: provided critical or conceptual support and revised the manuscript

Chapter 4: **Aurélie Bussy**, Raihaan Patel, Eric Plitman, Stephanie Tullo, Alyssa Salaciak, Saashi A. Bedford, Sarah Farzin, Marie-Lise Béland, Vanessa Valiquette, Christina Kazazian, Christine L. Tardif, Gabriel A. Devenyi, M. Mallar Chakravarty. *Hippocampal shape across the healthy lifespan and its relationship with cognition.* Neurobiology of Aging, October 2021. https://doi-org.proxy3.library.mcgill.ca/10.1016/j.neurobiolaging.2021.03.018

- Raihaan Patel : provided methodological and statistical support
- Eric Plitman : provided guidance in the conceptualization and in the image processing
- Stephanie Tullo, Alyssa Salaciak, Saashi A. Bedford, Sarah Farzin, Marie-Lise Beland, Vanessa Valiquette and Christina Kazazian : all participated in the data collection of the ADB dataset and in the data curation
- Christine L. Tardif : provided expertise in the ADB imaging protocol development
- Gabriel A. Devenyi : provided technical support to perform the image processing and the formal statistical analysis
- M. Mallar Chakravarty : supervised the study and provided guidance in conceptualization of the study, interpretations of results, and writing of the manuscript
- All authors: provided critical or conceptual support and revised the manuscript

Chapter 5: **Aurélie Bussy**, Raihaan Patel, Olivier Parent, Alyssa Salaciak, Saashi A. Bedford, Sarah Farzin, Stephanie Tullo, Sylvia Villeneuve, Judes Poirier, John CS Breitner, Gabriel A. Devenyi, PREVENT-AD Research Group, Christine L. Tardif, M. Mallar Chakravarty. *Combined structural and quantitative MRI reveal alterations in the hippocampus and cortex across the Alzheimer's disease spectrum.*

- Raihaan Patel : provided methodological and statistical support
- Olivier Parent : contributed to the image quality control
- Alyssa Salaciak, Saashi A. Bedford, Sarah Farzin and Stephanie Tullo : all participated in the data collection of the ADB dataset and in the data curation
- Sylvia Villeneuve, Judes Poirier and John CS Breitner : provided access to Presymptomatic Evaluation of Experimental or Novel Treatments for Alzheimer Disease (PREVENT-AD) dataset
- Gabriel A. Devenyi : provided technical support to perform the image processing and the formal statistical analysis
- Christine L. Tardif : provided expertise in the ADB imaging protocol development
- M. Mallar Chakravarty : supervised the study and provided guidance in conceptualization of the study, interpretations of results, and writing of the manuscript
- All authors: provided critical or conceptual support and revised the manuscript

Other related lead-author publications:

Aurélie Bussy, Jake P Levy, Tristin Best, Raihaan Patel, Lani Cupo, Tim Van Langenhove, Jørgen E Nielsen, Yolande Pijnenburg, Maria Landqvist Waldö, Anne M Remes,

Matthias L Schroeter, Isabel Santana, Florence Pasquier, Markus Otto, Adrian Danek, Johannes Levin, Isabelle Le Ber, Rik Vandenberghe, Matthis Synofzik, Fermin Moreno, Alexandre de Mendonça, Raquel Sanchez-Valle, Robert Laforce, Tobias Langheinrich, Alexander Gerhard, Caroline Graff, Chris R Butler, Sandro Sorbi, Lize Jiskoot, Harro Seelaar, John C van Swieten, Elizabeth Finger, Maria Carmela Tartaglia, Mario Masellis, Pietro Tiraboschi, Daniela Galimberti, Barbara Borroni, James B Rowe, Martina Bocchetta, Jonathan D Rohrer, Gabriel A Devenyi, M Mallar Chakravarty, Simon Ducharme; GENetic Frontotemporal dementia Initiative (GENFI) *Cerebellar and subcortical atrophy contribute to psychiatric symptoms in frontotemporal dementia.* Human Brain Mapping, March 2023, https://doi-org.proxy3.library.mcgill.ca/10.1002/hbm.26220

Other related co-authored publications

Etienne Aumont, **Aurélie Bussy**, Marc-André Bedard, Gleb Bezgin, Joseph Therriault, Melissa Savard, Jaime Fernandez Arias, Viviane Sziklas, Paolo Vitali, Nina Margherita Poltronetti, Vanessa Pallen, Emilie Thomas, Serge Gauthier, Mallar M. Chakravarty, Eliane Kobayashi, Pedro Rosa-Neto *Hippocampal subfield associations with memory depend on stimulus modality and retrieval mode.* In submission at Brain.

Olivier Parent, **Aurélie Bussy**, Gabriel A. Devenyi, Alyssa Dai, Manuela Costantino, Stephanie Tullo, Alyssa Salaciak, Saashi A. Bedford, Sarah Farzin, Marie-Lise Béland, Vanessa Valiquette, Sylvia Villeneuve, Judes Poirier, Christine L. Tardif, Mahsa Dadar, the PREVENT-AD Research Group, M. Mallar Chakravarty *Assessment of white matter hyperintensity severity using multimodal MRI in Alzheimer's Disease.* In submission.

Grace Pigeau, Manuela Costantino, Gabriel A. Devenyi, **Aurélie Bussy**, Olivier Parent,

M. Mallar Chakravarty *The impact of study design choices on significance and generalizability of canonical correlation analysis in neuroimaging studies.* In submission.

Olivier Parent, Emily Olafson, **Aurélie Bussy**, Stephanie Tullo, Nadia Blostein, Alyssa Dai, Alyssa Salaciak, Saashi A Bedford, Sarah Farzin, Marie-Lise Béland, Vanessa Valiquette, Christine L Tardif, Gabriel A Devenyi, M Mallar Chakravarty *High spatial overlap but diverging age-related trajectories of cortical magnetic resonance imaging markers aiming to represent intracortical myelin and microstructure.* Human Brain Mapping, March 2023, https://doi-org.proxy3.library.mcgill.ca/10.1002/hbm.26259

Raghav Mehta, Thomas Christinck, Tanya Nair, **Aurélie Bussy**, Swapna Premasiri, Manuela Costantino, M Mallar Chakravarthy, Douglas L Arnold, Yarin Gal, Tal Arbel *Propagating Uncertainty Across Cascaded Medical Imaging Tasks for Improved Deep Learning Inference.* IEEE transactions on medical imaging, February 2022, https://doi-org.proxy3.library.mcgill.ca/10.1109/tmi.2021.3114097

Eric Plitman, **Aurélie Bussy**, Vanessa Valiquette, Alyssa Salaciak, Raihaan Patel, Lani Cupo, Marie-Lise Béland, Stephanie Tullo, Christine L. Tardif, M. Natasha Rajah, Jamie Near, Gabriel A. Devenyi, M. Mallar Chakravarty *The impact of the Siemens Tim Trio to Prisma upgrade and the addition of volumetric navigators on cortical thickness, structure volume, and 1 H-MRS indices: An MRI reliability study with implications for longitudinal study designs.* NeuroImage, May 2021, https://doi-org.proxy3.library.mcgill.ca/10.1016/j.neuroimage.2021.118172

Presentation

Invited talks

1. **Bussy A**. *"Investigation of the hippocampus in physiological and pathological aging using multi-contrast and multi-modal imaging techniques"*; 22/02/2023; International lecture. Invited by the Cerebral Imaging Centre, Douglas Mental Health Institute, Montreal, Canada.

2. **Bussy A**. *"Investigation of the hippocampus in physiological and pathological aging using multi-contrast and multi-modal imaging techniques"* ; 18/11/2022; International lecture. Invited by the Center for Cognitive and Behavioral Brain Imaging at the Ohio State University.

3. **Bussy A**. *"Hippocampal volume and shape in aging; Methodological considerations"*. IPN retreat 2021; 04/10/2021; Local conference within McGill University. Invited by Pr. Sylvia Villeneuve.

4. **Bussy A**. *"Effects of MR sequence on hippocampal subfield volumes and relationship between hippocampal shape and age."* Hippocampal Subfield Group; 28/04/2021; International webinar. Invited by Pr Kelsey Canada.

5. **Bussy A**, Guma E, Cupo L, Patel R. *"Overview of multivariate analysis methods in Neuroimaging"*; 07/10/2020; Lecture at the Cerebral Imaging Centre, Douglas Mental Health Institute, Montreal, Canada. Invited by Pr Mallar Chakravarty

6. **Bussy A**. *"Applying MAGeT Brain for volumetric segmentation: a hands on tutorial"*. Montreal Aging & Dementia Conference; 26/12/2019; International conference at Montreal, Canada. Invited by Pr Natasha Rajah.

Oral Presentations - Conferences

1. **Bussy A**, Patel R, Parent O, Salaciak A, Farzin S, Tullo S, Villeneuve S, Poirier J, Breitner JCS, Devenyi GA, PREVENT-AD Research Group, Tardif CL, Chakravarty MM. *"Cortical morphometry and hippocampal microstructure predict aging and Alzheimer's disease progression."*. ISMRM 2023. Toronto, Canada ; International conference

2. **Bussy A**, Patel R, Parent O, Salaciak A, Farzin S, Tullo S, Villeneuve S, Poirier J, Breitner JCS, Devenyi GA, PREVENT-AD Research Group, Tardif CL, Chakravarty MM. *"Multivariate analysis of morphometric and quantitative magnetic resonance imaging metrics in aging and Alzheimer's disease"*. Quantitative MRI conference 2022. Virtual presentation.

3. **Bussy A**, Patel R, Salaciak A, Farzin S, Tullo S, Pelleieux S, Villeneuve S, Poirier J, Breitner JCS, Devenyi GA, PREVENT-AD Research Group, Tardif CL, Chakravarty MM. *"Multivariate analysis of morphometric and quantitative magnetic resonance imaging metrics in aging and Alzheimer's disease"*; Quebec Bio-imaging Network 2022 ; Sherbrooke.

4. **Bussy A**, Plitman E, Patel R, Tullo S, Salaciak A, Bedford SA, Farzin S, Béland ML, Valiquette V, Kazazian C, Tardif CL, Devenyi GA, Chakravarty MM. *"Hippocampal subfield volumes across the healthy lifespan and the effects of MR sequence on estimates"*; 2021 Leo and Rachel Hendlisz Award competition.

5. **Bussy A**, Levy J, Patel R, Cupo L, Devenyi GA, Chakravarty MM, Ducharme S, on behalf of the GENetic Frontotemporal dementia Initiative (GENFI). *"Cerebellar and subcortical volumes are associated with neuropsychiatric symptoms in genetic frontotemporal dementia"*; Douglas Research Day 2021; Local conference

6. **Bussy A**, Patel R, Plitman E, Tullo S, Salaciak A, Bedford SA, Farzin S, Béland ML, Devenyi GA, Chakravarty MM. *"Comparing the impact of T1; and T2-weighted*

acquisition on automated hippocampal subfield volume estimates"; SFN 2019, Chicago, US; International conference

7. **Bussy A**, Patel R, Plitman E, Tullo S, Salaciak A, Bedford SA, Farzin S, Béland ML, Devenyi GA, Chakravarty MM. *"The evolution of the hippocampus subfields volume across lifespan in healthy aging"*. Canadian College of Neuropsychopharmacology 2019 meeting, Montreal, Canada; International conference

Poster Presentation

1. **Bussy A**, Wearn A, Patel R, Baracchini G, Villeneuve S, Poirier J, Breitner JCS, Devenyi GA, Spreng RN, Chakravarty MM. *Cortical quantitative MRI metrics are sensitive to amyloid and tau PET in preclinical Alzheimer's disease.* OHBM 2023, Montreal, Canada ; International conference

2. **Bussy A**, Wearn A, Patel R, Baracchini G, Villeneuve S, Poirier J, Breitner JCS, Devenyi GA, Spreng RN, Chakravarty MM. *Cortical quantitative MRI metrics are sensitive to amyloid and tau PET in preclinical Alzheimer's disease.* HBHL 2023, Montreal, Canada ; Local conference

3. Parent O, **Bussy A**, Devenyi GA, Pigeau G, Costantino M, Tardif CL, Dadar M, Chakravarty MM. *Spatial clustering of white matter hyperintensities based on their microstructural properties.*; OHBM 2023, Montreal, Canada ; International conference

4. Simard LM, Immer K, **Bussy A**. *Quantification de la myéline dans le cerveau par ratio T1w/T2w, biomarqueur utilisant l'imagerie par résonance magnétique.* ACFAS 2023, Montreal, Canada ; International conference

5. Aumont E, **Bussy A**, Bezgin G, Therriault J, Savard M; Arias JM, Poltronetti NM, Pallen V, Thomas E, Vitali P, Chakravarty MM, Bedard MA, Rosa-Neto P. *Hippocam-*

pal subfield volumes and memory performances: the effects of stimulus modality and either free recall or recognition; AAIC, Amsterdam ; International conference

6. Legault-Denis C, Aumont E, Onuska K, Schmitz T, **Bussy A**, Chakravarty M, Soucy JP, Bedard MA. *"Bilateral cholinergic upregulation associated with CA2-CA3 hippocampal atrophy in cognitively unimpaired patients with Parkinson's disease: A combined MRI-PET study."*; ADPD 2023

7. Parent O, **Bussy A**, Devenyi GA, Dai A, Costantino M, Tullo S, Salaciak A, Bedford SA, Farzin S, Béland ML, Valiquette V, Tardif CL, Dadar M, Chakravarty MM. *"Multimodal assessment of white matter hyperintensity severity"*. SfN 2022, San Diego, United States ; International conference

8. **Bussy A**, Patel R, Salaciak A, Farzin S, Tullo S, Pelleieux S, Villeneuve S, Poirier J, Breitner JCS, Devenyi GA, PREVENT-AD Research Group, Tardif CL, Chakravarty MM. *"Multivariate analysis of morphometric and quantitative magnetic resonance imaging metrics in aging and Alzheimer's disease"*; ISMRM 2022, London, UK; International conference

9. Aumont E, **Bussy A**, Bezgin G, Savard M, Therriault J, Chakravarty MM, Bedard MA, Rosa-Neto P. *"Early visual memory loss in AD pathology continuum are predicted by specific lateralized hippocampal subfield atrophy"*. ADPD 2022

10. **Bussy A**, Levy J, Chakravarty MM, Ducharme S, on behalf of the GENFI; *"Cerebellar lobule volumes and neuropsychiatric symptoms in genetic frontotemporal dementia."*; American Neuropsychiatric Association 2021

11. Palmis S, Easson K, **Bussy A**, Gilbert G, Khairy M, Saint-Martin C, Chakravarty MM, Brossard-Racine M. *"Altered Cerebellar volume in youth born very preterm"*. 7th Annual Child Health and Human Development Research Day, Online (November, 12, 2021), Oral.

12. Parent O, Olafson E, **Bussy A**, Tullo S, Salaciak A, Bedford SA, Farzin S, Béland ML, Valiquette V, Tardif CL, Devenyi GA, Chakravarty MM. *"Comparing age trajectories of MRI cortical markers and myelin"*; SfN 2021

13. Premasiri S, **Bussy A**, Devenyi GA, Chakravarty MM "Cascaded 3D U;Net Model for Fast Automatic Segmentation of the Hippocampus"; OHBM 2021; International conference

14. Costantino M, Pigeau G, **Bussy A**, Blostein N, Devenyi GA, Markello R, Patel R, Gervais N, Chakravarty MM. *"Effects of pregnancy, and lifestyle risk factors on cortical thickness in healthy ageing"*; OHBM 2021

15. Palmis S, Easson K, **Bussy A**, Gilbert G, Khairy M, Saint-Martin C, Chakravarty MM, Brossard-Racine M. *"Altered Cerebellar volume in youth born very preterm"*. Congrès provincial de la recherche mère-enfant, Online (November 5, 2021), Poster.

16. **Bussy A**, Levy J, Chakravarty MM, Ducharme S, on behalf of the GENFI. *"Investigation of the cerebellar lobule volumes and neuropsychiatric symptoms in genetic FTD."*; SfN 2020; International conference

17. **Bussy A**, Plitman E, Patel R, Tullo S, Salaciak A, Bedford SA, Farzin S, Béland ML, Devenyi GA, Chakravarty MM. *"Volumetric, shape and microstructural alterations of the hippocampal subfields in healthy aging"*. Alzheimer's Association International Conference (AAIC) 2020, Amsterdam, Netherlands; International conference

18. **Bussy A**, Plitman E, Patel R, Tullo S, Salaciak A, Bedford SA, Farzin S, Béland ML, Devenyi GA, Chakravarty MM. *"Volumetric, shape and microstructural alterations of the hippocampal subfields in healthy aging"*. Alzheimer's Imaging Consortium (AIC) 2020, Amsterdam, Netherlands; International conference

19. **Bussy A**, Plitman E, Valiquette V, Karzazian C, Devenyi GA, Chakravarty MM.

"Impact of commonly used acquisition sequences on automated hippocampal subfield volume estimates"; OHBM 2020, Montréal, Canada

20. Plitman E, **Bussy A**, Valiquette V, Salaciak A, Rajah N, Near J, Devenyia GA, Chakravarty MM. *"Test;retest reliability of cortical thickness and structure volume in volumetric navigator sequences."* OHBM 2020, Canada

21. **Bussy A**, Snider JB, Coble D, Xiong C, Fagan AM, Cruchaga C, Benzinger TLS, Gordon BA, Hassenstab J, Bateman RJ and Morris JC on behalf of the Dominantly Inherited Alzheimer Network. *"Effect of apolipoprotein E4 on clinical, neuroimaging, and biomarker measures in noncarrier participants in the DIAN study"*; DIAD conference 2019, Los Angeles, US; International conference

22. **Bussy A**, Plitman E, Patel R, Tullo S, Salaciak A, Bedford SA, Farzin S, Béland ML, Devenyi GA, Chakravarty MM. *"The evolution of the hippocampus subfields volume across lifespan in healthy aging"*; IPN retreat 2019, Montreal, Canada; Local conference

23. **Bussy A**, Plitman E, Patel R, Tullo S, Salaciak A, Bedford SA, Farzin S, Béland ML, Devenyi GA, Chakravarty MM. *"The evolution of the hippocampus subfields volume across lifespan in healthy aging"*; Neurosymposium 2019, Montreal, Local conference

Original contributions

Chapter 3

The aim of our study was to identify the reasons for inconsistent results regarding the association between age and specific regions of the hippocampus. Indeed, various experimental design differences exist between studies but some important methodological factors have been overlooked. For example, different types of MRI sequence have been used in the literature, which might impact the quality and precision of the segmentation algorithms. Further, the age range and statistical models used to study age effect might alter the results. Overall, we demonstrated that one of the most widely used approach might be biased in the context of aging and therefore potentially impact studies investigating neurodegenerative disorders.

Chapter 4

The objective of this project was to investigate the hypothesis, originally proposed in Chapter 3, that the shape of the hippocampus changes over the course of an individual's life. Therefore, to study the surface-wise relationship between hippocampal shape and age, we derived two surface-based metrics and used a data-driven approach to study non-linear age-relationships. Additionally, we used a multivariate approach known as partial least square (PLS) to investigate the relationship between hippocampal shape and multiple key variables of interest such as age, sex, education, APOE-ϵ4 allele status and cognitive scores.

Chapter 5

In this last chapter, we wanted to investigate how the hippocampal microstructure, such as iron and myelin, might vary in the healthy lifespan and also across the AD spectrum. In order to determine whether the hippocampus or cortex was more informative about disease progression, we included both structures in our analyses. We used a data-driven parcellation of those structures based on indices of morphometry and microstructure. We then related our brain indices to several key variables of interest including lifestyle, cognitive, psy-

chological and medical information. Our findings demonstrated that cortical morphometry and hippocampal microstructure were the most strongly related to the disease progression, suggesting that they may serve as valuable indicators of the disease progression.

Funding and awards

The work within this thesis was possible thanks to many funding sources and awards that are graciously acknowledged here.

Scholarships

- **Healthy Brain for Healthy Life** - doctoral scholarship. 2022-2023
- **Alzheimer Society of Canada** - doctoral scholarship. 2019-2022

Travel awards

- **ISMRM Educational Stipend** - Travel award to attend ISMRM 2023 in Toronto, Canada. 2023/06
- **Quebec Bio-Imaging Network mentorship award** - QBIN CEGEP Mentorship Grant Program. 2022/07 to 2022/08
- **Quebec Bio-Imaging Network award** - Travel award to attend ISMRM 2022 in London, UK. 2022/05
- **ISMRM Educational Stipend** - Travel award to attend ISMRM 2022 in London, UK. 2022/05
- **Leo and Rachel Hendlisz award** - Douglas's second best paper. 2021/12

- **Roger J. Paiement Outreach award** - Travel award for AAIC. 2021/01
- **Brainhack Western award** - Travel award to attend Brainhack Western, London, Ontario, Canada. 2019/10
- **Quebec Bio-Imaging Network award** - Travel award to attend SFN 2019, Chicago, Illinois, USA. 2019/07

Chapter 1

Introduction

1.1 Rationale

About half of the world's population including Canada, the United States, and most nations in Europe live with low fertility rates, yet most of these countries still have growing populations due to immigration, and increases in life expectancy (Nations 2017). As the population ages, the proportion of older individuals is increasing at a rapid pace. One reason is due to the so-called "baby boomer" generation, which consists of large cohorts of individuals born between 1946 and 1965 (He, Goodkind, and Kowal 2016). These individuals currently represent approximately two-thirds of those aged 65 years and older. An increased demand for healthcare services is expected as the population ages, particularly for age-related conditions such as dementia, AD, and other neurodegenerative diseases. In this context, there is an urgent need for healthcare services that can meet the demands of older adults with multiple chronic health conditions (Jaul and Barron 2017). Therefore, it is crucial that healthcare systems prepare for this demographic shift, to not become overwhelmed and put the health of millions of individuals at risk.

In Canada in 2022, individuals aged 65 years and older represent a higher proportion of the population compared to the number of children aged 0 to 14 years old. This gap between

the number of older adults and children is growing and is in part due to sub-replacement fertility rates in Canada since the early 1970s (Statistics Canada, 2022). A sub-replacement fertility rate results in each new generation being smaller than the previous one in a given area. The United Nations defines sub-replacement fertility as a rate below approximately 2.1 children born per woman of childbearing age, although the threshold can be higher in some developing countries due to higher mortality rates (United Nations 2020). There are various factors that have contributed to the decline in fertility rates across the world, including but not limited to, changing social attitudes towards marriage and childbearing, economic factors, and access to reproductive technologies (Lightbourne R, S. Singh, and C. P. Green 1982; Götmark and Andersson 2020; Cheng et al. 2022). A recent example of external factor impacting fertility was the COVID pandemic which decreased fertility rate in countries such as Canada (Statistics Canada, 2022) and the United States (Lindberg et al. 2020). Overall, the low fertility rate is a significant contributor to rapid population aging and has long-term implications for various aspects of society. As the population ages, it puts increased stress on the labor market, public health care, and pension systems, leading to a range of socioeconomic challenges that must be addressed.

Further, healthcare costs are on the rise while the proportion of the working-age population, which was 69% in 2009, is predicted to decrease to 60% by 2036 (Statistics Canada). This demographic shift is expected to decrease the number of active workers, affecting the country's productivity and economic growth. To address this challenge, immigration rates in Canada have been increased. Since early 2020, over 1.2 million permanent and temporary immigrants came to Canada, accounting for nearly 90% of total population growth. By 2041, immigrants are projected to represent a third of Canada's population while it is currently 23% (Statistics Canada -2021 Census of Population). As a result, Canada is expected to experience significant socio-demographic changes, with an increased cultural and ethnic diversity of its population.

Overall, with an increasing number of older adults and a decreasing number of young peo-

ple, healthcare systems in most countries will be at stake in the near future. To address these challenges, the Canadian healthcare system has implemented a range of initiatives aimed at supporting healthy aging and improving healthcare for older adults (Public Health Agency of Canada, 2020). For example, there are a number of programs that focus on preventing and managing chronic diseases, such as diabetes and cardiovascular disease, which are more common in older adults. In addition, there is a growing recognition of the importance of research on aging and age-related conditions. The Canadian Institutes of Health Research has a specific focus on aging and neuroscience research, and funds a wide range of studies aimed at understanding the underlying mechanisms of aging and developing interventions to promote healthy aging.

1.2 Motivation

1.2.1 Why should we study physiological aging?

Aging is a gradual and continuous process of natural changes that occur throughout the lifespan. The term "normal," "pure," or "healthy" aging is frequently used to describe the universal physiological changes that occur in individuals who live long enough without developing any disorders. There are several important reasons to study normal aging (Fjell and Walhovd 2010).

Due to increased life expectancy, every country in the world is experiencing growth in both the size and the proportion of older persons in the population (World Health Organization 2016). Simultaneously, the prevalence to develop conditions such as hearing loss, cataracts, back and neck pain and osteoarthritis, diabetes, depression and dementia, increases in older age. However, there is significant variability in how individuals age. Some 70-year-old individuals will have similar physical and mental capacities to 30-year-old individuals, while others will demonstrate significant decline. This variability can be explained by two kinds of risk factors (Livingston et al. 2017). Immutable factors such as sex (Hägg and Jylhävä

2021), ethnicity (Ferraro, Kemp, and M. M. Williams 2017; Menkin et al. 2017), genetics (Finch and R E Tanzi 1997) or parental socioeconomic status (Agahi, B. A. Shaw, and Fors 2014) can impact how someone will age. But most importantly, modifiable factors such as education (Meeks and Murrell 2001), physical activity (Daskalopoulou et al. 2017), body weight (Fontana and Hu 2014), hypertension (Buford 2016), diabetes (E. S. Huang et al. 2014), alcohol (Caputo et al. 2012; Martins de Carvalho et al. 2019) or smoking consumption (Bernhard et al. 2007) impact individual's health in aging. Therefore, a better understanding of the modifiable risk factors associated with aging can be achieved by studying the brain and its changes over time. Subsequently, this could further be used to promote healthy aging and prevent age-related health issues.

Secondly, individuals experience several negative cognitive changes in aging such as decrease in processing speed (Sliwinski and Buschke 1999), impaired executive functions (Fjell, Sneve, et al. 2017) or decline in episodic memory (Nilsson 2003). These cognitive deficits then lead to functional deficits, which impedes activities of daily living of affected individuals. Studying how structural, functional and microstructural brain properties are related to those cognitive domains has the potential to reveal their putative neurobiological underpinnings.

Lastly, studying normal aging is necessary to clearly detect any deviation from this norm. There are multiple age-related pathologies such as AD (Bateman et al. 2012), Parkinson's disease (Gaig and Tolosa 2009) or frontotemporal dementia (Benussi et al. 2019) that present early brain alterations during the preclinical stage of the disease. More specifically in AD, individuals start showing brain alterations up to 25 years before symptom onset, while it is 20 years in Parkinson's disease, and 30 years in frontotemporal dementia (Katsuno et al. 2018). Early identification of these changes is essential for tracking disease progression and understanding the underlying causes or protective factors. This knowledge can help in developing effective interventions to prevent or slow down disease onset and progression.

1.2.2 Why should we study the hippocampus?

The hippocampus is a small, curved formation located deep in the temporal lobe of the brain. This structure has been intensely studied due to its critical role in learning, memory, and spatial navigation. The hippocampus is composed of several subregions, highly connected within the hippocampus itself as well as with the remainder of the brain, making it a complex and dynamic structure to study. The hippocampus is highly vulnerable to pathologies and is one of the most affected brain regions in multiple disorders, such as AD (West et al. 1994; Laakso, Soininen, et al. 1998), schizophrenia (Heckers 2001; Harrison 2004), epilepsy (Dam 1980; Huberfeld, Blauwblomme, and Miles 2015), and depression (Bear and Abraham 1996; S. Campbell and G. MacQueen 2004). It is therefore important to understand the functions of the hippocampus to gain insights into the underlying mechanisms of these conditions and help to develop better treatments.

Although numerous studies have investigated hippocampal changes in healthy aging, there are still important inconsistencies in the literature. For example, some studies have reported significant hippocampal volume loss with age (Nikolai V Malykhin, Y. Huang, et al. 2017; Raz et al. 2004), while others have not found any significant changes (Good et al. 2001; E V Sullivan et al. 1995). Similarly, some studies have reported age-related reductions in hippocampal neurogenesis (Cipriani et al. 2018; Sorrells et al. 2018), while others have found no changes with age (P. S. Eriksson et al. 1998; Moreno-Jiménez et al. 2021; Spalding et al. 2013).

One possible explanation for these inconsistencies is that studies differ in their methods, sample sizes, and participant characteristics (Bussy, Plitman, et al. 2021). For example, studies using different imaging techniques or different criteria for defining the hippocampus may yield different results. Additionally, sample sizes and participant characteristics, such as age range and health status, can also influence results. Another factor that may contribute to inconsistencies in the literature is the use of different outcome measures which can make it difficult to compare findings across studies. For example, some studies have

focused on hippocampal volume, while others have investigated changes in hippocampal shape or connectivity. Therefore, uncovering the most important methodological variations affecting reported age-related hippocampus changes would bring clarity to the significant heterogeneity in the literature.

The inconsistencies in the literature regarding hippocampal changes in healthy aging have important implications for understanding age-related cognitive decline and developing interventions to promote healthy aging. To address the inconsistencies in the literature, future research could focus on standardizing methods and outcome measures across studies. Large-scale, multi-site studies that include diverse samples and consistent methods and measures will help clarify the precise nature of hippocampal changes with healthy aging.

Additionally, more research is needed to understand the relationship between different aspects of hippocampal health, such as volume, shape, microstructural properties, and their implications for cognitive function in healthy aging. Understanding the complex interplay between these factors may help identify new targets for interventions to promote healthy aging and prevent cognitive decline.

1.2.3 Why should we use MRI?

MRI is a non-invasive imaging technique that uses magnetic fields and radio-frequency waves to produce high-resolution images of the human body, including the brain. The use of MRI has become increasingly popular in recent years due to its ability to provide detailed information about the structure and function of the brain.

Further, MRI has several benefits. First, it provides a high-resolution image of the brain with great anatomical detail. Presently, most structural MRI have a spatial resolution of 1 mm^3 while functional MRI often have isotropic resolutions equal or higher than 2 mm^3. This makes it possible to identify small structural changes in the brain, such as lesions, tumors, and brain atrophy. Second, MRI is a non-invasive technique that does not use ionizing radiation, which makes it a safe method for imaging the brain multiple times, or in

vulnerable population. This property of MRI makes it ideally suited for studying the brains of children, pregnant women or to acquire longitudinal datasets. Third, it can be used to study different aspects of brain function, including blood flow, metabolism, and diffusion or to estimate the tissue microstructure. This makes it a versatile technique for studying various neurological and psychiatric disorders.

Additionally, compared to other imaging modalities, MRI has multiple advantages. Indeed, computed tomography uses ionizing radiation and is less sensitive to soft tissues which is not suitable for studying the brain. Positron emission tomography (PET) uses radioactive tracers to study brain metabolism and neurotransmitter function. However, it has lower spatial resolution than MRI ($< 4\ mm^3$) and requires the injection of a radioactive substance. Lastly, single photon emission computed tomography is similar to PET but uses different radioactive tracers. It is less sensitive than PET and has lower spatial resolution than MRI. Overall, MRI is a powerful imaging modality for studying the brain. Its high spatial resolution, versatility, and non-invasive nature make it an attractive option for researchers and clinicians. Therefore, while other imaging modalities have their own advantages, they cannot match the resolution and versatility of MRI.

Overall, the aim of this thesis is to use the versatility of MRI to examine various aspects of the hippocampus, providing insight into its changes during aging and progression of AD.

1.3 Outline

This thesis comprises six chapters, each serving a distinct purpose. **Chapter 1** is the introduction, providing an overview of the research objectives and context. **Chapter 2** offers background material necessary to contextualize the rest of the chapters.

Chapter 3 presents a study aimed at characterizing age-related relationships between the volume of hippocampal subfields and peri-hippocampal white matter (WM) subregions. The impact of image acquisition choices (including standard isotropic T1w, high-resolution

isotropic T2w, and slab hippocampus-specific T2w) on hippocampal subfield volumes and their reliability is also critically assessed.

Chapter 4 uses morphological measurements to characterize shape-related modifications of the hippocampus associated with age. Additionally, we investigate the interaction between hippocampal shape and other factors known to be involved in age-related decline, such as sex, cognition, APOE-ϵ4 allele mutation, and education.

In **Chapter 5**, we use quantitative imaging techniques and morphometry to describe the hippocampal and cortical changes in healthy aging participants at different stages of the AD spectrum. We also investigate how multiple risk factors, lifestyle variables and cognitive information relate to qMRI metrics and morphometry.

Finally, **Chapter 6** presents a discussion of the obtained results and conclusions drawn from our studies.

Chapter 2

Background

2.1 Neuroanatomy

The human brain controls most of the functions of the body such as memory, motor, emotional, visual and auditory processing and can be broadly divided into the cerebrum, brainstem and cerebellum. The outer surface of the cerebrum is composed of grey matter (GM) and is named the cerebral cortex, while the inner core of the brain consists of WM. Importantly, the brain can be observed at different scales : from cellular alterations, to microstructural changes, to variations in brain structures or the entire brain itself.

2.1.1 Grey matter

2.1.1.1 Cell types

The two main types of cells in the brain are the neurons and the glial cells (or neuroglia). Neurons are classically described as being composed of three main parts (Figure 2.1 **a**): the dendrites which largely extend in a dendritic arborization close to the cell body (receive incoming information), the cell body (or soma) which contains the nucleus (receive incoming information and integrates information together) and the axon which is a long filament that typically conducts electrical impulses away from the cell body to the axon terminal (transmit

information to another neuron via its synapses). Glial cells include astrocytes, oligodendrocytes, ependymal cells, radial glia, microglia and the glymphatic system. Astrocytes provide physical and nutritional support for neurons (Vasile, Dossi, and Rouach 2017). Oligodendrocytes provide support and insulation to axons (Stadelmann et al. 2019). Ependymal cells create cerebrospinal fluid (CSF) and regulate neurotransmitters and hormone distribution in the brain (Del Bigio 2010). Radial glial cells regulate brain folding (Borrell and Götz 2014), plasticity and neurogenesis (Lindsey et al. 2018). Microglia are critical for the brain's internal immune system and act as the resident macrophages of the brain that help remove foreign or damaged material or cells (Graeber and Streit 2010). Microglia also play a crucial role in controlling neuronal activity, managing synaptic transmission, and shaping the creation, alteration, or removal of synaptic structures (Akiyoshi et al. 2018). The glymphatic system participates in waste elimination and helps distribute non-waste compounds in the brain (N. A. Jessen et al. 2015).

2.1.1.2 Cytoarchitecture

Cytoarchitecture or cytoarchitectonics is the microscopic study of the cellular composition and structural arrangement of neurons within the central nervous system (CNS). The similarity of the local organization and characteristics of the neurons (type, size, shape, density) are features that are used to define specific cytoarchitectural regions. The study of brain composition and organization started more than 250 years ago. In 1776, Francesco Gennari provided evidence of the presence of a white band which refers to a bundle of myelinated axons that run in a parallel manner to the cerebral cortex surface. This finding is considered as the first evidence that the cerebral cortex is not uniform in structure (Gennari 1782). In 1840, Jules Baillarger was the first neurologist to discover that the cerebral cortex was divided into six layers (Baillarger 1840). In the late nineteenth century, Golgi (Golgi 1885) and Cajal (Ramon Cajal and Azoulay 1909) set the foundations of the neuron theory by demonstrating the existence of synapses (gaps between neurons) confirming that neurons

function as independent cells and not as a single network. The examination of cortical cytoarchitecture started with the classic brain atlas developed by Korbinian Brodmann where cortical areas were parcellated based on their layer specific organization observable using the Nissl method of cell staining (Brodmann 1909). Following this pioneering work, additional atlases based on cytoarchitecture were proposed by Constantin von Economo and Georg N. Koskinas and others (Economo and Koskinas 1925) (Figure 2.1). New architectonic mapping of the human brain were developed using more recent computational tools to expand on previous parcellations with for example the BigBrain, a ultrahigh-resolution 3D brain reconstructed from thousands histological sections (Amunts, Lepage, et al. 2013; Amunts and Zilles 2015).

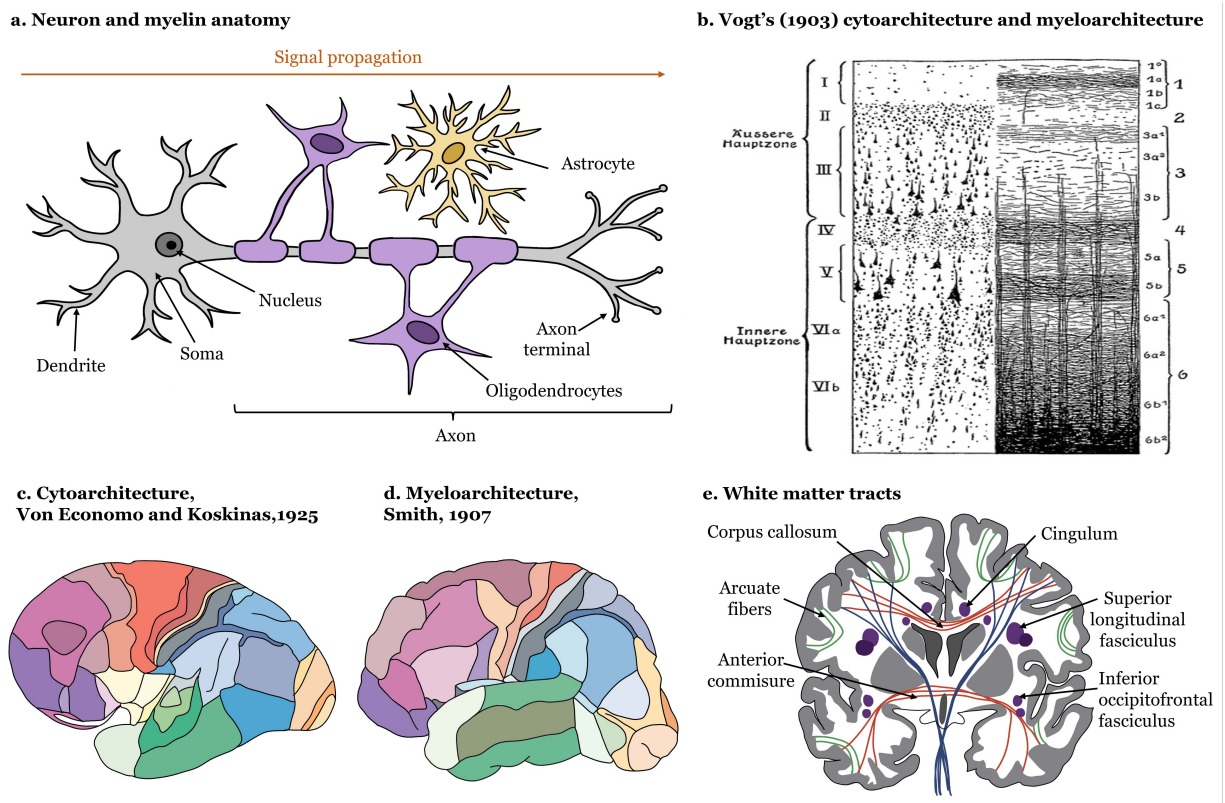

Figure 2.1: **a.** Schematic of a myelinated neuron. **b.** Cytoarchitectonic layers (designated with Roman numbers), and myeloarchitectonic layers (designated with Arabic numbers) (Vogt and Vogt 1903). **c.** Reproduction of the cytoarchitecture atlas (Economo and Koskinas 1925), **d.** Reproduction of the myeloarchitecture atlas (Grafton Elliot Smith 1907) and **e.** Representation of the main white matter tracts, inspired (Wycoco et al. 2013).

2.1.2 White matter

2.1.2.1 Myelin

In the CNS, oligodendrocytes are a type of neuroglia providing metabolic support and insulation, and facilitating saltatory conduction along axons (Emery 2010). Myelin is a lipid-rich multilamellar membrane produced by oligodendrocytes that is wrapped around the axons creating the myelin sheath. Its roles are to facilitate rapid propagation of electrical impulses (Saab and Nave 2017) and to provide metabolic substrates such as lactate and pyruvate to the underlying axon when there is a high axonal energy need (Saab, Tzvetanova, and Nave 2013; Stadelmann et al. 2019). In the vertebrate CNS, myelinated axons compose the white matter and account for around 40% of the CNS volume in humans.

2.1.2.2 Myeloarchitecture

In 1898, Oskar and Cécile Vogt founded a research center devoted entirely to the study of the structure and function of the central nervous system. Nissl stain was used to study the neuronal cell bodies, and the Weigert stain for myelinated nerve fibers. They defined 6 cytoarchitecture layers (Figure 2.1 **b**): (*I*) the cell-poor zonal layer, (*II*) the external granular layer, (*III*) the external pyramidal layer, (*IV*) the internal granular layer, (*V*) the internal pyramidal layer, and (*VI*) the multiform layer. They also defined 6 myeloarchitecture layers called : (*1*) the zonal layer, (*2*) the dysfibrous layer, (*3*) the suprastriate layer, (*4*) the external stria or outer stripe of Baillarger (dark band of tightly packed, tangential fibers) (*5a*) the intrastriate layer and (*5b*) the internal stria or inner stripe of Baillarger and (*6*) subdivided into the lamina *6a1*, *6a2*, *6b1* and *6b2* (transition to the subcortical WM) (Rudolf Nieuwenhuys 2013). Other cortical maps emerged from different myeloarchitectonic parcellations of the human brain (Figure 2.1 **d**) (A. W. Campbell 1904; Grafton Elliot Smith 1907).

Unlike the previously described methods, there are multiple newer techniques to assess the degree of myelination in WM in living humans. These include measures such as diffusion

tensor imaging (DTI) (Beaulieu 2002), magnetization transfer imaging (J G Sled and Pike 2001; John G Sled 2018), myelin water imaging (MacKay and Laule 2016), T1 mapping (Shams, Norris, and Marques 2019) and T1w/T2w ratio mapping (Glasser and Van Essen 2011).

2.1.3 Hippocampus

2.1.3.1 Hippocampal anatomy

The hippocampus is a complex structure embedded in the medial temporal lobe (MTL) (Figure 2.2 **a**) which has the shape of a curved, tapering tube, often compared to a seahorse. The hippocampus is a component of the archicortex, characterized by its unique three-layered cortical structure, consisting of a superficial molecular layer, a pyramidal cell layer, and a deep molecular layer. The superficial molecular layer can be further divided into stratum radiatum (proximal segment of the apical dendritic tree), stratum lacunosum (distal segment of the apical dendritic tree) and stratum moleculare (apical dendrites of pyramidal cells). The deeper molecular layer contains the alveus and stratum oriens (Figure 2.2 **c**). Together, the stratum radiatum, lacunosum and moleculare (SRLM) are often referred to as the "dark band" in MRI due to their dark contrast on T2w scans (J. L. Winterburn et al. 2013; Kulaga-Yoskovitz et al. 2015).

The hippocampus is not a unitary structure; rather it is composed of a set of subregions often referred to as the subfields. There is no consensus concerning which "subfields" make up the "hippocampal formation", but most authors include the CA, dentate gyrus (DG) and subiculum while some also include the presubiculum, parasubiculum, and entorhinal cortex (EC) (Yushkevich, R. S. C. Amaral, et al. 2015; Giovanni B Frisoni and Clifford R Jack 2015).

2.1.3.1.1 Cornus ammonis The CA of the hippocampus, also called "hippocampal proper", can be subdivided into four regions : CA1, CA2, CA3 and, sometimes, CA4 (Teyler

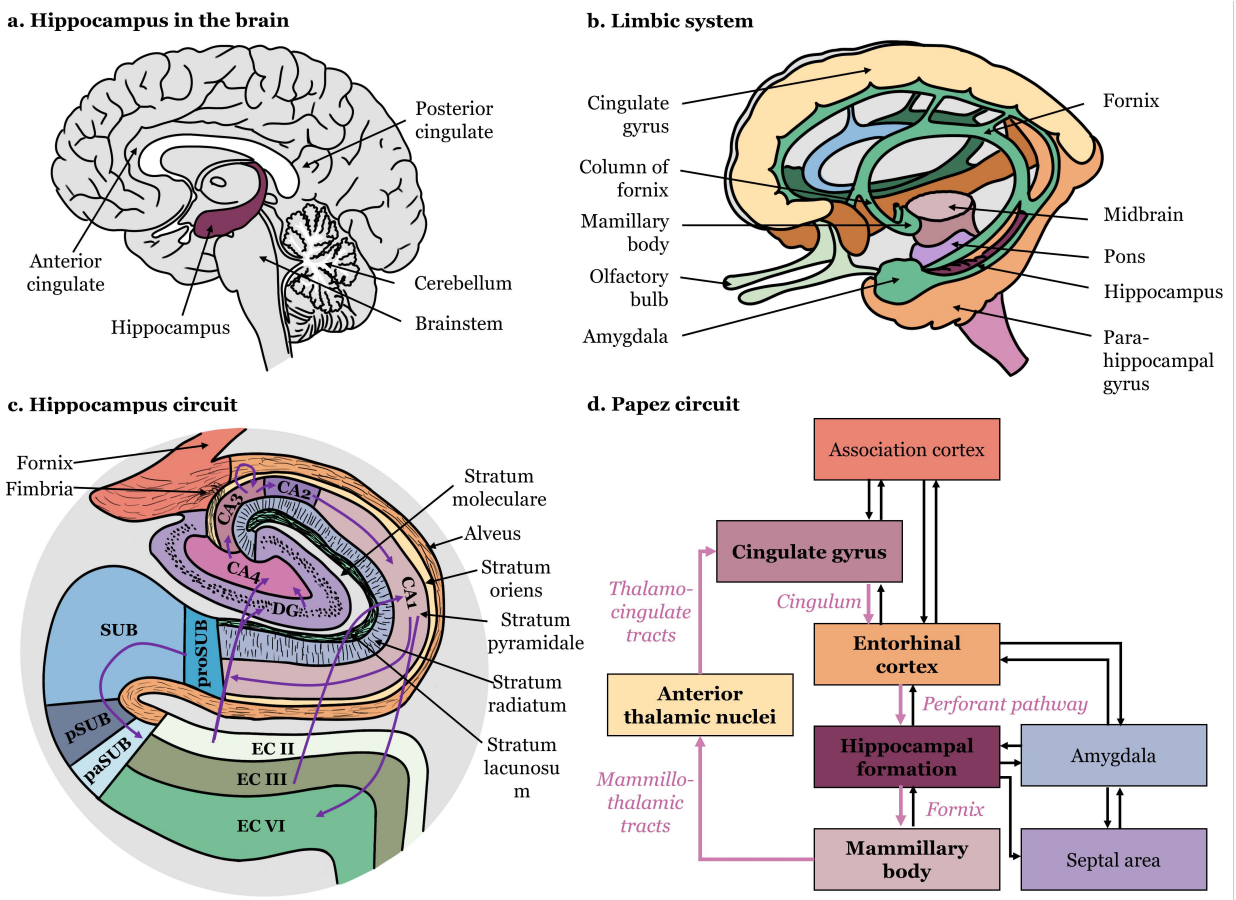

Figure 2.2: **a.** Visualization of the hippocampus in the brain on a sagittal view, **b.** Anatomic organization of the limbic structures, **c.** Representation of the hippocampus structure, with its different layers, subregions and projections, **d.** Simplified representation of the Papez circuit, its main structures (bold font) and projections (pink font).

and Discenna 1984).

CA1 is the largest region of the hippocampus proper, located between the subiculum and the CA2 and separated from the DG by the hippocampal sulcus. About 90% of its neurons are pyramidal cells (glutamatergic projection) while the rest are interneurons. Information reaches CA1 via two pathways: a) the direct pathway coming from axons of the EC layer *III* via the perforant pathway, or b) the indirect pathway from axons originating from layer *II* of the EC via the trisynaptic circuit. In return, pyramidal cells of CA1 project their axons to the subiculum and deep layers of the EC (mostly layer *V*; (D. G. Amaral and M P Witter 1989).

CA2 is a small region located between CA1 and CA3 which receives some input from layer *II* of the EC via the perforant path. CA2 pyramidal neurons can influence on CA1 and also can project to CA3 thus controlling hippocampal excitability. CA2 is also innervated by the hypothalamic supramammillary nucleus (Haglund, Swanson, and Köhler 1984) which has been shown to be active during social novelty exposure therefore contributing to social memory encoding (Robert et al. 2021).

CA3 subfield receives inputs from mossy fibers from the granule cells of the DG and from the EC via the perforant path. Most of the CA3 cells are pyramidal neurons which project mainly to the CA1 pyramidal neurons via the Schaffer collateral pathway. The CA3 pyramidal cells also have recurrent connections with other CA3 pyramidal cells or interneurons forming a recurrent network (Le Duigou et al. 2014). CA3 is considered to be the "pacemaker" of the hippocampus since it generates most of the synchronous bursting activity producing the hippocampal theta rhythm (Wittner and Richard Miles 2007).

CA4 is also called the hilius or hilar region and is sometimes considered as part of the DG since the CA4 pyramidal cells have a different morphology than other CA pyramidal cells. CA4 contains mossy fibers principally receiving inputs from granule cells in the DG and to a lesser extent from CA3 pyramidal cells. Importantly, more functions have been attributed to each subfield, and the functions described above for each subfield have been chosen as examples.

2.1.3.1.2 Dentate gyrus The DG is one of the brain regions where adult neurogenesis occurs in most mammalian species (Boldrini et al. 2018) except cetaceans (Patzke et al. 2015). However, the extent of adult neurogenesis in humans is still a topic of debate (Boldrini et al. 2018; Sorrells et al. 2018). The DG has been attributed with various mnemonic functions, such as pattern separation (Treves and Rolls 1994; Neunuebel and Knierim 2014; Madar, Ewell, and M. V. Jones 2019), novelty detection (Hunsaker, Rosenberg, and Kesner 2008), binding of information to spatial contexts, and working memory (Sasaki et al. 2018). The DG

is a structure of the hippocampal formation and consists of three distinct layers: an outer molecular layer, a middle granular layer, and an inner polymorphic layer. The principal cell type of the DG is the granule cell, mainly found in the granular layer. They receive information from the EC layer *II* via the perforant pathway and send information to the pyramidal cells of CA3 via mossy fibers.

2.1.3.1.3 Subiculum The subiculum, which lies between the hippocampus proper and other cortices, as well as several subcortical structures, plays a crucial role in memory consolidation (Ledergerber and Moser 2017). Studies using human brain imaging techniques such as fMRI have revealed heightened subicular activity during the recollection of the learning episode (Eldridge et al. 2005). The subicular complex includes the prosubiculum (ProS), subiculum, presubiculum (PSub), and parasubiculum (PaS) (Ding 2013). Despite its importance, this structure has been historically under-investigated (O'Mara et al. 2001) and considered to only be the hippocampal major output. Indeed, the subicular complex is the main output of the hippocampus, receiving mainly inputs from CA1 and EC layer *III*. It then projects to a variety of structures including the nucleus accumbens, septal nuclei, prefrontal cortex, lateral hypothalamus, mammillary nuclei, EC and amygdala.

2.1.3.1.4 White matter hippocampal subregions The hippocampal GM regions are surrounded by WM regions which are essential for the connection of the hippocampus to the rest of the brain. Those structures are not always included in neuroimaging analyses of the hippocampus despite their importance in limbic functions (Rajmohan and Mohandas 2007). The hippocampal WM subregions include three WM bundles, namely: alveus, fimbria and fornix and a nucleus called mammillary bodies (MB).

The alveus is a structure containing the axonal fibers from the DG and from the pyramidal neurons of CA3, CA2, CA1 and subiculum. Axons from the alveus then project to the fimbria which is a major tract for afferent and efferent fibers of the hippocampal formation. The fimbria covers the temporal parts of the hippocampus and projects into each crux of the

fornix. The bundles of fibers then merge in the midline of the brain to form the body of the fornix. The body then separates into the posterior and anterior fibers. The posterior fibers (or postcommissural fornix), derived from CA3, continue through the hypothalamus to the MB which then act as a relay between three main structures : the hippocampus, the thalamus and the tegmental nuclei (Peterson, Reddy, and Mayes 2022). The anterior fibers (or precommissural fornix), derived from the subiculum, project to the septal nuclei and nucleus accumbens of each hemisphere.

2.1.3.2 Hippocampal connectivity

2.1.3.2.1 Trisynaptic circuit The trisynaptic circuit was described by Santiago Ramon y Cajal (Ramón y Cajal 1899). It outlines a neural system in the hippocampus which involves three main regions classified according to their cell type (Figure 2.2 **c**). The first projection is between the EC layer *II* to the granule cells of the DG, via the perforant path. The DG then projects on the CA3 pyramidal cells via mossy cell fibers. CA3 then projects to CA1 pyramidal cells via the Schaffer collaterals. Together, the DG, CA3 and CA1 form the trisynaptic pathway. Finally, CA1 projects to various structures including the subiculum, the EC layer *VI* (D. G. Amaral 1993).

2.1.3.2.2 Papez circuit In 1937, James Papez described a neural pathway including structures from the limbic system implicated in the control of emotion (Papez 1937). The limbic system includes several brain structures such as the amygdala, thalamus, hypothalamic nuclei, cingulate gyrus and the corpus callosum (Figure 2.2 **d**). The Papez circuit projects from the hippocampal formation (subiculum) to the MB, via the postcommissural fornix. A mammillary tract facilitates communication between the MB and the anterior thalamic nuclei, which in turn is connected to the cingulate cortex, via the thalamocortical nuclei. Finally, a projection from the cingulate cortex connects to the EC, subiculum and hippocampus, forming a neuronal loop of information flow.

2.1.3.2.3 Antero-posterior axis connectivity Multiple sources of evidence have shown that the hippocampus is connected to other structures in the brain through an antero-posterior axis. The anterior hippocampus (aHPC) and the posterior hippocampus (pHPC) are often separated by the coronal plane containing the uncal apex. Alternative separations along the antero-posterior axis are dividing the hippocampus as three parts called "head", "body" and "tail", each including about a third of the distance along the long axis of the hippocampus. The aHPC is reciprocally connected to the amygdala (Duvernoy 2005; C. D. Smith et al. 2009), ventromedial prefrontal cortex, insula and nucleus accumbens demonstrating its involvement in emotion and motivation regulation processes (Murty et al. 2010). Most of the DG has been shown to be in the pHPC (N V Malykhin et al. 2010) suggesting that most hippocampal neurogenesis takes place in the pHPC. Further, place cells which are cells specialized in spatial memory and navigation have been shown to principally be in the pHPC (Woollett and Maguire 2011). Consequently, many have proposed that the pHPC is a key structure for spatial processing.

2.2 Physiological aging

2.2.1 Effect on neurophysiology

2.2.1.1 Macrostructural modification

2.2.1.1.1 Grey matter GM volume decreases over the course of the adult lifetime, although the rate at which this occurs in different brain regions vary (Hedman et al. 2012). Generally, many studies have observed a "last-in, first-out" pattern, which refers to late developing areas such as the prefrontal cortex being the last to mature and the first to show age-related deterioration, while early maturing regions like the visual and auditory cortex are less susceptible to GM atrophy (Tamnes et al. 2013; Bethlehem et al. 2022). One notable exception to the typical pattern of late-maturing areas being most affected by atrophy in

aging is the medial temporal lobe, which includes the hippocampus and amygdala. While these areas demonstrate late development, they are specifically vulnerable to atrophy in older age (Sowell et al. 2003).

In terms of specific GM measures, previous research has shown that the SA and CT are genetically independent of each other (Panizzon et al. 2009; Hofer et al. 2020), highlighting that they are complementary in describing cortical morphology. In general, significant reductions in SA, CT, and volume have been reported across most of the cortex over time, with the greatest change occurring in volume, followed by thickness, and lower variation in SA (Storsve et al. 2014). In addition to the global volume decrease throughout the cortex, there is evidence of accelerated volume change with age particularly in the entorhinal cortex (Fjell, Westlye, et al. 2014).

Importantly, the border between GM and WM can become less distinct with age on some magnetic resonance (MR) image contrasts due to changes in the content of myelin within the cortex and in the superficial WM (Westlye, Walhovd, Anders M Dale, Espeseth, et al. 2009). This can negatively affect the reported measurements of both the thickness and SA of the cortex, since a shift of the GM-WM border into the WM would result in a decrease in SA estimates, while also partially counteracting the age-related reduction in thickness (D H Salat et al. 2009; Natu et al. 2019). In addition, a recent study conducted by our laboratory revealed that although there was a high spatial overlap between intracortical myelin and microstructure measures, we observed distinct age-related trajectories depending on which cortical magnetic resonance imaging markers were selected (Parent et al. 2023). This finding underscores the importance of choosing the appropriate metrics when conducting studies on cortical changes over time.

2.2.1.1.2 White matter Cross-sectional and longitudinal studies suggest that WM volume follows a inverted-U shaped pattern across the adult lifespan, with increases of myelin up to around age 50 and accelerated decline thereafter (Westlye, Walhovd, Anders M Dale,

Bjørnerud, et al. 2010).

Most studies on age-related trajectories in human WM have used DTI, which has shown an age-related decreases in water diffusion coherence (lower fractional anisotropy (FA)) and higher magnitude of water diffusion (higher mean diffusivity (MD)) (Cox et al. 2016). DTI measures may be confounded by changes in axonal dispersion, fiber crossing, myelination, or axonal densities (Beaulieu 2002), leading to the development of the neurite orientation dispersion and density imaging (NODDI) model (H. Zhang et al. 2012). NODDI appears to be more sensitive to age-related variation than conventional DTI measures (Kodiweera et al. 2016) and has been used to demonstrate that axonal packing decreases with age and that nonlinear age-related models better approximate data for most tracts (Cox et al. 2016). Multi-parameter mapping (MPM) is a qMRI methodology that can estimate magnetization transfer and relaxation rates R1 and R2, which provide sensitivity to local myelination and/or iron deposition (Weiskopf et al. 2013). Metrics derived from MPM have successfully captured significant demyelination in WM with age, particularly in later life (Callaghan et al. 2014; Slater et al. 2019).

2.2.1.1.3 Hippocampus The hippocampus has been widely studied in the context of ageing given its associations with many cognitive functions susceptible to age-related decline (Fjell, Walhovd, Fennema-Notestine, et al. 2009). However, inconsistent results have been observed regarding the volume of which hippocampal subfield is the most affected in aging.

To study the hippocampus *in vivo* using MRI, researchers have used various anatomical definitions of the subfields (R. S. C. Amaral et al. 2018; Iglesias, Augustinack, et al. 2015; Yushkevich, J. B. Pluta, et al. 2015; Olsen et al. 2019; J. L. Winterburn et al. 2013), as well as different image segmentation protocols (La Joie, Fouquet, et al. 2010; Yushkevich, Hongzhi Wang, et al. 2010; Pipitone et al. 2014). Initial volumetric studies of the hippocampus were conducted using manual delineation. A previous study (S G Mueller et al. 2007) found a linear volumetric decrease in CA1 when comparing younger to older adults, and

in a subsequent study that included more individuals, they also found a significant volume decline in CA3/DG (Susanne G Mueller and Weiner 2009). Further studies have shown a linear relationship of the CA1/2 volume with age (Shing et al. 2011; Naftali Raz, Daugherty, et al. 2015) and a decrease in the EC volume and CA1-SRLM width in older adults compared to younger individuals (Geoffrey A Kerchner et al. 2014). A linear effect of age on the subiculum volume was observed (La Joie, Fouquet, et al. 2010), with a relatively preserved CA1 and CA2/3/4/DG volumes when considering changes in a group of individuals between 19 and 68 years old. In a follow-up study, a linear decrease of the subiculum volume, a nonlinear decrease in CA1 volume around the age of 50, and no significant changes in the other subfields were observed (Flores, La Joie, Landeau, et al. 2015).

The results highlight the need to consider methodological guidelines (including subfield definitions, segmentation techniques, image types, age range of subjects, and age modeling) to address the discrepancies in previous studies. A thorough understanding of how each of these experimental design choices affects the hippocampus' age-related changes is essential for gaining insight into the structure's typical development and for effectively investigating hippocampal disorders.

2.2.1.2 Microstructure

2.2.1.2.1 Cellular The aging brain undergoes a series of cellular alterations that can contribute to age-related cognitive decline and neurodegenerative diseases. These alterations include changes in neuronal morphology and function, as well as changes in glial cell numbers and function.

One of the most prominent cellular-level alteration is a loss of neurons (Edler et al. 2020), particularly in regions of the brain important for memory and higher-order cognitive processes. Studies have shown that aging is associated with a decline in the number of synapses and dendritic spines, which are crucial for neural communication and plasticity (Dickstein et al. 2013; Petralia, Mattson, and Yao 2014). Further, aging is associated with alterations in

neuronal gene expression, including increases in the expression of genes involved in oxidative stress and inflammation, and reductions of the cellular metabolism genes (Bishop, T. Lu, and Yankner 2010).

In addition to changes in neuronal structure and function, aging is also associated with alterations in the number and function of glial cells. Astrocytes and microglia, play important roles in supporting neuronal function and maintaining brain homeostasis (Kono, Ikegaya, and Koyama 2021). Advanced age has been associated with a decline in the number of astrocytes (Jiang and Cadenas 2014) and microglia (Peters, Josephson, and Vincent 1991; Hefendehl et al. 2014), as well as changes in their morphology and function. Other cellular alterations seen in the aging brain include changes in mitochondrial function (Grimm and Eckert 2017), and accumulation of misfolded proteins such as β-amyloid peptide (Aβ) and hyperphosphorylated microtubule associated protein tau (ptau), which are associated with AD (Basaiawmoit and Rattan 2010; Soto 2003).

2.2.1.2.2 Iron Iron is an essential nutrient that plays a vital role in several biological processes, including oxygen transport (Thirupathi and Chang 2019) and DNA synthesis (Puig et al. 2017). In the brain, iron is required for neurotransmitter synthesis (Youdim and A. R. Green 1978), myelin production (Morelli et al. 2012; Todorich et al. 2009), and energy metabolism (S. Zhang et al. 2022). However, excessive accumulation of iron in the brain can lead to neurodegeneration (Núñez et al. 2012) and cognitive decline (Howard et al. 2022; Ayton et al. 2020).

Under normal conditions, oligodendrocytes are the most common cell type containing iron in the brain (James R Connor and Menzies 1996; Todorich et al. 2009). However, neurons, microglia, and oligodendrocytes all express ferritin indicating that they all have the capacity to store iron (J R Connor, Boeshore, et al. 1994; Reinert et al. 2019). Ferritin is a storage protein enclosing large amounts of iron in a soluble, non-toxic form (Munro and Linder 1978). A large amount of iron can also be sequestered in neuromelanin granules

in dopaminergic neurons of the substantia nigra and noradrenergic neurons of the locus coeruleus (Zecca et al. 2001; Double et al. 2003).

Studies have shown that the concentration of iron in the brain increases with age, and this increase is particularly pronounced in certain regions of the brain such as the caudate nucleus, putamen, red nucleus, substantia nigra, and dentate nucleus (Y. Li et al. 2020; Salami et al. 2021). Decreases in brain iron mobility in AD, consistent with the hypothesis that iron homeostasis is disrupted in the aging brain, have been reported (J R Connor, Snyder, et al. 1992). For example, there is specific evidence that iron and ferritin levels were higher in AD but transferrin levels were lower in the GM of the motor cortex. Taken together these findings suggest diminished iron mobility in this brain region which might increase potential iron-induced oxidative damages (J R Connor, Snyder, et al. 1992).

2.2.1.2.3 Myelin The process of myelination begins during fetal development (Jakovcevski et al. 2009) and continues throughout childhood and adolescence, with significant myelination occurring in the first two decades of life (Arain et al. 2013). Studies have shown that there is a gradual decline in myelin integrity (reduction of myelin sheaths thickness and impairment of its function) with age, particularly in the frontal lobes (Callaghan et al. 2014), which are involved in higher-order cognitive functions such as decision making, problem solving, and attention. Multiple hypotheses exist regarding retrogenesis, the process by which degenerative mechanisms reverse the order of acquisition in normal development. According to the "gain-predicts-loss" hypothesis, there is a mirror-symmetric relationship between development and aging in terms of the rate of change: any gains achieved before reaching the peak will be followed by corresponding losses after reaching the peak (Yeatman, Wandell, and Mezer 2014).

One of the key myelin-related changes that occurs in aging is a reduction in the number and size of oligodendrocytes, the cells that produce and maintain myelin sheaths (Dimovasili et al. 2023; F. Wang et al. 2020). This reduction in oligodendrocyte numbers and activity

is thought to contribute to age-related declines in cognitive function (Bowley et al. 2010) and increased susceptibility to neurodegenerative diseases such as AD (Z. Cai and Xiao 2016; Butt, De La Rocha, and Rivera 2019). Another myelin-related change that occurs in aging is an increase in the expression of inflammatory markers and oxidative stress, which can damage myelin and compromise its ability to function properly (Domingues et al. 2016; Perry, Nicoll, and C. Holmes 2010).

2.2.2 Cognitive variation during aging

All the previously described brain alteration processes have downstream effects on the cognition of the elderly.

2.2.2.1 Memory

While many older adults feel that their memory performance is deteriorating as they age, objective assessments of memory reveal a more nuanced picture. Subjective memory complaints are often correlated with mood states rather than objective memory performance (Yates, Clare, Woods, and MRC CFAS 2017; Yates, Clare, Woods, F. E. Matthews, et al. 2015). Inter-individual differences in age-related memory trajectories and the existence of older adults who show little evidence of decline have led researchers to propose the concept of "reserve" to explain how some individuals are better able to cope with brain and cognitive changes as they age. Brain reserve refers to individual differences in the brain itself (Stern 2009), while cognitive reserve refers to individual differences in how people process tasks (Stern 2002).

The study of age-related cognitive decline and pathology, such as AD, has been a major focus of research. However, some researchers argue that the distinction between normal and pathological aging is insufficient to describe the heterogeneity found among healthy older adults, and instead suggest distinguishing between "usual" and "successful" aging (Rowe and Kahn 1987).

The available evidence suggests that total GM is positively associated with global cognition, abstract reasoning, and processing speed, but not with memory (Tisserand et al. 2004; Staff et al. 2006; Kaup et al. 2011). Older adults with thicker cortex in several regions demonstrate better "fluid" cognitive ability (Fjell, Walhovd, Reinvang, et al. 2006). In contrast, global WM is unrelated with global cognition, but positively associated with abstract reasoning and processing speed, and unassociated with memory (Tisserand et al. 2004; Staff et al. 2006).

Executive function is the domain most often studied in relationship to the anatomy and function of the frontal lobe. Studies generally support a positive relationship between the size of frontal lobe regions and executive function (Hänninen et al. 1997; Zimmerman et al. 2006), although some studies found no relationship or an inverse relationship (Tullberg et al. 2004; Van Petten et al. 2004).

There is relatively strong evidence that larger hippocampal-formation structure predicts better memory performance (Tisserand et al. 2004; Hackert et al. 2002; J. T. O'Brien et al. 1997). Compared to the hippocampal formation, the relationships between cognition and other temporal lobe measurements were less frequently investigated (Golomb et al. 1996; Lupien et al. 1998; Toledo-Morrell et al. 2000) and showed weaker associations with memory performance.

Associations between parietal, occipital, subcortical, and cerebellar brain measures and cognition have been rarely studied among older adults. Limited findings included a positive relationship between amygdala and putamen volume and memory (Zimmerman et al. 2006), and some papers found that larger cerebellar volume relates to better memory (Paradiso et al. 1997; Won et al. 2022).

2.2.2.2 Excecutive function

Executive functions are cognitive processes that include planning, initiation, shifting, monitoring, and inhibition of behaviours which are crucial for daily tasks, problem solving, and

planning (A. Diamond 2013). The development and aging of executive functions show variable profiles, with development from childhood into early adulthood (V. A. Anderson et al. 2001; Garon, Bryson, and I. M. Smith 2008; Best, P. H. Miller, and L. L. Jones 2009) and a decline into older age (Ferguson, Brunsdon, and Bradford 2021). The development of each executive function component occurs at different rates, with cognitive flexibility shown to mature by age 12 (Cragg and Nation 2008; P. Anderson 2002) while working memory, inhibition, and planning continue to develop into young adulthood (Bedard et al. 2002; B. R. Williams et al. 1999). Cognitive performance peaks in young adulthood with declines in various aspects of cognition emerging as early as 20 or 30 years old (Zelazo et al. 2014).

Neuroimaging studies have also revealed changes in the structure of brain regions that underlie executive functions in middle-aged and older adults. In a meta-analysis, it was reported that among healthy adults, having a larger prefrontal cortex, particularly in its lateral section, is linked with superior performance on executive function tests (Yuan and Naftali Raz 2014). Four studies reported that older adults with lower baseline hippocampal volume showed steeper declines in executive function (Hohman et al. 2017; Leong et al. 2017). One study found that 2-year changes in CT of the right occipital cortex were negatively correlated with simultaneous performance changes in executive function tasks (Möller et al. 2016). A negative correlation between changes in MD in the inferior and superior longitudinal fasciculi and performance changes in a version of the Stroop task over a period of three years suggested that WM microstructure is related to decline in inhibitory control, independently of participant age (Moon et al. 2017).

2.2.2.3 Processing speed

Processing speed refers to the ability of an individual to perform cognitive tasks quickly and efficiently, including tasks that involve attention, memory, and problem-solving. Two studies found that having a more intact hippocampal GM at baseline, indicated by lower MD, and experiencing less decline in whole brain GM volume were associated with reduced declines

in processing speed over three years (Anblagan et al. 2018; Ritchie et al. 2015) . Positive correlated changes over two years between indices of WM microstructure (i.e., decreases in FA and increases in MD) of the corticospinal tract and processing speed suggested that individuals with less intact WM microstructure in the corticospinal tract exhibit steeper declines in processing speed (Köhncke et al. 2016). Further, the relationship between processing speed and white matter hyperintensities (WMH) is well described (George Bartzokis, David Sultzer, et al. 2004; Lampe et al. 2019; Roseborough et al. 2023).

2.3 Pathological aging - Alzheimer's disease spectrum

AD is the leading cause of dementia worldwide, affecting over 44 million people globally, including more than 600,000 in Canada (2022 Alzheimer Society of Canada). It is expected that one million Canadians will have dementia by 2030 due to the aging population and limited effectiveness of available treatments.

2.3.1 Neuropathology

AD pathology demonstrates two main hallmarks: the accumulation of Aβ plaques and neurofibrillary tangles (NFT) composed of ptau proteins (Braak and E. Braak 1991b). Both pathologies start to accumulate during the preclinical stage, years before symptoms appear (Bateman et al. 2012).

2.3.1.1 Amyloid beta

The main component of senile plaques, Aβ peptide, is derived from the proteolytic cleavage of a larger glycoprotein named amyloid precursor protein (APP). APP is an integral membrane protein expressed in many tissues, particularly in the synapses of neurons, and plays a central role in AD pathogenesis (R. J. O'Brien and Wong 2011). APP has been implicated as a regulator of synaptic formation and repair, anterograde neuronal transport,

and iron export. Human APP can be processed via two alternative pathways: amyloidogenic and non-amyloidogenic (G.-F. Chen et al. 2017). APP is first cleaved by α-secretase (non-amyloidogenic pathway) or β-secretase (amyloidogenic pathway). The amyloidogenic processing of APP thus involves sequential cleavages by β- and γ-secretases at the N and C termini of Aβ. The fragment of APP generated by β-secretase cleavage can be internalized and further processed by γ-secretase at multiple sites to produce cleavage fragments of different sizes, including the main final Aβ forms, the 40-amino acid form of Aβ (Aβ40) and the 42-amino acid form of Aβ (Aβ42) (H. Zheng and Koo 2011).

Over time, Aβ monomers can aggregate into oligomers, then into insoluble amyloid fibrils which eventually form extracellular amyloid plaques. Amyloid fibrils are larger and insoluble, while amyloid oligomers are soluble and may spread throughout the brain. The "amyloid cascade hypothesis" proposes that Aβ aggregation into plaques leads to neurotoxicity and dementia. Aβ interacts with transition metals such as copper, zinc, and iron (Lovell et al. 1998; Bayer et al. 2003; Maynard et al. 2002).

The binding of Aβ to various receptors can lead to neuronal toxicity. Aβ oligomers can induce mitochondrial dysfunction and oxidative stress in AD neurons, resulting in a massive calcium influx and toxicity in neurons (Reiss et al. 2018). However, the production of Aβ is normally counterbalanced by various processes such as proteolytic degradation, cell-mediated clearance, active transport out of the brain, and deposition into insoluble aggregates. Aβ released into the extracellular space can be transported between different compartments and can also be cleared by chaperone proteins such as apolipoprotein E (Apo-E). The transport of Aβ across the blood-brain barrier (BBB) is critical in regulating brain Aβ levels (Yoon and AhnJo 2012).

Histopathological studies show that Aβ deposition in the brain follows a stereotypical pattern, starting in the transentorhinal cortex, spreading first into the entorhinal cortex and hippocampus. Eventually Aβ spreads to other neocortical regions with first the association cortices in the frontal and parietal lobes before invading the rest of the cortex in later stages

(Braak and E. Braak 1991b) (Figure 2.3). Abnormal Aβ levels in the CSF can be detected before becoming abnormal on Aβ-PET scans (Bateman et al. 2012; Palmqvist et al. 2016). As the disease progresses, Aβ level in the CSF decreases as Aβ becomes sequestered into amyloid plaques in the brain.

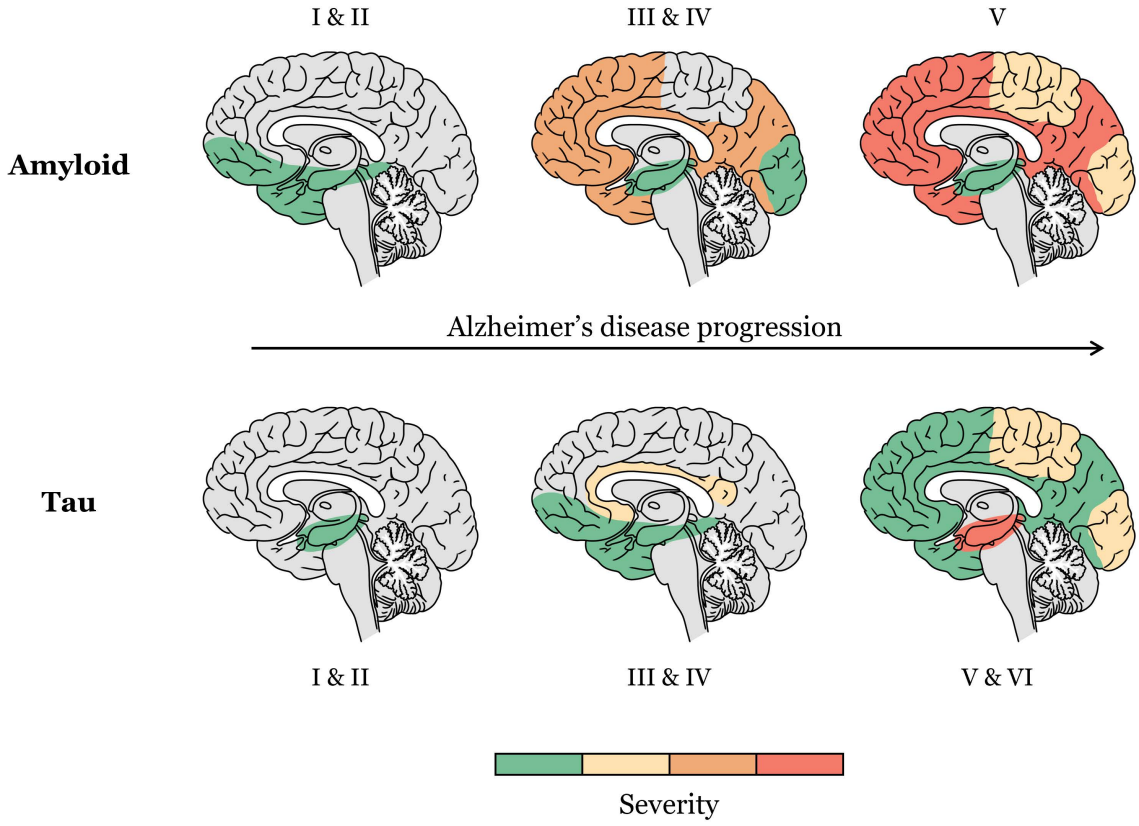

Figure 2.3: Schematic representation of the Braak and Braak amyloid and tau stages during the progression of AD. Color codes for severity of the amyloid and tau protein accumulation (green : less severe, red : most severe). *Inspired by (Swarbrick et al. 2019)*

2.3.1.2 Tau

The tau protein has been implicated in various neurodegenerative diseases such as AD, frontotemporal dementia, Parkinson's disease, and progressive supranuclear palsy. Human tau is a microtubule-associated protein that is primarily present in the axons of the CNS. Tau is hydrophilic and intrinsically disordered, meaning that it is highly flexible and mobile, with a low content of secondary structures (E.-M. Mandelkow and E. Mandelkow 2012). As

originally described, tau protein is essential for microtubule assembly and stability (Weingarten et al. 1975). Microtubules are protein polymers of the cytoskeleton that play a role in cell shape, mitosis, and intracellular transport (Lasser, Tiber, and Lowery 2018). Tau's interactions with microtubules can be direct, such as binding, stabilization, and promotion of microtubule assembly, or indirect, affecting other proteins that may or may not interact with microtubules by themselves.

In normal conditions, tau undergoes phosphorylation which enables it to bind to tubulin along the axons, and helps in stabilizing and assembling microtubules (W. Noble et al. 2013). However in neurodegenerative conditions, tau protein gets excessively phosphorylated, which leads to its detachment from microtubules. When hyperphosphorylated and detached from microtubules, tau accumulates in neurites and neuronal cell bodies. It then forms insoluble intracellular aggregates or inclusion bodies, such as NFT, which are one of the major pathological features of AD (Neddens et al. 2018).

Pathological tau can be released to the extracellular space due to various mechanisms, including cell death, neuronal activity, and microvesicle (Clavaguera et al. 2009). Once released, pathological tau must enter recipient cells via endocytosis, where it can be degraded, re-secreted, or where it can mediate misfolding of wild-type tau (Frost, Jacks, and M. I. Diamond 2009). Recipient cells preferentially take up short, low-molecular-weight tau fibrils. Tau aggregates can transfer between connected cells and induce misfolding, leading to tauopathy propagation across different brain regions in a prion-like fashion (affected cells propagate the tauopathy to connected cells) (Dujardin and Hyman 2019; B. B. Holmes and M. I. Diamond 2014). In AD individuals, the formation of NFT is initially observed in the transentorhinal cortex (part of the MTL, see Figure 2.3) and then progresses to the anterior hippocampus, followed by adjacent limbic and temporal cortex, association isocortex, and ultimately to the primary sensory cortex (Heiko Braak and Del Tredici 2015; Cho et al. 2016).

2.3.1.3 Brain atrophy

Hippocampal atrophy is a well-established and validated biomarker of AD progression, and its volume has shown to be related to the different pathological stages of AD progression. Multiple studies have reported that the hippocampal volume in AD patients is 15% to 40% smaller than in healthy controls (HC). Hippocampal volume is involved early and progressively, correlating with Braak staging and neuronal counts both in dementia and aging (Bobinski et al. 2000; C R Jack Jr, Dickson, et al. 2002). The annual hippocampal atrophy rates were reported to be three time faster in AD patients than in HC (Barnes et al. 2009). Longitudinal measures of change in hippocampal volume in AD patients correlated with clinical decline (C R Jack Jr, Petersen, Y. Xu, P. C. O'Brien, G E Smith, Ivnik, Boeve, et al. 2000). However, hippocampal atrophy is not specific to AD (Sankar et al. 2017) and may lack sensitivity and specificity at the mild cognitive impairment (MCI) stage, as it can be present in non-AD forms of dementia (Laakso, Partanen, Riekkinen, et al. 1996; Elder et al. 2017). Studies assessing hippocampal subfields showed that they are differentially affected by AD pathology compared to controls, with patients showing a clear involvement of the head of the hippocampus, especially in CA1 (Chételat et al. 2008; Iglesias, Augustinack, et al. 2015; La Joie, Perrotin, et al. 2013).

Cortical atrophy in AD initially affects the MTL, specifically the EC and hippocampus, before spreading to the rest of the cortex in a temporal-parietal-frontal trajectory (Giovanni B Frisoni, Prestia, et al. 2009; Lerch, Jens C Pruessner, et al. 2005). Motor areas are typically unaffected until late stages of the disease. The pattern of atrophy is closely linked with the severity of the disease and the emergence of clinical symptoms. Memory deficits appear when atrophy is initially limited to the MTL, while executive functions, language, perception, memory, and awareness decline at later stages when neocortical deficits are present (Lerch, Jens C Pruessner, et al. 2005; Apostolova et al. 2008). The pattern of atrophy in AD is different from that observed in normal aging, with age-related atrophy predominantly occurring in the sensorimotor and visual cortices and to small frontal areas. The AD-specific

topographic pattern of atrophy represents a well-established MRI 'signature' or 'fingerprint' of typical AD and shows potential clinical validity (Ossenkoppele et al. 2015). However, there are cases that deviate from the 'typical' AD phenotype, and studies increasingly suggest that these cases are associated with distinct MRI phenotypes.

Other subcortical regions demonstrate atrophy in AD progression. For example, amygdala atrophy in AD is associated with global cognitive functioning as well as aberrant motor behaviours (Poulin et al. 2011) and *post-mortem* studies have revealed substantial amygdala neuronal loss (Vereecken, Vogels, and Nieuwenhuys 1994; Scott et al. 1992). *Post-mortem* studies have also revealed that AD pathology can be observed in certain nuclei of the thalamus during the early stages of the disease (Braak and E. Braak 1991a; Xuereb et al. 1991).

2.3.1.4 Genetic risk factors

Genetically, AD is divided into two forms: early-onset familial early onset Alzheimer's disease (EOAD) and late onset Alzheimer's disease (LOAD). EOAD is often caused by rare and highly penetrant mutations in three genes: *APP*, *presenilin 1 (PSEN1)* and *presenilin 2 (PSEN2)*. Conversely, LOAD is caused by numerous genetic risk factors of relatively high frequency but low penetrance and, by environmental and epigenetic factors.

APP is located on chromosome 21 and encodes APP, which is processed by two enzymes, β- and γ-secretase, to produce the Aβ peptide that accumulates in the brains of AD patients. *PSEN1* and *PSEN2* are located on chromosomes 14 and 1, respectively, and encode proteins that form a complex with other proteins to act as a catalytic center for -secretase, one of the enzymes responsible for the production of Aβ. Mutations in these genes can lead to increased production of Aβ and cause EOAD with high penetrance (Bertram et al. 2007).

Apo-E is the main gene which has been investigated for genetic association with AD. The ϵ4 allele of *Apo-E* leads to a dose-dependent increase in AD risk of approximately three-fold for heterozygous ϵ4 carriers and of almost 15 for ϵ4 homozygous as compared to non-carriers. In contrast, the rarer ϵ2 allele appears to exert protective effects or healthier aging when

inherited with the $\epsilon 3$ allele as compared to homozygous $\epsilon 3$ allele carriers (C.-C. Liu et al. 2013).

2.3.2 Neuropsychology

Cognitive impairments in AD develop gradually over many years, starting with memory and progressing to executive function, language, and visuospatial abilities. Dementia is the final stage of the disease and is diagnosed when cognitive deficits impair daily living activities. AD is viewed as a continuum, starting with the preclinical stage, followed by MCI and ending with dementia (Sperling et al. 2011).

2.3.2.1 Subjective cognitive impairment

Subjective cognitive impairment (SCI) refers to self-reported cognitive decline, such as memory problems or difficulties with concentration, that are perceived by an individual but are not detected on standardized cognitive testing (F. Jessen et al. 2014). SCI is often considered a transitional stage between normal cognitive aging and MCI, which is a more objective and measurable decline in cognitive function that affects daily life activities.

2.3.2.2 Mild cognitive impairment

MCI is a condition characterized by cognitive decline that is more than what would be expected for an individual's age and education level but does not significantly affect daily activities. It differs from dementia, which has more severe and widespread cognitive deficits that significantly impact daily function. MCI has been consistently linked to a higher risk of developing dementia, especially AD dementia (Gauthier et al. 2006).

2.3.2.3 Alzheimer's dementia

The early NFT changes in AD pathology occurs in the MTL structures, which are critical for episodic memory function. As a result, the main clinical hallmark of AD pathology is the

deficit in the ability to learn and remember new information. However, amyloid pathology, which likely occurs years prior to the onset of symptoms, is not particularly abundant in the medial temporal lobe but instead in the regions comprising the "default mode network" (Buckner, Andrews-Hanna, and Schacter 2008). Numerous studies have shown that patients with AD are impaired on episodic memory tests due to ineffective consolidation or storage of new information (Delis et al. 1991).

Mildly demented patients with AD often show impairments on language and semantic tests such as object naming, verbal fluency, and semantic categorization (Hodges, D P Salmon, and Butters 1991; Butters et al. 1987; Martin and Fedio 1983). Deficits in executive functions, working memory and visuospatial abilities are often present early in AD progression and can even be present at the MCI stage (Sandra Weintraub, Wicklund, and David P Salmon 2012).

2.3.2.4 Clinical diagnosis

The diagnosis of AD is typically made through a combination of clinical evaluation, cognitive testing, and imaging studies. Indeed, diagnosis of AD can be challenging, and the use of multiple diagnostic methods is often necessary to confirm the diagnosis.

First, when individuals present with memory concerns, doctors take a detailed medical history to assess the onset and progression of symptoms and perform a physical exam to check for any potentially underlying medical conditions which may explain the cognitive deficits. They may administer cognitive tests to evaluate memory, language, attention, and problem-solving skills to determine the extent of cognitive impairment. Mini mental state examination (MMSE) and Montreal cognitive assessment (MoCA) are two routine cognitive screening tests rated on a 30-point scale which have been wildly used to stage individuals on the AD spectrum. While similar, they present some differences (Trzepacz et al. 2015). MMSE is known to have a ceiling effect for normal individuals (scores 24 or higher), which reduces the likelihood to detect predementia stages (Spencer et al. 2013). Further, it has

shown poor sensitivity for distinguishing MCI individuals (Tombaugh and McIntyre 1992). MoCA has been developed to address some limitations of MMSE by including different cognitive categories such as visuospatial, executive, naming, memory, attention, language, abstraction and orientation. MoCA has been shown to be more sensitive than the MMSE for the detection of MCI and mild AD with a score < 25 as optimal cutoff point for a diagnosis of cognitive impairment (Nasreddine et al. 2005).

Blood tests may be done to rule out other conditions that can cause similar symptoms and genetic testing may be done in some cases to evaluate the risk of AD. Imaging assessments such as MRI may be ordered to look for structural changes in the brain that may indicate AD or investigate the potential existence of a lesion that may rule out AD diagnosis. Amyloid PET scans may be used to confirm the presence of amyloid plaques, even though it is not always used in clinics due to the high financial costs.

2.4 Magnetic resonance imaging

Nuclear magnetic resonance (NMR) is a physical principle simultaneously described by two authors (Bloch 1946) and (Purcell, Torrey, and Pound 1946). This physical phenomenon demonstrates that the nuclei of atoms in a static magnetic field resonate when a secondary oscillating magnetic field is applied. A few years later, tumoral tissues were found to have significantly different magnetic properties compared to normal tissue (Damadian 1971), highlighting the huge potential of NMR in biomedical applications. Following these discoveries, Paul Lauterbur developed a method to generate the first 2D and 3D MRI images (Lauterbur 1973). In 1977, Peter Mansfield invented the technique of echo-planar imaging (EPI), a data acquisition technology which made it possible to acquire images more quickly alongside the development of two dimensional MR images reconstruction (Mansfield and Maudsley 1977), endorsing further the potential of MRI in clinical settings. At present, MRI is a standard medical imaging technique, having the potential of being non-invasive, being usable in all

regions of the body, demonstrating great tissue contrasts and being very versatile.

2.4.1 Principle of nuclear magnetic resonance

The basic building blocks of matter are atoms, which can be found in solids, liquids, and gases. An atom comprises a positively charged nucleus surrounded by negatively charged electrons. The nucleus contains one or more protons (positively charged particles) and one or more neutrons (uncharged particles). The most abundant element in the body is hydrogen and is found in many molecules, including water. In fact, the brain is composed of approximately 80% water. Water molecules are composed of two hydrogen atoms (H^+) and one oxygen atom. Each hydrogen atom contains a single proton in its nucleus (Figure 2.4.1 **a**). Protons have quantum properties (McRobbie et al. 2017), referred to as nuclear spin, which causes them to act like tiny rotating magnets, with a magnetic moment associated with their rotation (Figure 2.4.1 **b**). This magnetic moment interacts with an external magnetic field, causing the proton to precess around the direction of the magnetic field with a characteristic frequency known as the Larmor frequency ω_0, in $rad.s^{-1}$). The frequency of precession of a H^+ is directly proportional to the strength of the external magnetic field (B_0, measured in T) and the gyromagnetic ratio (γ, measured in $rad.s^{-1}.T^{-1}$) of the H^+. This relationship is expressed mathematically as eq. 2.1.

$$\omega_0 = B_0.\gamma \tag{2.1}$$

In the context of magnetic resonance, the behavior of spinning charged particles, such as electrons or protons, is described by quantum mechanics. Under normal conditions, the magnetic moments of the particles are randomly oriented, and the sum of the magnetic moments generated by a large number of spins (i.e particles that have an intrinsic property of spin) results in a net magnetic moment of zero (Figure 2.4.1 **c**). However, when these particles are placed in a strong magnetic field, the spins align themselves with the external

field. The spins can align and precess around the main axis of the external field, either in the same direction ("parallel", "spin-up"or "low-energy") or in the opposite direction ("anti-parallel", "spin-down" or "high-energy"). A property defined by the Boltzmann equation (2.2) states that there is a small but significant excess of spins in the spin-up state creating a net magnetization M in the same direction of B_0 (Figure 2.4.1 **d**).

$$\frac{N^-}{N^+} = e^{\frac{-E}{kT}} \tag{2.2}$$

Where E is the energy difference between the spin states, k is Boltzmann's constant (1.3805 x 10^{-23} J.Kelvin^{-1}), and T is the temperature in Kelvin.

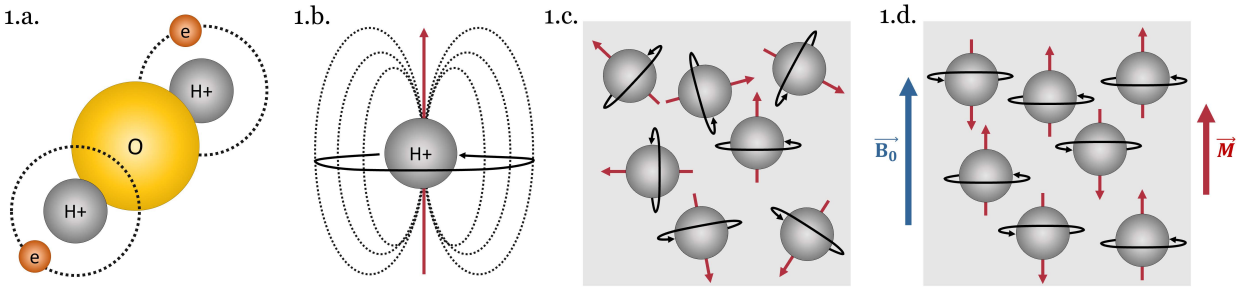

Figure 2.4: **a.** Schematic of a water molecule with one oxygen and two hydrogen atoms. **b.** Simplified figure of the nuclear magnetic moment from the spin of one proton. Seven spins (protons) in two conditions: **c.** In absence of an external magnetic field, the spins are randomly oriented such that the sum of their magnetization in a given voxel is M=0. **d.** In the presence of a static magnetic field B_0, the spins are aligned with B_0, either in the same direction or in the opposite direction. If we sum the magnetic moments of all the spins we always obtain a small excess magnetization in the same direction as B_0, called the net magnetization (M).

2.4.2 Relaxation

At equilibrium, the net magnetization vector M is along the external magnetic field B_0 and is called the equilibrium magnetization M_0. In this configuration, the component of M along the z-axis (M_z or "longitudinal magnetization") is equal to M_0 whereas the component of M in the x-y plane (M_{xy} or "transversal relaxation") is zero (Figure 2.5 **a1**). By applying an additional electromagnetic radiofrequency (RF) pulse at the Larmor frequency perpendicular

to B_0, often called "B_1", the magnetization M is tipped in the transversal plane (Figure 2.5 **a2**). Here, we take the example of an flip angle (α)=90for the explanation and figures such as during the pulse B_1, $M_z = 0$ and $M = M_{xy}$, however note that in reality it can vary between 0and 180. When we remove the pulse B_1, M returns, or relaxes, towards equilibrium along B_0 direction (figure 2.5 **a3-4**). The time constant describing how M_z returns to its equilibrium value is called the spin-lattice (or "longitudinal") relaxation time T1, while the time constant of the return to equilibrium of the transverse magnetization M_{xy}, is called the spin-spin (or "transversal") relaxation time T2.

2.4.2.1 Longitudinal relaxation

The B_1 pulse is a brief electromagnetic pulse that is used to manipulate the spins in a sample. The pulse causes the spins to absorb energy and transition to a higher energy state. After the B_1 pulse, the spins begin to lose energy due to interactions with their surrounding environment (or "lattice"). This loss of energy causes the spins to return to their original energy state, which is known as the thermal equilibrium state. The rate at which this process occurs is measured by the longitudinal relaxation time T1. T1 is defined as the time it takes for the nuclear spin magnetization M_z to recover 63% of its equilibrium value after the B_1 pulse (2.3).

$$M_z = M_0(1 - e^{\frac{-t}{T1}}) \tag{2.3}$$

To ease the visualization and the understanding of the relaxation phenomenon, a rotating frame of reference is used to simplify the complex precession of the spins (Figure 2.5 **b1-5**). In this rotating frame, there is no precession of M around B_0, and the B_1 field is not rotating but appears static. However, note that those mechanisms are more complex when represented in the laboratory frame (Figure 2.5 **d**).

2.4.2.2 Transversal relaxation

At equilibrium, the magnetization in the transverse plane is null (Figure 2.5 **b1**), because all the spins are rotating around the z axis with a random orientation. During the B_1 pulse, all the spins rotate around the z axis at the Larmor frequency in the xy plane, the spins are in "phase coherence", and the transverse magnetization is maximum (Figure 2.5 **b2**). When B_1 stops, in addition to the global rotation around the z axis, two additional mechanisms create the dephasing of the protons.

The spin-spin dephasing is caused by the local magnetic field that each spin creates at the macroscale (Figure 2.4.1 **b**). This phenomenon will cause each spin to experience a slightly different magnetic field causing dephasing of all the spins over time (Figure 2.5 **b**) (Resing and Torrey 1963). This will cause reduction of the transversal magnetization M_{xy} over time (Figure 2.5 **c2**). The time constant which describes the spin-spin relaxation is called T2 such that only 37% of the maximum magnetization M_{xy} remains at time T2 (2.4). Note that T1 and T2 relaxation are occurring simultaneously with the only restriction that T2 is always less than or equal to T1.

$$M_{xy} = M_{xy_0}.e^{\frac{-t}{T2}} \tag{2.4}$$

In addition to the spin-spin relaxation, the spins also undergo a field dephasing effect characterized by the local field inhomogeneities (Truong et al. 2006) such as the main magnetic field inhomogeneity, the differences in magnetic susceptibility among various tissues or materials, chemical shift, and gradients applied for spatial encoding. The combination of T2 relaxation and the local field inhomogeneities relaxation is characterized by the time constant T2*. For instance, in the presence of a linear field variation across a voxel, T2* is shorter than T2 (Figure 2.5), and their relationship can be expressed by the following equation (2.5).

$$\frac{1}{T2*} = \frac{1}{T2} + \frac{1}{T2'} \tag{2.5}$$

where T2' represents the contributions from field heterogeneities across a voxel $\frac{1}{T2'} = \gamma.\Delta.B_{inhom}$.

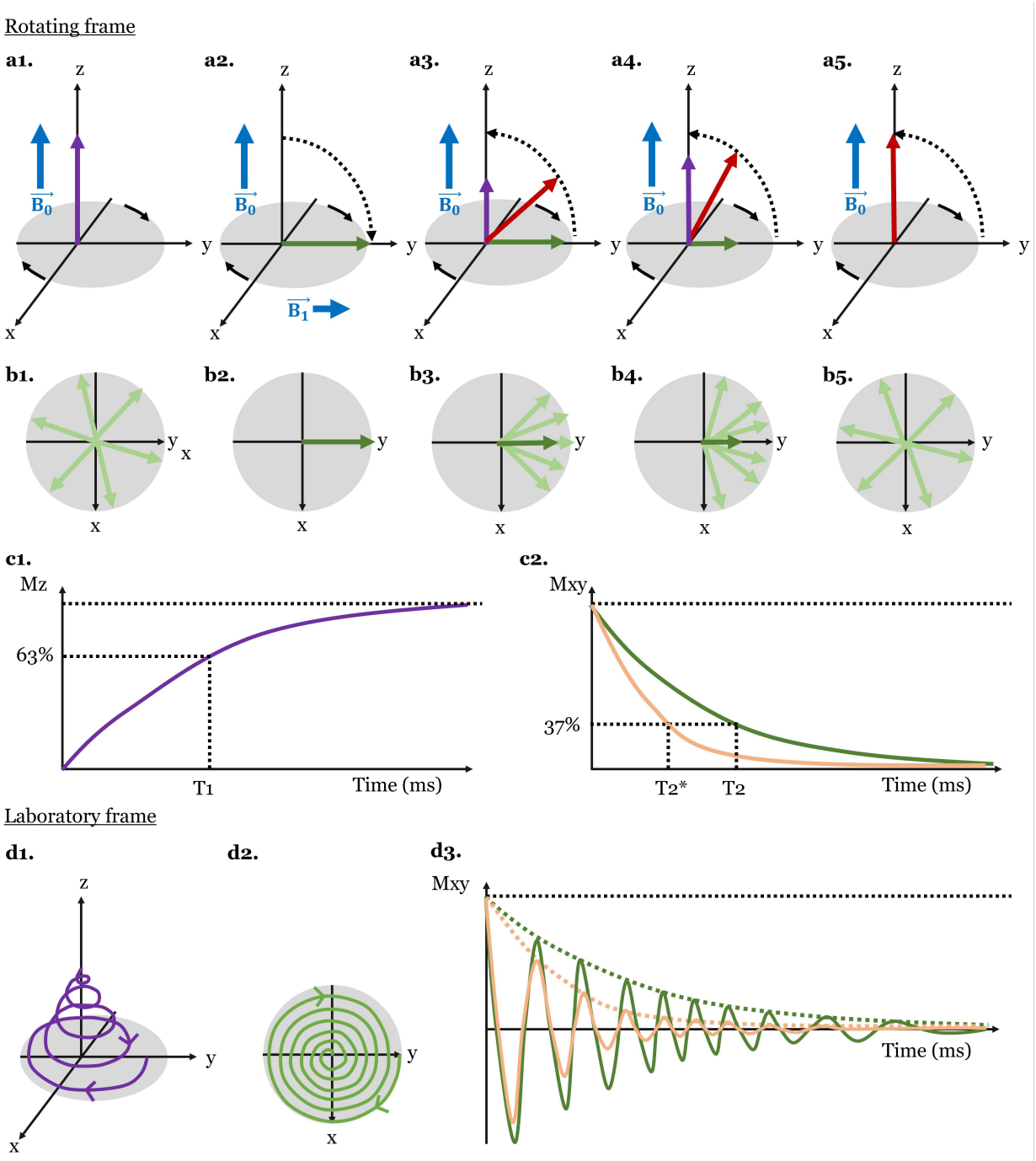

Figure 2.5: **a.** Representation in a rotating frame of the effect of a RF pulse followed by a relaxation. **a1.** Under a strong magnetic field B_0 and at equilibrium, the net magnetization is entirely along the z axis. **a2.** Once we apply an additional RF pulse B1 perpendicular to B_0, we flip the magnetization in the xy plane. **a3-4.** As soon as we stop B_1, the magnetization starts to grow back along the z axis. **a5.** When the system is back at equilibrium, the magnetization is in the same state as in 1.a., before B1 pulse. **b.** Representation in a rotating frame of the phase of the spins. **b1.** Before B_1, the spins are randomly distributed (light green arrows). **b2.** During B_1, the spins are in "phase coherence". **b3-4.** The spins are dephasing over time, inducing a reduction of the magnetization M_{xy} (dark green arrows). **c.** Representation of the **c1.** longitudinal relaxation over time and the T1 time constant and **c2.** transversal relaxation over time and the T2 and T2* time constants. **d.** Representation in the laboratory frame of **d1.** the net magnetization in 3D over time after an RF pulse, **d2.** the transversal relaxation in the xy plane over time after an RF pulse and **d3.** the magnetization M_{xy} over time.

2.4.2.3 Magnetic susceptibility

Magnetic susceptibility (χ) is a physical property of materials that describes their response to an external magnetic field. It is a measure of how easily a material becomes magnetized when subjected to a magnetic field, as well as how much the magnetic field is distorted by the presence of the material. The magnetic susceptibility of a material depends on a number of factors, including its chemical composition and temperature. In general, materials with unpaired electrons, such as iron, cobalt, and nickel, are described as paramagnetic molecules because they have high magnetic susceptibilities and are strongly attracted to magnetic fields. Other materials, such as aluminum and copper, have very low magnetic susceptibilities and are essentially non-magnetic. On the other hand, diamagnetic substances, such as calcium and myelin are weakly repelled by the magnetic field (Table 2.1).

Therefore, by estimating the magnetic susceptibility of the tissue using susceptibility MRI, it is possible to gain insight into the quantity of iron and myelin at the voxel level. Indeed, previous studies have shown that the two main contributors to susceptibility variations in the brain are iron and myelin content (Fukunaga et al. 2010; Stüber et al. 2014).

	Diamagnetic	Paramagnetic
Susceptibility X (ppm)	Negative (~-10)	Positive (>500)
Electrons	No unpaired electrons	At least one unpaired electron
Spin alignment with Bo	Opposite or anti-parallel	Same or parallel
Examples	Myelin, water, fat, calcium, most biological tissues	Iron, ferritin, steel, contrast agents
Effect on magnetic field	Very weakly repealed	Attracted
	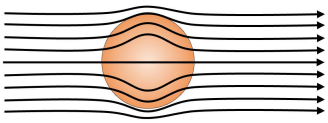	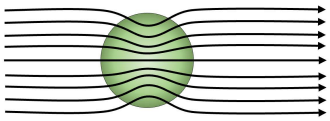

Table 2.1: Summary of the differences between diamagnetic and paramagnetic molecules and their differential effect on the magnetic field.

2.4.3 Weighted magnetic resonance imaging

MRI is a versatile imaging technique that can provide a variety of images, each of them derived from different magnetic properties. Here, "standard" or "conventional" MRI can be used to designate "weighted" scans and are a type of scans often used in the clinical routine to diagnose and monitor neurological diseases. "T1-weighted" and "T2-weighted" are the most common images and this nomenclature is used to indicate the type of MR pulse sequence parameters employed. The idea behind this naming system is to imply which tissue parameter dominates the image contrast (T1, T2, spin-density, diffusion, susceptibility...). The sequence parameters that mostly influence the weighting are the repetition time (repetition time (TR); time between two RF pulses) and the echo time (echo time (TE); time between the RF pulse and the echo).

2.4.3.1 T1-weighted images

T1w scan is a type of MRI scan that uses a specific set of parameters to highlight the differences in the longitudinal relaxation of protons in different tissues. T1w scans are the most common images acquired since they provide a good contrast between tissue types (Mugler and Brookeman 1990). Tissues with short T1 (fast longitudinal recovery) will appear

brighter than those with long T1 since M_z will be higher before the second excitatory pulse (Figure 2.4.3.1 **c**). T1w scans are often called "anatomical" or "structural" images as these image-types provide clear boundaries between different tissues.

In order to achieve that, the contribution of T2 and proton density (PD) needs to be reduced (however, note that in all T1w scans, there is always some contribution of T2 and PD effects). In order to amplify the contribution of the T1 effect, a short TR is used to maximize the differences of longitudinal relaxation between tissues and a short TE is used to minimize T2 differences between tissues (Figure 2.4.3.1 **c**).

2.4.3.2 T2-weighted images

T2w scan is a type of MRI scan that uses a specific set of parameters to highlight the differences in the transversal relaxation of protons in different tissues. In general, T2w scans display dark WM, gray GM and bright fluids. Pathological processes usually increase the water content in tissues therefore most lesions appear as a signal increase on T2w images. Those images are widely used for brain lesion detection such as astrocytomas, glioblastomas, infarction and multiple sclerosis plaques.

To obtain a T2w scan, a long TR is needed to minimize the longitudinal relaxation differences between tissues, and a relatively long TE (not too long to avoid a full decay of transverse magnetization) to maximize the T2 differences between tissues (Figure 2.4.3.1 **d**). These long time parameters are the reason why T2w scans are often longer than the T1w scans.

2.4.4 Quantitative magnetic resonance imaging

While very informative, weighted scan intensity can be sensitive to various neurobiological processes. Indeed, those scans are related to a mixture of physical properties and will also be dependent on protocol settings and hardware parameters such as the magnetic field strength, inhomogeneities of the RF pulses and RF coil sensitivities. However, in qMRI, a parametric map can be obtained by acquiring at least two images of the same tissue location (Figure

2.4.3.1 **e-f**). For example, using two images with differing amounts of T2 weighting but similar scanner parameters otherwise, an exponential decay can be fitted to estimate the tissue parameter T2. In this case, individual pixel values now have a numerical meaning (T2 values in milliseconds, at each location in the brain), rather than representing signal intensity on an arbitrary scale in the case of a weighted scan. Another advantage of qMRI, is how reliable and reproducible it is compared to traditional MRI protocol (Y. Lee et al. 2019).

2.4.4.1 T1 mapping

A T1 map reflects the longitudinal relaxation time constant T1 at each voxel and depends on the microstructural composition of the tissue. It can vary based on (a) the concentration and the properties of macromolecules such as myelin content (Lutti et al. 2014) and axon diameter (Harkins, J. Xu, et al. 2016), (b) the iron content (Vymazal, Righini, et al. 1999) and (c) the proton density (Gelman et al. 2001). Increased myelin and iron content leads to a T1 reduction while increased water content induces a T1 lengthening. Therefore, T1 in WM is shorter than in GM due to the higher myelin concentration and T1 in CSF is long. T1 mapping has been used in the context of different clinical applications. In multiple sclerosis (MS), qMRI techniques can be useful to quantify pathological tissue changes inside macroscopic lesions, in diffuse tissue damage and in normal-appearing tissues. Increased T1 values in normal-appearing brain tissues in MS patients, even at early stages of the disease have been demonstrated (Griffin et al. 2002; Vrenken et al. 2006). Studies have also used T1 mapping to investigate disease-related tissue pathology in Parkinson's disease (Vymazal, Righini, et al. 1999) or even early detection of tumor progression (Lescher et al. 2015).

2.4.4.2 T2 mapping

A T2 map reflects the transverse relaxation time T2 at each voxel assuming a perfect RF pulse without inhomogeneities (Figure 2.4.3.1 **e**). In order to measure T2, a refocusing pulse

is applied to rephase the protons and counteract the effects of the external magnetic field inhomogeneity. In order to sample the transverse relaxation and extract T2 values, multiple 180° pulses are applied to produce multiple echoes free of magnetic field inhomogeneity. Quantitative T2 mapping can be used as a single-component to give insight into the microstructure contained within a single voxel or it can be used to extract various types of information. Increase water leads to T2 increases while increase iron and myelin lead to a decrease of T2 (House et al. 2006). In most brain sites, T2-relaxation values increases with age, interpreted as higher free tissue water (Kumar et al. 2012).

2.4.4.3 T2* mapping

T2* relaxation time is related to the dephasing caused by the molecular interactions (Figure 2.4.1) and the local external magnetic field inhomogeneities (Brown et al. 2014). These inhomogeneities can be attributed to various factors, including the challenge of producing a uniform high-intensity magnetic field across a large volume, as well as variations in the magnetic susceptibility of different types of tissues (J. Duyn 2013). Contrary to the case of T2 mapping, no 180° refocusing pulses are used for T2* mapping since both the T2 effect and the magnetic field inhomogeneity effect are of interest. Note that since no pulses are applied, more dephasing occurs, leading to a faster relaxation for T2* than for T2.

While both myelin and iron content decrease T2* (Christine Lucas Tardif et al. 2016a), *postmortem* analyses have demonstrated iron to be the dominant source of contrast in T2* maps (Langkammer et al. 2010; Stüber et al. 2014). T2* has demonstrated different sorts of hypointense abnormalities and improved disease diagnostics compared to standard T1 and T2 imaging (Tsushima and Endo 2006; Chavhan et al. 2009). Also, different regions of the brain exhibit T2* changes due to different biological phenomenon. For example, the hippocampus (Naftali Raz, Rodrigue, and Haacke 2007) and the basal ganglia (Cherubini et al. 2009) have demonstrated significant T2* changes with age while the substantia nigra is impacted in Parkinson's disease (Lehéricy et al. 2012).

2.5 Image processing

2.5.1 Structural MRI

2.5.1.1 Preprocessing

MR images are typically affected by various types of artifacts that must be minimized before any quantitative metric estimation pipeline can be applied. To improve the quality of MR images, several preprocessing steps are commonly applied to adjust their geometric or intensity space, making subsequent processing and analysis easier.

2.5.1.1.1 Denoising One of the primary challenges of working with MR images is the presence of random noise introduced during image acquisition, which leads to uncertainties in the measures derived from structural MRI. The goal of denoising is to improve the image quality by reducing the noise component while preserving the image features (Vaishali, K. K. Rao, and G. V. S. Rao 2015). One approach is to average multiple acquisitions directly in the scanner which can effectively reduce MR image noise, but it is not commonly used in clinical settings because it significantly increases the acquisition time. Instead, filtering methods are typically applied during the preprocessing stage of many analysis pipelines (A. Singh and J. Singh 2016).

There are many denoising methods available in the literature. The earliest denoising methods had the drawback of removing high-frequency signal components, thereby blurring the edges in the images while removing noise (**Gonzalez2006-eg**; Buades, Coll, and Morel 2005). For instance, classical low-pass filters like the Gaussian filter exhibit this drawback. Other denoising methods are based on patch-wise image processing approaches that exploit the sparseness or self-similarity properties of the medical images, or both. A spatially adaptive non-local means filter was proposed an automatically estimated the local noise level (Manjón, Coupé, et al. 2010) (Figure 2.7 **a.**).

2.5.1.1.2 Inhomogeneity Correction In MR imaging, signal intensity inhomogeneity is a common artifact caused by imperfections in the RF coils and object-dependent interactions (J G Sled, Zijdenbos, and A C Evans 1998). This artifact manifests as a low-frequency variation in signal intensity across the image, which can negatively impact quantitative analysis methods such as image registration and segmentation. Bias field correction, also known as inhomogeneity correction, is a technique used to correct for this artifact (Belaroussi et al. 2006).

One commonly utilized tool is the N4ITK algorithm, which is often referred to as N4 correction in literature (Tustison et al. 2010). This method is an advance of the previously developped N3 correction (J G Sled, Zijdenbos, and A C Evans 1998). Initially, the image input is downsized to a low resolution and a b-spline is fitted to the inhomogeneity in the intensity. Subsequently, the fitted non-uniformity is subtracted from the initial image and the corrected image is employed in a subsequent iteration, which is performed at a higher resolution. This process is repeated until convergence is reached, ultimately maximizing the high frequency content of the tissue intensity distribution (Figure 2.7 **b.**).

a. T1 and T2 values for two tissue types

	T1 (msec)	T2 (msec)
Tissue A	350	100
Tissue B	500	150

b. TR and TE values for different contrasts

	T1-weighted	T2-weighted
TE (msec)	10	100
TR (msec)	300	1500

c. T1-weighted acquisition mechanism

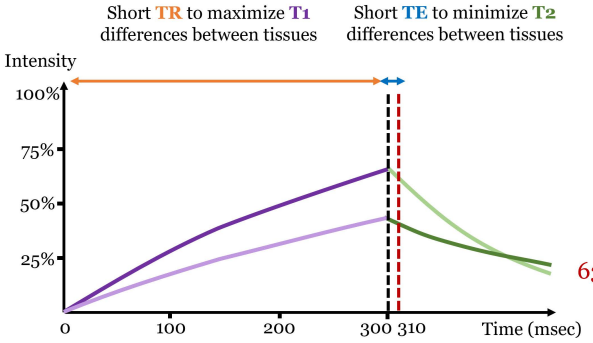

d. T2-weighted acquisition mechanism

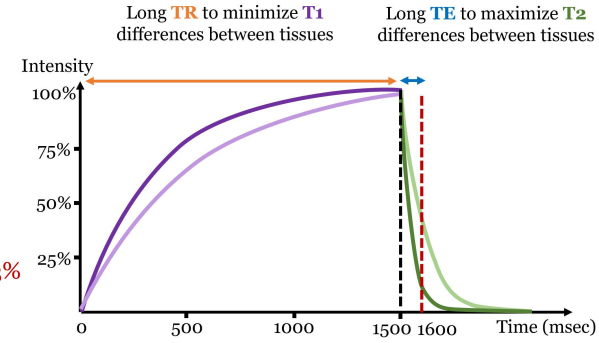

63%

e. Quantitative T1 acquisition mechanism

1. Acquire intensity at different time during T1 relaxation
2. Reconstruct longitudinal relaxation from those information
3. Calculate the time T1 at which 63% of the recovery is completed

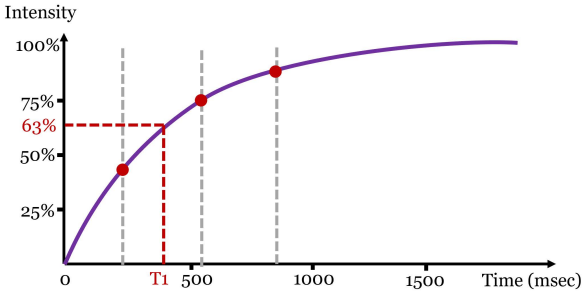

f. Quantitative T2 acquisition mechanism

1. Acquire intensity at different time during T2 relaxation
2. Reconstruct transverse relaxation from those information
3. Calculate the time T2 at which only 37% of the magnetization is left

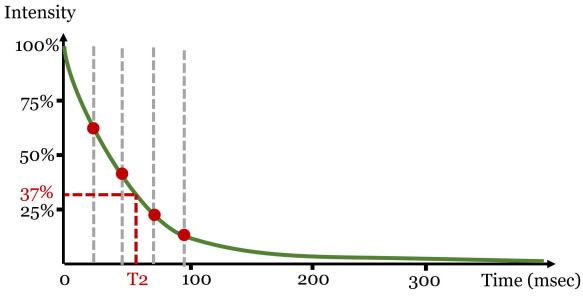

Figure 2.6: Example of **a.** T1 and T2 values for two tissue types, **b.** TR and TE values for different contrasts, **c.** T1w acquisition mechanism, **d.** T2w acquisition mechanism, **e.** Quantitative T1 acquisition mechanism and **f.** Quantitative T2 acquisition mechanism.

a. Raw vs denoised MRI (grey colors)

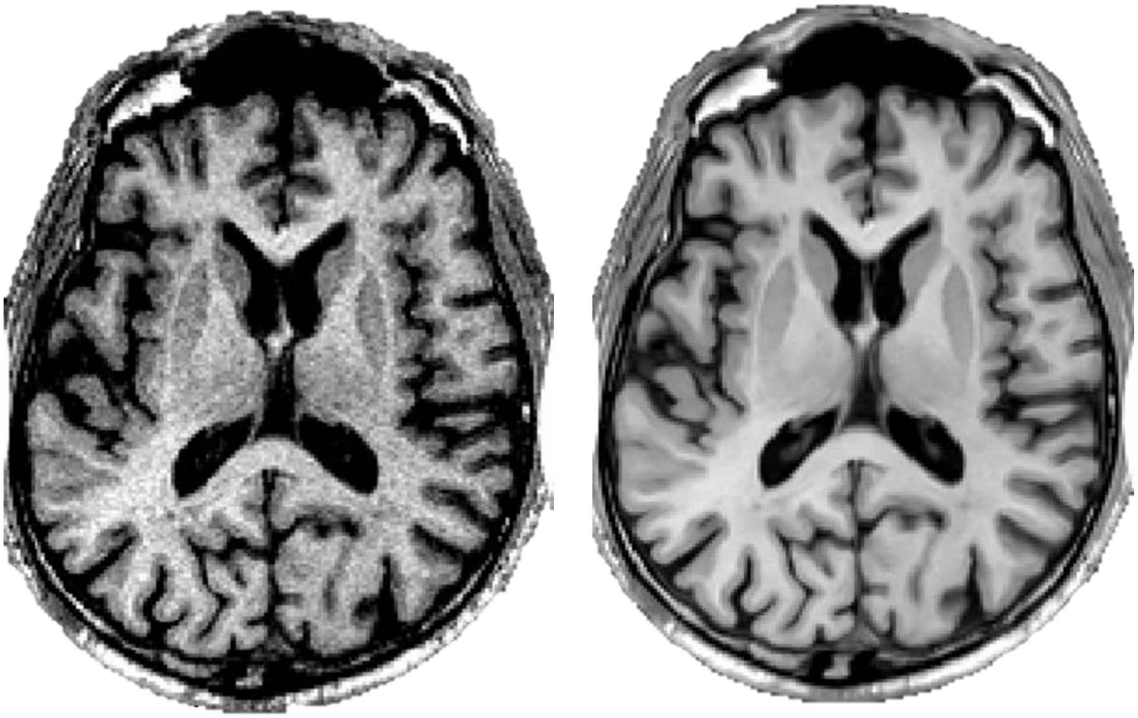

b. Raw MRI vs bias field corrected MRI (spectral colors)

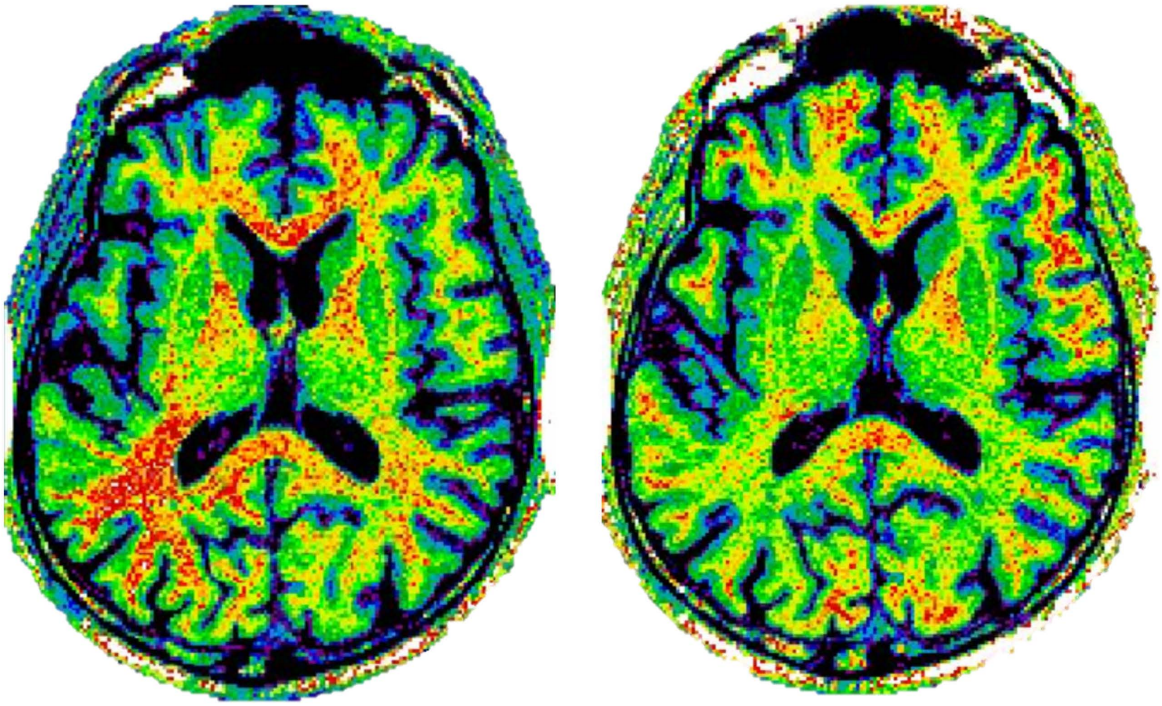

Figure 2.7: Example of preprocessing steps : **a.** Raw T1w MRI image and denoised image (Manjón, Coupé, et al. 2010). **b.** Raw T1w MRI image and bias field corrected using minc-bpipe algorithms (Bussy, Plitman, et al. 2021).

2.5.1.2 Image registration

Medical research, particularly neuroscience research, uses medical images to investigate disease processes and understand normal development and aging. In many of these studies, multiple images are acquired from subjects at different times and often with different imaging modalities. In this context, it is often desirable to compare images obtained from patient to controls or study single subjects imaged multiple times. Image registration, also known as image fusion, matching, or warping, is the process of aligning two or more images (Oliveira and Tavares 2014). The goal is to use mathematical transformations to align the images into a common coordinate space. In neuroscience, the ability of image registration to establish a point-to-point correspondence allows for comparisons between two images that are neuroanatomically homologous (Toga and P. M. Thompson 2001) as a means to allow for the comparison of MRI data across different subjects, modalities, datasets, and studies. Multiple medical applications use image registration including surgery simulation (Castro et al. 2006), assisted/guided surgery (Arbel et al. 2004), brain atlas creation (Collins et al. 1994; Alan C Evans et al. 2012; Chakravarty, Sadikot, et al. 2008), multimodal analysis (Maes et al. 1997), and more. Image registration is often one of the first steps in a pipeline and it can be describe by both linear and nonlinear registrations (Oliveira and Tavares 2014).

2.5.1.2.1 Linear registration Linear registration is a widely used technique that estimates the translations, rotations, scales, and shears required to align one image with another. The defining characteristic of linear registration is that it preserves parallel lines, even after the transformation is applied (Maintz and Viergever 1998). Linear transformations can be categorized based on which specific transformations are employed (Toga and P. M. Thompson 2001). A 6-parameter transformation includes only three translations and three rotations and therefore can not account for differences in image size. A 9-parameter transformation includes three scaling factors for each direction (x, y, and z) to adjust for differences in size in addition to the 6-parameter transformation. Finally, a 12-parameter transformation

includes three shears in addition to the 9-parameter transformation. These transformations fall under the class of affine transformations. Most automated methods operate based on intensity-based features of the images and aim to minimize intensity differences or maximize a measure of image similarity between images post-transformation. Multiple metrics can be optimized, such as mean squared difference, cross-correlation, correlation ratio, or mutual information (Collins et al. 1994; Dadar et al. 2018). Although linear registration methods are commonly used in neuroimaging software, their degrees of freedom are limited (Brian B Avants et al. 2011; Maintz and Viergever 1998). However, because our brain exhibit significant variability and each individual has differential cortical patterning, linear registration is often not enough to correctly register two individual brains.

2.5.1.2.2 Non-linear registration Nonlinear registration methods can supplement linear registration by accounting for local morphological differences between two brain images. Nonlinear methods minimize these differences using spatially varying deformations, allowing for variations in transformation depending on location. Nonlinear registration methods have significantly more degrees of freedom than linear methods, providing greater flexibility to capture local deformations (Maintz and Viergever 1998; Sotiras, Davatzikos, and Paragios 2013). Nonlinear registration algorithms output deformation fields at a voxel level, which can be analyzed to measure changes in brain morphology(Ashburner et al. 1998; John Ashburner and Friston 2000).

Mathematically, image registration is an ill-posed problem, meaning that it does not have a unique and stable solution. Therefore, image registration is typically phrased as a variational problem that involves finding a solution that balances data fit and regularization (Ruthotto and Modersitzki 2015). To ensure existence and uniqueness of solutions, a regularization step is added to the problem to ensure that the solutions to the variational problem are plausible for the specific application (Tihonov 1963). One popular method of regularization is elastic registration, which assumes that the objects being imaged deform elastically (Periaswamy

and Farid 2003). An external force is applied to deform one object to minimize the distance to the other object, while an internal force is given by an elastic model. The registration process stops when external and internal forces balance, resulting in an equilibrium state. Additionally, prior knowledge or expectations of the transformation can be incorporated into the model to improve its accuracy. For example, local rigidity constraints can be used in applications where images show bones or other objects that behave approximately rigidly (Ruthotto, Hodneland, and Modersitzki 2012; J. Zhang et al. 2015). Nonlinear registration schemes may fail if the geometrical difference between the images is too large. To overcome this, a preregistration step with a rigid transformation model is usually employed.

2.5.1.3 Segmentation methods

Image segmentation aims to divide an image into regions that are homogeneous, non-overlapping, and meaningful based on attributes such as texture or intensity (Despotović, Goossens, and Philips 2015). The outcome of this process is either an image with labels representing each region or contours that delineate the boundaries of each region. Brain MRI typically involves classifying image elements into three main tissue types such as GM, WM and CSF, but specific structures of interest can also be segmented such as the hippocampus (J. L. Winterburn et al. 2013). These segmentation results are useful in various applications, such as analyzing anatomical structures, examining pathological regions, planning surgeries, and visualizing data.

2.5.1.3.1 Manual segmentation Manual segmentation refers to the process of segmenting and labeling medical images by a human. This method is considered to be the most accurate but it remains a time-consuming and labor-intensive process. Operators must go through each slice of a 3D image, which can take a significant amount of time. Despite intra- and inter-operator variability (Collier et al. 2003), manual segmentation is still widely used to define a surrogate for true delineation, called "ground truth" and is often used to

quantitatively evaluate automated segmentation methods.

2.5.1.3.2 Intensity-based methods Several intensity-based segmentation methods exist to classify individual pixels or voxels based on their intensity. Thresholding is the simplest and most widely used image segmentation method. It uses the intensity histogram to determine intensity values (ie thresholds) which separate the desired classes (Sezgin and Sankur 2004). For example, Otsu's segmentation is a commonly used technique to separate pixels into two classes (Nyo et al. 2022). However, thresholding does not take into account the spatial characteristics of an image, such as neighborhood information, making it sensitive to noise and intensity inhomogeneities.

Region growing, also known as region merging, is another technique for extracting a connected region of the image (Park and C. Lee 2009). It works by selecting a seed point (i.e., a pixel or voxel) that belongs to the object of interest, which can be done either manually or automatically. Then, the method examines all neighboring pixels/voxels, and if their intensities are similar enough, they are added to the growing region (Passat et al. 2005). Region growing is relatively easy to implement and produces good results. However, segmentation quality can depend on the seed point selection. A tangential technique called edge-based methods extract brain regions based on edges. It is a technique widely used in the brain extraction tool (BET) employed by FSL (S. M. Smith 2002). This technique uses both a deformable model and image-based forces to fit the brain surface.

Clustering methods are unsupervised segmentation methods that partition an image into clusters of pixels or voxels sharing similar intensities (Mirzaei and Adeli 2018). The most commonly used clustering methods are the k-means clustering (J. MacQueen 1967) and the fuzzy k-means clustering methods (Bensaid et al. 1996). Clustering methods are reasonably insensitive to noise or intensity inhomogeneities and offer good segmentation reliability (Cardenas et al. 2001).

2.5.1.3.3 Atlas-based methods Atlas-based segmentation is a common technique used in medical image analysis to automatically segment structures of interest. In this approach, a pre-existing and pre-segmented atlas of the human brain is used as a reference image to segment new brain images. The reference brain is manually segmented by an expert to obtain an atlas which delineates structures of interest. In a model-based segmentation, one template brain is registered to the image (Arata et al. 1995; Csernansky et al. 1998). The same transformation is then applied to the atlas to obtain the atlas in the subject space. This technique is fast but it is based on a specific brain anatomy which is not necessarily representative of the subject brain, and it is susceptible to errors if the registration is inaccurate.

Multi-atlas segmentation involves registering multiple atlases (i.e., pre-segmented images) to the target image and combining them to generate a final segmentation (Klein et al. 2005; Hongzhi Wang et al. 2013). The basic idea behind multi-atlas segmentation is to combine the registered atlases to generate a consensus segmentation, which represents the most likely segmentation of the target image based on the information contained in the atlases. Using multiple atlases improves the accuracy of the segmentation (Iglesias and Sabuncu 2015), however it increases the computational time of the segmentation.

2.5.1.4 Hippocampal segmentation

2.5.1.4.1 Manual segmentation The hippocampus is a complex structure which has been the focus of a lot of segmentation methods. Early studies of the hippocampus relied on manual segmentation using anatomical landmarks visible in histological or MRI sections. However, this approach is time-consuming and subject to variability across different researchers (R. S. C. Amaral et al. 2018; Chakravarty, Sadikot, et al. 2008; Laura E M Wisse, Daugherty, et al. 2017). Indeed, due to the anatomical variability of the hippocampus, multiple laboratories have developed their own segmentation protocol reaching more than 20 distinct manual segmentation protocols, making comparisons across laboratories difficult

(Yushkevich, R. S. C. Amaral, et al. 2015; Giovanni B Frisoni and Clifford R Jack 2015). Therefore, various semi- and fully-automated techniques have been developed in the last decades.

2.5.1.4.2 Probabilistic segmentation Two of the most employed segmentation tools use a probabilistic approach. FreeSurfer is a fully automated segmentation method that can be used to segment the hippocampus but also other brain structures (Bruce Fischl, David H Salat, Busa, et al. 2002). The tool is based on a probabilistic atlas built with ultra-high resolution *ex vivo* MRI data (0.13 mm isotropic) which were manually labelled. *Ex vivo* and *in vivo* T1w were combined into a single computational atlas of the hippocampal formation (Iglesias, Augustinack, et al. 2015). Then, Freesurfer applies non-linear registrations to align images to a standardized space. It subsequently employs a probabilistic framework based on Markov random fields to estimate the probability of each voxel belonging to a specific structure (Bruce Fischl, David H Salat, Busa, et al. 2002; Bruce Fischl, David H Salat, Kouwe, et al. 2004). FSL implements a Bayesian probabilistic model and a training dataset consisting of 336 subjects to identify structures based on their intensity and shape profiles (Patenaude et al. 2011).

2.5.1.4.3 Atlas-based segmentation Automatic segmentation of hippocampal subfields (ASHS) is another software package that uses a combination of multi-atlas label fusion and learning-based error correction to segment the hippocampal subfields (Yushkevich, J. B. Pluta, et al. 2015). Both an isotropic T1w scan and an anisotropic T2w scan ($0.4 \times 0.4 \times 2.0\ mm^3$) are necessary to perform this segmentation. Multiple Automatically Generated Templates (MAGeT) uses a subset of images from an unlabelled dataset, called a template library, to propagate the manually delineated atlas segmentation (Chakravarty, Steadman, et al. 2013; Pipitone et al. 2014). The registration process involves non-linear transformations between atlas and template library images, as well as between each template library image and each image in the unlabelled dataset (Figure 3.10). These transformations are

then used to warp atlas segmentation to each unlabelled image, creating a set of candidate labels for each image. The candidate labels are fused using a majority voting approach at the voxel level. Finally, HIPpocampus subfield Segmentation (HIPS) is a multi-contrast version of a patch matching segmentation method (Coupé, Manjón, et al. 2011; Giraud et al. 2016).

2.5.1.5 Deformation based morphometry

Deformation based morphometry (DBM) is a method used to study structural differences in brain shape. It involves using deformation or vector fields to compare the relative position of specific brain structures across subjects or within subject across multiple timepoints. To achieve this, all subjects' brain images must first be spatially normalized and registered to a group-wise average image or a template image (M K Chung et al. 2001).

The registration process usually involves several steps. Initially, the images undergo linear rigid alignment with six degrees of freedom. The next step involves a 12-parameter transformation, followed by nonlinear registration (Ashburner et al. 1998). The goal of this method is to ensures that all images are in the same stereotaxic space, allowing for voxel-by-voxel comparisons (M K Chung et al. 2001; John Ashburner and Friston 2000). DBM treats deformation fields as vector fields representing absolute displacement or absolute Jacobian determinants, enabling the investigation of all linear and non-linear transformations required to register a subject to the study average brain. Relative Jacobian determinants explicitly model only the non-linear part of the deformations and remove residual global linear transformations attributable to differences in total brain size (M K Chung et al. 2001).

Chapter 3

Hippocampal subfield volumes across the healthy lifespan and the effects of MR sequence on estimates

Aurélie Bussy[1], Eric Plitman[2], Raihaan Patel[3], Stephanie Tullo[1], Alyssa Salaciak[4], Saashi A. Bedford[2], Sarah Farzin[4], Marie-Lise Béland[4], Vanessa Valiquette[1], Christina Kazazian[4], Christine Lucas Tardif[5], Gabriel A. Devenyi[2], M. Mallar Chakravarty[6], Alzheimer's Disease Neuroimaging Initiative

1 - Computional Brain Anatomy (CoBrA) Laboratory, Cerebral Imaging Centre, Douglas Mental Health University Institute, Montreal, QC, Canada, Integrated Program in Neuroscience, McGill University, Montreal, Canada.

2 - Computional Brain Anatomy (CoBrA) Laboratory, Cerebral Imaging Centre, Douglas Mental Health University Institute, Montreal, QC, Canada; Department of Psychiatry, McGill University, Montreal, QC, Canada.

3 - Computional Brain Anatomy (CoBrA) Laboratory, Cerebral Imaging Centre, Douglas Mental Health University Institute, Montreal, QC, Canada, Department of Biological and

Biomedical Engineering, McGill University, Montreal, QC, Canada.

4 - Computional Brain Anatomy (CoBrA) Laboratory, Cerebral Imaging Centre, Douglas Mental Health University Institute, Montreal, QC, Canada.

5 - Department of Biological and Biomedical Engineering, McGill University, Montreal, QC, Canada; McConnell Brain Imaging Centre, Montreal Neurological Institute, Montreal, QC, Canada; Department of Neurology and Neurosurgery, McGill University, Montreal, QC, Canada.

6 - Computional Brain Anatomy (CoBrA) Laboratory, Cerebral Imaging Centre, Douglas Mental Health University Institute, Montreal, QC, Canada; Integrated Program in Neuroscience, McGill University, Montreal, Canada; Department of Psychiatry, McGill University, Montreal, QC, Canada; Department of Biological and Biomedical Engineering, McGill University, Montreal, QC, Canada.

3.1 Preface

In **Chapter 3**, we sought to understand the reasons behind the inconsistent findings regarding the relationship between age and specific regions of the hippocampus. We observed that various studies differ in their experimental designs and use of different types of MRI sequences which may affect the accuracy and precision of the segmentation algorithms. Additionally, the age range and statistical models used to investigate the age-volume relationships can influence the outcome.

Here, we analyzed multiple datasets of MR scans from 1,690 healthy individuals aged 18 to 95 years. We used different types of image sequences, including T1w, high-resolution T2w, and slab T2w images, to examine the hippocampal subfields and surrounding WM regions. Our analysis revealed that certain subregions, like SRLM and fornix, experienced significant volume reduction with age, while the CA1 subfield remained relatively preserved. Moreover, we found that the choice of image modality influenced the age-related relationships

observed in the subfield volumes. In summary, our study suggests that experimental design differences and the choice of imaging modality can explain the inconsistent results in relating hippocampal subfield volumes to age. This manuscript was published in *NeuroImage* in 2021 (Bussy, Plitman, et al. 2021).

3.2 Abstract

The hippocampus has been extensively studied in various neuropsychiatric disorders throughout the lifespan. However, inconsistent results have been reported with respect to which subfield volumes are most related to age. Here, we investigate whether these discrepancies may be explained by experimental design differences that exist between studies. Multiple datasets were used to collect 1690 magnetic resonance scans from healthy individuals aged 18–95 years old. Standard T1w (magnetization prepared rapid acquisition by gradient echo (MPRAGE) sequence, 1 mm^3 voxels), high-resolution T2w (SPACE sequence, 0.64 mm^3 voxels) and slab T2w (Slab; 2D turbo spin echo (TSE), 0.4 $\times$0.4 $\times$2 mm^3 voxels) images were included. The MAGeT Brain algorithm was used for segmentation of the hippocampal GM subfields and peri- hippocampal WM subregions. linear mixed-effect model (lmer) and Akaike information criterion (AIC) were used to examine linear, second or third order natural splines relationship between hippocampal volumes and age. We demonstrated that SRLM and fornix subregions expressed the highest relative volumetric decrease, while the cornus ammonis 1 presented a relative volumetric preservation of its volume with age. We also found that volumes extracted from slab images demonstrated different age-related relationships compared to volumes extracted from T1w and T2w images. The current work suggests that although T1w, T2w and slab derived subfield volumetric outputs are largely homologous, modality choice plays a meaningful role in the volumetric estimation of the hippocampal subfields.

3.3 Introduction

Medial temporal lobe structures, particularly the hippocampus, have been extensively studied for their involvement in various neuropsychiatric disorders such as AD (Bobinski et al. 2000; Braak and E. Braak 1991b; L. A. v. d. Pol et al. 2006; W. Zhao et al. 2019), schizophrenia (Dwork 1997; Heckers 2001; Nelson et al. 1997), major depression disorder (S. Campbell and G. MacQueen 2004; Nikolai V Malykhin, Carter, et al. 2010; Stockmeier et al. 2004), and frontotemporal dementia (Laakso, G B Frisoni, et al. 2000; Muñoz-Ruiz et al. 2012). To better contextualize group differences in case-control studies, an understanding of normative variation of hippocampal structure across the adult lifespan is critical. This information is crucial in order to better understand how deviations from this trajectory may precede the frank onset (or even the prodromes) of various neuropsychiatric disorders. Unfortunately, current studies investigating the relationship between hippocampus structure and age have rendered inconsistent results.

An examination of studies that report upon the relationship between hippocampal volume and age in healthy aging highlights these inconsistencies: some studies report global preservation (Good et al. 2001; E V Sullivan et al. 1995; Edith V Sullivan, Marsh, and Pfefferbaum 2005), while others report overall reduction (Bussy, Snider, et al. 2019; Kurth, Cherbuin, and Luders 2017; Nikolai V Malykhin, Y. Huang, et al. 2017; Raz et al. 2004). More recently, several studies have begun to characterize this relationship at the level of the GM hippocampal subfields, including CA 1, 2, 3 and 4, subiculum and SRLM, using innovative new techniques (Olsen et al. 2019; Pipitone et al. 2014; J. L. Winterburn et al. 2013; Yushkevich, J. B. Pluta, et al. 2015). In most studies reviewed in (Flores, La Joie, Landeau, et al. 2015), the CA1 and subiculum appear to be most impacted by aging. However, in other recent studies, the CA1 (R. S. C. Amaral et al. 2018; Voineskos et al. 2015) and subiculum (Daugherty et al. 2016) have been shown to be relatively preserved. In the present work, we suggest that the observed discrepancies in findings may be explained by the study design disparities - across a range of methodological choices - that exist between

studies.

First, a key methodological difference is the anatomical definition of the hippocampal subfields. This issue is controversial and thus, different atlases are used in the literature (R. S. C. Amaral et al. 2018; Iglesias, Augustinack, et al. 2015; J. Winterburn et al. 2015; Yushkevich, J. B. Pluta, et al. 2015; Yushkevich, R. S. C. Amaral, et al. 2015). In order to facilitate the segmentation of small subfields, protocols use diverse definitions of subfields, which include CA1 combined with CA2 (A. R. Bender et al. 2018), CA3 combined with DG (Flores, La Joie, Landeau, et al. 2015), CA3 combined with CA4 and DG (Shing et al. 2011) or CA4 solely combined with DG (J. Winterburn et al. 2015; L E M Wisse et al. 2012). Second, various segmentation protocols are employed to study the subfields, including manual delineation (La Joie, Fouquet, et al. 2010; S G Mueller et al. 2007), semi-automated approaches (Yushkevich, Hongzhi Wang, et al. 2010), and automated methods (Iglesias, Augustinack, et al. 2015; Pipitone et al. 2014; Van Leemput et al. 2009; Yushkevich, J. B. Pluta, et al. 2015).

Of note, a recent effort has been started by the Hippocampal Subfields Group (`http://www.hippocampalsubfields.com/`) to develop a harmonized protocol based on expert consensus and histological evidence as a means to facilitate comparison of findings across subject groups (Olsen et al. 2019; Laura E M Wisse, Daugherty, et al. 2017). However, despite these significant and important efforts, there remains two additional aspects related to study design that are outside the scope of segmentation protocols, namely: 1) the non-linear relationship of the hippocampal subfield volumes with age, 2) the MRI acquisition protocols. Further, to completely characterize the age-related trends of the hippocampal circuitry, it is critical to examine the examination of peri-hippocampal WM subregions such as alveus, fornix, fimbria and MB. The current manuscript primarily focuses on the impact of these two components.

Importantly, previous studies have examined diverse participant age ranges. While some cohorts consider the entire adult lifespan (R. S. C. Amaral et al. 2018; S G Mueller et al.

2007; F. Zheng et al. 2018), others only assess subjects older than 65 (Giovanni B Frisoni, Ganzola, et al. 2008; Laura E M Wisse, Biessels, et al. 2014). These variations can lead to inconsistencies in findings, since it is well-accepted that the relationship between brain structures and age is typically non-linear (Coupé, Catheline, et al. 2017; Tullo et al. 2019); thus, sampling a smaller age range can lead to conclusions that should not be used to interpret data outside that range. Nonetheless, only a few studies have investigated the non-linear relationships between age and hippocampal subfield volumes (Flores, La Joie, Landeau, et al. 2015; Nikolai V Malykhin, Y. Huang, et al. 2017; S G Mueller et al. 2007; Ziegler et al. 2012).

MRI protocols are highly heterogeneous in the literature and its impact on hippocampal subfield definitions is still not clear. Indeed, studies have used standard T1w images (R. S. C. Amaral et al. 2018; Chételat et al. 2008; Giovanni B Frisoni, Ganzola, et al. 2008), more specialized T2w images (S G Mueller et al. 2007; Laura E M Wisse, Biessels, et al. 2014) or proton-density-weighted (PDw) images (Flores, La Joie, Landeau, et al. 2015; La Joie, Fouquet, et al. 2010). Further, the resolution used to examine hippocampal subfields is highly variable across these image acquisitions. For example, studies used isotropic whole brain scans at 0.7 mm^3, 1 mm^3 (Pereira et al. 2014; Laura E M Wisse, Biessels, et al. 2014) (typically for T1w images, and rarely T2w) or $0.78 \times 0.78 \times 1.5$ mm^3 resolution (Voineskos et al. 2015), or "slab" scans at $0.4 \times 0.4 \times 2$ mm^3 resolution (Susanne G Mueller and Weiner 2009) (typically for T2w and PDw images). The latter is acquired in a region of interest that covers the amygdala and hippocampus either partially or entirely from its anterior to posterior extent. Taken together, these different acquisition parameters may contribute to volume estimation differences potentially explaining the variation observed in age-related subfield relationships. Further, there are very few studies that used high-resolution isotropic scans which allow for the visualization of the molecular layers (i.e. "dark band") of the hippocampus, often considered a prerequisite landmark for manual or automated identification of hippocampal subfields (S. H. Eriksson et al. 2008; J. L. Winterburn et al. 2013; Laura

E M Wisse, Daugherty, et al. 2017). Also, there have been suggestions in several studies that slab T2w or PDw scans should be preferentially used in the study of hippocampal subfields to obtain coronal high resolution (La Joie, Fouquet, et al. 2010; Yushkevich, J. B. Pluta, et al. 2015). Concurrently, there has also been minimal investigation with respect to the use of higher resolution isotropic images for this purpose (L E M Wisse et al. 2012; Laura E M Wisse, Biessels, et al. 2014). Finally, given that the hippocampus and its subfields make up a critical circuit in the brain's memory network, some groups (Iglesias, Augustinack, et al. 2015), including ours (R. S. C. Amaral et al. 2018; Christine L Tardif, Devenyi, et al. 2018), have begun to include the peri-hippocampal WM in studies examining the hippocampal subfields. This is a critical step forward towards examining this specific anatomy at the circuit level.

Given the inconsistency in the literature, there is a clear need to better characterize age-related relationships between the volume of the hippocampal subfields and peri-hippocampal WM subregions while performing a critical assessment of experimental design choices. Here, we examine the role of image acquisition (including standard isotropic T1w, high-resolution isotropic T2w and slab hippocampus-specific T2w) on hippocampal subfield volumes, while assessing the reliability of the hippocampal subfield measures.

3.4 Methods

3.4.1 Image acquisition and participants

3.4.1.1 Image acquisition types

Here, we examine three different scan types from multiple sources. These data come from multiple datasets collected by our group and publicly available datasets (described further in Section 3.4.1.2). These scan types were targeted because two of them (standard T1w MPRAGE and slab T2w 2D TSE) have been commonly used in the hippocampal subfield

literature. The final one, a high-resolution whole brain T2w acquisition, is introduced here as a methodology that potentially addresses some of the limitations with respect to resolution and field-of-view (FOV).

• T1w: This is the protocol most commonly used in neuroimaging studies and has been extensively employed to study the hippocampus, among other structures (Pereira et al. 2014). Here, we used the Alzheimer's Disease Neuroimaging Initiative (ADNI) MPRAGE protocol (Clifford R Jack Jr, Bernstein, et al. 2008; Mugler and Brookeman 1990), since these parameters have been commonly used to investigate hippocampus physiology and pathology.

• Slab T2w 2D TSE: This protocol uses the same ADNI oblique acquisition with 2 mm thick slices perpendicular to the long axis of the hippocampus and 0.4 mm x 0.4 mm in the coronal plane. Recently, this sequence became the standard procedure to study the hippocampus subfields. Users typically take advantage of the high-resolution of the coronal plane to segment the subfields while sacrificing resolution through the anterior-posterior direction. While the type of scanner field has been investigated in regard to the hippocampal measurements (Derix et al. 2014; Marques and Norris 2018; Parekh et al. 2015), it is still unclear what the design trade-off of the anisotropic scans does in terms of consistency and precision of the measurement.

• High-resolution 0.64 mm^3 T2w: This protocol uses the SPACE sequence, a 3D TSE sequence with slab selective, variable excitation pulse. It has been developed in our laboratory for the purpose of increasing the resolution and subfield contrast in the hippocampus. Furthermore, this sequence provides isotropic images across the whole brain and allows for the use of standard linear and nonlinear registration methods that expect whole-brain coverage (Chakravarty, Steadman, et al. 2013).

3.4.1.2 Datasets

The five datasets used to examine the relationship of the hippocampal subfields with age are outlined below, and all include some variation of the acquisition methods described in

	ADB (np=52) (ns=100)	*ADNI (np=135) (ns=233)*	*Cam-CAN (np=376) (ns=376)*	*HA (np=84) (ns=167)*	*Test-retest (np=18) (ns=54)*	*Overall (np=665) (ns=930)*
Age						
Mean (SD)	69.3 (5.7)	71.6 (6.9)	49.9 (17.2)	46.4 (16.1)	26.8 (5.6)	55.4 (18.5)
Median [Min, Max]	69.5 [56.0, 81.0]	70.0 [56.0, 93.0]	49.0 [18.0, 85.0]	46.0 [18.0, 80.0]	26.0 [20.0, 42.0]	61.0 [18.0, 93.0]
Sex						
F	61 (61.0%)	160 (68.7%)	196 (52.1%)	93 (55.7%)	33 (61.1%)	543 (58.4%)
M	39 (39.0%)	73 (31.3%)	180 (47.9%)	74 (44.3%)	21 (38.9%)	387 (41.6%)
Sequence						
T1	52 (52.0%)	135 (57.9%)	376 (100.0%)	84 (50.3%)	18 (33.0%)	665 (71.5%)
T2	48 (48.0%)	0 (0.0%)	0 (0.0%)	83 (49.7%)	18 (33.0%)	149 (16.0%)
Slab	*0 (0.0%)*	*98 (42.1%)*	*0 (0.0%)*	*0 (0.0%)*	*18 (33.0%)*	*116 (12.5%)*

Table 3.1: Demographics by dataset: Final sample after motion and segmentation quality control (QC) across Healthy Aging (HA), ADB, ADNI, Cambridge Centre for Ageing and Neuroscience (Cam-CAN) and Test-retest datatsets. *np = number of participants; ns = number of scans.*

Datasets	Contrast	Sequence	TE (ms)	TR (ms)	TI (ms)	α	Matrix	Resolution (mm^3)	Scan time (mm:ss)
HA	T1w	MPRAGE	2.98	2300	900	9	256 × 240 × 176	1	05:12
ADB	T1w	MPRAGE	2.98	2300	900	9	256 × 240 × 176	1	05:12
ADNI	T1w	MPRAGE	min full echo	2300	900	9	256 × 240 × 208	1	06:20
Cam-CAN	T1w	MPRAGE	2.99	2250	900	9	256 × 240 × 192	1	04:32
Test/retest	T1w	MPRAGE	2.01	2300	900	9	256 × 240 × 208	1	05:12
HA	T2w	SPACE	198	2500	/	/	350 × 350 × 263	0.64	13:22
ADB	T2w	SPACE	198	2500	/	/	350 × 350 × 263	0.64	10:02
Test/retest	T2w	SPACE	198	2500	/	/	350 × 350 × 263	0.64	07:35
ADNI	T2w	T2w 2D TSE	50	8020	/	150	175 × 175 × 60	0.39 × 0.39 × 2	04:20
Test/retest	T2w	T2w 2D TSE	76	8020	/	150	150 × 150 × 60	0.39 × 0.39 × 2	06:34

Table 3.2: Scanning parameters of the different sequences in the different datasets. TE= echo time, TR= repetition time, TI = inversion time, α= flip angle. More details in Supplementary material - Acquisition parameters.

the previous section. All the datasets collected by our group at the Douglas Mental Health University Institute were approved by its Research Ethics Board.

• HA. This dataset was collected and scanned on a 3T Siemens Trio MRI scanner using a 32-channel head coil at the Douglas Mental Health University Institute, Montreal, Quebec, Canada, and contains 111 participants aged 18–80 (Tullo et al. 2019). We analyzed two types of MRI images: standard MPRAGE (1 mm^3) and high-resolution T2w (TSE; 0.64 mm^3).

• ADB. This dataset was also collected and scanned on a 3T Siemens Trio MRI scanner using a 32-channel head coil at the Douglas Mental Health University Institute, Montreal, Quebec, Canada, (Tullo et al. 2019). From this study, we used 68 healthy elderly participants (56–81). The same acquisition protocol as the HA dataset was used, providing standard MPRAGE (1 mm^3) and high-resolution T2w (TSE sequence; 0.64 mm^3).

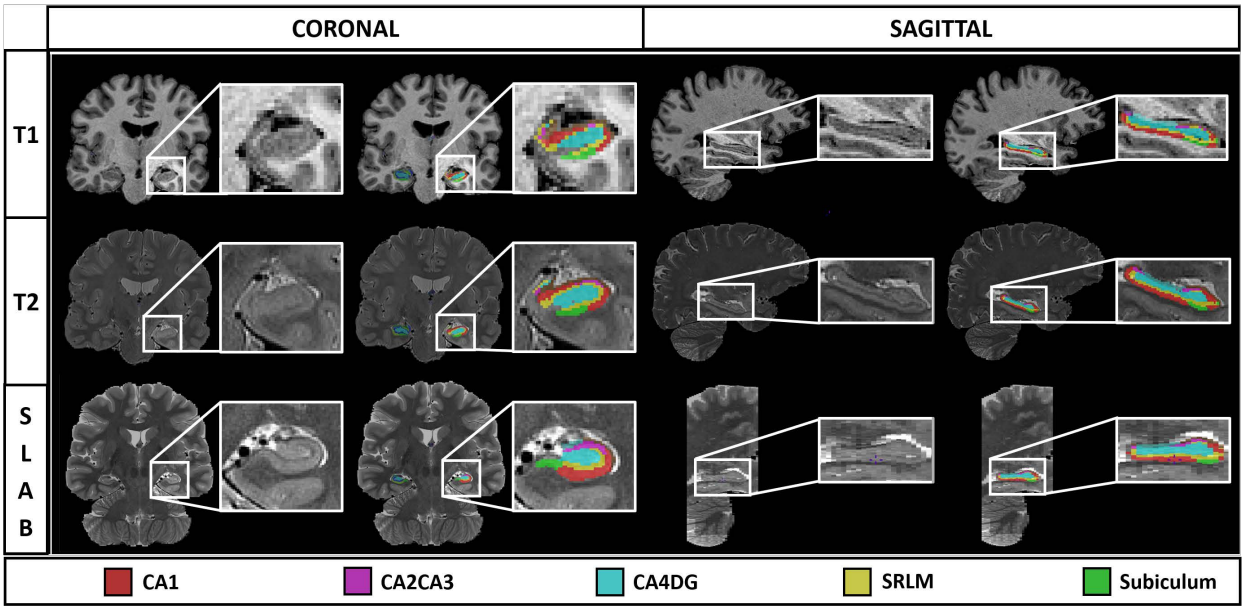

Figure 3.1: Example of coronal and sagittal views of a participant's scans: T1w (1 mm^3), T2w (0.64 mm^3) and slab (0.4 $\times$0.4 $\times$2 mm^3) without and with the labels obtained from our segmentation protocol.

• ADNI. ADNI is a publicly available multicenter study from which we included 317 healthy participants, aged 56–95, scanned on 3T General Electric, Philips or Siemens scanners, depending on the acquisition's site. We used two types of MRI images: standard MPRAGE (1 mm^3) (Clifford R Jack Jr, Bernstein, et al. 2008) and slab T2w 2D TSE with 2 mm thick slices perpendicular to the long axis of the hippocampus and 0.4 mm dimensions in the coronal plane (S G Mueller et al. 2007; Susanne G Mueller, Yushkevich, et al. 2018; Thomas et al. 2004).

• Cam-CAN. Cam-CAN is a large-scale dataset collecting MRI scans at the Medical Research Council Cognition and Brain Sciences Unit in Cambridge, England, using a 3T Siemens TIM Trio scanner with a 32-channel head coil (Shafto et al. 2014; J. R. Taylor et al. 2017). We included 652 healthy individuals (aged 18–88) with standard MPRAGE (1 mm^3).

• Test-retest. Test-retest dataset was collected at the Douglas Mental Health University Institute, Montreal, Canada. Twenty-one healthy participants aged 20–42 were recruited and scanned using a 3T Siemens PRISMA scanner. These participants underwent three different MR sequence acquisitions that reproduce the three different types of acquisitions

described above: standard MPRAGE (1 mm^3), high-resolution T2w (TSE sequence; 0.64 mm^3) and slab T2w 2D TSE sequence (0.4 × 0.4 × 2 mm^3).

The total number of scans after QC of the images (see Section 3.4.2), was 930, and consisted of individuals aged 18–93 (58.4% female) (Table 3.1; Demographics of the initially included participants before scan QC and preprocessing summarized in supplementary Table 3.3). Complete demographics and QC inclusion/exclusion criteria are available in Supplementary material; age distribution of the participants included in the analyses can be found in Supplementary figure 3.8. The main acquisition parameters are provided in Table 3.2 and more details given in Supplementary material - Acquisition parameters.

3.4.2 Image processing

3.4.2.1 Raw quality control

Structural MR images are particularly sensitive to subject motion, often resulting from involuntary movements (e.g. cardiac or respiratory motion, and drift over time). The effects of motion, including blurring and ringing, negatively impact the quality of structural MRI data (Bellon et al. 1986; Reuter, Tisdall, et al. 2015; T. B. Smith and Nayak 2010). QC of all raw images was performed by a rater (AB) using the QC procedure previously developed in our laboratory (Bedford et al. 2020); https://github.com/CoBrALab/documentation/wiki/Motion-Quality-Control-(QC)-Manual .

3.4.2.2 Preprocessing

The minc-bpipe-library pipeline https://github.com/CobraLab/minc-bpipe-library was employed to preprocess and standardize T1w images using N4 bias field correction (Tustison et al. 2010), registration to Montreal Neurological Institute (MNI) space using bestlinreg (Collins et al. 1994; Dadar et al. 2018), standardization of the field-of-view and orientation of the brain using an inverse-affine transformation of a MNI space head mask, and extraction of the brain using BEaST (Eskildsen et al. 2012) . The pipeline produces

brain masks and QC images to quickly evaluate all steps of the pipeline. T2w and slab images preprocessing consists of the following steps: rigid registration of T1w to T2w or slab scan (Collins et al. 1994; Dadar et al. 2018) , application of the transform file to the T1w brain masks obtained by the minc-bpipe-library pipeline to create T2w or slab brain masks, N4 correction, and extraction of T2w or slab brains using T2w or slab brain masks.

3.4.2.3 Automated hippocampus segmentation

The MAGeT Brain algorithm, a modified automated multi-atlas technique (Chakravarty, Steadman, et al. 2013; Pipitone et al. 2014), was used for segmentation of the hippocampal subfields. The MAGeT brain algorithm and documentation related to its use are available on https://github.com/CobraLab/documentation/wiki. This method uses a set of five high-quality atlases, manually segmented on 0.3 mm isotropic T1w and T2w brains, as input. We used the definitions of the GM subfields (CA1, combined CA2 and CA3 (CA2CA3), combined CA4 and dentate gyrus (CA4DG), SRLM and subiculum) (J. L. Winterburn et al. 2013) and the definitions of WM subregions (fimbria, fornix, alveus and MB) of the hippocampus (R. S. C. Amaral et al. 2018) (Figure 3.1). Specifically, the atlases and the corresponding T1w images have been used to segment T1w images while the atlases and the corresponding T2w images have been used to segment T2w isotropic images and T2w slab images. We used either T1w or T2w images to reduce, to the best of our ability, the bias of having one sequence type with higher contrast and intensity similarity with the image brains of the atlases.

For each sequence-type within a specific dataset (e.g. high-resolution T2w data in the ADB dataset), we first ran a "best template selection" stage https://github.com/CoBrALab/documentation/wiki/Best-Templates-for-MAGeT in order to select the 21 subjects with highest quality atlas-to-template segmentation. This best template selection is a MAGeT run for which we only perform the registration between the five atlases and all the subjects. The atlases-to-subjects segmentations obtained from this run are carefully qual-

ity controlled to select the 21 subjects who give the best initial segmentation. Then, the full MAGeT run is completed using these 21 subjects as a template library to segment all the subjects (see supplementary figure 3.10 for a schematic illustration of the full MAGeT-Brain segmentation run). Furthermore, to the best of our abilities, the 21 templates were balanced in age and sex in the same way that the entire dataset of interest, to obtain a representative set of templates. This step computationally increases the number of atlases to 105 candidate labels (21 templates x 5 atlases) specific to each dataset (since derived from the subjects of interest). Finally, the 105 candidate labels for each subject were fused using a majority vote technique to obtain final labels, in order to improve segmentation by reducing error propagation compared to traditional atlas-based segmentation procedures (Chakravarty, Steadman, et al. 2013; Iosifescu et al. 1997; Makowski et al. 2018; Pipitone et al. 2014; Svarer et al. 2005). MAGeT Brain uses affine and SyN nonlinear registration, which are registration options provided as part of the Advanced Normalization Tools [ANTS; (B B Avants et al. 2008)]. Segmentations were conducted using a focused region-of-interest (ROI) based registration step for each hemisphere independently. ROI masks were generated by converting all labels to a single value mask and then dilated with a 3 mm radius kernel in order to focus both affine and nonlinear registration, a method which reduces computational time and improves segmentation accuracy (Chakravarty, Sadikot, et al. 2008; Chakravarty, Mallar Chakravarty, et al. 2009).

For the slab segmentation, in both the "best template selection "or full MAGeT runs, the initial bulk alignment of the slab images were facilitated using their corresponding whole brain T1w images (since the small FOV is not optimal for accurate registrations). First, within-subject affine registrations were performed between slab and whole brain T1w images by using the label masks to handle mismatched FOV. Then, affine registrations were performed using the whole brain T1w images between atlases/templates and templates/subjects. Finally, nonlinear registrations were computed between the slabs images to obtain precise hippocampi segmentation.

The rater (AB) quality controlled the final labels by visual inspection following the QC procedure implemented by our group https://github.com/CobraLab/documentation/wiki/MAGeT-Brain-Quality-Control-(QC)-Guide to only include high quality segmentation in the statistical analyses.

3.4.3 Statistical analysis

3.4.3.1 Relationship between age and normalized hippocampal subfield volumes

To draw general conclusions on the association between each subfield volume with age, we first combined all the datasets together in order to account for the variability in image resolution, sequence, and age range commonly encountered in the literature (Yushkevich, J. B. Pluta, et al. 2015). Lmer (from lmerTest 3.1–0 package in R 3.6.1) and natural spline (ns from splines package) were used to examine the relationship between hippocampal volumes and age. To study different age relationships for each structure of interest, the AIC (Akaike 1974) was used to find the relative quality of each statistical model using either linear, second, or third order natural splines. To minimize the loss of information, the model with the lowest AIC was considered the best fit for the data (Mazerolle 2006). Sex was used as a fixed effect, and dataset (ADB, ADNI, HA, CamCAN, Test-retest), MRI sequence (T1, T2, slab), and subject were modelled as random effects for all statistical analyses. In addition, ICV was used to account for interindividual variability in head size (Daugherty et al. 2016; Flores, La Joie, Landeau, et al. 2015). We used z-scored ICV (scale function) to help the fit of the model 3.1.

$$\begin{aligned} Volume \sim ns(Age, n) + Sex + scale(ICV) + \\ (1|Sequence) + (1|Dataset) + (1|Subject) \end{aligned} \tag{3.1}$$

To determine the extent to which each subfield participates in global hippocampus atrophy with age, we then assessed the relationship between each GM or WM subfield volume and age, while covarying for total hippocampal GM volume (CA1 + CA2CA3 + CA4DG +

Subiculum + SRLM volumes) or WM volume (fimbria + fornix + MB + alveus volumes), respectively, as well as ICV, 3.2 and 3.3.

$$VolumeGM \sim ns(Age, n) + Sex + scale(ICV) + scale(HIPGM) + (1|Sequence) + (1|Dataset) + (1|Subject) \quad (3.2)$$

or

$$VolumeWM \sim ns(Age, n) + Sex + scale(ICV) + scale(HIPWM) + (1|Sequence) + (1|Dataset) + (1|Subject) \quad (3.3)$$

For each analysis described above, we used a Bonferroni correction to correct for multiple comparisons across our 18 structures (five GM subfields and four WM subregions per hemisphere), at a $p<0.05$ threshold for significance, resulting in a significance level of $p<0.0028$ (only corrected p-values reported throughout this paper). To visualize these results, we used two different techniques. We first used these coefficients to create the predicted volume divided by the predicted volume at age 18 for a subject of mean ICV and mean ipsilateral hippocampal GM or WM volume when applicable. This allows us to assess the age relative volume change of each subfield with respect to its baseline volume (Figures 3.2, 3.3 and 3.4). The second type of representation was done using the fixed effect coefficients of the statistical models described above to create the corresponding relationship of the volume with age (Supplementary figures 3.11, 3.12 and 3.13). Of note, both visualization techniques show similar shapes with the first relating these slopes in percent volume change with age whereas the second illustrates volume change with age. APOE-ϵ4 allele gene is often studied in aging population since it is associated with higher risk of both early-onset and late-onset sporadic AD (Corder et al. 1993) as well as age-related cognitive impairment (Rawle et al. 2018). While some authors described that APOE-ϵ4 allele allele was associated with hippocampal, amygdalar and entorhinal cortex atrophy (Cherbuin et al. 2007), others did not find any structural differences between APOE-ϵ4 allele carriers and noncarriers (Habes et al.

2016) or even that APOE-ϵ4 allele noncarriers had more pronounced age-related atrophy (Bussy, Snider, et al. 2019; Gonneaud et al. 2016). Although not the primary interest of this paper, age-related APOE-ϵ4 allele effect was investigated in a subset of 203 genotyped participants (52 ADB-T1, 48 ADB-T2, 52 HA-T1 and 51 HA-T2) with models investigating the interaction of APOE-ϵ4 allele with age. No APOE-ϵ4 allele effect was found to be related to hippocampal volume with age. Therefore, APOE-ϵ4 allele was discarded in our following analyses.

3.4.3.2 Impact of sequence type on the relationship between hippocampal subfield volumes with age

We studied the impact of the sequence type on the relationship between hippocampal subfield volumes with age 3.4. Here, we examined whether the intercept and/or slope of the predicted model was influenced by sequence-type after covarying by sex, ICV, and ipsilateral hippocampal GM or WM volume as fixed effects, and dataset and subjects as random effects.

$$\begin{aligned} Volume \sim ns(I(Age-18), n) * Sequence + Sex + scale(ICV) + \\ scale(HIPGM) + (1|Dataset) + (1|Subject) \end{aligned} \tag{3.4}$$

Figure 3.5 illustrate the relationship between age and hippocampal subfield volumes when extracting from T2w and slab images, compared to when extracting using T1w data. To visualize that, we used model coefficients to predict T1w, T2w, and slab subfield volumes divided by the predicted volume at age 18 for a subject of mean ICV, and mean ipsilateral hippocampal GM or WM volume extracted from T1w images. The goal of dividing by the predicted volume at age 18 extracted from T1w images, regardless of sequence, was to remove the potential effect of over- or under-estimation of a specific sequence and thus to focus on the age-related relationship differences. Supplementary figure 3.14 represent the significant over- or under-estimation of the volumes, in addition to the significant age-related relationships encountered when using solely model coefficients to predict T1w, T2w, and slab subfield

volumes.

3.4.3.3 Impact of sequence type on volume estimates

Given the use of various MRI parameters to study the hippocampus subfields in the literature, we used the Test-retest dataset to compare the volume estimates from T1w, T2w, and slab sequences in the same participants to see how these diverse parameters impact subfield volumes estimation. A dependent 2-group Wilcoxon signed rank test was performed to compare the volume estimates from T1w, T2w, and slab sequences. Here, we used a Bonferroni correction significance level adjusted for 54 multiple comparisons (18 subregions x 3 sequence types), resulting in a significance level of $p<0.00093$. Intraclass correlation coefficient (ICC) (psych 1.8.12 package) were determined to reflect the degree of consistency (ICC [3.1]) between the volume estimates of the different sequences. ICCs were interpreted according to previously established criteria: "excellent": 1.00–0.75, "good": 0.74–0.60, "fair": 0.59–0.40, and "poor": 0.39–0.00 (Cicchetti 1994). The mean percentage volume difference was determined to calculate the extent of the differences in the volume estimations for each sequence.

3.4.3.4 Contrast to noise ratio

Effect of age on the hippocampal subfields contrast has been demonstrated in a study (Knight et al. 2016). Therefore, we developed a protocol to assess the contrast to noise ratio (CNR) in our data. We defined small masks in the CA1 and in the CA4DG of the hippocampal head, and in the temporal lobe WM (J. L. Winterburn et al. 2013). Supplementary figure 3.16 illustrates how each mask was defined as ten consecutive voxels. First, we used T1w and high-resolution T2w scans on HA dataset to investigate the CNR relationship with age between 20 and 80. We randomly chose four participants (two females and two males) per decade. Second, we used T1w and T2w slab scans on ADNI dataset to investigate the CNR relationship with age between 60 and 90. Here, we randomly chose four participants (two

females and two males) per 5 year bin. The CNR was calculated using the following formula 3.5 (Knight et al. 2016; J. L. Winterburn et al. 2013).

$$CNR = \frac{|WM - GM|}{\sqrt{var(GM) + var(WM)}} \tag{3.5}$$

where WM and GM represent the mean WM and GM intensities within the mask, respectively and var(WM) and var(GM) represent the variance of the two tissue classes within the mask. Linear models were used to investigate the effect of age and Bonferroni correction was used to correct for multiple comparisons.

3.4.3.5 HIPS comparison

HIPS (Manjón, Romero, and Coupe 2022; Romero, Coupé, and Manjón 2017) was applied to all the T1w scans of our datasets to investigate the differences of segmentation technique with MAGeT. We decided to investigate this other segmentation technique since it uses the same atlases as MAGeT (J. L. Winterburn et al. 2013). HIPS segmentation has been performed thanks to volBrain website (`www.volbrain.upv.es`), labels were manually quality controlled with our standard procedure and 689 individuals with good labels with both MAGeT and HIPS segmentations were analyzed. lmer investigating the interaction between the segmentation technique (MAGeT vs HIPS) and age were performed (see supplementary figure 3.18). Sex, ICV and right or left total hippocampal GM volume were used as a fixed effect, and dataset and subject were modelled as random effects for the statistical analyses. AIC was used to find the relative quality of each statistical model and demonstrated that all subfields were best explained using a third order natural splines. Bonferroni correction was applied on 10 structures (five bilateral GM subfields), at a $p<0.05$ threshold for significance, resulting in a significance level of $p<0.005$.

3.4.3.6 ASHS comparison

ASHS (Yushkevich, J. B. Pluta, et al. 2015)] was applied to the 98 slab scans of the ADNI dataset to investigate the differences of volume estimation com- pared to MAGeT outputs. We decided to investigate this segmentation technique since ASHS segmentation protocol uses slab-specific atlases with anisotropic resolution. The atlases themselves were developed using serial histological data (Adler, J. Pluta, et al. 2014; Duvernoy 2005; J. Pluta et al. 2012). The goal was to examine whether MAGeT segmentation on the slab images performed properly despite the mismatched resolution between our atlases and the slab images. Here, the absolute hippocampal volumes were expected to be different from MAGeT and ASHS, since the atlases of each technique define the hippocampal subfield boundaries differently (Yushkevich, R. S. C. Amaral, et al. 2015). However, the aim was to investigate whether the segmentation techniques gave similar age-relationships. Lmer including the interaction between the segmentation technique (MAGeT vs ASHS) and age were performed (see supplementary figure 3.19). Sex, ICV and right or left total hippocampal GM volume were used as a fixed effect, and subject was modelled as random effect for the statistical analyses. AIC was used to find the relative quality of each statistical model and demonstrated that all subfields were best explained using third order natural splines. Bonferroni correction was applied on the 8 structures [bilateral CA1, CA2CA3 in ASHS), CA4DG (defined as DG in ASHS) and Subiculum], at a $p<0.05$ threshold for significance, resulting in a significance level of $p<0.00625$.

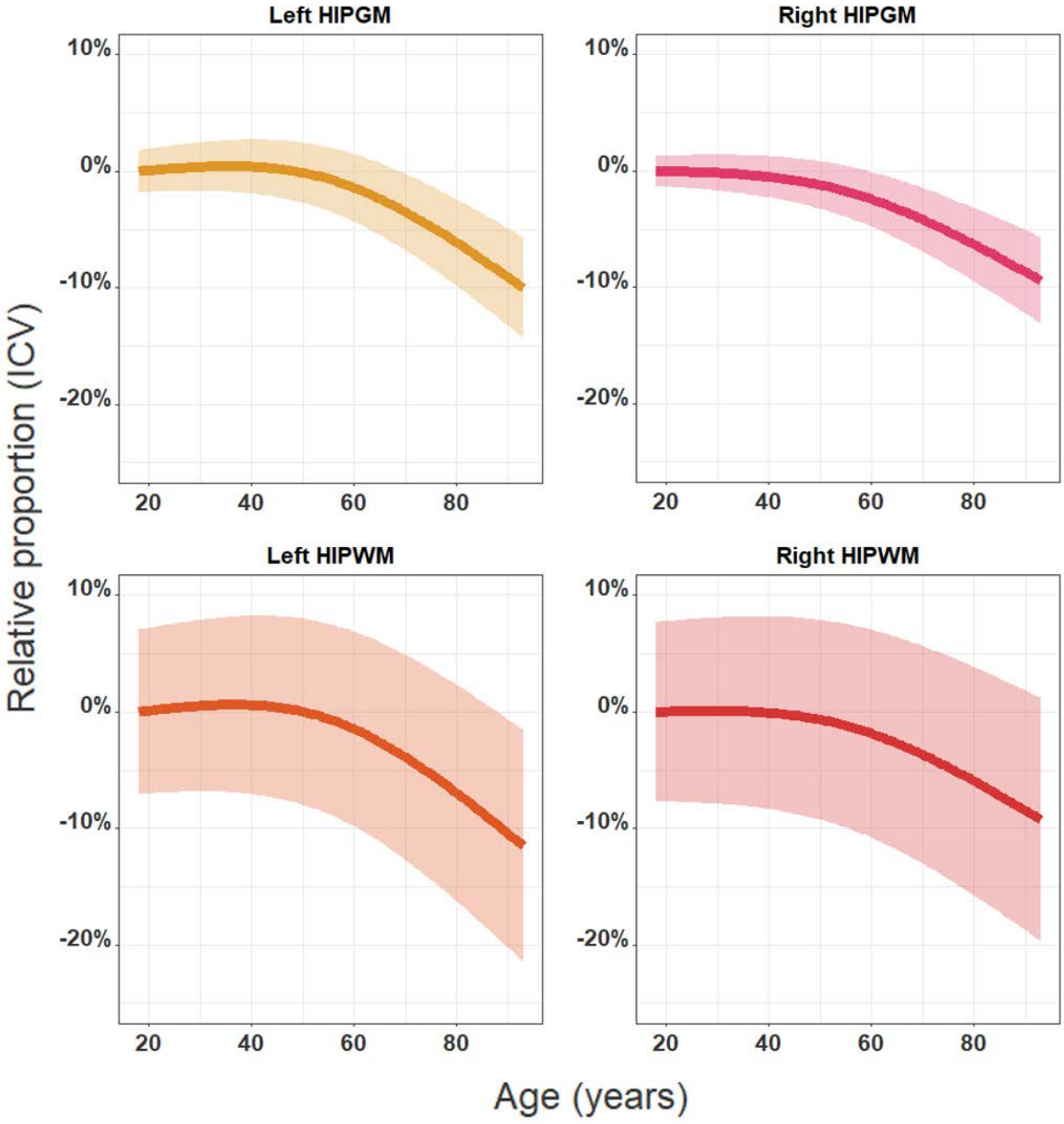

Figure 3.2: Best fit models showing the relationships between age and the relative proportion of the hippocampus using the predicted volume at age 18 for a subject of mean ICV as baseline (same model with volume instead of relative proportion in Supplementary figure 3.11). Best fit models displayed for each structure covaried by ICV and sex as fixed effects and dataset, sequence, and subjects as random effects. Second order relationships were found to be the best fit model for all the structures: right HIPGM ($p = 3.33 \times 10^{-4}$), right HIPWM ($p = 1.05 \times 10^{-3}$), left HIPGM ($p = 2.27 \times 10^{-5}$) and left HIPWM ($p = 1.18 \times 10^{-5}$).

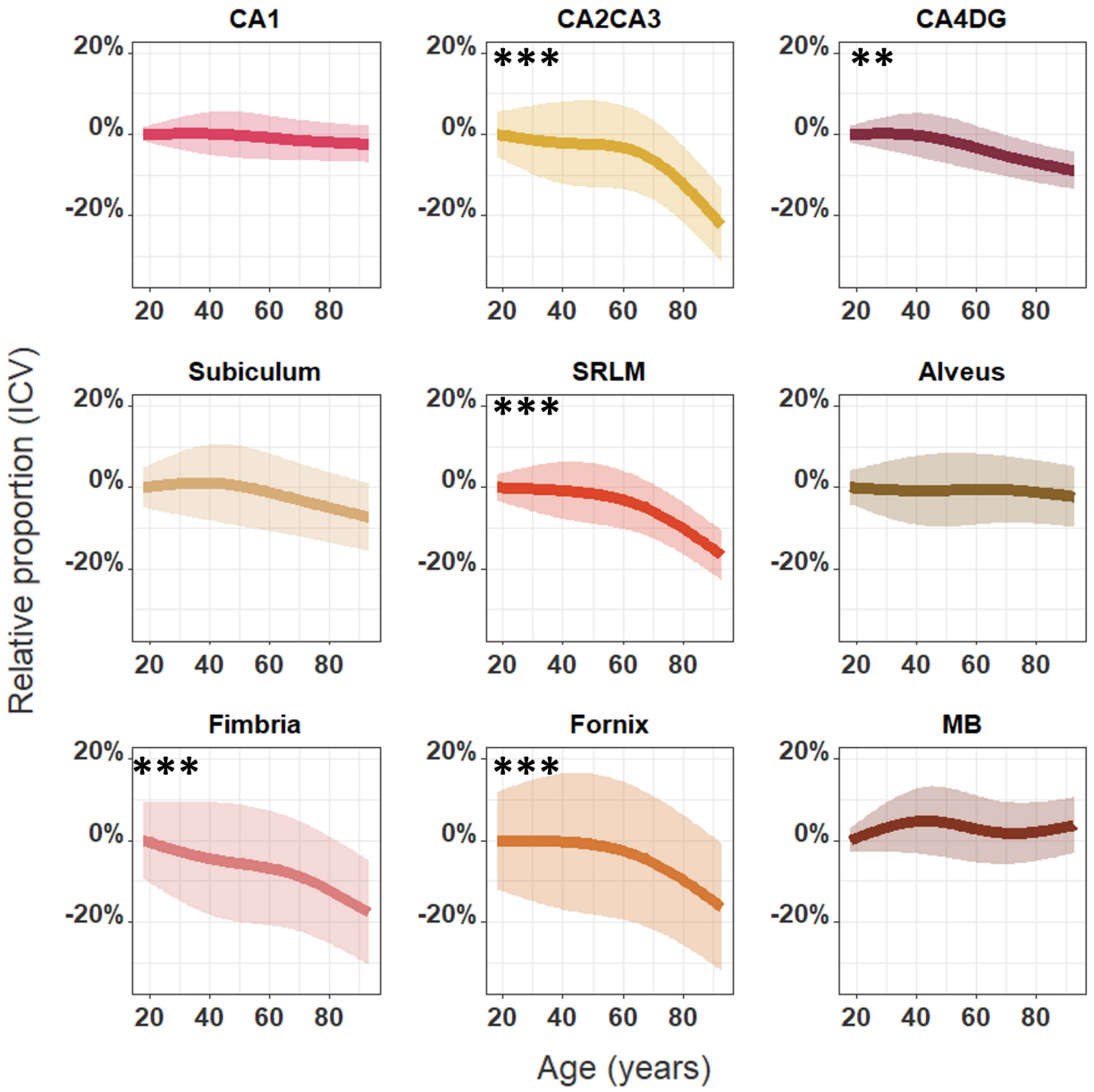

Figure 3.3: Best fit models showing the relationships between age and the relative proportion of the right hippocampal subfields, using the predicted volumes at age 18 for a subject of mean ICV as baseline (same model with volume instead of relative proportion in Supplementary figure 3.12). Best fit models displayed for each subfield covaried by ICV and sex as fixed effects and dataset, sequence, and subject as random effects. Significant monotonic decreases were found for the right CA2CA3 ($p = 3.55 \times 10^{-7}$), CA4DG ($p = 4.28 \times 10^{-3}$), SRLM ($p = 7.74 \times 10^{-7}$), fimbria ($p = 9.45 \times 10^{-4}$) and fornix ($p = 1.79 \times 10^{-4}$). Similar relationships were found in the left hemisphere. $*p<0.05$; $**p<0.01$ and $***p<0.001$ after Bonferroni correction.

3.5 Results

3.5.1 Relationship between hippocampal subfield volumes and age

3.5.1.1 All datasets normalized by the ICV

After covarying for ICV and assessing linear, second- and third-order relationships with age using the AIC, second-order models demonstrated to be the best fit for bilateral GM and WM hippocampus (Figure 3.2): right HIPGM ($p = 3.33 \times 10^{-4}$), right HIPWM ($p = 1.05 \times 10^{-3}$), left HIPGM ($p = 2.27 \times 10^{-5}$) and left HIPWM ($p = 1.18 \times 10^{-5}$). These results show that, when accounting for head size difference, the relative volumes of the bilateral hippocampi were reduced by approximately 10% between age 18 and 93, with a steeper decline after age 50. To test which subfields are involved in this 10% relative volume decrease of the hippocampi with age, individual subfield relationships with age were examined. Third-order models were observed to be the best fit for all hippocampal subfields bilaterally (Figure 3.3 and Supplementary figure 3.12). Significant monotonic decreases were found for the right CA2CA3 ($p = 3.55 \times 10^{-7}$), CA4DG ($p = 4.28 \times 10^{-3}$), SRLM ($p = 7.74 \times 10^{-7}$), fimbria ($p = 9.45 \times 10^{-4}$) and fornix ($p = 1.79 \times 10^{-4}$). These results indicate that relative volumes of the CA2CA3, SRLM, fimbria and fornix decreased by approximately 20%, while CA4DG decreased by 10% between age 18 and 93. Interestingly, volumetric impairments seem to start earlier in CA4DG, SRLM and fimbria compared to the CA2CA3 and fornix, which seem relatively preserved until age 60. Similar relationships were found in the left hemisphere. In contrast, the bilateral CA1, subiculum, alveus and MB did not express significant relationships with age, and therefore were not implicated in the global volume decrease of the hippocampus.

3.5.1.2 All datasets normalized by the hippocampal volume

In the right hemisphere, when covarying for ipsilateral hippocampal GM or WM volume and ICV, all hippocampal subfield volumes were shown to have a best fit third-order relationship

with age. Significant monotonic increases were found for the relative proportion of the right CA1 ($p = 1.19 \times 10^{-10}$). The relative volume of CA1 demonstrated a 7% increase between age 18 and 93. Significant monotonic decreases were found for the right CA2CA3 ($p = 3.19 \times 10^{-4}$) and SRLM ($p = 5.29 \times 10^{-6}$) (Figure 3.4 and Supplementary figure 3.13). These results indicate that relative volumes of the CA2CA3 decreased by approximately 15% and SRLM by 5% between age 18 and 93. No significant volume interaction with age was found for the right CA4DG, subiculum, alveus, fimbria, fornix and MB. Similar relationships were found in the left hemisphere.

3.5.1.3 Impact of sequence on subfield volume relationship with age

T1w volumes demonstrated significant linear increases for CA1 ($p = 2.65 \times 10^{-6}$), decreases for fimbria ($p = 9.85 \times 10^{-3}$) and third-order relationships for CA2CA3 ($p = 6.59 \times 10^{-5}$) and SRLM ($p = 1.33 \times 10^{-5}$) highlighting a steeper decline after age 60 for these subfields (Figure 3.5 A). Compared to T1w, significant differences were found with slab for the CA1 ($p = 0.0102$) and MB ($p = 3.47 \times 10^{-14}$), demonstrating a steeper increase with age, while CA4DG ($p = 1.93 \times 10^{-3}$) and fornix ($p = 9.41 \times 10^{-7}$) manifested a stronger decline with age. Volumes estimated from the T2w sequence exhibited similar relationships with age when compared to volumes estimated from T1w, except that T2w expressed steeper increase for CA1 ($p = 5.49 \times 10^{-4}$). In Figure 3.5 A, the different age relationships for each sequence are represented without intercept difference to emphasize the effect of age on the estimation. While not plotted, we see in Table 3.12B (and in more details in Supplementary figure 3.14) that slab intercepts were smaller for CA1, CA2CA3, subiculum, fimbria,and MB, while they were higher for CA4DG and SRLM. In addition, compared to T1w volumes, T2w volumes expressed smaller intercepts for CA2CA3, subiculum, and fimbria and higher intercepts for CA4DG, SRLM and fornix. Similar relationships were found in the left hemisphere.

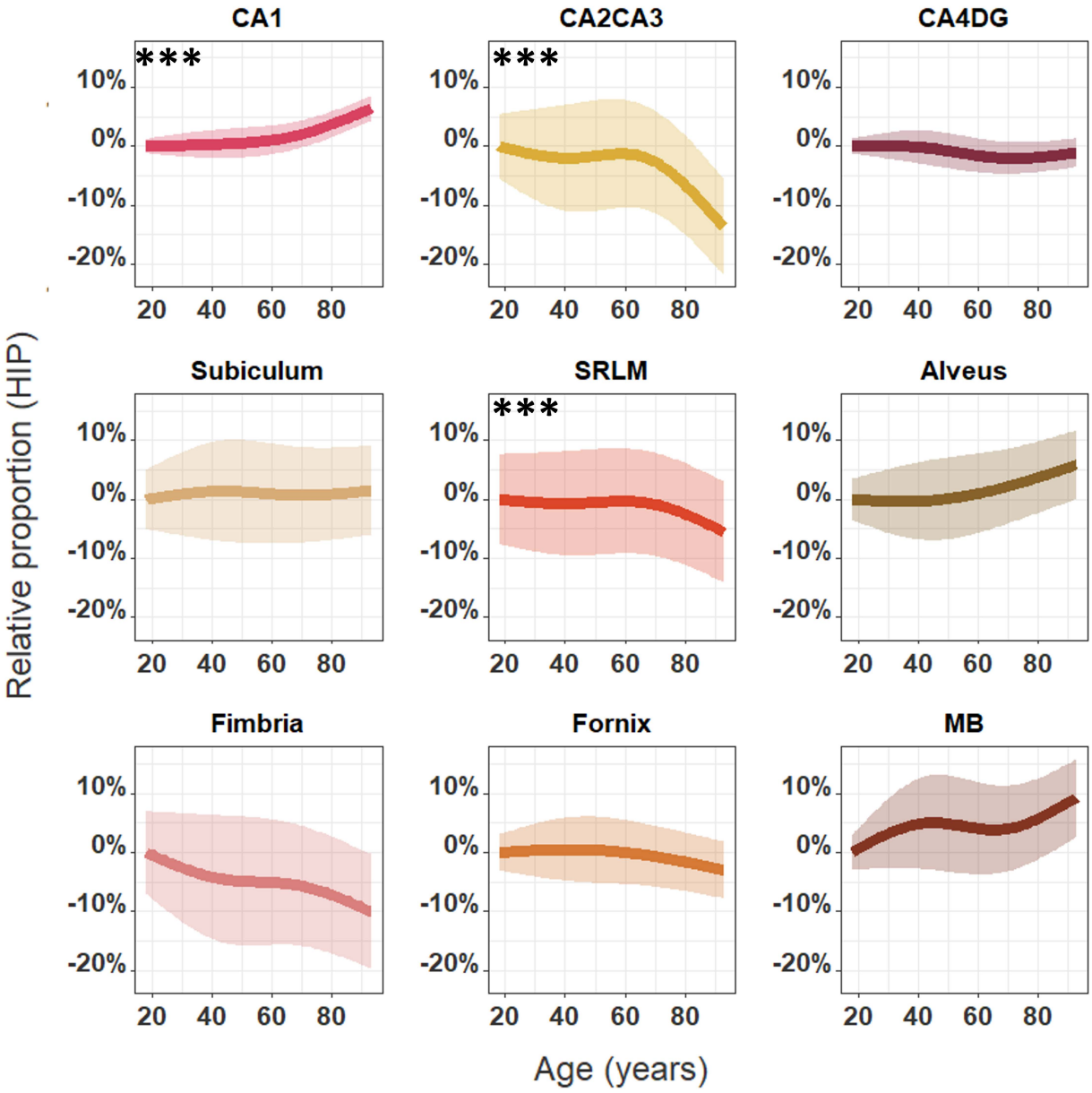

Figure 3.4: Best fit models showing the relationships between age and the relative proportion of the right hippocampal subfields, using the predicted volumes at age 18 for a subject of mean ICV and mean right hippocampal GM or WM volume as baseline (same model with volume instead of relative proportion in Supplementary figure 3.13). Best fit model displayed for each subfield covaried by right hippocampal GM or WM volume, ICV and sex as fixed effects and dataset, sequence, and subject as random effects. Significant monotonic increases were found for the right CA1 ($p = 1.19 \times 10^{-10}$) and significant monotonic decreases were found for the right CA2CA3 ($p = 3.19 \times 10^{-4}$) and SRLM ($p = 5.29 \times 10^{-6}$). $*p<0.05$; $**p<0.01$ and $***p<0.001$ after Bonferroni correction.

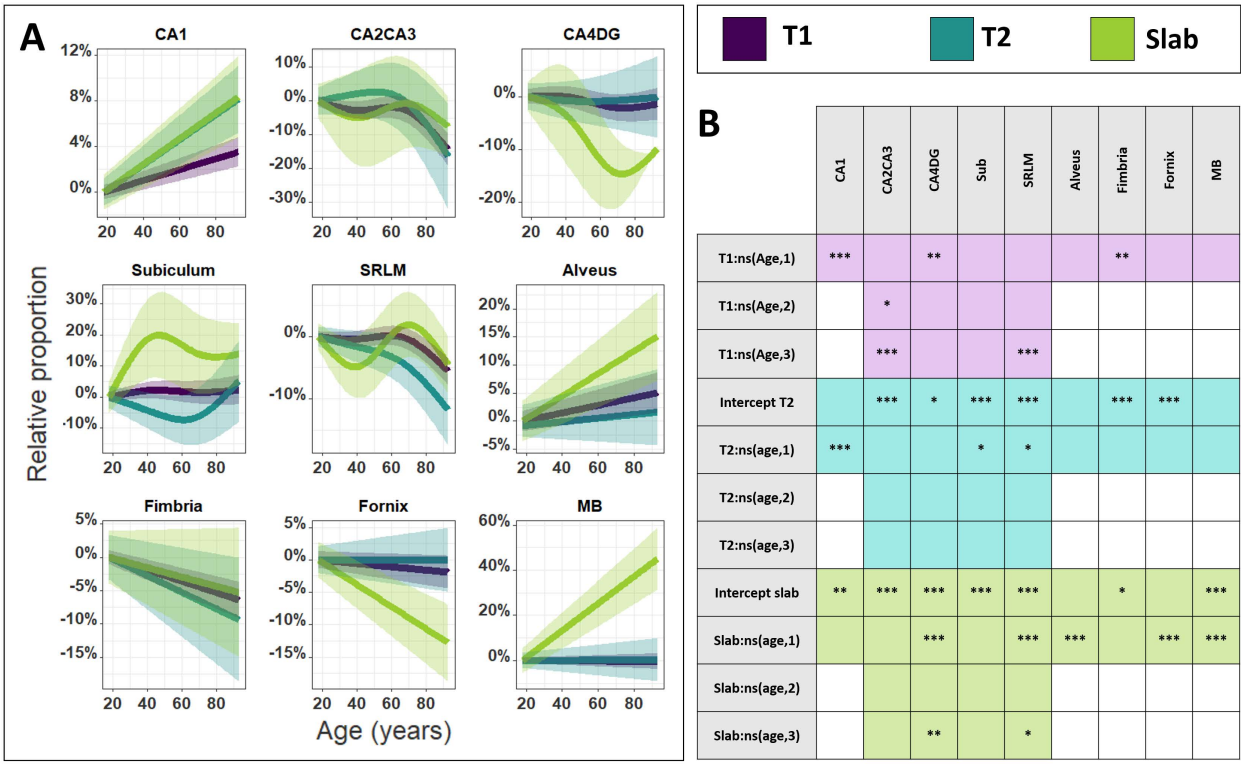

Figure 3.5: **A**. Estimated fixed effect plots showing the relationships, separated by sequence-type, between age and the relative proportion of the right hippocampal subfields, using the predicted volume at age 18 for a subject of mean ICV and mean ipsilateral hippocampal GM or WM volume extracted from T1w images as baseline. Best fit model displayed for each subfield covaried by ipsilateral hippocampal GM or WM volume, ICV, and sex as fixed effects and dataset, sequence, and subject as random effects. **B**. Table describing the significant coefficients for the different relationships with age and the intercepts. T1w was used as reference sequence in the model and demonstrated a significant linear increase for CA1 ($p = 2.65 \times 10^{-6}$), decrease for fimbria ($p = 9.85 \times 10^{-3}$) and third order decrease for CA2CA3 ($p = 6.59 \times 10^{-5}$) and SRLM ($p = 1.33 \times 10^{-5}$). Significant differences were found with slab compared to T1w, with the CA1 ($p = 0.0102$) and MB ($p = 3.47 \times 10^{-14}$), demonstrating a steeper increase with age, while CA4DG ($p = 1.93 \times 10^{-3}$) and fornix ($p = 9.41 \times 10^{-7}$) showing a steeper decline with age. Best fit models estimated from the T2w sequence exhibited similar relationships with age than the models obtained with T1w images except that T2w expressed steeper increases with age for CA1 ($p = 5.49 \times 10^{-4}$). Supplementary figure 3.14 described in more details the significant intercept differences. Similar investigations made in the left hemisphere. $*p<0.05$; $**p<0.01$ and $***p<0.001$ after Bonferroni correction.

3.5.2 Impact of different sequence on hippocampal subfield volumes estimates

We compared the volume estimates of the right hippocampal subfields obtained from T1w, T2w, and slab sequences within the same subjects (Figure 3.6). Significant differences were obtained between T1w and slab sequences for all the subfields except the SRLM. These results demonstrated that T1w images lead to larger volume estimates than the slab sequence, on average by 11.2% (Supplementary Table 3.4), except for the CA4DG which is larger using slab images. T2w images appeared to render similar volumes compared to T1w images, except for the CA2CA3, which was larger when extracted from T1w. Moreover, T2w volumes estimates were on average 8.1% larger than the volumes extracted from slab sequences. These findings suggest that, while we cannot rule which sequence provides the most accurate volume estimation due to a lack of ground truth, slab images appear to estimate smaller volumes compared to other acquisitions Finally, ICC (3,1) was used to calculate the consistency between each dataset volume estimates (Figure 3.7). High ICC values were mostly found between T1w and slab sequences. We can also observe that the left hippocampus revealed lower ICC in most subfields. Subregions exhibiting poor consistency included left fimbria and fornix.

3.5.3 Contrast to noise ratio analysis

No significant age effect was found on the CNR of the CA1 and CA4DG using the T1w, high-resolution T2w or slab T2w images of the HA or ADNI datasets (supplementary Figure 3.17).

3.5.4 HIPS segmentation analysis

Hippocampal subfield volumes extracted from HIPS or MAGeT segmentation techniques were investigated with age. Subtle significant differences in the right CA1 and in the left

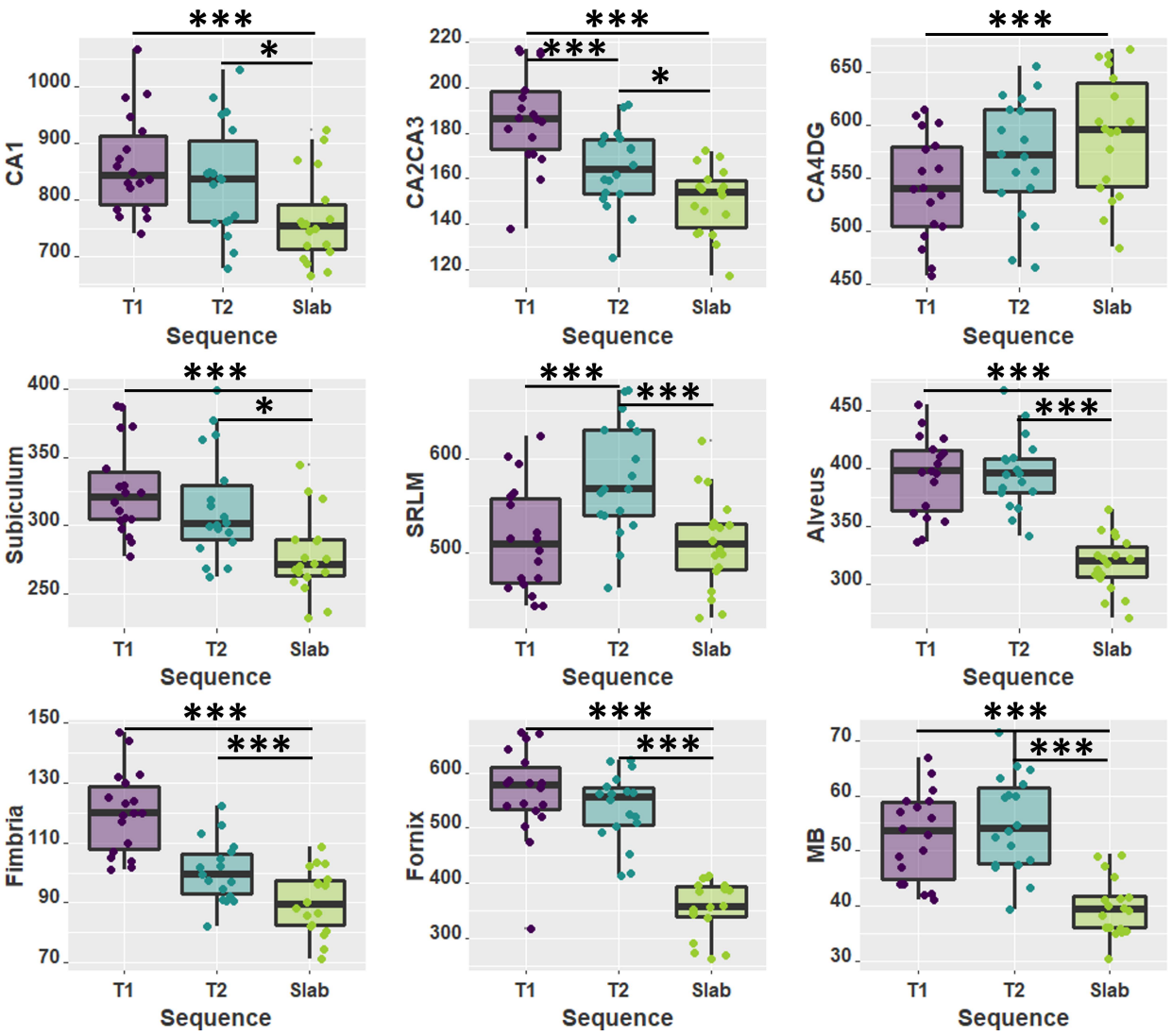

Figure 3.6: Boxplots illustrating the right volume estimates from T1w, T2w and slab sequences from the same participants as well as the dependent 2-group Wilcoxon signed rank test results (Supplementary Table 3.3). Similar results were found in the left hemisphere (Supplementary figure 3.15). $*p<0.05$; $**p<0.01$ and $***p<0.001$ after Bonferroni correction for 54 comparisons (18 subfields x 3 sequence types).

CA4DG were found (supplementary Figure 3.18). However, the CA2CA3 illustrated clear age-relationship differences between the techniques, potentially because of biases due to its small subfield size. For all the other subfields, our results were identical with HIPS or MAGeT techniques.

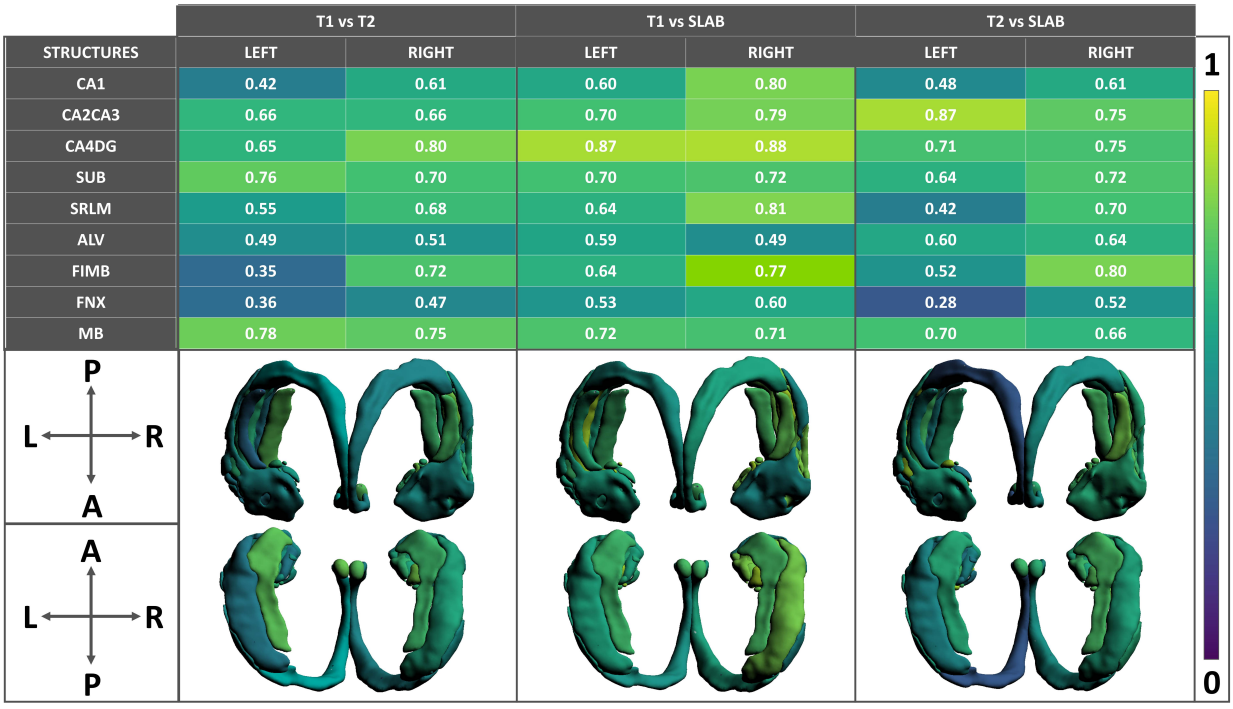

Figure 3.7: Representation of ICC consistency (3,1) of hippocampal subfields volume estimates from T1w, T2w, and slab images. Colour scale serves as an indicator of the ICC values: yellow for an ICC of 1 and dark blue for an ICC of 0.

3.5.5 ASHS segmentation analysis

Hippocampal volumes extracted from ASHS and MAGeT segmentation techniques were investigated with age. Overall, ASHS volumes were significantly larger in the CA1, CA4DG and subiculum subfields and smaller in the CA2CA3 subfields. However, in all the subfields, no significant difference was found in the age-relationship of the volumes extracted from MAGeT and ASHS techniques (supplementary Figure 3.19).

3.6 Discussion

The aim of this paper was to examine the hippocampal subfields and WM subregions throughout healthy aging. Normalized for ICV, we found that all subfields and WM subregions expressed a volumetric decrease with age, with the exception of CA1, subiculum, alveus and MB. These findings are in contradiction with previous investigations that demonstrated

a significant impact of age on the CA1 (Daugherty et al. 2016; Flores, La Joie, Landeau, et al. 2015; Shing et al. 2011; Laura E M Wisse, Biessels, et al. 2014; Wolf et al. 2015). Although, other studies found no volumetric change with age for the CA1 (Voineskos et al. 2015) or even an increase with age for the CA1 and alveus when accounting for ipsilateral hippocampal volume (R. S. C. Amaral et al. 2018). No clear age-related relationship between the CA1–3 volumes with age was demonstrated in another study, with a significant decrease in the body but not in the head and tail (Nikolai V Malykhin, Y. Huang, et al. 2017). Regarding WM subregions, the alveus, fimbria and fornix have been previously mostly used as anatomical landmarks for the GM subfields definition (La Joie, Fouquet, et al. 2010; Nikolai V Malykhin, Y. Huang, et al. 2017; S G Mueller et al. 2007; L E M Wisse et al. 2012). In the present study, WM subregions were considered as an integral part of the hippocampal circuitry. CA1 and alveus were found to be stable with age which reproduces, using a larger sample, previous findings from our group (R. S. C. Amaral et al. 2018).

Researchers have consistently shown the CA1 subfield to be the first hippocampal subfield to be impacted in AD (Adler, Laura E M Wisse, et al. 2018; R. S. C. Amaral et al. 2018; Flores, La Joie, and Gaël Chételat 2015; Giovanni B Frisoni, Ganzola, et al. 2008). Further, *post-mortem* studies of AD individuals have also found hippocampal amyloid and fibrillary tangles to firstly accumulate in CA1 (Braak and E. Braak 1991b; Heiko Braak, Alafuzoff, et al. 2006). Therefore, we suggest that CA1 preservation in healthy aging could be of interest to identify early changes in hippocampus volume trajectories. SRLM has also been found to be especially impacted in patients with AD (Adler, Laura E M Wisse, et al. 2018) as well as to a greater extent in APOE-ϵ4 allele carriers (Geoffrey A Kerchner et al. 2014). Thus, it is interesting that our results also indicate a strong age-related atrophy in this subfield, although we did not find any APOE-ϵ4 allele effect. This could be in part because we did not have APOE-ϵ4 allele genotyping for a subset of our participants, preventing us from having enough data to fully investigate this genetic effect.

Complementary analyses were performed using ipsilateral hippocampal GM or WM vol-

umes normalization. To our knowledge, this is the first study that analyzed the subfield volumetric relationship with respect to age while including global hippocampal atrophy. SRLM and fornix subregions expressed the highest relative volumetric impairment while the CA1 presented a relative volumetric preservation of its volumes with age. These findings replicate the results that we found using ICV normalization and provided a reasonable indication that the CA1 is a relatively preserved hippocampal subfield in healthy aging. Dissimilarities with other publications could be explained by the variability of the hippocampal subfield atlases definition used in the literature (Yushkevich, R. S. C. Amaral, et al. 2015). Indeed, we have previously found similar increases of the CA1 volumes (R. S. C. Amaral et al. 2018) after normalization using the same atlases and segmentation protocol in another cohort.

We hypothesize that the variability in findings within the literature may also be a function of the methodology used. For example, some groups approximated the hippocampal volumes using solely three contiguous slices (Daugherty et al. 2016) while others used nine slices (La Joie, Fouquet, et al. 2010). Other studies have also expressed concern regarding the probable undersegmentation of CA1 and oversegmentation of the CA2–3 with FreeSurfer 5.3 (Flores, La Joie, Landeau, et al. 2015). Also, only a few studies previously examined the WM subregions of the hippocampus (R. S. C. Amaral et al. 2018; Nikolai V Malykhin, Y. Huang, et al. 2017; Voineskos et al. 2015), potentially because slab sequences do not always provide proper FOV to study the entire hippocampal circuitry.

Also, in the present study, we included participants aged from 18 to 93, an age range which is larger than what is used in most papers studying the effect of age in the hippocampus subfields (Dounavi et al. 2020; S G Mueller et al. 2007; Wolf et al. 2015). Almost all the significant relationships with age demonstrated third order relationship, often with an inflection point close to 60 years old. Similarly, a critical age in the acceleration of hippocampal degeneration was previously identified at 63 years old (Yang et al. 2013).

Further, we investigated if our results were driven by a CNR relationship with age, since another study found a significant decrease in the hippocampal subfields with age (Knight

et al. 2016). However, no age relationship of the CNR was found in our datasets which comforted us in our finding that the age effects that we identified were not related to a loss of contrast. However, while we defined our masks following a manual segmentation procedure previously used (Kulaga-Yoskovitz et al. 2015; J. L. Winterburn et al. 2013; B. Wood et al. 2015), others (Knight et al. 2016) have defined their WM masks in the SRLM. Thus, these protocol differences may explain the discrepancy regarding the CNR relationship with age in the hippocampus. Further, more investigation in regard to the age effect on the CNR would be of interest since we noticed a subtle downward trend in some hippocampal subfields using T2w images, particularly in light of the difference in ROIs used to examine the CNR.

A recent study compared different techniques to measure hippocampal subfield volumes and found that slab images were more sensitive to amyloid deposition and mild cognitive impairment status than whole brain T1w images (Susanne G Mueller, Yushkevich, et al. 2018). Also, slab images have demonstrated highly consistent results with those from T1w images and slightly better detection of group effects in atrophy rates between patients with cognitive impairment and controls (Das et al. 2012). In our study, we found that volumes extracted from slab images demonstrated different age-related relationships than the volumes extracted from whole brain T1w and T2w images. This could be explained by the relatively small number of participants having a slab image in our study. Indeed, 64% of our original slab scans had to be excluded due to high motion artifact or incomplete coverage of hippocampal GM and WM subregions (Susanne G Mueller, Yushkevich, et al. 2018) compared to 43% for T1w and 25% for T2w (Supplementary figure 3.9). Of note, it is unclear how consistent QC has been applied in other slab volumetric studies.

To our knowledge, our paper used, for the first time, a high-resolution isotropic whole brain T2w sequence with isotropic voxel dimensions of 0.64 mm. The main advantage is that this acquisition provides a voxel volume of 0.26 mm^3 compared to 0.32 mm^3 for the commonly used slab sequence or 1 mm^3 for T1w sequence. Additionally, it allows for a clear delineation of the SRLM due to the hypo-intense contrast obtained in T2 contrast (Dounavi

et al. 2020; Iglesias, Augustinack, et al. 2015). This is of importance since it provides well-defined internal anatomical landmarks for segmentation protocols. T2w results primarily demonstrated similar results to T1w volume estimates with the supplementary benefit of demonstrating higher precision of segmentation according to visual inspection of the labels.

The results presented in this paper should be interpreted with respect to several considerations and limitations. First, an important consideration is that this study aims to draw a global conclusion in how the different hippocampal subfields evolve across the lifespan using cross-sectional data. Thus, even though longitudinal analysis would be essential and more appropriate to assess the "true" relationship of the hippocampal subfield volumes and age, these studies require tremendous resources, time and dedication from the participants. Therefore, in the context of our research, since no longitudinal study used various sequences on healthy participants to study the hippocampus subfields, we used cross-sectional studies to approximate and study this topic.

Secondly, to create this study, we used datasets from multiple sites. This led to different inclusion criteria with regards to how each site defined healthy participants (Supplementary methods). Also, participants were scanned in different scanners, especially in the ADNI dataset, which itself included multiple sites. To counterbalance this issue, we performed rigorous preprocessing, QC (Bedford et al. 2020), and statistical analyses to standardize the quality and the intensity of the images included in this study to the best of our ability.

In addition, the differing results with the slab scans must be interpreted carefully since this dataset was limited to 116 participants. Unfortunately, we did not have access to slab data from healthy participants across the entire lifespan. That is why we decided to include the Test-retest dataset in order to increase the age-range of the slab sequence analyses. Thus, complementary analyses including more participants with a full coverage across the adult lifespan for the three modalities would be beneficial to validate these findings.

A significant challenge in the MRI subfield literature is the validation or derivation of the underlying segmentation protocols based on histological segmentation. To this end, few

groups have successfully developed protocols that incorporate histology due to the scarcity of tissue and the significant challenge of histology-to-MRI nonlinear registration. The few groups that have derived their atlases from a histologically informed delineation, have to some extent used different strategies. For example, some (Jordan DeKraker et al. 2018) have relied heavily on the work from Ding (Ding and Van Hoesen 2015) while the work from Adler (Adler, J. Pluta, et al. 2014) relies more heavily on the Duvernoy (Duvernoy, Cattin, and Risold 2013). Thus, within the field there is still a lingering lack of clarity with respect to what "histologically-informed" methodologies to use. While there are still ongoing attempts to reconcile these disparities through the development of a harmonized subfield protocol that is informed, in some way, by the consensus segmentation of histological data (Olsen et al. 2019; Laura E M Wisse, Daugherty, et al. 2017), this remains a work in progress.

Nonetheless, it is important for us to acknowledge that, in the present paper, proper validation of the correspondence to ground-truth histology was unfortunately not possible. However, the atlases used were based on histological boundaries and rigorous QC was completed to only include segmentations following these atlases histological rules (R. S. C. Amaral et al. 2018; J. L. Winterburn et al. 2013). Besides, in the current paper, we have examined the interplay between the acquisition technique and two additional segmentation algorithms that have been developed precisely for hippocampal subfield studies (Romero, Coupé, and Manjón 2017; Yushkevich, R. S. C. Amaral, et al. 2015). All of these techniques, including our own (Pipitone et al. 2014), which have been previously validated against manual segmentation.

Further, regarding the quality of segmentation, MAGeT has been developed to create a large template library given a much smaller sized input atlas library and then uses this template library in basic multi-atlas segmentation. The critical step here is that choosing 21 templates [optimal template number as demonstrated in previous work (Pipitone et al. 2014)], led to having 105 atlas-to-template labels before doing a label fusion with the majority vote technique. Concretely, even if up to 52 atlas-to-template labels were giving erroneous

information, these errors would not be propagated, because more than half (>53) would give correct information, which reduces tremendously the probability of propagating an error. Also, as reported in (Bhagwat, Pipitone, et al. 2016), there is minimal impact in the quality of the segmentation according to the label fusion technique choice.

Another limitation relevant to the generalization of our findings is that our study is to a considerable extent dependent on our segmentation protocol (Chakravarty, Steadman, et al. 2013; Pipitone et al. 2014). Although MAGeT Brain has been validated by several studies (Makowski et al. 2018; Pipitone et al. 2014) and widely used to study the hippocampal subfields (Patel, Steele, et al. 2020; Christine L Tardif, Devenyi, et al. 2018; Voineskos et al. 2015), it remains that our subfield definitions are one among the multitude of atlases used in the literature. Supplementary results comparing MAGeT and HIPS (Manjón, Romero, and Coupe 2022; Romero, Coupé, and Manjón 2017) segmentation techniques demonstrated almost similar relationships with age, highlighting that the relative preservation of the left CA1 with age for example was not due to a bias coming from MAGeT technique. Nonetheless, since HIPS uses the same atlases as MAGeT (J. L. Winterburn et al. 2013), here we solely investigated the impact of the segmentation technique choice but we did not investigate the impact of different subfield definitions. Thus, we also investigated ASHS segmentation technique which uses slab-specific anisotropic atlases as inputs. We did not find any difference in the volumetric age-relationships between MAGeT and ASHS outputs. However, as expected, overall volume differences were found between ASHS and MAGeT outputs, due to their different hippocampal subfield definitions. This highlights the importance of the work done by the Hippocampal Subfields Group (`http://www.hippocampalsubfields.com/`), which aims to standardize the definition of the medial temporal lobe segmentation, and to establish guidelines for subfield boundaries based on reference atlases and neuroanatomical landmarks visible *post-mortem* and on MRI (Olsen et al. 2019; Yushkevich, R. S. C. Amaral, et al. 2015). A critical follow-up study would be to repeat this study to compare the effect of the MRI sequence using the complete and validated segmentation protocol described by

the Hippocampal Subfield Group.

Outside of the sequence resolution and acquisition parameters, other parameters can impact segmentation quality. Of importance, the signal to noise ratio (SNR), CNR and partial volume effect (PVE) are critical measures. Specifically, small regions (<200 mm^3) such as CA2CA3, fimbria or MB subregions or regions that are not very thick relative to the voxel size, such as the SRLM, may be prone to the effects of PVE. The extent of the impact of PVE on our final results remains unclear, and thus interpretations of age-related trends should be done with caution. Nonetheless, previous work (G A Kerchner et al. 2010) has noted that the SRLM adjacent to the CA1 as being sensitive to the ageing process, which is in line with our findings. Additionally, other types of reliability measures, such as sharpness (Fonov and Louis Collins 2018; T. B. Shaw et al. 2019), would be of interest in future work.

A recently published commentary has highlighted concerns regarding the use of 1 mm^3 isotropic T1w scans for hippocampal subfield volumes studies (Laura E M Wisse, Gaël Chételat, et al. 2020). While this work is important and demonstrates the need to consider carefully the advantages and drawbacks of using T1w 1 mm^3 images, a balanced discussion on other sequence benefits and flaws have not been reviewed. In light of our findings, we would like to advocate that a careful examination of the trade-offs between the different acquisition types should be done.

Another limitation of this paper is that we only used volumetric measurements to study the hippocampus. Nonetheless, other techniques could be used such as morphological methods which have previously provided spatially localized information about age-related hippocampal modifications (Voineskos et al. 2015; Yang et al. 2013). Another approach using hippocampal thickness, curvature, inner and outer surface textures and gyrification, has proven subfield-specific AP differences (DeKraker et al. 2020). The main advantage of morphological analyses is that it is independent from subfield definitions, which could be of interest while a consensus definition of the subfields is attained and published by the Hippocampal subfield group or to look at more local and subtle age-related changes.

For researchers interested in volumetric relationships with age, we advocate the use of large age-range datasets since we demonstrated that most of our age-related relationships were non-linear with an inflection point occurring at approximately age 60. Slab anisotropic scans seemed to find different age-effects compared to those found with T1w and T2w isotropic images. Also, because of the characteristics of slab scans, we would suggest to be especially careful in the volume approximation of small structures, such as CA2CA3, fornix or MB, since these structures can be locally thinner than 2 mm. Moreover, we advise researchers using slab datasets to keep in mind that it is likely that in general the subfield volumes are smaller compared to the estimation from standard T1w images (Das et al. 2012). Also, while slab images have the great advantage of having the highest in-plane resolution where some of the most complicated subfield anatomical variation may occur, it clearly does so at the sacrifice of lower resolution in the anterior-to-posterior direction. Furthermore, the resulting voxel volume for the slab images used would be 0.32 mm^3 compared to 0.26 mm^3 for the T2w isotropic images we propose here. Finally, previous work from our own group demonstrated that the length of the long-axis is an important characteristic in the relationship of the hippocampus with age (Voineskos et al. 2015). Other groups have demonstrated a more highly curved hippocampus along the long axis in relation to age (Yang et al. 2013). In this context, we believe that the hippocampal shape modifications with age will cause issues at the level of resolving subfield borders that will increasingly "fall through the cracks" of the out of plane resolution limitations of the slab acquisition. To this end, it is critical to better examine the trade-offs between the different acquisition types carefully. Further, while investigating the accuracy of the segmentation protocols that we used (MAGeT, HIPS and ASHS) in the context of a "curving "hippocampus with age would be of interest, assessing the hippocampal shape would require a completely separate set of methods and analyses (such as voxel-based morphometry, deformation-based morphometry, or MAGeT surface-based morphometry measures for example), which unfortunately would be out of the scope of this study.

Finally, for new scanning protocols, we encourage researchers to consider using high-resolution isotropic T2w images, which have shown promising sensitivity and accuracy. T2w images also demonstrated smaller volumes in most of the subfields compared to T1w images, but we predict that they may better estimate the "true "volumes since they have higher isotropic resolution and contrast in key areas. T2w images rendered the same age-related relationships as T1w in most structures, although stronger age-related relationships were identified for the CA1 when compared to T1w images. Furthermore, high-resolution T2w images have demonstrated high-quality segmentation from visual inspection compared to slab and T1w scans (Figure 3.1), and provide whole brain images that permit hippocampal WM subregion investigation.

To conclude, we compared a wide range of datasets attempting to elucidate the relationship between hippocampal subfields with age. Certain subfields appeared to show reliable and reproducible relationships with age across various datasets. Nonetheless, the sensitivity of slab images to age-related changes in the hippocampus subfields deserves further exploratory analysis.

3.7 Supplementary materials

3.7.1 Participants

- **HA dataset** Here, we recruited 112 healthy individuals aged 18 to 80 and composed of 53 males and 58 females. The study was approved by the Research Ethics Board of the Douglas Mental Health University Institute in Montreal, Canada and written informed consent from all participants was obtained. Individuals with a history of PTSD, ADD/ADHD, bipolar disorder, schizophrenia, Alzheimer's, Parkinson's disease, physical injuries such as head trauma and concussion, alcohol or substance abuse were excluded. Participants with a MMSE score between 24-30 were considered eligible.

- **ADB dataset** ADB study evaluates volumetric differences in the architecture of brain circuitry in healthy seniors, seniors with MCI, and seniors with AD. For the purpose of the present study, we only included 66 healthy seniors, aged 56-81, 27 males and 41 females. We used the same inclusion and exclusion criteria than for the HA cohort for the recruitment of this sample.

- **ADNI dataset** ADNI is a publicly available longitudinal multicenter study which began in 2004 and was created to examine the progression of AD. Here we focused on the ADNI-3 cohort (Weiner et al. 2017) and included cross-sectional information from 317 healthy participants, aged 56-95, 118 males and 199 females. To be included in the ADNI cohort, participants must have MMSE scores between 24-30, a CDR of 0 and be non-depressed, non-MCI, and nondemented. Participants with any significant neurologic disease, evidence of infection, infarction, or other focal lesions or with a history of alcohol or substance abuse were excluded.

- **Cam-CAN dataset** Cam-CAN is a large-scale cross-sectional research project from the University of Cambridge, England and was launched in October 2010. Epidemiological, cognitive, and neuroimaging data were acquired to understand how individuals

can best retain cognitive abilities into old age. 652 healthy individuals, aged 18-88, 322 males and 330 females were included in our study. Participants were required to be cognitively healthy (MMSE 24-30), to meet hearing, vision, and English language ability criteria necessary for completing experimental tasks, and to be free of MRI or MEG contraindications and neurological or serious psychiatric conditions.

- **Test-retest dataset** The purpose of the test-retest dataset is to compare the volume estimates of the hippocampal subfields using different sequences of acquisition within the same subjects. Eighteen participants free of neurological disorders, aged 20-42 with a mean age of 26.9 including 7 males and 11 females were recruited in Montreal, Quebec, Canada.

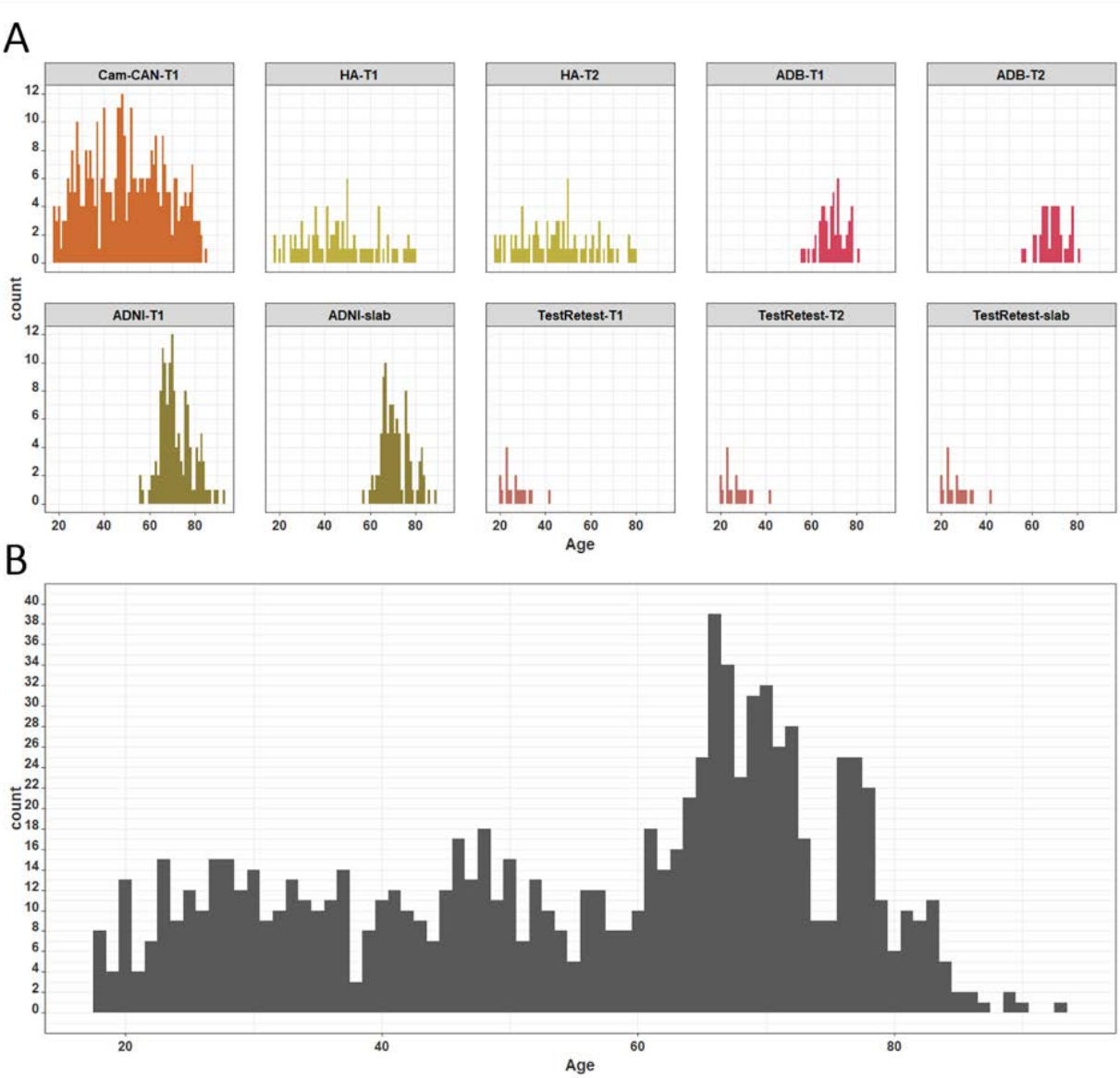

Figure 3.8: **A)** Age distribution by dataset and sequence type, **B)** Age distribution of the entire dataset.

3.7.2 Acquisition parameters

T1w 3D MPRAGE : TR=2300 ms, TE=2.01 ms, inversion time (TI)=900 ms, resolution =1 mm isotropic, FOV=192 x 240x 192 mm, flip angle=9 degrees, GRAPPA factor = 2, echo spacing=7.4 ms, bandwidth=240 Hz/Px.

High Resolution T2w 3D SPACE : TR=2500 ms, TE=198 ms, resolution = 0.64 mm , FOV =263 x 350 x 350 mm, CAIPIRINHA imaging, GRAPPA acceleration factor=2,

bandwidth=625 Hz/Px , echo train duration=483 ms, turbo factor=143.

Slab T2w 2D TSE: TR=8020 ms, TE=76 ms, slice thickness=2 mm, FOV=150 x 150 x 60 mm, flip angle=150 degrees, base resolution=384, 30 slices, interleaved slice acquisition, echo spacing=15.3 ms, bandwidth=107 Hz/Px, echo train per slice=48, turbo factor=8.

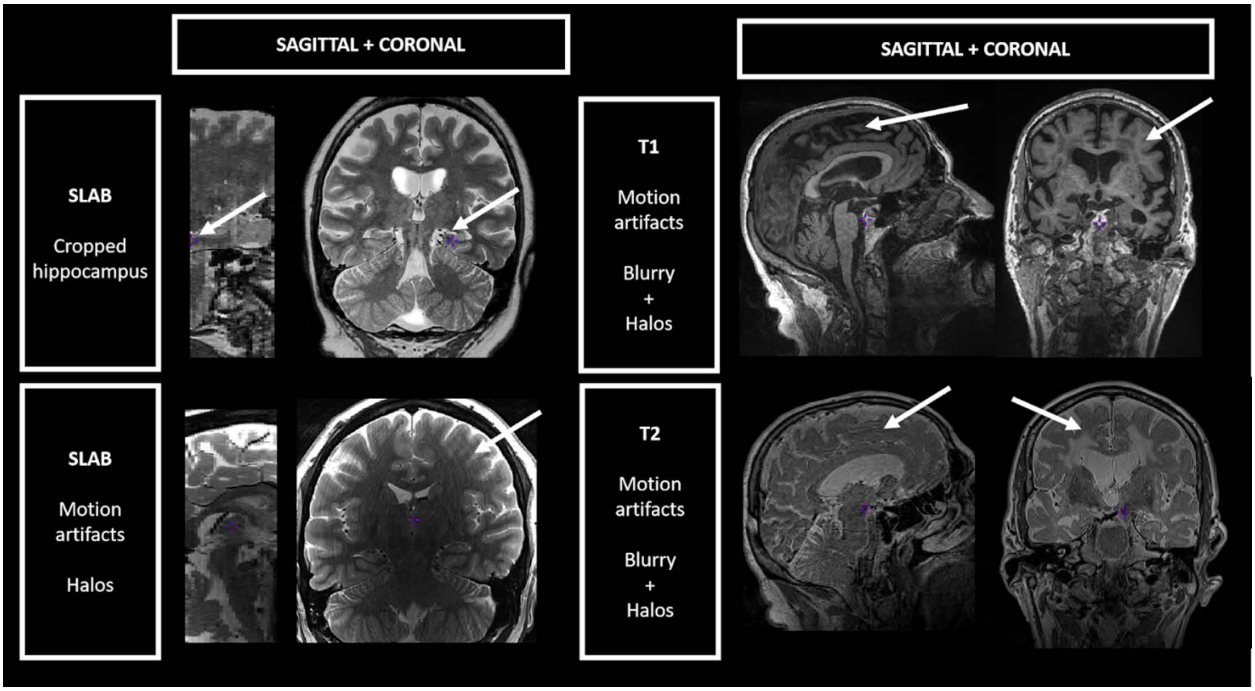

Figure 3.9: Examples of scans discarded due to inappropriate FOV or high motion artifacts. White arrows were added to indicate scan problems.

3.7.3 MAGET segmentation

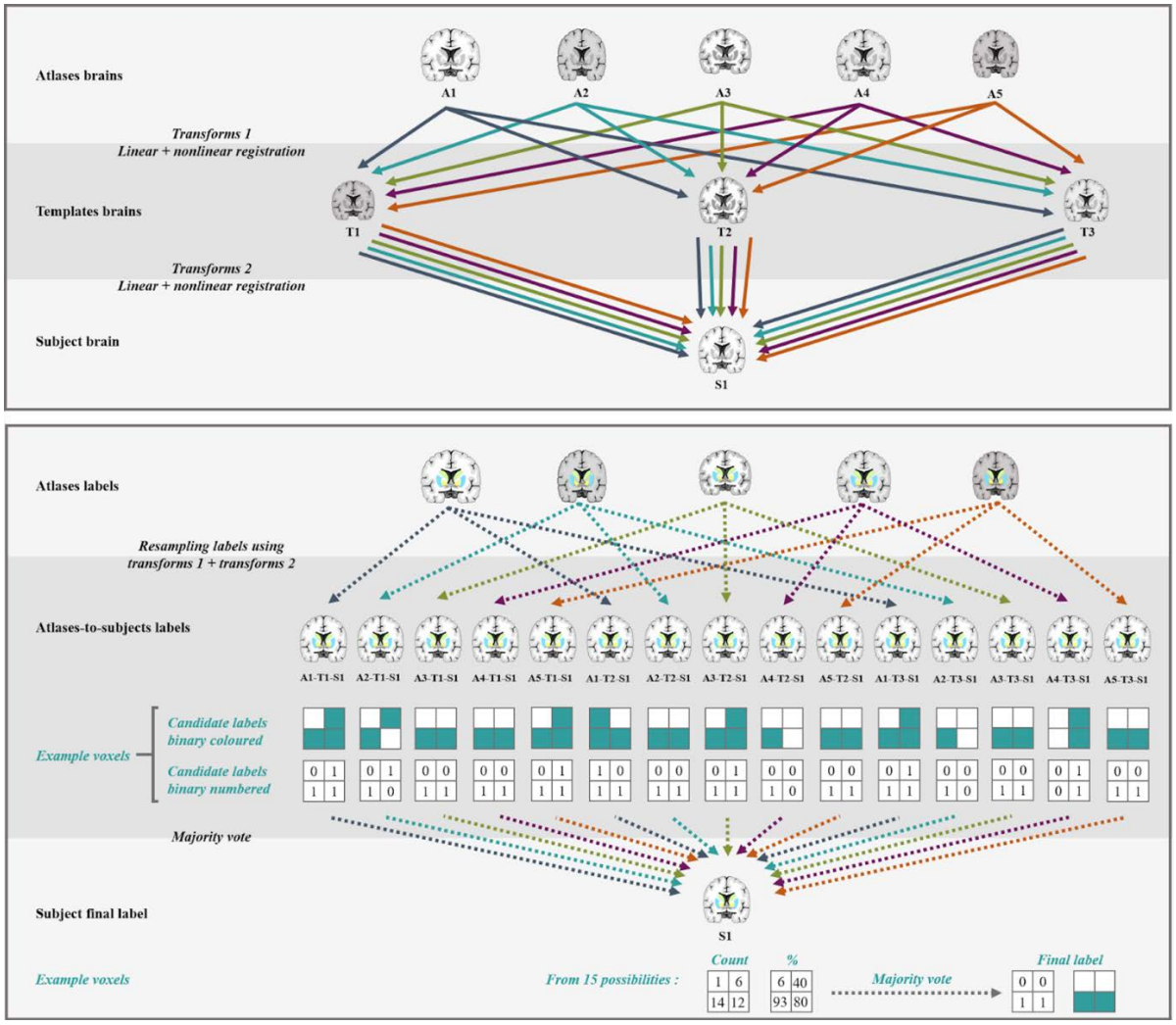

Figure 3.10: A schematic illustration of MAGeT segmentation. Upper figure: In this example, 5 atlases are used to segment one subject. The template library is created by sampling (either randomly or representatively) from the subject images; in this example 3 subjects were selected as templates (odd number of templates are prefered to avoid having even votes). Each atlas brain is registered to each template brain and each template is registered to the subjects. Lower figure: The atlases labels are propagated to each subject image by using the concatenated transformations (atlas-to-template + template-to-subject), creating 15 candidate labels (5 atlases x 3 templates). The candidate labels for each subject are then fused into a final segmentation by using majority vote.

3.7.4 All datasets normalized by the ICV

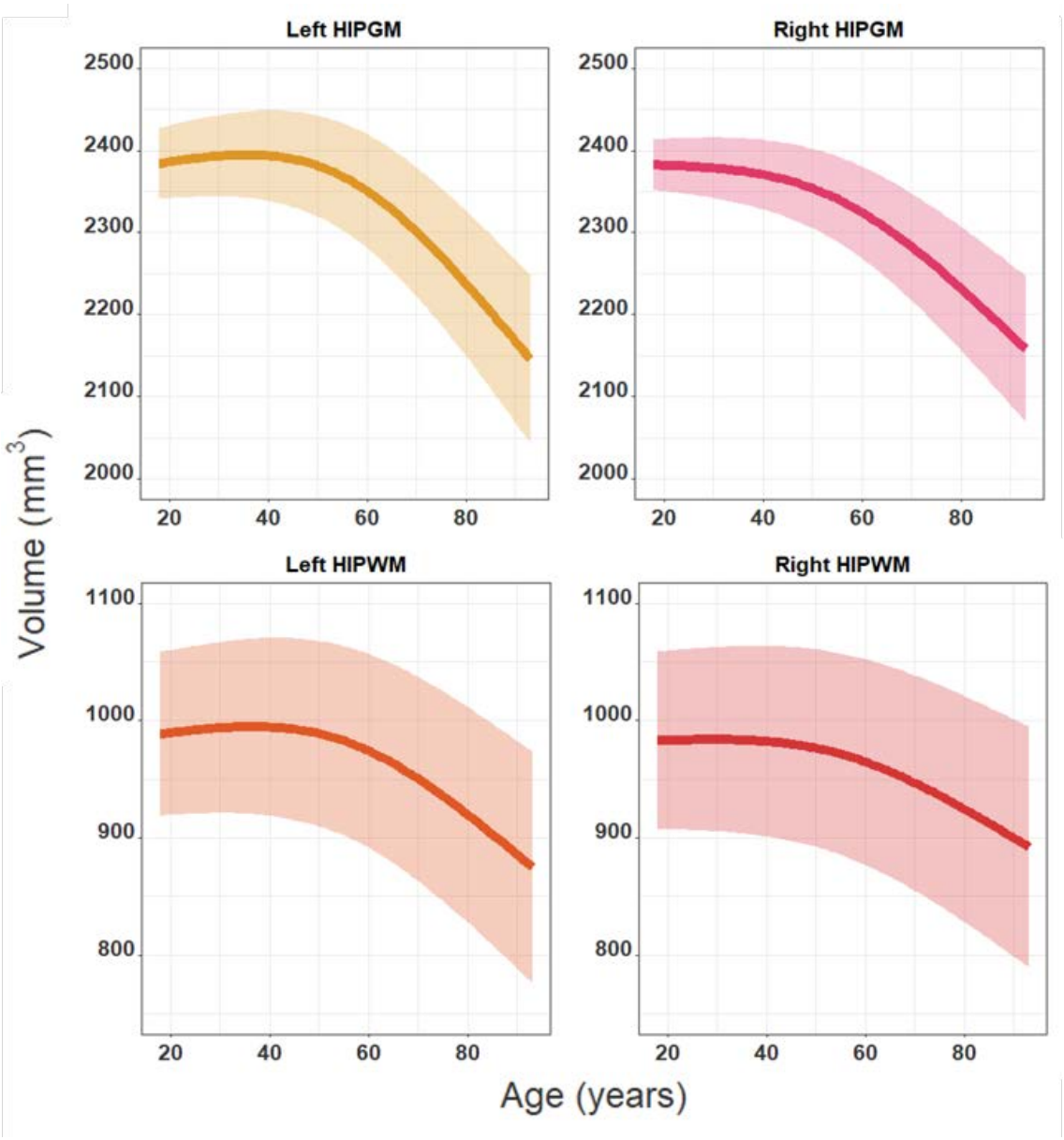

Figure 3.11: Best fit models showing the relationships between age and the hippocampal volume covaried by ICV and sex as fixed effects and dataset, sequence, and subjects as random effects. Second order relationships were found to be the best fit model for all the structures : right HIPGM (p=3.33x10-4), right HIPWM (p=1.05x10-3), left HIPGM (p=2.27x10-5) and left HIPWM (p=1.18x10-5).

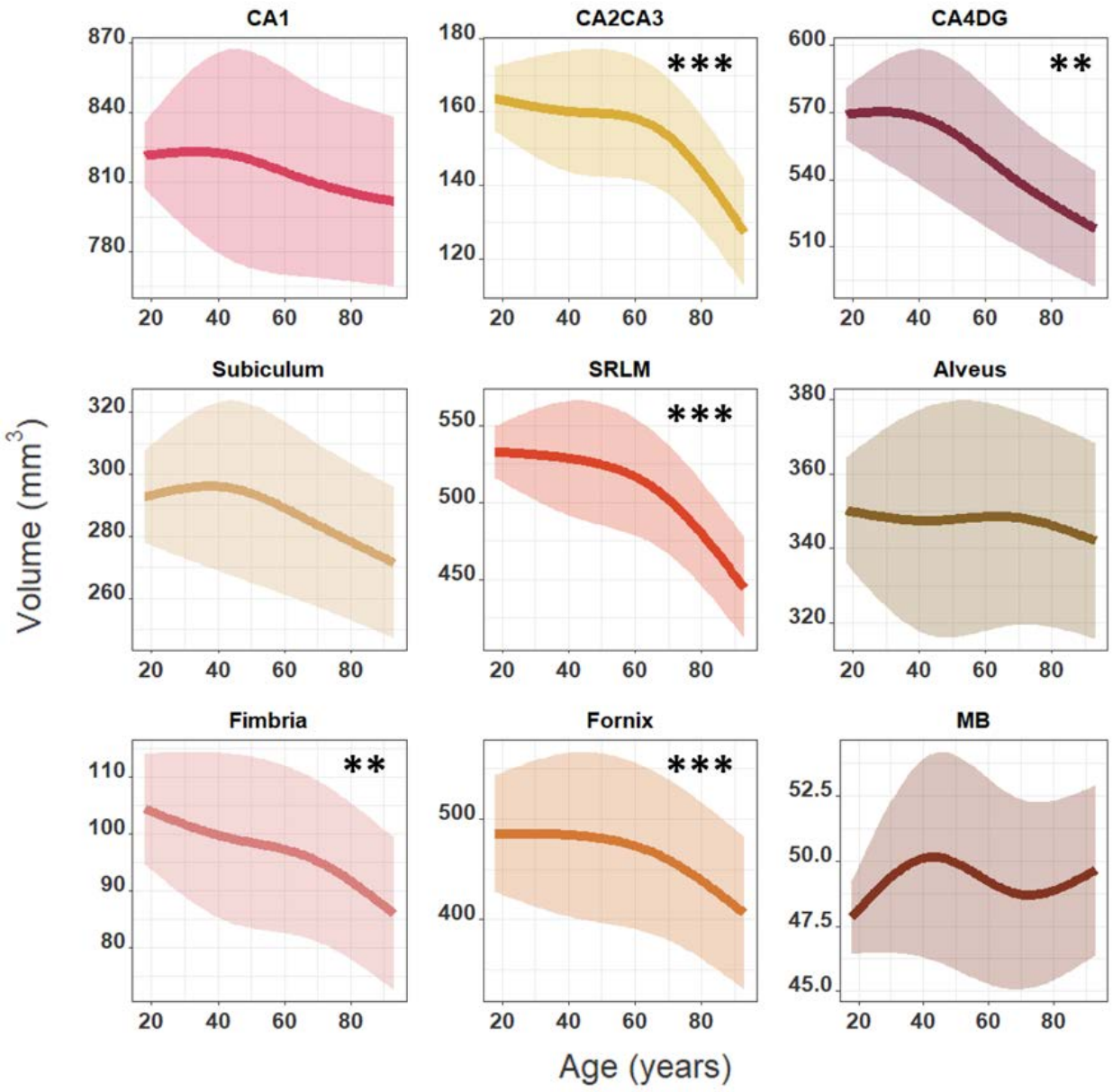

Figure 3.12: Best fit models showing the relationships between age and the volume of the right hippocampal subfields. Best fit models displayed for each subfield covaried by ICV and sex as fixed effects and dataset, sequence, and subject as random effects. Significant monotonic decreases were found for the right CA2CA3 (p=8.42x10-7), CA4DG (p=0.0085), SRLM (p=1.60x10-6), fimbria (p=0.0024) and fornix (p=4.79x10-4). Similar relationships were found in the left hemisphere. * p<0.05; ** p<0.01 and *** p<0.001 after Bonferroni correction.

3.7.5 All datasets normalized by the hippocampal volume

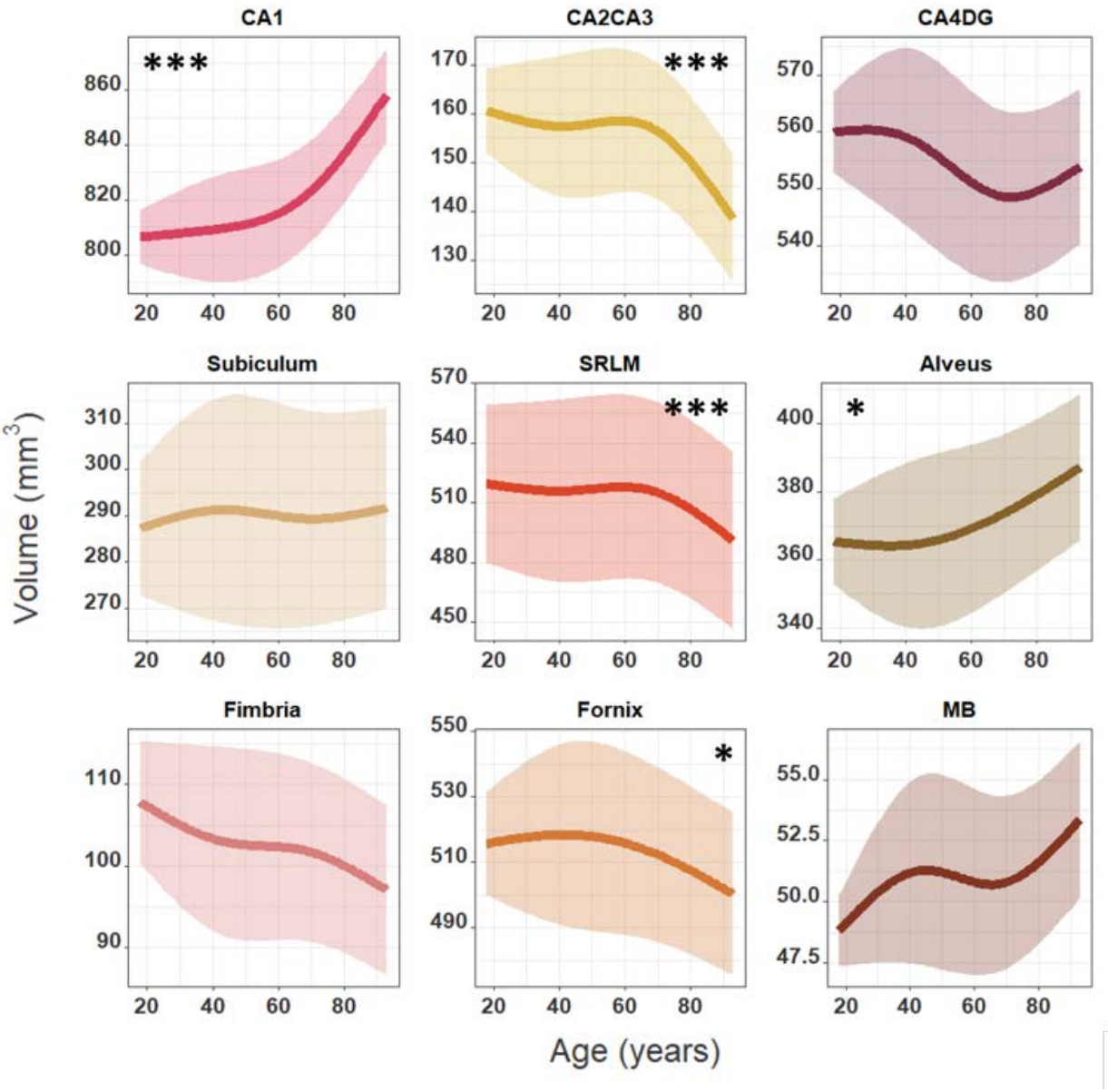

Figure 3.13: Best fit models showing the relationships between age and the volume of the right hippocampal subfields. Best fit models displayed for each subfield covaried by right hippocampal GM or WM volume, ICV and sex as fixed effects and dataset, sequence, and subject as random effects. Significant monotonic increases were found for the right CA1 (p=1.37x10-10) and alveus (p=0.010) and significant monotonic decreases were found for the right CA2CA3 (p=5.11x10-4), SRLM (p=7.99x10-7) and fornix (p=0.034). Similar relationships were found in the left hemisphere. * p<0.05; ** p<0.01 and *** p<0.001 after Bonferroni correction.

3.7.6 Impact of sequence on subfield volume relationship with age

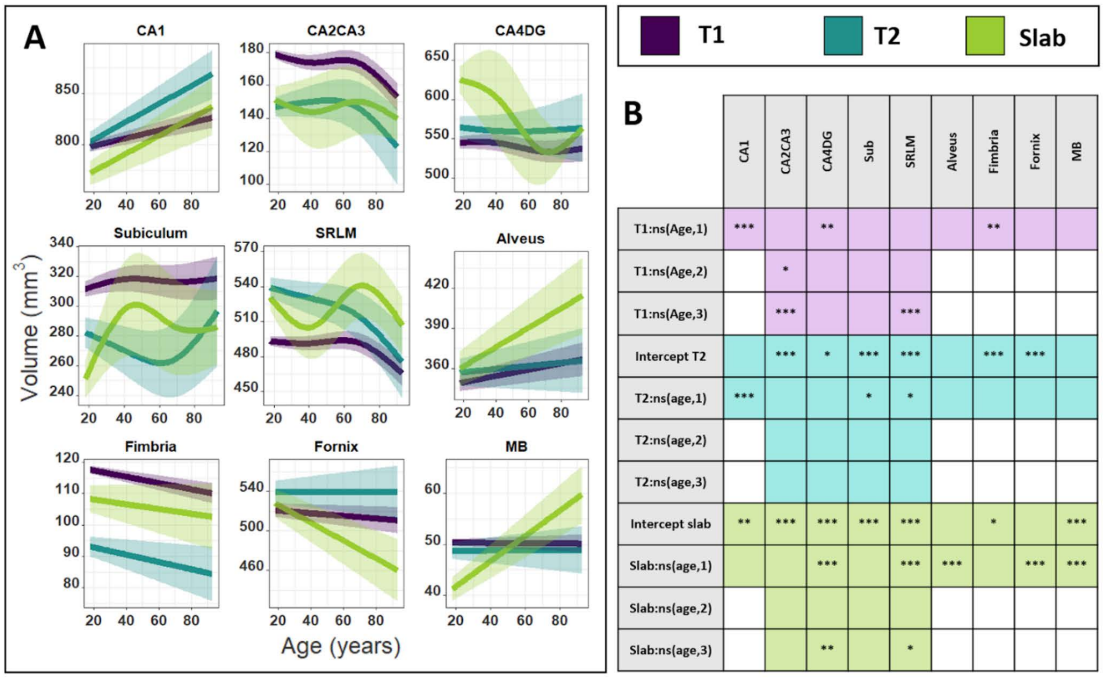

Figure 3.14: **A.** Estimated fixed effect plots showing the relationships, separated by sequence-type, between age and right hippocampal subfield volumes. Best fit models displayed for each subfield covaried by right hippocampal GM or WM volume, ICV and sex as fixed effects and dataset, sequence, and subject as random effects. **B.** Table describing the significant coefficients for the different relationships with age and the intercepts. T1w was used as reference sequence in the model and demonstrated a significant linear increase for CA1 (p=2.65x10-6), decrease for fimbria (p=9.85x10-3) and third order decrease for CA2CA3 (p=6.59x10-5) and SRLM (p=1.33x10-5). Significant differences were found with slab compared to T1w, with the CA1 (p=0.0102) and MB (p=3.47x10-14), demonstrating a steeper increase with age, while CA4DG (p=1.93x10-3) and fornix (p=9.41x10-7) showing a steeper decline with age. Best fit models estimated from the T2w sequence exhibited similar relationships with age than the models obtained with T1w images, except that T2w expressed steeper increase with age for CA1 (p=5.49x10-4). Furthermore, slab demonstrated significant smaller intercepts for CA1, CA2CA3, subiculum, fimbria, MB and larger intercepts for CA4DG and SRLM. T2w demonstrated significant smaller intercepts for CA2CA3, subiculum, fimbria and larger intercepts for CA4DG, SRLM and fornix. * p<0.05; ** p<0.01 and *** p<0.001 after Bonferroni correction.

3.7.7 Impact of different sequence on hippocampal subfield volumes estimates

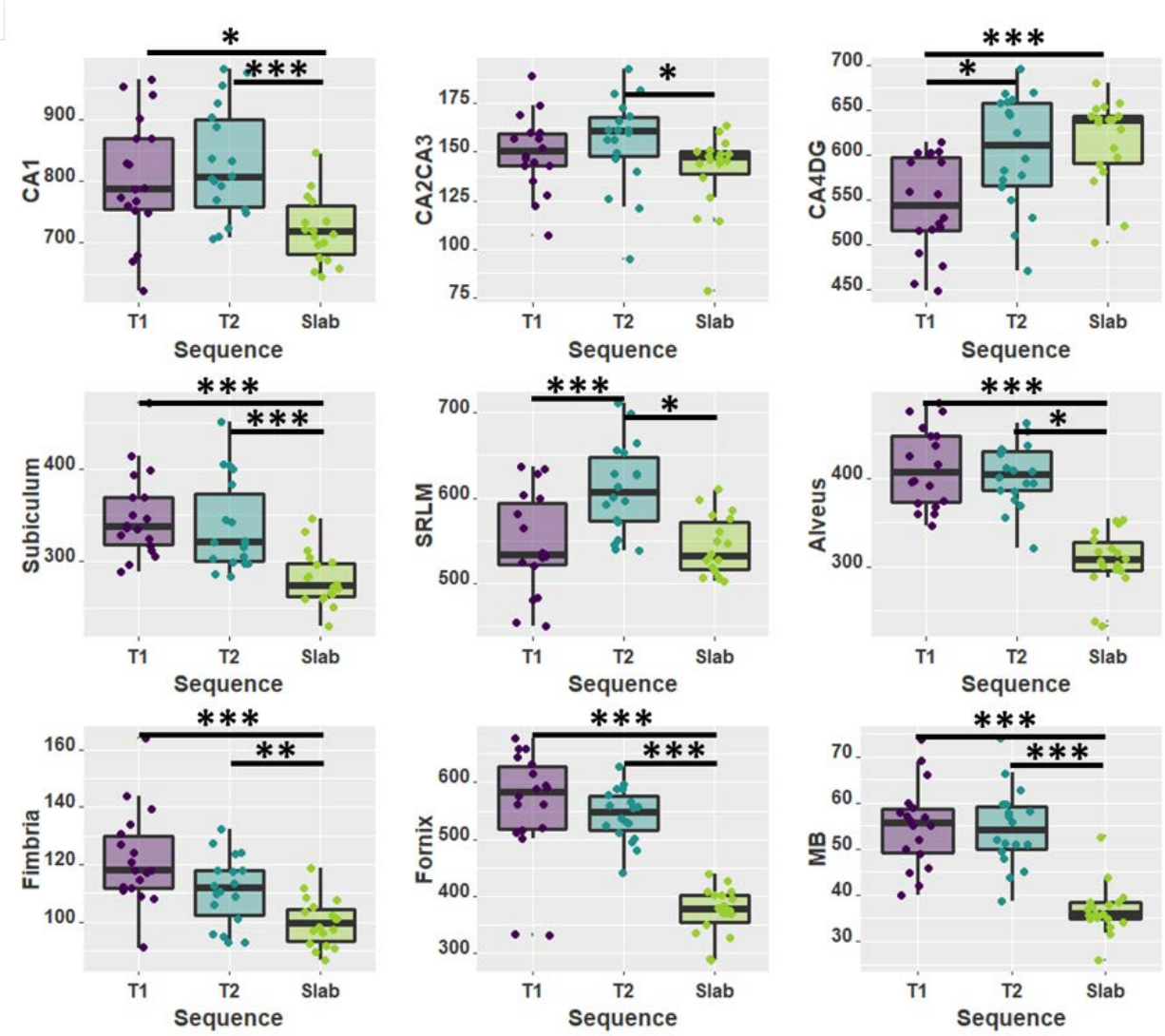

Figure 3.15: Boxplot comparing the left volume estimates from T1w, T2w and slab sequences from the same participants. Statistical tests performed using dependent 2-group Wilcoxon signed rank test. * $p<0.05$; ** $p<0.01$ and *** $p<0.001$ after Bonferroni correction for 54 comparisons (18 subfields x 3 sequence types).

3.7.8 CNR mask creation

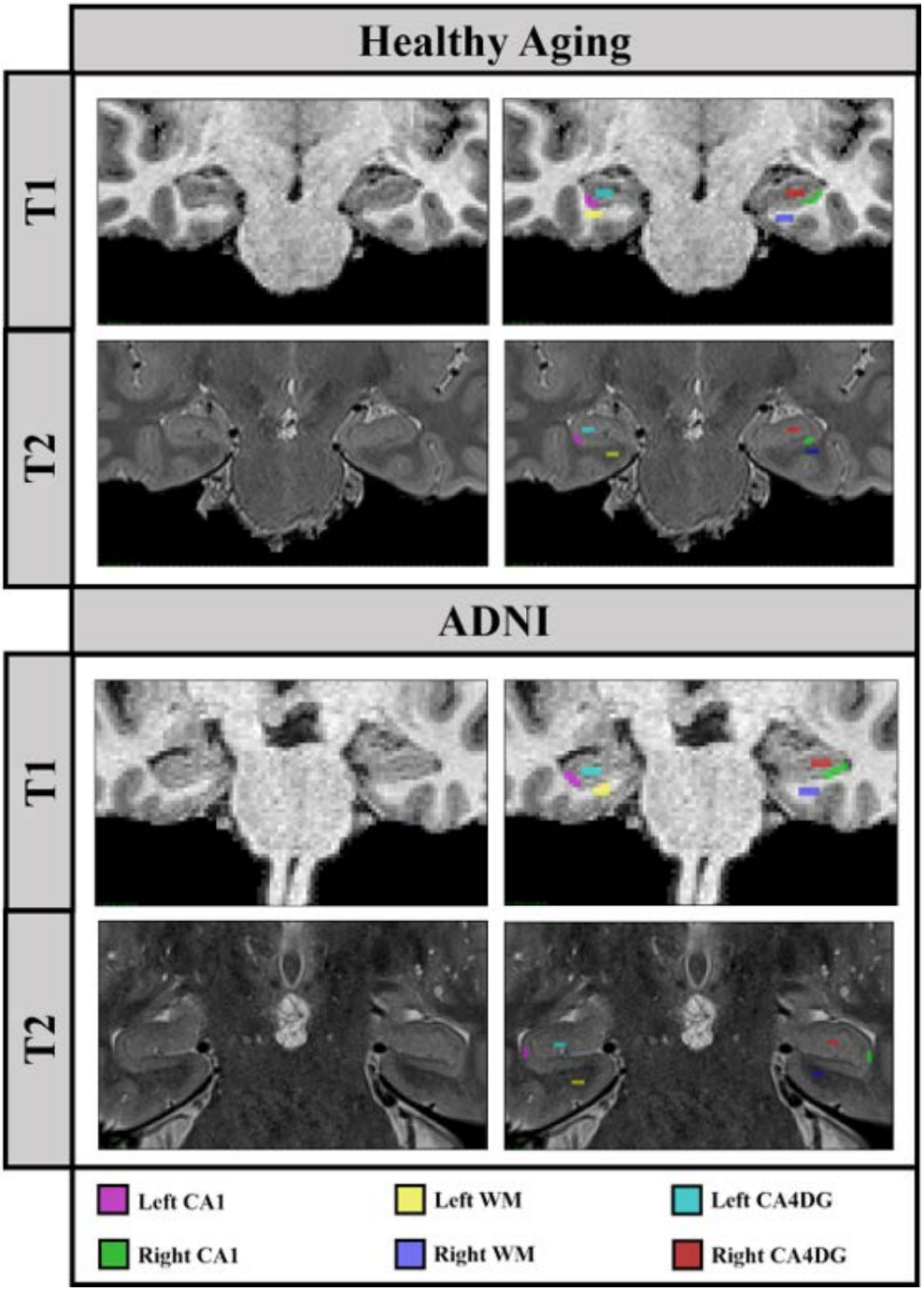

Figure 3.16: Examples of the mask definitions of the CA1, CA4DG and WM in one participant (25 years old male) from the HA dataset (masks defined in both T1w and T2w images) and one participant (66 years old female) from the ADNI dataset (masks defined in both T1w and slab images).

3.7.9 CNR relationship with age

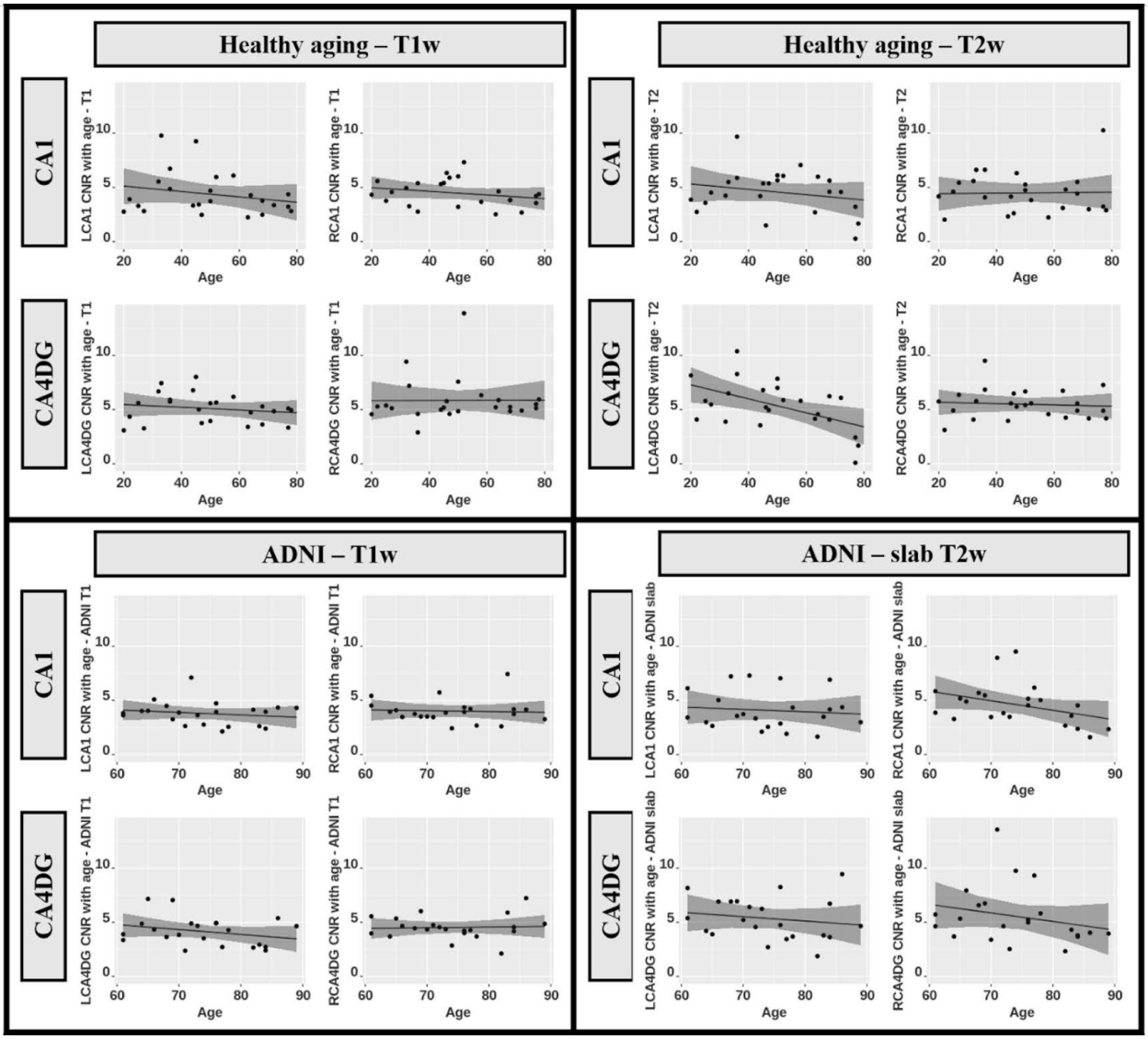

Figure 3.17: CNR in T1w and T2w images from HA and ADNI dataset. Left CA4DG in HA T2w demonstrated a significant decrease with age. However, with Bonferroni correction, no subfield indicated a significant CNR change with age.

3.7.10 HIPS comparison

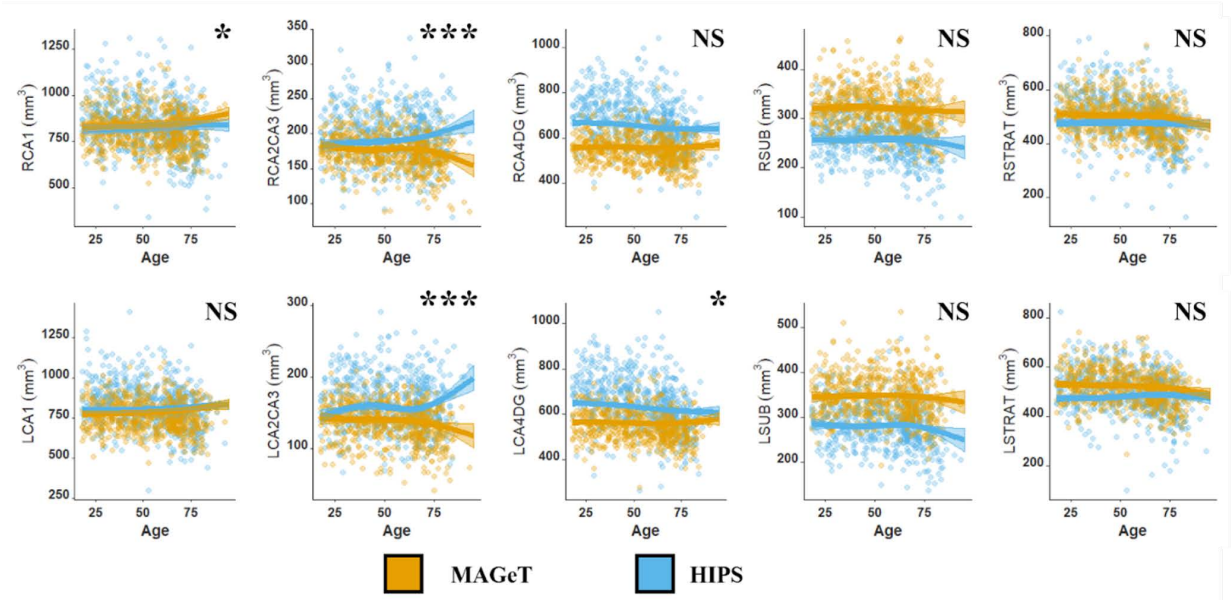

Figure 3.18: Comparison of the hippocampal subfields age-relationships between HIPS (in blue) and MAGeT (in orange) techniques. Third order models displayed for each subfield covaried by ICV, right or left total hippocampal volume, and sex as fixed effects and, dataset and subject as random effects. * $p<0.05$; ** $p<0.01$ and *** $p<0.001$ after Bonferroni correction.

3.7.11 ASHS comparison

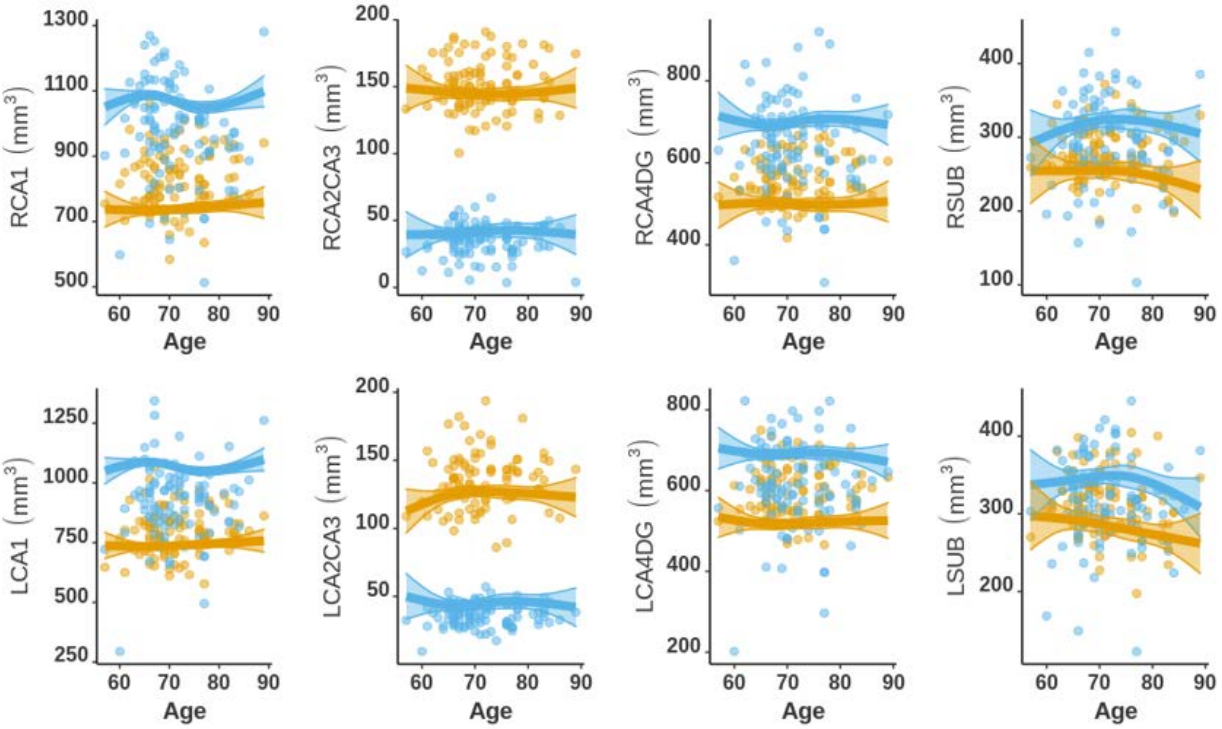

Figure 3.19: Comparison of the hippocampal subfields age-relationships between ASHS (in blue) and MAGeT (in orange) techniques. Third order models displayed for each subfield covaried by ICV, right or left total hippocampal volume, and sex as fixed effects and, subject as random effects. None of the subfields expressed a significant effect of the segmentation technique on the age-relationships.

3.7.12 Demographic information

	ADB (np=68) (ns=136)	**ADNI** (np=317) (ns=617)	**Cam-CAN** (np=652) (ns=652)	**HA** (np=111) (ns=222)	**Test-retest** (np=21) (ns=63)	**Overall** (np=1169) (ns=1690)
Age						
Mean	69.7	73.9	54.3	45.6	27.0	60.6
(SD)	(5.7)	(8.0)	(18.6)	(16.4)	(5.9)	(18.8)
Median	70.0	72	54.5	44.0	27.0	67
[Min, Max]	[56.0, 81.0]	[56.0, 95.0]	[18.0, 88.0]	[18.0, 95.0]	[20.0, 42.0]	[18.0, 95.0]
Sex						
F	82 (60.3%)	387 (62.7%)	330 (50.6%)	116 (52.3%)	39 (61.9%)	954 (58.4%)
M	54 (39.7%)	230 (37.3%)	322 (49.4%)	106 (47.7%)	24 (38.1%)	736 (41.6%)
Sequence						
T1	68 (50.0%)	317 (51.4%)	652 (100%)	111 (50.0%)	21 (33.0%)	1169 (69.2%)
T2	68 (50.0%)	0 (0.0%)	0 (0.0%)	111 (50.0%)	21 (33.0%)	200 (11.8%)
Slab	0 (0.0%)	300 (48.6%)	0 (0.0%)	0 (0.0%)	21 (33.0%)	321 (19.0%)

Table 3.3: Demographics by dataset: Initial sample across HA, ADB, ADNI, and Cam-CAN. *np = number of participants; ns = number of scans.*

3.7.13 Supplementary tables

3.7.14 Comparison volume estimates from T1w, T2w and slab sequences

	Left						Right					
	T1 vs T2		T1 vs Slab		T2 vs Slab		T1 vs T2		T1 vs Slab		T2 vs Slab	
	%	p value	%	p value	%	p value	%	p value	%	p value	%	p value
CA1	-3.9	NS	9.6	0.018	12.3	NS	2.8	NS	11.2	8.2e-4	8.1	0.01
CA2CA3	-4.1	NS	6.0	NS	9.5	NS	11.6	0.0029	19.4	4.1e-4	8.5	0.01
CA4DG	-11.4	0.018	-13.5	4.1e-4	-2.4	0.018	-5.1	NS	-9.2	8.2e-4	-4.1	NS
Subiculum	3.0	NS	19.0	4.1e-4	16.0	NS	3.7	NS	14.7	8.2e-4	11.1	0.020
SRLM	-12.6	8.2e-4	0.2	NS	10.6	8.2e-4	-12.8	0.0012	0.5	NS	11.4	4.1e-4
Alveus	1.7	NS	25.1	4.1e-4	23.5	NS	-1.0	NS	19.0	7.6e-6	19.6	4.1e-4
Fimbria	7.9	NS	17.3	4.1e-4	9.5	NS	15.9	0.012	24.7	0.012	10.2	0.027
Fornix	0.1	NS	31.9	4.1e-4	30.9	NS	3.0	NS	36.5	7.6e-6	33.7	4.1e-4
MB	0.0	NS	32.7	4.1e-4	32.2	NS	-5.1	NS	23.7	7.6e-6	26.9	4.1e-4

Table 3.4: Percentage of volume difference between each sequence type and p-values obtained with dependent 2-group Wilcoxon signed rank test used to compare the volume estimates from T1w, T2w and slab sequences. Bonferroni correction adjusted for 54 multiple comparisons (18 subfields x 3 sequence types) employed. Bold p-values demonstrate significant results.

References Chapter 3

Adler, Daniel H, John Pluta, et al. (Jan. 2014). "Histology-derived volumetric annotation of the human hippocampal subfields in postmortem MRI". en. In: *Neuroimage* 84, pp. 505–523.

Adler, Daniel H, Laura E M Wisse, et al. (Apr. 2018). "Characterizing the human hippocampus in aging and Alzheimer's disease using a computational atlas derived from ex vivo MRI and histology". en. In: *Proc. Natl. Acad. Sci. U. S. A.* 115.16, pp. 4252–4257.

Akaike, Hirotugu (1974). "A New Look at the Statistical Model Identification". In: *Springer Ser. Statist.*, pp. 215–222.

Amaral, Robert S C et al. (Apr. 2018). "Manual segmentation of the fornix, fimbria, and alveus on high-resolution 3T MRI: Application via fully-automated mapping of the human memory circuit white and grey matter in healthy and pathological aging". en. In: *Neuroimage* 170, pp. 132–150.

Avants, B B et al. (Feb. 2008). "Symmetric diffeomorphic image registration with cross-correlation: evaluating automated labeling of elderly and neurodegenerative brain". en. In: *Med. Image Anal.* 12.1, pp. 26–41.

Bedford, Saashi A et al. (Mar. 2020). "Large-scale analyses of the relationship between sex, age and intelligence quotient heterogeneity and cortical morphometry in autism spectrum disorder". en. In: *Mol. Psychiatry* 25.3, pp. 614–628.

Bellon, E M et al. (Dec. 1986). "MR artifacts: a review". en. In: *AJR Am. J. Roentgenol.* 147.6, pp. 1271–1281.

Bender, Andrew R et al. (Feb. 2018). "Optimization and validation of automated hippocampal subfield segmentation across the lifespan". en. In: *Hum. Brain Mapp.* 39.2, pp. 916–931.

Bhagwat, Nikhil, Jon Pipitone, et al. (July 2016). "Manual-Protocol Inspired Technique for Improving Automated MR Image Segmentation during Label Fusion". en. In: *Front. Neurosci.* 10, p. 325.

Bobinski, M et al. (2000). "The histological validation of post mortem magnetic resonance imaging-determined hippocampal volume in Alzheimer's disease". en. In: *Neuroscience* 95.3, pp. 721–725.

Braak, H and E Braak (1991b). "Neuropathological stageing of Alzheimer-related changes". In: *Acta Neuropathol.* 82.4, pp. 239–259.

Braak, Heiko, Irina Alafuzoff, et al. (Oct. 2006). "Staging of Alzheimer disease-associated neurofibrillary pathology using paraffin sections and immunocytochemistry". en. In: *Acta Neuropathol.* 112.4, pp. 389–404.

Bussy, Aurélie, Eric Plitman, et al. (June 2021). "Hippocampal subfield volumes across the healthy lifespan and the effects of MR sequence on estimates". en. In: *Neuroimage* 233, p. 117931.

Bussy, Aurélie, B Joy Snider, et al. (Mar. 2019). "Effect of apolipoprotein E4 on clinical, neuroimaging, and biomarker measures in noncarrier participants in the Dominantly Inherited Alzheimer Network". en. In: *Neurobiol. Aging* 75, pp. 42–50.

Campbell, Stephanie and Glenda MacQueen (2004). "The role of the hippocampus in the pathophysiology of major depression". In: *J. Psychiatry Neurosci.* 6.

Chakravarty, M Mallar, M Mallar Chakravarty, et al. (2009). "Comparison of piece-wise linear, linear, and nonlinear atlas-to-patient warping techniques: Analysis of the labeling of subcortical nuclei for functional neurosurgical applications". In: *Hum. Brain Mapp.* 30.11, pp. 3574–3595.

Chakravarty, M Mallar, Abbas F Sadikot, et al. (Dec. 2008). "Towards a validation of atlas warping techniques". en. In: *Med. Image Anal.* 12.6, pp. 713–726.

Chakravarty, M Mallar, Patrick Steadman, et al. (Oct. 2013). "Performing label-fusion-based segmentation using multiple automatically generated templates". en. In: *Hum. Brain Mapp.* 34.10, pp. 2635–2654.

Cherbuin, Nicolas et al. (Oct. 2007). "Neuroimaging and APOE genotype: a systematic qualitative review". en. In: *Dement. Geriatr. Cogn. Disord.* 24.5, pp. 348–362.

Chételat, G et al. (Jan. 2008). "Three-dimensional surface mapping of hippocampal atrophy progression from MCI to AD and over normal aging as assessed using voxel-based morphometry". en. In: *Neuropsychologia* 46.6, pp. 1721–1731.

Cicchetti, Domenic V (1994). "Guidelines, criteria, and rules of thumb for evaluating normed and standardized assessment instruments in psychology". In: *Psychol. Assess.* 6.4, p. 284.

Collins, D L et al. (Mar. 1994). "Automatic 3D intersubject registration of MR volumetric data in standardized Talairach space". en. In: *J. Comput. Assist. Tomogr.* 18.2, pp. 192–205.

Corder, E H et al. (Aug. 1993). "Gene dose of apolipoprotein E type 4 allele and the risk of Alzheimer's disease in late onset families". en. In: *Science* 261.5123, pp. 921–923.

Coupé, Pierrick, Gwenaelle Catheline, et al. (Nov. 2017). "Towards a unified analysis of brain maturation and aging across the entire lifespan: A MRI analysis". en. In: *Hum. Brain Mapp.* 38.11, pp. 5501–5518.

Dadar, Mahsa et al. (July 2018). "A comparison of publicly available linear MRI stereotaxic registration techniques". en. In: *Neuroimage* 174, pp. 191–200.

Das, Sandhitsu R et al. (Apr. 2012). "Measuring longitudinal change in the hippocampal formation from in vivo high-resolution T2-weighted MRI". en. In: *Neuroimage* 60.2, pp. 1266–1279.

Daugherty, Ana M et al. (Feb. 2016). "Age differences in hippocampal subfield volumes from childhood to late adulthood". en. In: *Hippocampus* 26.2, pp. 220–228.

DeKraker, J et al. (Feb. 2020). "Hippocampal subfields revealed through unfolding and unsupervised clustering of laminar and morphological features in 3D BigBrain". en. In: *Neuroimage* 206, p. 116328.

DeKraker, Jordan et al. (Feb. 2018). "Unfolding the hippocampus: An intrinsic coordinate system for subfield segmentations and quantitative mapping". en. In: *Neuroimage* 167, pp. 408–418.

Derix, Johanna et al. (2014). "Visualization of the amygdalo-hippocampal border and its structural variability by 7T and 3T magnetic resonance imaging". In: *Hum. Brain Mapp.* 35.9, pp. 4316–4329.

Ding, Song-Lin and Gary W Van Hoesen (2015). "Organization and detailed parcellation of human hippocampal head and body regions based on a combined analysis of Cyto- and chemoarchitecture". In: *J. Comp. Neurol.* 523.15, pp. 2233–2253.

Dounavi, Maria-Eleni et al. (Mar. 2020). "Volumetric alterations in the hippocampal subfields of subjects at increased risk of dementia". In: *Neurobiol. Aging* 91, pp. 36–44.

Duvernoy, Henri M (June 2005). *The Human Hippocampus: Functional Anatomy, Vascularization and Serial Sections with MRI*. en. Springer Science & Business Media.

Duvernoy, Henri M, Francoise Cattin, and Pierre-Yves Risold (June 2013). *The Human Hippocampus: Functional Anatomy, Vascularization and Serial Sections with MRI*. en. Springer Science & Business Media.

Dwork, A J (1997). "Postmortem Studies of the Hippocampal Formation in Schizophrenia". In: *Schizophr. Bull.* 23.3, pp. 385–402.

Eriksson, Sofia H et al. (Jan. 2008). "PROPELLER MRI visualizes detailed pathology of hippocampal sclerosis". en. In: *Epilepsia* 49.1, pp. 33–39.

Eskildsen, Simon F et al. (Feb. 2012). "BEaST: brain extraction based on nonlocal segmentation technique". en. In: *Neuroimage* 59.3, pp. 2362–2373.

Flores, Robin de, Renaud La Joie, and Gaël Chételat (Nov. 2015). "Structural imaging of hippocampal subfields in healthy aging and Alzheimer's disease". en. In: *Neuroscience* 309, pp. 29–50.

Flores, Robin de, Renaud La Joie, Brigitte Landeau, et al. (Feb. 2015). "Effects of age and Alzheimer's disease on hippocampal subfields: comparison between manual and FreeSurfer volumetry". en. In: *Hum. Brain Mapp.* 36.2, pp. 463–474.

Fonov, Vladimir S and D Louis Collins (Mar. 2018). "Comparison of different methods for average anatomical templates creation: do we really gain anything from a diffeomorphic framework?" en.

Frisoni, Giovanni B, Rossana Ganzola, et al. (Dec. 2008). "Mapping local hippocampal changes in Alzheimer's disease and normal ageing with MRI at 3 Tesla". en. In: *Brain* 131.Pt 12, pp. 3266–3276.

Gonneaud, Julie et al. (Oct. 2016). "Relative effect of APOE $\epsilon 4$ on neuroimaging biomarker changes across the lifespan". en. In: *Neurology* 87.16, pp. 1696–1703.

Good, C D et al. (July 2001). "A voxel-based morphometric study of ageing in 465 normal adult human brains". en. In: *Neuroimage* 14.1 Pt 1, pp. 21–36.

Habes, M et al. (Sept. 2016). "Relationship between APOE Genotype and Structural MRI Measures throughout Adulthood in the Study of Health in Pomerania Population-Based Cohort". en. In: *AJNR Am. J. Neuroradiol.* 37.9, pp. 1636–1642.

Heckers, S (2001). "Neuroimaging studies of the hippocampus in schizophrenia". en. In: *Hippocampus* 11.5, pp. 520–528.

Iglesias, Juan Eugenio, Jean C Augustinack, et al. (July 2015). "A computational atlas of the hippocampal formation using ex vivo, ultra-high resolution MRI: Application to adaptive segmentation of in vivo MRI". en. In: *Neuroimage* 115, pp. 117–137.

Iosifescu, D V et al. (July 1997). "An automated registration algorithm for measuring MRI subcortical brain structures". en. In: *Neuroimage* 6.1, pp. 13–25.

Jack Jr, Clifford R, Matt A Bernstein, et al. (2008). "The Alzheimer's disease neuroimaging initiative (ADNI): MRI methods". In: *Journal of Magnetic Resonance Imaging: An Official Journal of the International Society for Magnetic Resonance in Medicine* 27.4, pp. 685–691.

Kerchner, G A et al. (Oct. 2010). "Hippocampal CA1 apical neuropil atrophy in mild Alzheimer disease visualized with 7-T MRI". en. In: *Neurology* 75.15, pp. 1381–1387.

Kerchner, Geoffrey A et al. (Feb. 2014). "APOE ϵ4 worsens hippocampal CA1 apical neuropil atrophy and episodic memory". en. In: *Neurology* 82.8, pp. 691–697.

Knight, Michael J et al. (Dec. 2016). "Quantitative T1 and T2 MRI signal characteristics in the human brain: different patterns of MR contrasts in normal ageing". en. In: *MAGMA* 29.6, pp. 833–842.

Kulaga-Yoskovitz, Jessie et al. (Nov. 2015). "Multi-contrast submillimetric 3 Tesla hippocampal subfield segmentation protocol and dataset". en. In: *Sci Data* 2, p. 150059.

Kurth, Florian, Nicolas Cherbuin, and Eileen Luders (Dec. 2017). "The impact of aging on subregions of the hippocampal complex in healthy adults". en. In: *Neuroimage* 163, pp. 296–300.

La Joie, Renaud, Marine Fouquet, et al. (Nov. 2010). "Differential effect of age on hippocampal subfields assessed using a new high-resolution 3T MR sequence". en. In: *Neuroimage* 53.2, pp. 506–514.

Laakso, M P, G B Frisoni, et al. (June 2000). "Hippocampus and entorhinal cortex in frontotemporal dementia and Alzheimer's disease: a morphometric MRI study". en. In: *Biol. Psychiatry* 47.12, pp. 1056–1063.

Makowski, Carolina et al. (Apr. 2018). "Evaluating accuracy of striatal, pallidal, and thalamic segmentation methods: Comparing automated approaches to manual delineation". en. In: *Neuroimage* 170, pp. 182–198.

Malykhin, Nikolai V, Rawle Carter, et al. (Sept. 2010). "Structural changes in the hippocampus in major depressive disorder: contributions of disease and treatment". en. In: *J. Psychiatry Neurosci.* 35.5, pp. 337–343.

Malykhin, Nikolai V, Yushan Huang, et al. (Nov. 2017). "Differential vulnerability of hippocampal subfields and anteroposterior hippocampal subregions in healthy cognitive aging". en. In: *Neurobiol. Aging* 59, pp. 121–134.

Manjón, José V, José E Romero, and Pierrick Coupe (Jan. 2022). "A novel deep learning based hippocampus subfield segmentation method". en. In: *Sci. Rep.* 12.1, p. 1333.

Marques, José P and David G Norris (2018). "How to choose the right MR sequence for your research question at 7 T and above?" In: *Neuroimage* 168, pp. 119–140.

Mazerolle, Marc (Jan. 2006). "Improving data analysis in herpetology: using Akaike's Information Criterion (AIC) to assess the strength of biological hypotheses". en. In: *Amphib-reptil.* 27.2, pp. 169–180.

Mueller, S G et al. (May 2007). "Measurement of hippocampal subfields and age-related changes with high resolution MRI at 4T". en. In: *Neurobiol. Aging* 28.5, pp. 719–726.

Mueller, Susanne G and Michael W Weiner (June 2009). "Selective effect of age, Apo e4, and Alzheimer's disease on hippocampal subfields". en. In: *Hippocampus* 19.6, pp. 558–564.

Mueller, Susanne G, Paul A Yushkevich, et al. (2018). "Systematic comparison of different techniques to measure hippocampal subfield volumes in ADNI2". In: *NeuroImage: Clinical* 17, pp. 1006–1018.

Mugler III, John P and James R Brookeman (1990). "Three-dimensional magnetization-prepared rapid gradient-echo imaging (3D MP RAGE)". In: *Magn. Reson. Med.* 15.1, pp. 152–157.

Muñoz-Ruiz, Miguel Ángel et al. (Dec. 2012). "Structural MRI in frontotemporal dementia: comparisons between hippocampal volumetry, tensor-based morphometry and voxel-based morphometry". en. In: *PLoS One* 7.12, e52531.

Nelson, Michael D et al. (1997). "Hippocampal volume reduction in schizophrenia as assessed by magnetic resonance imaging: A meta-analytic study". In: *Schizophr. Res.* 24.1-2, p. 153.

Olsen, Rosanna K et al. (Dec. 2019). "Progress update from the hippocampal subfields group". en. In: *Alzheimers. Dement.* 11, pp. 439–449.

Parekh, Mansi B et al. (May 2015). "Ultra-high resolution in-vivo 7.0T structural imaging of the human hippocampus reveals the endfolial pathway". en. In: *Neuroimage* 112, pp. 1–6.

Patel, Raihaan, Christopher J Steele, et al. (Feb. 2020). "Investigating microstructural variation in the human hippocampus using non-negative matrix factorization". en. In: *Neuroimage* 207, p. 116348.

Pereira, Joana B et al. (Apr. 2014). "Regional vulnerability of hippocampal subfields to aging measured by structural and diffusion MRI". en. In: *Hippocampus* 24.4, pp. 403–414.

Pipitone, Jon et al. (Nov. 2014). "Multi-atlas segmentation of the whole hippocampus and subfields using multiple automatically generated templates". en. In: *Neuroimage* 101, pp. 494–512.

Pluta, John et al. (2012). "In vivo analysis of hippocampal subfield atrophy in mild cognitive impairment via semi-automatic segmentation of T2-weighted MRI". en. In: *J. Alzheimers. Dis.* 31.1, pp. 85–99.

Pol, L A van de et al. (2006). "Hippocampal atrophy in Alzheimer disease: Age matters". In: *Neurology* 66.2, pp. 236–238.

Rawle, Mark James et al. (2018). "Apolipoprotein-E (Apoe) $\epsilon 4$ and cognitive decline over the adult life course". In: *Transl. Psychiatry* 8.1.

Raz, N et al. (Feb. 2004). "Differential aging of the medial temporal lobe: a study of a five-year change". en. In: *Neurology* 62.3, pp. 433–438.

Reuter, Martin, M Dylan Tisdall, et al. (Feb. 2015). "Head motion during MRI acquisition reduces gray matter volume and thickness estimates". en. In: *Neuroimage* 107, pp. 107–115.

Romero, José E, Pierrick Coupé, and José V Manjón (Dec. 2017). "HIPS: A new hippocampus subfield segmentation method". en. In: *Neuroimage* 163, pp. 286–295.

Shafto, Meredith A et al. (Oct. 2014). "The Cambridge Centre for Ageing and Neuroscience (Cam-CAN) study protocol: a cross-sectional, lifespan, multidisciplinary examination of healthy cognitive ageing". en. In: *BMC Neurol.* 14, p. 204.

Shaw, Thomas B et al. (Dec. 2019). "Non-linear realignment improves hippocampus subfield segmentation reliability". en. In: *Neuroimage* 203, p. 116206.

Shing, Yee Lee et al. (Feb. 2011). "Hippocampal subfield volumes: age, vascular risk, and correlation with associative memory". en. In: *Front. Aging Neurosci.* 3, p. 2.

Smith, T B and K S Nayak (2010). "MRI artifacts and correction strategies". In: *Imaging Med.*

Stockmeier, Craig A et al. (Nov. 2004). "Cellular changes in the postmortem hippocampus in major depression". en. In: *Biol. Psychiatry* 56.9, pp. 640–650.

Sullivan, E V et al. (July 1995). "Age-related decline in MRI volumes of temporal lobe gray matter but not hippocampus". en. In: *Neurobiol. Aging* 16.4, pp. 591–606.

Sullivan, Edith V, Laura Marsh, and Adolf Pfefferbaum (July 2005). "Preservation of hippocampal volume throughout adulthood in healthy men and women". en. In: *Neurobiol. Aging* 26.7, pp. 1093–1098.

Svarer, Claus et al. (Feb. 2005). "MR-based automatic delineation of volumes of interest in human brain PET images using probability maps". en. In: *Neuroimage* 24.4, pp. 969–979.

Tardif, Christine L, Gabriel A Devenyi, et al. (Feb. 2018). "Regionally specific changes in the hippocampal circuitry accompany progression of cerebrospinal fluid biomarkers in preclinical Alzheimer's disease". en. In: *Hum. Brain Mapp.* 39.2, pp. 971–984.

Taylor, Jason R et al. (2017). "The Cambridge Centre for Ageing and Neuroscience (Cam-CAN) data repository: Structural and functional MRI, MEG, and cognitive data from a cross-sectional adult lifespan sample". In: *Neuroimage* 144, pp. 262–269.

Thomas, David L et al. (June 2004). "High-resolution fast spin echo imaging of the human brain at 4.7 T: implementation and sequence characteristics". en. In: *Magn. Reson. Med.* 51.6, pp. 1254–1264.

Tullo, Stephanie et al. (2019). "MR-based age-related effects on the striatum, globus pallidus, and thalamus in healthy individuals across the adult lifespan". In: *Hum. Brain Mapp.* 40.18, pp. 5269–5288.

Tustison, Nicholas J et al. (June 2010). "N4ITK: improved N3 bias correction". en. In: *IEEE Trans. Med. Imaging* 29.6, pp. 1310–1320.

Van Leemput, Koen et al. (2009). "Automated segmentation of hippocampal subfields from ultra-high resolution in vivo MRI". In: *Hippocampus* 19.6, pp. 549–557.

Voineskos, Aristotle N et al. (Aug. 2015). "Hippocampal (subfield) volume and shape in relation to cognitive performance across the adult lifespan". en. In: *Hum. Brain Mapp.* 36.8, pp. 3020–3037.

Weiner, Michael W et al. (May 2017). "The Alzheimer's Disease Neuroimaging Initiative 3: Continued innovation for clinical trial improvement". en. In: *Alzheimers. Dement.* 13.5, pp. 561–571.

Winterburn, Julie et al. (Nov. 2015). "High-resolution In Vivo Manual Segmentation Protocol for Human Hippocampal Subfields Using 3T Magnetic Resonance Imaging". en. In: *J. Vis. Exp.* 105, e51861.

Winterburn, Julie L et al. (July 2013). "A novel in vivo atlas of human hippocampal subfields using high-resolution 3 T magnetic resonance imaging". en. In: *Neuroimage* 74, pp. 254–265.

Wisse, L E M et al. (July 2012). "Subfields of the hippocampal formation at 7 T MRI: in vivo volumetric assessment". en. In: *Neuroimage* 61.4, pp. 1043–1049.

Wisse, Laura E M, Geert Jan Biessels, et al. (Sept. 2014). "Hippocampal subfield volumes at 7T in early Alzheimer's disease and normal aging". en. In: *Neurobiol. Aging* 35.9, pp. 2039–2045.

Wisse, Laura E M, Gaël Chételat, et al. (2020). "Hippocampal subfield volumetry from structural isotropic 1 mm 3 MRI scans: A note of caution". In: *Hum. Brain Mapp.* 42.2, pp. 539–550.

Wisse, Laura E M, Ana M Daugherty, et al. (Jan. 2017). "A harmonized segmentation protocol for hippocampal and parahippocampal subregions: Why do we need one and what are the key goals?" en. In: *Hippocampus* 27.1, pp. 3–11.

Wolf, Dominik et al. (Oct. 2015). "Differential associations of age with volume and microstructure of hippocampal subfields in healthy older adults". en. In: *Hum. Brain Mapp.* 36.10, pp. 3819–3831.

Wood, Bryony et al. (2015). "Magnetic resonance scanning and image segmentation procedure at 3 T for volumetry of human hippocampal subfields". In: *Biomed. Spectrosc. Imaging* 4.2, pp. 197–208.

Yang, Xianfeng et al. (Nov. 2013). "Evolution of hippocampal shapes across the human lifespan". en. In: *Hum. Brain Mapp.* 34.11, pp. 3075–3085.

Yushkevich, Paul A, Robert S C Amaral, et al. (May 2015). "Quantitative comparison of 21 protocols for labeling hippocampal subfields and parahippocampal subregions in in vivo MRI: towards a harmonized segmentation protocol". en. In: *Neuroimage* 111, pp. 526–541.

Yushkevich, Paul A, John B Pluta, et al. (Jan. 2015). "Automated volumetry and regional thickness analysis of hippocampal subfields and medial temporal cortical structures in mild cognitive impairment". en. In: *Hum. Brain Mapp.* 36.1, pp. 258–287.

Yushkevich, Paul A, Hongzhi Wang, et al. (Dec. 2010). "Nearly automatic segmentation of hippocampal subfields in in vivo focal T2-weighted MRI". en. In: *Neuroimage* 53.4, pp. 1208–1224.

Zhao, Weina et al. (Mar. 2019). "Trajectories of the Hippocampal Subfields Atrophy in the Alzheimer's Disease: A Structural Imaging Study". en. In: *Front. Neuroinform.* 13, p. 13.

Zheng, Fenglian et al. (Oct. 2018). "The Volume of Hippocampal Subfields in Relation to Decline of Memory Recall Across the Adult Lifespan". en. In: *Front. Aging Neurosci.* 10, p. 320.

Ziegler, Gabriel et al. (Oct. 2012). "Brain structural trajectories over the adult lifespan". en. In: *Hum. Brain Mapp.* 33.10, pp. 2377–2389.

Chapter 4

Hippocampal shape across the healthy lifespan and its relationship with cognition

Aurélie Bussy[1], Raihaan Patel[2], Eric Plitman[3], Stephanie Tullo[1], Alyssa Salaciak[4], Saashi A. Bedford[3], Sarah Farzin[4], Marie-Lise Béland[4], Vanessa Valiquette[1], Christina Kazazian[4], Christine Lucas Tardif[5], Gabriel A. Devenyi[3], M. Mallar Chakravarty[6]

1 - Computional Brain Anatomy (CoBrA) Laboratory, Cerebral Imaging Centre, Douglas Mental Health University Institute, Montreal, QC, Canada, Integrated Program in Neuroscience, McGill University, Montreal, Canada.

2 - Computional Brain Anatomy (CoBrA) Laboratory, Cerebral Imaging Centre, Douglas Mental Health University Institute, Montreal, QC, Canada; Department of Psychiatry, McGill University, Montreal, QC, Canada.

3 - Computional Brain Anatomy (CoBrA) Laboratory, Cerebral Imaging Centre, Douglas Mental Health University Institute, Montreal, QC, Canada, Department of Biological and Biomedical Engineering, McGill University, Montreal, QC, Canada.

4 - Computional Brain Anatomy (CoBrA) Laboratory, Cerebral Imaging Centre, Douglas Mental Health University Institute, Montreal, QC, Canada.

5 - Department of Biological and Biomedical Engineering, McGill University, Montreal, QC, Canada; McConnell Brain Imaging Centre, Montreal Neurological Institute, Montreal, QC, Canada; Department of Neurology and Neurosurgery, McGill University, Montreal, QC, Canada.

6 - Computional Brain Anatomy (CoBrA) Laboratory, Cerebral Imaging Centre, Douglas Mental Health University Institute, Montreal, QC, Canada; Integrated Program in Neuroscience, McGill University, Montreal, Canada; Department of Psychiatry, McGill University, Montreal, QC, Canada; Department of Biological and Biomedical Engineering, McGill University, Montreal, QC, Canada.

4.1 Preface

In **Chapter 4**, we sought to explore the hypothesis, initially introduced in **Chapter 3**, which suggests that the shape of the hippocampus undergoes changes throughout a person's life. To investigate the surface-wise connection between hippocampal shape and age, we developed two surface-based metrics and employed a data-driven approach to examine non-linear age-related patterns. Furthermore, we used a multivariate technique called PLS to explore the association between hippocampal shape and important variables of interest, including age, sex, education, APOE-ϵ4 allele status, and cognitive scores.

We found that age-related changes in the hippocampus were characterized by an antero-posterior effect on SA and a medial-lateral effect on displacement, indicating an increase in curvature with age. These findings were consistent with lower cognitive scores and being female. Therefore, the study suggested that the age-related changes in hippocampal shape might contribute to the differences in volume estimation between slab images and isotropic scans observed in **Chapter 3**. This manuscript was published in *Neurobiology of Aging* in

2021 (Bussy, Patel, et al. 2021).

4.2 Abstract

The study of the hippocampus across the healthy adult lifespan has rendered inconsistent findings. While volumetric measurements have often been a popular technique for analysis, more advanced morphometric techniques have demonstrated compelling results that highlight the importance and improved specificity of shape-based measures. Here, the MAGeT Brain algorithm was applied on 134 healthy individuals aged 18–81 years old to extract hippocampal subfield volumes and hippocampal shape measurements, namely: local SA and displacement. We used linear-, second- or third-order natural splines to examine the relationships between hippocampal measures and age. In addition, PLS analyses were performed to relate volume and shape measurements with cognitive and demographic information. Volumetric results indicated a relative preservation of the right CA1 with age and a global volume reduction linked with older age, female sex, lower levels of education and cognitive performance. Vertex-wise analysis demonstrated an SA preservation in the anterior hippocampus with a peak during the sixth decade, while the posterior hippocampal SA gradually decreased across lifespan. Overall, SA decrease was linked to older age, female sex and, to a lesser extent lower levels of education and cognitive performance. Outward displacement in the lateral hippocampus and inward displacement in the medial hippocampus were enlarged with older age, lower levels of cognition and education, indicating an accentuation of the hippocampal "C" shape with age. Taken together, our findings suggest that vertex-wise analyses have higher spatial specificity and that sex, education, and cognition are implicated in the differential impact of age on hippocampal subregions throughout its anteroposterior and medial-lateral axes.

4.3 Introduction

The role of the hippocampus in normal behavior and across neuropsychiatric disorders has been a major topic of clinical and neuroscientific research since the initial investigations of Scoville and Milner on patient H.M. (Scoville and Milner 1957). Since these pioneering investigations, altered hippocampal structure and function have been implicated in several neuropsychiatric disorders, such as AD (Convit et al. 1997; R. S. C. Amaral et al. 2018), schizophrenia (Nelson et al. 1997), major depressive disorder (J D Bremner et al. 2000; Videbech and Ravnkilde 2004; Treadway et al. 2015), post-traumatic stress disorder (J Douglas Bremner et al. 2003; Apfel et al. 2011), and frontotemporal dementia (Laakso, G B Frisoni, et al. 2000; Muñoz-Ruiz et al. 2012; Chapleau et al. 2020). Moreover, the relationship between hippocampal structure and age across the adult lifespan has also been of interest towards setting a "baseline" of hippocampal morphology, against which disorders implicating this region may be compared. However, previous findings investigating hippocampal changes with age have rendered inconsistent results (La Joie, Fouquet, et al. 2010; Flores, La Joie, Landeau, et al. 2015; Bussy, Plitman, et al. 2021) and potential sources of this inconsistency are discussed below.

Although whole hippocampal volume can be studied using standard volumetric MRI (Sabuncu et al. 2011; Sankar et al. 2017; Schoemaker et al. 2016), there is mounting evidence that variation at the level of the hippocampal subfields provides additional insight into neuropsychiatric disorders and healthy aging. However, it is presently unclear which subregions of the hippocampus are the most impacted through the course of the adult lifespan. Indeed, some studies have demonstrated a predominant decrease of the CA)1 and subiculum volumes with age (Shing et al. 2011; Laura E M Wisse, Biessels, et al. 2014; Flores, La Joie, Landeau, et al. 2015; Wolf et al. 2015; Daugherty et al. 2016), while others have shown a relative preservation of the CA1 volume compared to global hippocampal atrophy with age (R. S. C. Amaral et al. 2018; Bussy, Plitman, et al. 2021). These contradictory results might potentially be explained by the use of various hippocampal subfield definitions and

segmentation techniques across existing literature (Yushkevich, R. S. C. Amaral, et al. 2015; Laura E M Wisse, Daugherty, et al. 2017; Bussy, Plitman, et al. 2021).

To date, studies investigating the hippocampus across the adult lifespan have largely been limited to the examination of volumetric information. However, different morphological techniques have been shown to provide spatially localized information about age-related hippocampal modifications, independent of finer-grain neuroanatomical definitions (Yang et al. 2013; Voineskos et al. 2015). For example, some groups have reported inward deformations in the hippocampal head of older adults (Yang et al. 2013). Additionally, voxel-based regression analyses demonstrated that age-related variation occurred mostly in the head and tail of the hippocampus (J C Pruessner et al. 2001). Furthermore, significant patterns of inward displacement modifications in the hippocampal head and outward displacement in the hippocampal body have been found to be associated with age (Voineskos et al. 2015). In contrast, another study found a higher impact of age in the posterior hippocampus rather than in the hippocampal head (Kalpouzos et al. 2009).

There are several other factors that may impact findings from previous studies. For example, previous normative aging studies have examined various age ranges, with some researchers considering large spans of the adult lifespan (S G Mueller et al. 2007; Flores, La Joie, and Gaël Chételat 2015; R. S. C. Amaral et al. 2018; F. Zheng et al. 2018; Bussy, Plitman, et al. 2021), while others only investigated elderly individuals (Giovanni B Frisoni, Ganzola, et al. 2008; Laura E M Wisse, Biessels, et al. 2014). Despite previous analyses showing non-linear relationships between brain volume and age (Coupé, Catheline, et al. 2017; Tullo et al. 2019; Bussy, Plitman, et al. 2021), non-linear relationships with age are still rarely investigated, especially in morphometric studies (Yang et al. 2013).

The role of the hippocampus in episodic and working memory has previously been established (Driscoll et al. 2003; Eichenbaum 2004). Additionally, the protective role of high level of education on the hippocampus has been demonstrated (K. G. Noble et al. 2012). Moreover, cognitive abilities earlier in life moderates the relationship between hippocampal

volume and cognition in middle age (Vuoksimaa et al. 2013). Researchers have also established the impact of sex on disorders where hippocampal dysfunction and degeneration are implicated (Fleisher et al. 2005; Fisher, David A Bennett, and H. Dong 2018). Moreover, APOE-ϵ4 allele genotype has been recognized as a genetic risk factor for hippocampal age-related and AD-related atrophy (Pievani et al. 2011; O'Dwyer et al. 2012). However, to our knowledge, all these factors have rarely been studied in relation to hippocampal shape (Voineskos et al. 2015).

To extend our understanding of hippocampal subfield volumetry and morphology throughout the lifespan, the aim of this paper is to investigate the associations between age and hippocampal structure. We further investigate the relationship with different factors known to influence age-related variation such as biological sex, education, and APOE-ϵ4 allele genotype. Finally, we also use a multivariate technique to connect hippocampal morphometry, demographic characteristics, and cognition. To the best of our knowledge, this is a novel approach given that previous work typically investigates hippocampal morphometry using univariate analyses, linear models, or group comparisons to principally analyze the effect of one variable at the time (L. Wang et al. 2003; Yang et al. 2013; Voineskos et al. 2015; Q. Dong et al. 2019). Here, we explore the interaction of different variables at the same time, which allows us to draw conclusions about the influence of each variable towards overall vertex-wise shape modification.

4.4 Methods

4.4.1 Participants

Participants were selected from 2 datasets collected by our group; namely, the HA and ADB datasets. These datasets were previously used and described by our group, in one study investigating the striatum, globus pallidus, and thalamus (Tullo et al. 2019) and in another examining the effects of MR sequence on hippocampal subfield volumes estimates (Bussy,

Plitman, et al. 2021). Both HA and ADB datasets were approved by the Research Ethics Board of the Douglas Research Centre, Montreal, Canada and written informed consent was collected from all participants. 112 healthy individuals aged 18–80 (55 males and 57 females) and 66 healthy seniors aged 56–81 (25 males and 41 females) were selected from the HA and ADB datasets, respectively. Exclusion criteria included having a history of neurological disease, psychiatric disorder, major structural neurological abnormalities or pathologies, history of brain damage or concussion, current or recent use of psychoactive substances, intellectual disability, a MMSE (M. F. Folstein, S. E. Folstein, and McHugh 1975) score below 24, having less than 6 years of formal education, and any contraindications to MRI.

The initial dataset, which is described in Supplementary Table 4.2, summarizes the demographic information of the 178 participants initially included in the study. Table 4.1 describes the demographic information of the 134 individuals ("Full" dataset) for which the preprocessing and processing steps passed our QC (see 4.4.3 Raw quality control and 4.4.7 Output quality control). These participants were included for the age analyses using vertex-wise linear mixed-effect analyses (See 4.4.9 Statistics). Table 4.1 also includes demographics for the 85 individuals ("APOE4" dataset) who passed QC and with known APOE-ϵ4 allele genotype, repeatable battery for the assessment of neuropsychological status (RBANS) (Randolph et al. 1998), MMSE, and years of education. These participants were included in subfield-wise hippocampal volume analyses and PLS analyses (See 4.4.9 Statistics).

4.4.2 Imaging acquisition

All participants were scanned on a 3T Siemens Tim Trio MRI scanner using a 32-channel head coil at the Douglas Research Centre, Montreal, Quebec, Canada. T1w images were acquired using parameters established by the ADNI MPRAGE protocol (Clifford R Jack Jr, Bernstein, et al. 2008). T1w acquisition parameters were TE/TR = 2.98 ms/2300 ms, TI = 900 ms, α= 9°, 256 × 240 × 176 matrix, GeneRalized Autocalibrating Partial Parallel

	APOE4 - 85 participants			FULL - 134 participants		
	ADB (n = 44)	HA (n = 41)	Overall (n = 85)	ADB (n = 54)	HA (n = 80)	Overall (n = 134)
Age						
Mean	70.0	51.6	61.1	69.9	47.2	56.4
(SD)	(5.64)	(17.4)	(15.7)	(5.4)	(16.2)	(17.1)
Median	70.0	50.0	66.0	70.0	46.0	62.5
[Min, Max]	[57.0, 81.0]	[18.0, 80.0]	[18.0, 81.0]	[57.0, 81.0]	[18.0, 80.0]	[18.0, 81.0]
Sex						
Female	28 (63.6%)	23 (56.1%)	51 (60.0%)	32 (59.3%)	46 (57.5%)	78 (58.2%)
Male	16 (36.4%)	18 (43.9%)	34 (40.0%)	22 (40.7%)	34 (42.5%)	56 (41.8%)
APOE4						
Non-carriers	30 (68.2%)	28 (68.3%)	58 (68.2%)			
Carriers	14 (31.8%)	13 (31.7%)	27 (31.8%)			
Education						
Mean	16.4	16.7	16.6			
(SD)	(3.98)	(3.42)	(3.70)			
Median	16.0	17.0	16.0			
[Min, Max]	[10.0, 31.0]	[10.0, 26.0]	[10.0, 31.0]			
RBANS						
Mean	95.0	103.0	98.7			
(SD)	(12.7)	(15.9)	(14.8)			
Median	92.5	104.0	99.0			
[Min, Max]	[71.0, 123.0]	[57.0, 132.0]	[57.0, 132.0]			
MMSE						
Mean	28.6	28.7	28.6			
(SD)	(1.53)	(1.54)	(1.53)			
Median	29.0	29.0	29.0			
[Min, Max]	[24.0, 30.0]	[24.0, 30.0]	[24.0, 30.0]			

Table 4.1: Complete demographic information of the 85 individuals who passed motion and segmentation QC and with complete APOE-ϵ4 allele genotyping, RBANS total score, MMSE, and years of education by dataset and demographics of the "Full" dataset with the 134 participants used for the vertex-wise age analyses

Acquisition (GRAPPA) of 2, bandwidth = 238 Hz/pixel, 1.00 mm isotropic voxel dimensions, and scan time 5:12.

4.4.3 Raw quality control

Involuntary movements such as cardiac or respiratory motion can lead to motion artifacts and may negatively impact the quality of structural MRI images (Bellon et al. 1986; T. B. Smith and Nayak 2010; Reuter, Tisdall, et al. 2015) and any quantitative outputs derived from these images (Reuter, Tisdall, et al. 2015; Alexander-Bloch et al. 2016). QC of all raw images was performed by one of the authors (AB) using the QC procedure previously developed in our laboratory (Bedford et al. 2020) https://github.com/CoBrALab/documentation/wiki/Motion-Quality-Control-Manual.

4.4.4 Preprocessing

Image preprocessing was used to standardize the overall quality of the T1w images prior to processing. The minc-bpipe-library pipeline https://github.com/CobraLab/minc-bpipe-library was applied to T1w images and consists of several steps, including: N4 bias field correction (Tustison et al. 2010), registration to MNI space (ICBM 2009c Nonlinear Symmetric) using bestlinreg (Collins et al. 1994; Dadar et al. 2018), and standardization of the field-of-view by using a MNI head mask transformed into native space using the linear transformation estimated at the prior stage. Finally, any voxels outside the head mask were cropped, the orientation of the brain was standardized, and the brain was extracted using Brain Extraction based on nonlocal Segmentation Technique (BEaST) (Eskildsen et al. 2012).

4.4.5 Volumetric analysis

Segmentation of the hippocampal subfields was performed using the MAGeT Brain algorithm (Pipitone et al. 2014; Chakravarty, Steadman, et al. 2013). GM subfields included the CA1, CA2CA3, CA4DG, SRLM and subiculum; these were defined in five high-resolution atlases. These atlases have been previously manually segmented on 0.3 mm isotropic T1w and T2w MRI-based atlases (J. L. Winterburn et al. 2013) and the segmentation procedure was validated using both manual segmentation, comparisons to other pipelines, and simulations (Pipitone et al. 2014).

As described in our recent work (Bussy, Plitman, et al. 2021), MAGeT Brain was used to segment each dataset independently, with a first run for ADB dataset and another for HA dataset. First, a "best template selection" stage https://github.com/CoBrALab/documentation/wiki/Best-Templates-for-MAGeT was performed in order to select the 21 subjects with the highest quality of atlas-to-template segmentation in each dataset independently. Next, these 21 subjects were used to populate the template library in order to segment all the subjects of each dataset. This step improves the quality of the atlas-to-template

segmentation by artificially increasing the number of candidate labels to 105 (21 templates × 5 atlases). A majority vote technique was then used on these 105 candidate labels to obtain final labels (Pipitone et al. 2014; Chakravarty, Steadman, et al. 2013; Makowski et al. 2018), which, when coupled with the atlas inflation strategy, performs similarly to or exceeds performance of recent advances in label fusion techniques (Bhagwat, Pipitone, et al. 2016). Affine and SyN nonlinear registrations from the Advanced Normalization Tools (ANTS; (B B Avants et al. 2008) are used within the MAGeT brain algorithm. ROI located at each hippocampal subfield label were used to create single value masks. These masks were then dilated with a 3-mm radius kernel in order to focus both affine and nonlinear registration, a method which reduces computational time and improves segmentation accuracy (Chakravarty, Sadikot, et al. 2008; Chakravarty, Mallar Chakravarty, et al. 2009).

4.4.6 Shape analysis

The MAGeT pipeline also provides morphometric (SA and displacement) measurements (Raznahan et al. 2014; Voineskos et al. 2015; P. Shaw et al. 2014; Janes et al. 2015). An average neuroanatomical representation was created for the hippocampal GM through group-wise nonlinear registration of the 5 atlases previously defined in (J. L. Winterburn et al. 2013); this representation was referred to as the "model" (Figure 4.1 **A**). This model provides a common space for analysis of surface-based metrics from which we derived a mesh of the hippocampal surfaces, composed of 1200 vertices/hemisphere. Then, a surface-based metric (Lerch, Carroll, et al. 2008) was used to estimate the local shape variation of our subjects with the model as a reference. Finally, SA (examining expansion or contraction) and displacement (examining inward or outward) were calculated using vertex-wise analysis (Figure 4.1 **B** et **C**).

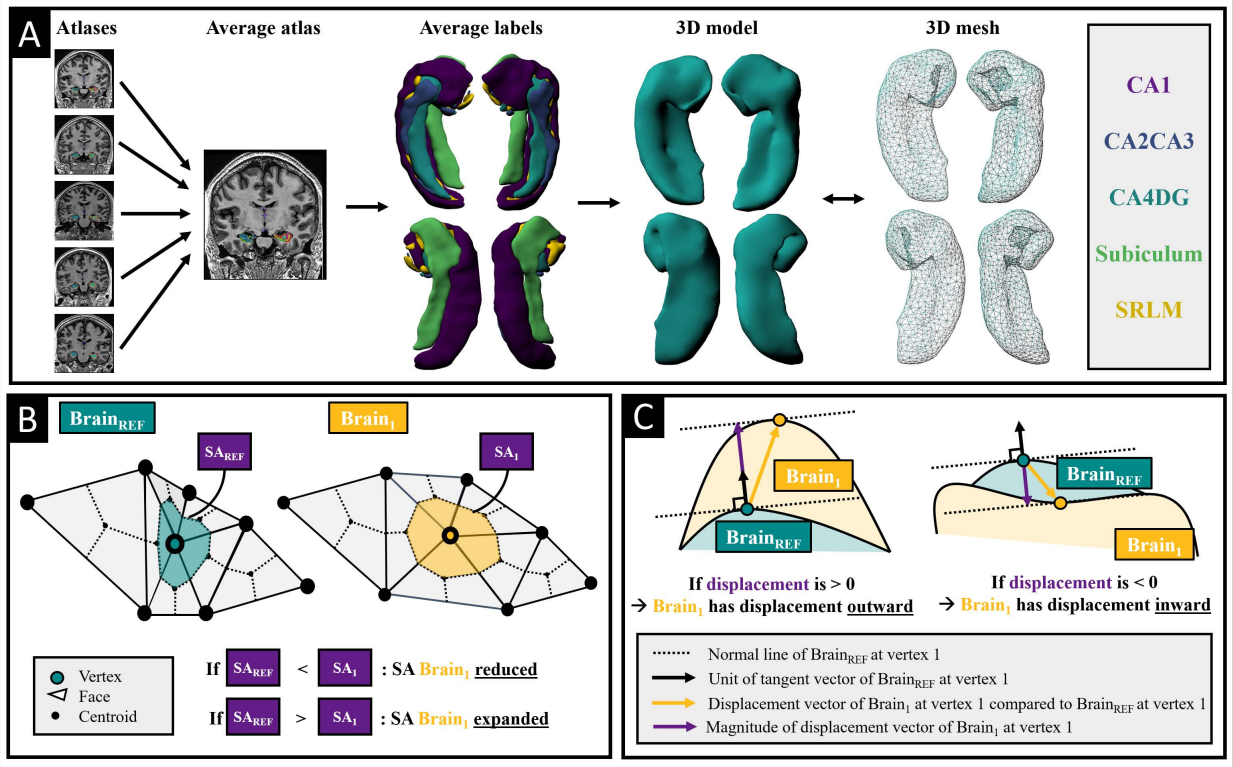

Figure 4.1: Schematic representation of the major analysis streams presented. **A** The five hippocampal atlases were nonlinearly registered to create an average brain. The same transformations were applied on the 5 hippocampal labels to obtain the 5 atlases in a common space, and labels were fused in common space using majority vote. An average 3D hippocampal model was created along with a 3D mesh in order to perform surface-based morphological analyses. **B** SA was calculated using the Voronoï method of parcellation around each vertex. The SA of the brain of interest was then compared to the SA of the corresponding vertex in the reference brain. **C** Displacement measure was calculated using the magnitude of the displacement vector between a vertex and the corresponding vertex in the reference brain.

4.4.7 Output quality control

QC of the final labels by visual inspection was conducted following the procedure implemented by our group (https://github.com/CobraLab/documentation/wiki/MAGeT-Brain-Quality-Control-(QC)-Guide). All QC was conducted by one of the authors (AB) to only include high quality segmentation in the statistical analyses.

4.4.8 Subfields objects

From the 5 brains used previously to define our 5 atlases (J. L. Winterburn et al. 2013), average brains and labels were previously created (Voineskos et al. 2015). Mango software (version 4.1 developed by Research Imaging Institute, UTHSCSA; (Lancaster et al. 2011)) was used to create 3D objects of each subfield to visually help comparison between our morphological measurements and the hippocampal subfields (Figure 4.1 **A**).

4.4.9 Statistics

4.4.9.1 Age-relationship models

First, we sought to examine the impact of age on our morphometric and volumetric measures while accounting for factors like sex, genetic risk, education and cognition. The "APOE4" dataset of 85 individuals (Table 4.1) was used to investigate the hippocampal subfield volume changes with age while the "FULL" dataset of 134 individuals was used to examine the relationship between the vertex-wise morphological measures and age. This allowed us to take advantage of the higher number of participants to extract vertex-wise relationships with age. lmer (from lmerTest 3.1-2 package for subfield-wise analysis or vertexLmer from RMINC 1.5.2.2 package for vertex-wise analysis in R 3.6.3) and natural splines (ns from splines package) were used to model linear, second, or third order age relationships, either for subfield-wise volumes or vertex-wise measurements.AIC (Akaike 1974) was used to investigate the most appropriate age relationships across the multiple models. The model with the lowest AIC was selected and was considered to best fit the data (Mazerolle 2006); see also previous work from our group (Tullo et al. 2019; Bedford et al. 2020). The models with the lowest AIC and the models with the second lowest AIC were also compared by calculating the difference between the 2 AIC values, called delta. Delta was then plotted vertex-wise to create a confidence map for the model's choice, and delta was interpreted following previously defined guidelines (Burnham and D. R. Anderson 2004). All statistical

models and the confidence map are described in detail within the supplementary material.

For the subfield-wise analysis, sex, intracranial volume, APOE-ϵ4 allele status, education, MMSE, and RBANS were included as fixed effects, while dataset was included as a random effect. Bonferroni correction was performed to correct for multiple comparisons across our 12 structures (bilateral total hippocampus and five GM subfields per hemisphere), at a $p < 0.05$ threshold for significance, resulting in a significance level of $p < 0.00417$ (only corrected p-values reported throughout this paper).

For the vertex-wise analysis, sex was included as a fixed effect, while dataset was included as a random effect. A 5% false-discovery rate (FDR) correction was applied to control for the expected proportion of "discoveries" that are false (Yoav Benjamini and Hochberg 1995; Benjamini et al. 2001). After selecting the best fit for each vertex, lmer (from lmerTest 3.1-2 package in R 3.6.3) and which.max and which.min functions were used to calculate the age for which SA and displacement were at the maximum and minimum, respectively.

4.4.9.2 PLS analysis

After establishing the baseline with more common univariate measures, we sought to examine how morphometry and volume covaries with factors that we know are implicated in the ageing process, such as sex, genetic risk, education and cognition. PLS, a multivariate technique that transforms the predictors to a smaller set of uncorrelated components and subsequently performs least squares regression on these newly defined components, was performed on the APOE-ϵ4 allele dataset. The goal of PLS is to identify a set of latent variable (LV)s, that explain patterns of covariance between "brain" and "cognitive/demographic" data with the constraint that LVs explain as much of the covariance between the two matrices as possible. Mathematically, each LV will describe linear combinations of the "brain" and "cognitive/demographic" data that maximally covary. Two separate PLS analyses were used; the first to investigate the relationships between the hippocampal subfield volumes and cognitive/demographic information, and the second to relate shape measurements with

cognitive/demographic information. In this work, we first used 2 input matrices composed of the "brain" data and the "cognitive/demographic" data detailed in Table 4.1 **A**. Here, our "brain" data included the volume of each hippocampal subfield (matrix size 85 × 10). Our "cognitive/demographic" data contained age, sex, years of education, MMSE, APOE-ϵ4 allele status, and RBANS score for each subject (matrix size 85 × 6). Second, for the vertex-wise PLS, our "brain" data included either vertex-wise measurements of the SA or displacement in each hippocampus (matrix size 85 × 1215 or 85 × 1152). Our "cognitive/demographic" data contained age, sex, years of education, APOE-ϵ4 allele status, and RBANS scores for each subject (matrix size 85 × 5). We also ran PLS using "ns(age,2)" or "ns(age,3)" instead of "age" (Supplementary Figs. 4.10 and 4.11) and no qualitative difference was observed from these analyses.

Following a statistical protocol described in previous works (Anthony Randal McIntosh and Lobaugh 2004; Krishnan et al. 2011; Anthony R McIntosh and Mišić 2013; Zeighami et al. 2019; Patel, Steele, et al. 2020), each LV was then tested statistically using permutation testing. First, row permutations (10,000 times) of the input "brain" matrix were subject to PLS in order to obtain a distribution of singular values with the hypothesis that a permuted "brain" matrix will eliminate the initial brain-cognitive relationships. From these permutations, a nonparametric p-value was calculated for each LV expressing the degree to which the singular value obtained from the original matrices was associated with chance. A p-value threshold of 0.05 was selected to demonstrate which LV had at least a 95% chance of not being associated with a random correlation in the original matrices.

Second, the degree to which each "brain" and "cognitive/demographic" variable contributes to a given LV was tested using bootstrap resampling. The rows of the "brain" and "cognitive/demographic" matrices were randomly sampled with replacement to generate 10,000 new sets of matrices, this time maintaining initial brain-cognitive relationships (in contrast to the permutation tests described above). Each bootstrapped pair was subject to PLS in order to create a distribution of singular vector weights for each variable. The

ratio of the singular vector weight over the standard error of the weight, called a bootstrap ratio (BSR), represents the contribution and reliability of a "brain" variable. We used a BSR threshold of 2.58, analogous to a p-value of 0.01. Meanwhile, the distribution of singular vector weights of each cognitive variable is used to obtain a 95% confidence interval (Krishnan et al. 2011; Anthony Randal McIntosh and Lobaugh 2004; Nordin et al. 2018; Zhou et al. 2012; Zeighami et al. 2019).

4.4.10 CAMCAN replication dataset

Cam-CAN is a large-scale dataset collecting MRI scans at the Medical Research Council Cognition and Brain Sciences Unit in Cambridge, England. The images were acquired using a 3T Siemens TIM Trio scanner with a 32-channel head coil (Shafto et al. 2014; J. R. Taylor et al. 2017). We included 652 healthy individuals (aged 18-88) with standard MPRAGE (1 mm3). Similar preprocessing and processing steps were applied and after quality control, 350 participants (age range 18–85, mean age 49.95; 182 females/168 males) were included in our statistical analyses. Linear models with sex as covariate and natural splines were used to model linear, second, or third order age relationships, similarly as in 4.4.9.1 Age-relationship models.

4.5 Results

4.5.1 Subfield-wise

Here, after testing linear, second- and third-order relationships between each subfield and age using the AIC, we observed a third-order relationship of volumes with age. Both hippocampi and all the subfields, except the right CA1, were significantly decreasing with greater age (Figure 4.2 **A**). Most subfields expressed a slight and steady decrease until age 60, followed by an accelerated association until age 80. PLS analysis demonstrated that the left and right hippocampus and their subfields were each associated with one significant LV, explaining

93.7% and 90.9% of the covariance, respectively (Figure 4.2 **B**). In the right hemisphere, decrease in all the subfield volumes was associated with older age (R = 0.38, 95% CI = [0.23,0.53]), female sex (R = 0.56, 95% CI = 0.45,0.67), low education (R = -0.22, 95% CI = -0.42,-0.03), low RBANS total score (R = -0.20, 95% CI = -0.38,-0.02) and low MMSE score (R = -0.24, 95% CI = -0.41,-0.06). Left LV1 identified a pattern in which decreased volumes in the CA1, CA4DG, subiculum, SRLM and ICV were associated with older age (R = 0.38, 95% CI = 0.23,0.55), lower MMSE score (R = -0.18, 95% CI = -0.36, 0), and female sex (R = 0.49, 95% CI = 0.37,0.62).

4.5.2 Vertex-wise

4.5.2.1 Surface area

In Figure 4.3 **A**, we use AIC at each vertex to show that, within the hippocampal structure, there are different types of age relationships. The right hippocampus had principally linear relationships with age in the body/tail, and a second- or third-order relationship in the head of the hippocampus. The left hippocampus demonstrated a second-order relationship in the head, while the body and tail were best described linearly or with a third-order relationship with age. The vertices showing a significant effect of age are displayed in Figure 4.3 **B**. A significant linear decrease with age was found in the tail of the hippocampus, while the head of the hippocampus indicated significant second- or third-order relationships with age. Using these best models, we found that the maximum SA was largely found at 18 years old, except in the head of the hippocampus, which showed a maximum SA at 60 years old (Figure 4.3 **C**). Moreover, the minimum SA was reached at 81 years old, except in some local areas, like the uncus, which demonstrated a minimum SA at 18 years old. In Figure 4.3 **D**, we plotted peak vertices of these different significant relationships with age. Of note, the second- and third-order curves corroborated that, for some vertices, the SA was preserved until the age of 60 years old.

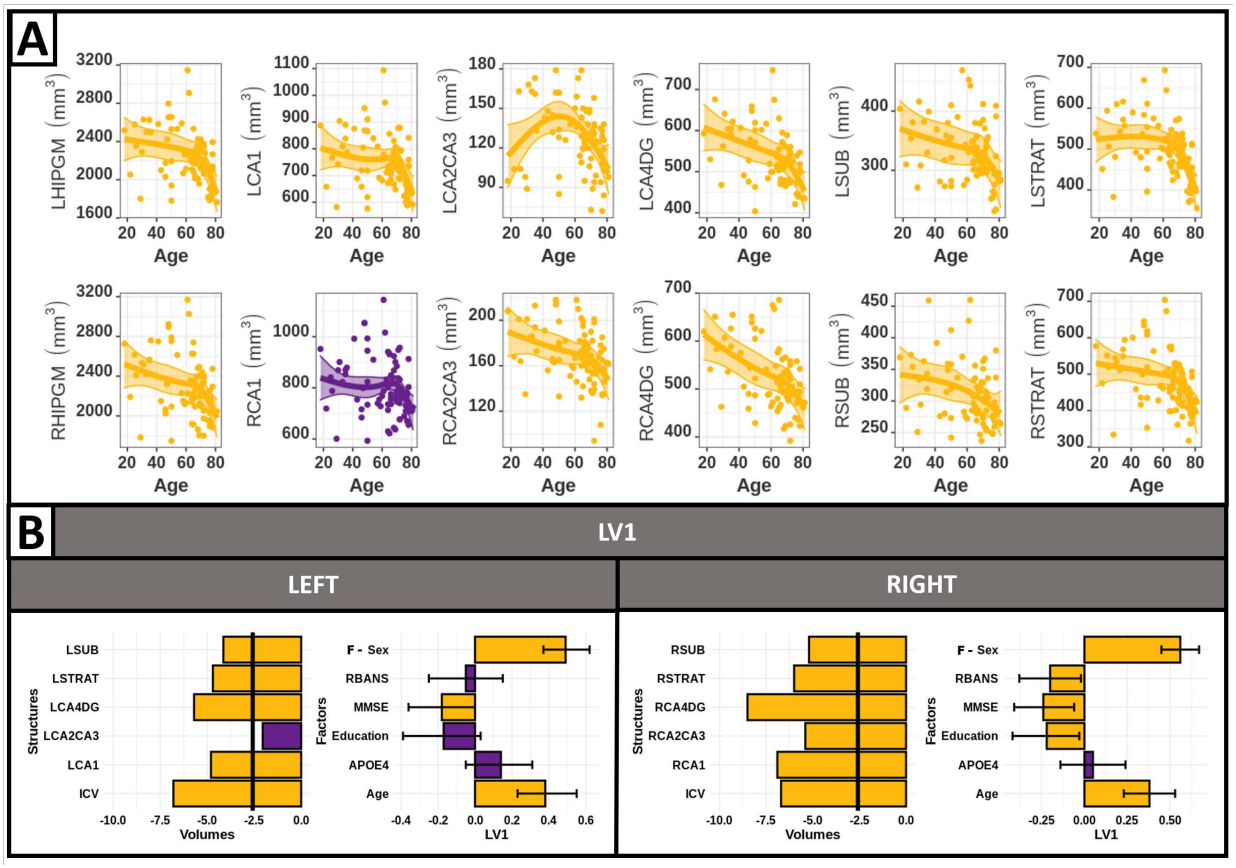

Figure 4.2: **A** Third order relationships between age and the hippocampal subfields volumes. Purple: nonsignificant; yellow: $p < 0.05$ after Bonferroni correction. Supplementary Table 4.3 illustrates t-values and uncorrected p-values. **B** PLS between the left/right hippocampal subfield volumes and the demographic information identified one significant LV on each hemisphere ($p < 0.05$). Right LV1 explained 93.7% and left LV1 explained 90.9% of the covariance. **Left side**: Bar plots describe the correlation of each subfield variable with the LV, yellow identifies variables significantly contributing to the LV. Black vertical line corresponds to a BSR threshold of 2.58. **Right side**: Bar plots describe the correlation of each demographic variable with the LV, with error bars denoting the 95% confidence interval, thus yellow identifies variables significantly contributing to the LV. Black vertical line corresponds to a BSR threshold of 2.58. BSR, bootstrap ratio; LV, latent variables. (For interpretation of the references to color in this figure legend, the reader is referred to the Web version of this article.)

4.5.2.2 Displacement

Here, we studied the relationship between age and displacement measures for each hippocampal vertex. In Figure 4.4 **A**, we used AIC at each vertex of the hippocampus, and found different types of age relationships. The models showing a significant effect of age are

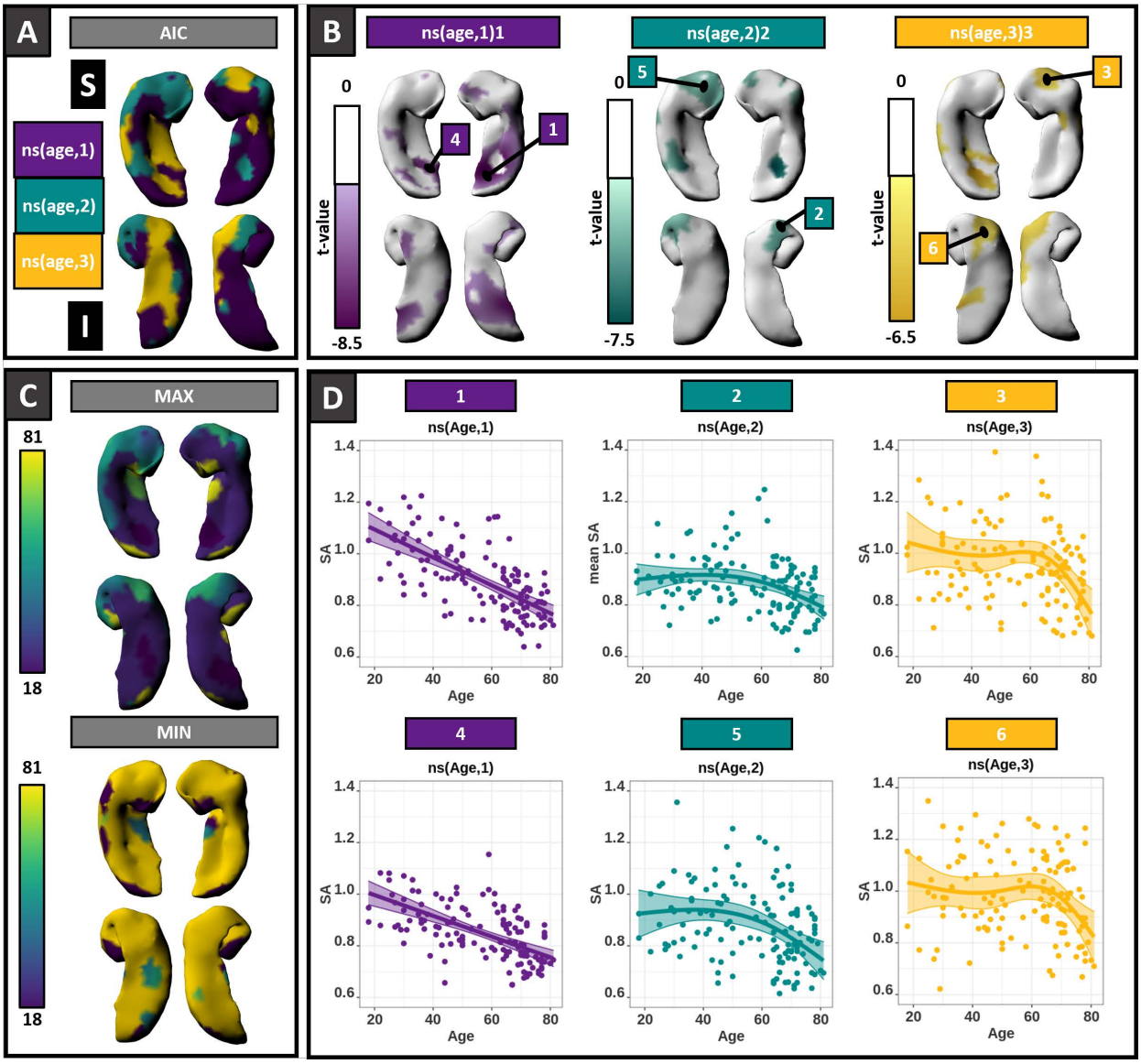

Figure 4.3: **A** SA vertex-wise best fit age-relationship models as determined by AIC; purple for linear, cyan for second order and yellow for third order relationships with age; S: superior view; I: inferior view. **B** Representation of significant age effects using the best model at each vertex (only higher order predictor shown) and the location of 6 significant peak vertices. t-value maps correspond to significant p-values (corrected at FDR 5%). **C** Using the best model at each vertex, representation of the age for which SA was at its maximum or minimum. **D** Plots of the SA of 6 peak vertices with age. FDR, false-discovery rate; SA, Surface area. (For interpretation of the references to color in this figure legend, the reader is referred to the Web version of this article.)

displayed in Figure 4.4 **B**. A significant positive linear relationship with age was found in the inferior lateral hippocampus, while a significant negative relationship was found in the

medial tail of the hippocampus. Significant positive second-order best models were located in the lateral hippocampus, while negative second-order models were situated in the right head and medial body of the hippocampus. Finally, a local positive third-order displacement was contained in the left superior uncus, while a negative third-order model was found in the left inferior uncus. Significant negative linear relationships were also observed, especially in the inferior medial tail of the hippocampus. Significant negative second-order models were in the right superior head and along the medial body of the hippocampus. A third-order negative displacement was located in the inferior left uncus. In general, the maximum displacement was found at an older age laterally and at a younger age in the superior body and medial inferior tail (see Figure 4.4 **C**). Conversely, the minimum displacement was found in the superior tail and inferior head of the hippocampus. In Figure 4.4 **D**, we plotted peak vertices of the different significant displacement change with age.

4.5.3 Partial least squares analysis

4.5.3.1 Surface area

For SA, PLS demonstrated three significant LVs, with the LV1 for the right hippocampus explaining 79%, the LV2 for the right hippocampus explaining 15% and the LV1 for the left hippocampus explaining 68% of the covariance (Figure 4.5). Right LV1 represents a pattern in which decreased overall right SA is associated with older age (R = 0.39, 95% CI = 0.25,0.53), female sex (R = 0.55, 95% CI = 0.44,0.67), low education (R = -0.22, 95% CI = -0.40,-0.03) and RBANS scores (R = -0.22, 95% CI = -0.44,-0.04). Left LV1 identifies a pattern in which decreased SA in the dorsal hippocampus is associated with older age (R = 0.41, 95% CI = 0.31,0.57) and female sex (R = 0.33, 95% CI = 0.18,0.51). Thus, similarly to the subfield-wise PLS, age and female sex are key factors explaining the hippocampal SA modifications. Also, the right hemisphere SA is more impacted by lower cognitive performance and levels of education. Significant effects of age impact regional SA, such that the right hemisphere with the right LV2 pattern shows an increased SA in medial

tail and decrease SA in the uncus to be associated with younger age (R = -0.55, 95% CI = -0.75,-0.20).

4.5.3.2 Displacement

For displacement, PLS analysis demonstrated 3 significant LVs with the right LV1 explaining 52%, right LV2 explaining 29% and left LV1 explaining 77% of the covariance (Fig. 4.6). Right LV1 showed a pattern in which outward displacement in the superior head and the medial tail, as well as inward displacement in the lateral body, was associated with younger age (R = -0.69, 95% CI = -0.78,-0.63). Left LV1 identified a pattern in which outward displacement in the superior body and inferior medial hippocampus, as well as inward displacement in the lateral hippocampus, was associated with younger age (R = -0.62, 95% CI = -0.72,-0.54), high RBANS score (R = 0.28, 95% CI = 0.13,0.44) and higher levels of education (R = 0.23, 95% CI = 0.08, 0.40). In contrast to what was observed previously in the volumes and SA analyses, here, cognition and education appear to have an effect on the left hippocampus. Interestingly, a sex effect was only found in the right hemisphere with the right LV2, identifying a pattern in which inward displacement in the hippocampus head was associated with female sex (R = 0.41, 95% CI = 0.37,0.59) and lower education levels (R = -0.24, 95% CI = -0.43,-0.13).

4.5.4 Replication dataset - age analyses

4.5.4.1 Surface area

In Supplementary Fig. 4.7A, we used AIC at each vertex to investigate different types of age relationships. Most of the hippocampi vertices expressed linear or second-order age relationships as best models. The vertices showing a significant effect of age were displayed in Supplementary Fig 4.8B. Significant linear decrease or second-order decrease with age were found in the tail of the hippocampus, while the head of the hippocampus did not indicate significant relationships with age. Using these best models, we found that the maximum

SA was largely found at 18 years old, except in the superior head and inferior body of the hippocampus which showed a maximum SA at ≈ 50 years old (Supplementary Fig. 4.8C). Moreover, the minimum SA was reached at 81 years old, except in some local areas, such as the lateral body of the hippocampus, which demonstrated a minimum SA at 18 years old. In Supplementary Fig. 4.8D, we plotted peak vertices of these different significant relationships with age.

4.5.4.2 Displacement

We also studied the relationship between age and displacement measures for each hippocampal vertex in the Cam-CAN dataset. In Supplementary Fig. 4.9A, we used AIC at each vertex of the hippocampus, and found different types of age relationships. The models showing a significant effect of age were displayed in Supplementary Fig. 4.9B. A significant positive linear relationship with age was found in the uncus, while a significant negative relationship was found in the medial tail of the hippocampus. Significant positive second-order best models were located in the lateral hippocampus, while negative second-order models were situated in the medial tail of the hippocampus. Finally, a local positive third-order displacement was contained in the lateral tail, while a negative third-order model was found in the left inferior uncus. In general, the maximum displacement was found at an older age laterally and at a younger age in the superior body and medial inferior tail (see Supplementary Fig. 4.9C). Conversely, the minimum displacement was found in the superior tail and inferior head of the hippocampus. In Supplementary Fig. 4.9D, we plotted peak vertices of the different significant displacement change with age.

4.6 Discussion

The aim of this paper was to investigate the relationship between age and hippocampal structure throughout the healthy lifespan. To address this topic, we used standard subfield-wise

volumetric as well as vertex-wise SA and displacement measurements. To summarize, we found an accelerated decrease across hippocampal volumes after 60 years old and an overall decreased volume associated with older age and female sex. Vertex-wise, we found an overall preservation of the SA in the hippocampal head while the body and tail expressed a reduced SA with age. Further, an outward displacement was found in the lateral hippocampi, while an inward displacement was found in the medial hippocampi with age, possibly demonstrating an accentuation of the hippocampal curvature with age. Additionally, we found that females had a stronger decrease of SA with age while sex had a lower effect on the displacement. Further, while APOE-ϵ4 allele was not found to be associated with our results, lower education and cognitive scores were correlated with lower SA in the right hippocampus. Moreover, higher education and cognitive scores were correlated with stronger inward and outward patterns of displacement in the left hippocampus. Hence, these results may suggest that preserved global cognition and greater education lead to altered hippocampal morphometry potentially resulting in greater curvature with age.

Moreover, we found a similar overall pattern of age-relationships for our vertex-wise results using two different datasets. Indeed, using the Cam-CAN dataset as an independent replication dataset, we have demonstrated that no evolution with age of the SA was found in the head of the hippocampi and a decrease of the SA was observed with age in the body and tail of the hippocampi. Further, the displacement results also demonstrated an identical pattern of change with age in the replication dataset, with an outward displacement in the lateral hippocampi and in the uncus, while an inward displacement was found in the medial hippocampi. These results highlight that our findings are replicable and consistent across different samples.

Subfield-wise investigation demonstrated third-order relationships for all the hippocampal subfield volumes with age, highlighting an accelerated volumetric decrease after the age of 60. These results are in line with previous studies demonstrating a faster rate of hippocampal volumes decline during the sixth decade in healthy aging (Yang et al. 2013; Nobis et al. 2019;

Bussy, Plitman, et al. 2021). Right CA1 volume appeared to be relatively less impacted by age, reproducing previous results from our group (Voineskos et al. 2015; Bussy, Plitman, et al. 2021; R. S. C. Amaral et al. 2018). Further, hippocampal volume analyses examining the influence of demographic factors emphasized that volume loss in most subfields (all except left CA2CA3) was strongly associated with older age and female sex, and to a lesser extent, in the right hemisphere, with lower cognitive performance and lower levels of education.

These results are in agreement with the literature; hippocampal subfield volumes are known to reduce during aging (Clifford R Jack Jr, Wiste, et al. 2015; Flores, La Joie, Landeau, et al. 2015). Moreover, lower levels of education (K. G. Noble et al. 2012) and low cognitive performance (O'Shea et al. 2016) are known to be risk factors for hippocampal atrophy. Also, we found that female sex was predominantly associated with low volumes and correlated with lower levels of education and cognition. Interestingly, hippocampal volumes have been found to be positively linked to associative memory in older women but not in men (Z. Zheng et al. 2017). Overall, this pattern of correlation between volumes and demographic characteristics was interesting but did not provide any information about the spatial specificity of these relationships since all subfields were implicated, except the left CA2CA3.

To investigate the spatial specificity of the impact of age in more depth, we ran vertex-wise analysis that demonstrated different patterns of age relationships throughout the hippocampal structure. The body/tail manifested a SA linear decrease, while the head suggested second- and third-order relationships with age. These findings illustrated a relative preservation of the anterior hippocampal SA with a peak during the sixth decade, while the posterior hippocampal SA gradually decreased across lifespan. Moreover, overall decrease of SA was linked to older age, female sex and, to a lesser extent in the right hemisphere, lower cognitive performance and lower levels of education. These results replicated the correlations found between the volumes and the cognitive/demographic factors described above. In addition, older age was specifically linked to lower SA in the right posterior hippocampus.

SA results are in agreement with previous findings demonstrating a stronger impact of aging in the posterior hippocampus (Nikolai V Malykhin, Y. Huang, et al. 2017; Langnes et al. 2020). Additionally, evidence of anterior/posterior (AP) anatomical and functional differences in the hippocampus have been highlighted by various studies. Namely, studies have indicated gradients of anatomical extrinsic connectivity with cortical and subcortical structures along the hippocampus long axis (Bryan A Strange et al. 2014). Further, the posterior hippocampus appears to be specifically involved in spatial memory, while the anterior hippocampus is more involved in stress responses and emotional behavior (Fanselow and H.-W. Dong 2010). Another recent study demonstrated that the anterior hippocampus showed higher functional connectivity with the anterior temporal lobe, orbitofrontal, inferior frontal gyrus, and premotor cortex, while the posterior hippocampus was more functionally connected to the medial and lateral frontal lobe, inferior parietal lobule, precuneus, and occipital lobes (Tang et al. 2020). This AP axis appeared to be related to hippocampal gene expression providing evidence of a molecular AP gradient (Vogel et al. 2020). Additionally, several previous and recent studies have suggested a hippocampal AP functional and anatomical gradient (B A Strange et al. 1999; Bryan A Strange et al. 2014; Vos de Wael et al. 2018; Przeździk et al. 2019). Ultimately, our analyses support previous findings demonstrating a hippocampal AP axis. Also, our results indicate that the specific impact of age in the posterior hippocampus could illustrate that posterior hippocampal functions and connections might be more vulnerable than those in the anterior portion of the hippocampus.

In the present paper, analyses also indicated outward displacement with older age in the lateral hippocampus and inward displacement with older age in the medial hippocampus. Further, PLS analyses also strengthened this finding, demonstrating medial outward displacement and lateral inward displacement associated with younger age, and, to a lesser extent in the left hemisphere, higher levels of cognition and education. Interestingly, this pattern was distinct from the sex effect, which was found in the head of the hippocampus, in which inward displacement was associated with low education and female sex. Education

has often been considered an influential factor in cognitive performance and hippocampal volume or microstructure (Piras et al. 2011) as well as a protective factor against mild cognitive impairment (Wada et al. 2018) and AD dementia (Meng and D'Arcy 2012; Groot et al. 2018). Gender inequality with regards to education is predictable since older women from our datasets were born in a socioeconomic period when they were less encouraged to pursue higher education than men (Permanyer and Boertien 2019). This could explain why female sex and low education are associated with age, and potentially contribute to our observed higher prevalence of women for hippocampal impairment-like measures. Furthermore, gender inequality regarding education could partly be responsible for the increased risk of developing AD in women (Beam et al. 2018).

In the cortex, gray matter volume is defined as the product of SA and thickness. Therefore, measures of cortical volume are thought to reflect structural properties that could be specific to cortical SA or to CT (Panizzon et al. 2009). Further, the neurons of the cerebral cortex have been shown to be organized into radial cell sacks called ontogenetic columns that are perpendicular to the surface of the brain (Rakic 1995; Mountcastle 1997; Pasko Rakic 2007). Also, it is well-known that the size of the cortical SA depends on the number of ontogenetic columns, whereas CT is influenced by the number of cells within a column (Rakic 1988). Therefore, we could extrapolate the same theory on the hippocampal SA, which would suggest that the preferential SA decrease in the body/tail of the hippocampus with age reflects a reduced number of ontogenetic columns with advanced age. This reduced SA in the posterior hippocampus could potentially result in reduced hippocampal connectivity with the rest of the brain structures. Further, since previous studies have demonstrated that the posterior hippocampus is more associated with memory and spatial navigation (Bryan A Strange et al. 2014), we could expect that the reduced posterior SA leads to an impairment in these functions. Also, while displacement metric is different from CT, the interpretation of the CT could be expanded to the displacement, where inward displacement might reflect a lower number of cells within a column. However, since we have inward displacement in

one side of the hippocampus and outward displacement in the other side of the hippocampi, our findings suggest that rather than seeing a decreased hippocampal thickness, we see a reshaping and a curving of the hippocampus with age.

Previously, medial/lateral (ML) gradient was found to correlate with an estimation of myelin content in the hippocampus, with the medial hippocampus having a higher myelin content (Vos de Wael et al. 2018). Further, a recent paper using a non-negative matrix factorization technique to cluster the hippocampus demonstrated that the medial hippocampus cluster was the most myelinated (Patel, Steele, et al. 2020). Similarly, intracortical myelin was found to be the highest in the subiculum, which is the most medial hippocampal subfield (Jordan DeKraker et al. 2018). Therefore, we hypothesize that the inward medial displacement with age observed in our study could potentially be associated with an age-related myelin decrease.

Interestingly, no effect of APOE-ϵ4 allele genotype was established in our analysis, neither for the subfield volumes nor for the morphological measurements. Similarly, in a previous study performed in our laboratory, while APOE-ϵ4 allele genotype demonstrated a trend for local inward displacement in the medial hippocampal head and outward displacement in the inferior head, these effects were not significant after 5% FDR correction (Voineskos et al. 2015). These outcomes are contradictory to previous findings showing increased atrophy rates in the hippocampus of APOE-ϵ4 allele carriers (Shi et al. 2014; B. Li et al. 2016; Q. Dong et al. 2019). Nevertheless, other studies have found no evidence for a significantly greater rate of atrophy with increasing age (J. L. Taylor et al. 2014), nor even a stronger effect of age on hippocampal atrophy in the APOE-ϵ4 allele non-carriers (Gonneaud et al. 2016; Bussy, Snider, et al. 2019).

Furthermore, in our PLS analyses, we demonstrated that the anterior hippocampal vertices already demonstrating decline in the first decades of life (expressing a linear decrease with age) were the ones highly associated with low cognition and education as well as with female sex. Moreover, SA relative preservation in the head of the hippocampus seems to

be relatively well colocalized within the anterior CA1 subfield (see Figure 4.1), which might help to explain the relative preservation of CA1 volumes with age that we found when using subfield-wise measures. Nonetheless, this result seems to be in agreement with a previous study showing a similar finding on the CA1 preservation with age using a voxel-based morphometry technique (La Joie, Fouquet, et al. 2010).

Volumetric measures have the drawbacks of being directly impacted by the definition of the hippocampal subfields (which is highly inconsistent among research groups (Yushkevich, R. S. C. Amaral, et al. 2015; Bussy, Plitman, et al. 2021)), by the quality of segmentation, and only gives global information which does not reflect local changes. In turn, vertex-wise measurements provide local information which can be independently calculated in each vertex, do not depend on any *a priori* subfield definition and allow independent vertex-wise statistical analyses. In the present study, using vertex-wise analysis, we demonstrated that the SA was differentially impacted by age along the AP axis. These results could not have been observed at all using subfield-wise measurements since the hippocampal subfields are structures defined along the AP axis. Further, the AP differences that we found are not based on *a priori* AP or head/body/tail segmentations but rather are based on data-driven results. Also, regarding our displacement findings, while we might assume that a subiculum volume decrease could be analogous to an inward medial hippocampal displacement and that an increase of the CA1 volume could be analogous to the outward displacement seen laterally (even though displacement could be driven by the inner hippocampal subfields such as the DG), we would still miss the information suggesting an accentuation of the "C" shape with age.

Further, several previous studies that have parsed the hippocampus have used subjective and variable ways to define different regions of the hippocampus, both in terms of the manner by which the head, body and tail subregions were parsed (Duvernoy, Cattin, and Risold 2013; Nikolai V Malykhin, Y. Huang, et al. 2017) as well as the definitions of the anterior and posterior hippocampus. These methodological discrepancies could potentially explain some

of the contradictory results, specifically that of anterior hippocampus volumes being more impacted by age, for example (Ta et al. 2012; Gordon et al. 2013). In the present paper, we believe that a methodological strength is that we performed our analyses with the goal of optimizing the statistics performed on our datasets; notably, the AIC method was used to select the best fit curves for each vertex (Akaike 1974; Mazerolle 2006). Accordingly, we found spatially well-defined and relatively bilateralized clusters of vertices, behaving either in a linear, second-, or third- order fashion, highlighting clear differences of age-related relationships throughout the hippocampus. We further investigated these model choices by calculating the difference between the AIC of the two best models for each vertex (Burnham and D. R. Anderson 2004). These analyses demonstrated that for most voxels, AICmin provides a similar quality of fit than AICsecond, except for most of the voxels demonstrating third-order models in AICmin and which have considerable support over second-order models in AICsecond (Burnham and D. R. Anderson 2004). Further, our replication dataset exhibited fairly dissimilar AIC patterns for both SA and displacement, demonstrating that these AIC maps might not be generalizable. However, while the AIC maps looked dissimilar between our 2 datasets, when looking specifically at the significant vertex-wise models, we demonstrated that they were found in similar areas and that they demonstrated similar age relationships (Figs. 4.3B, 4.4B and Supplementary Figs. 4.8B and 4.9B). Therefore, this demonstrates that despite dissimilar AIC maps, our significant vertex-wise results and overall patterns of SA and displacement changes with age can be generalized to healthy aging populations.

The EC is a structure known to connect a variety of cortical areas with the hippocampus. Sensory inputs are integrated in the superficial layers of the EC while layers *II* and *III* project to the hippocampus. Specifically, neurons from layer *II* project to the DG and CA3 through the perforant pathway, whereas layer *III* projects to the CA1 and subiculum through the mossy fibers (Strien, Cappaert, and M P Witter 2009; Menno P Witter et al. 2017). The hippocampal circuitry ends with the subiculum projecting back to the layers *V* and *VI* of

the EC, which has widespread cortical and subcortical projections. Selective vulnerability of neurons in layer *II* of the EC have been demonstrated in aging and AD (Gómez-Isla et al. 1996; Kordower et al. 2001; Stranahan and Mattson 2010). These results highlight a stronger age-susceptibility in layer *II* than in layer *III*. This could help explain our results since we have shown a higher age-related susceptibility in layer *II* projections, i.e. CA2CA3 and CA4DG subfields (Small et al. 2011), than in layer *III* projections, i.e. CA1 and subiculum. Indeed, some studies have demonstrated that regions with higher connection demonstrate selective vulnerability to disease-associated atrophy patterns (Seeley et al. 2009; Zhou et al. 2012; Shafiei et al. 2020).

Hippocampal development undergoes rapid growth and morphological modifications during the perinatal months. The hippocampal shape is likely influenced by the rate of neural progenitor migration in the developmental period and by neurogenesis in the DG until adulthood (Nowakowski and Rakic 1981; Kornack and Rakic 1999). Another study demonstrated that similar numbers of intermediate neural progenitors were found in the DG as well as comparable numbers of glia and mature granule neurons in cognitively normal individuals aged 14–79, indicating that neurogenesis persists throughout the course of healthy aging (Boldrini et al. 2018). Moreover, a study examining the impact of prematurity on the hippocampal shape demonstrated that at age 7, preterm children had greater hippocampal expansion in the AP direction and contraction along the medial border compared to full term children (D. K. Thompson et al. 2014). Interestingly, this shows that perinatal development has the same effect of aging that we observed later in life (i.e., an accentuation of the "C" shape). This leads us to hypothesize that the shape modification seen with age in our results is the continuation of the normal brain development and reorganization and not necessarily a marker of aging specific atrophy.

An important limitation to acknowledge is that this paper used cross-sectional data to investigate age-related hippocampal changes. While our results exhibit an interesting and promising understanding of hippocampal aging, we should keep in mind that longitudinal

data would be necessary to validate these findings. Furthermore, the use of larger datasets could be relevant for such a validation study, as well as the use of higher resolution scans. Indeed, we previously demonstrated the impact of contrast and resolution on the hippocampal subfield volumes relationships with age (Bussy, Plitman, et al. 2021)(Bussy et al. 2021). Here, we decided to use T1w images because our morphometry technique is currently only applicable on T1w scans. However, further efforts to replicate these results using high resolution isotropic T2w images would be desirable.

To conclude, this paper aimed to describe the age-related relationships of the hippocampus volume and shape. Subfield-wise investigation demonstrated that the majority of the hippocampal subfields had accelerated volume decrease after 60 years old. Vertex-wise analysis provided more local information, showing a SA preservation in the anterior hippocampus, while the posterior hippocampus SA decreased linearly with age. Finally, displacement examination demonstrated a reinforcement of the hippocampus curvature with age.

4.7 Supplementary materials

4.7.1 Statistical models

Linear mixed-effects models (lmer from lmerTest 3.1-2 package in R 3.6.3) and natural splines (ns from splines package) were used to model linear, second, or third order age relationships for subfield-wise volumes. Akaike information criterion [AIC; (Akaike 1974)] was used to investigate the most appropriate age relationships across the multiple models. The model with the lowest AIC was selected and was considered to best fit the data (Mazerolle 2006). Sex, intracranial volume, APOE-ϵ4 allele status, education, MMSE, and RBANS were included as fixed effects, while dataset was included as a random effect 4.1.

$$Volume = ns(Age, n) + Sex + ICV + Education + MMSE + RBANS + (1|Dataset) \tag{4.1}$$

Linear mixed-effects models (vertexLmer from RMINC 1.5.2.2 package in R 3.6.3) and natural splines were used to model linear, second, or third order age relationships for vertex-wise measurements. AIC was used to investigate the most appropriate age relationships across the multiple models. The model with the lowest AIC was selected and was considered to best fit the data. Sex was included as fixed effects while dataset was included as a random effect 4.2.

$$SA\ ns(Age, n) + Sex + (1|Dataset) \tag{4.2}$$

4.7.2 Demographic information

	INITIAL		
	ADB (n=66)	**HA (n=112)**	**Overall (n=178)**
Age			
Mean (SD)	69.8 (5.74)	45.5 (16.4)	54.6 (17.9)
Median [Min, Max]	70.0 [56.0, 81.0]	44.0 [18.0, 80.0]	59.0 [18.0, 81.0]
Sex			
F	41 (62.1%)	57 (50.9%)	98 (55.1%)
M	22 (37.9%)	55 (49.1%)	80 (44.9%)

Table 4.2: Initial demographics of the 178 participants included before motion QC.

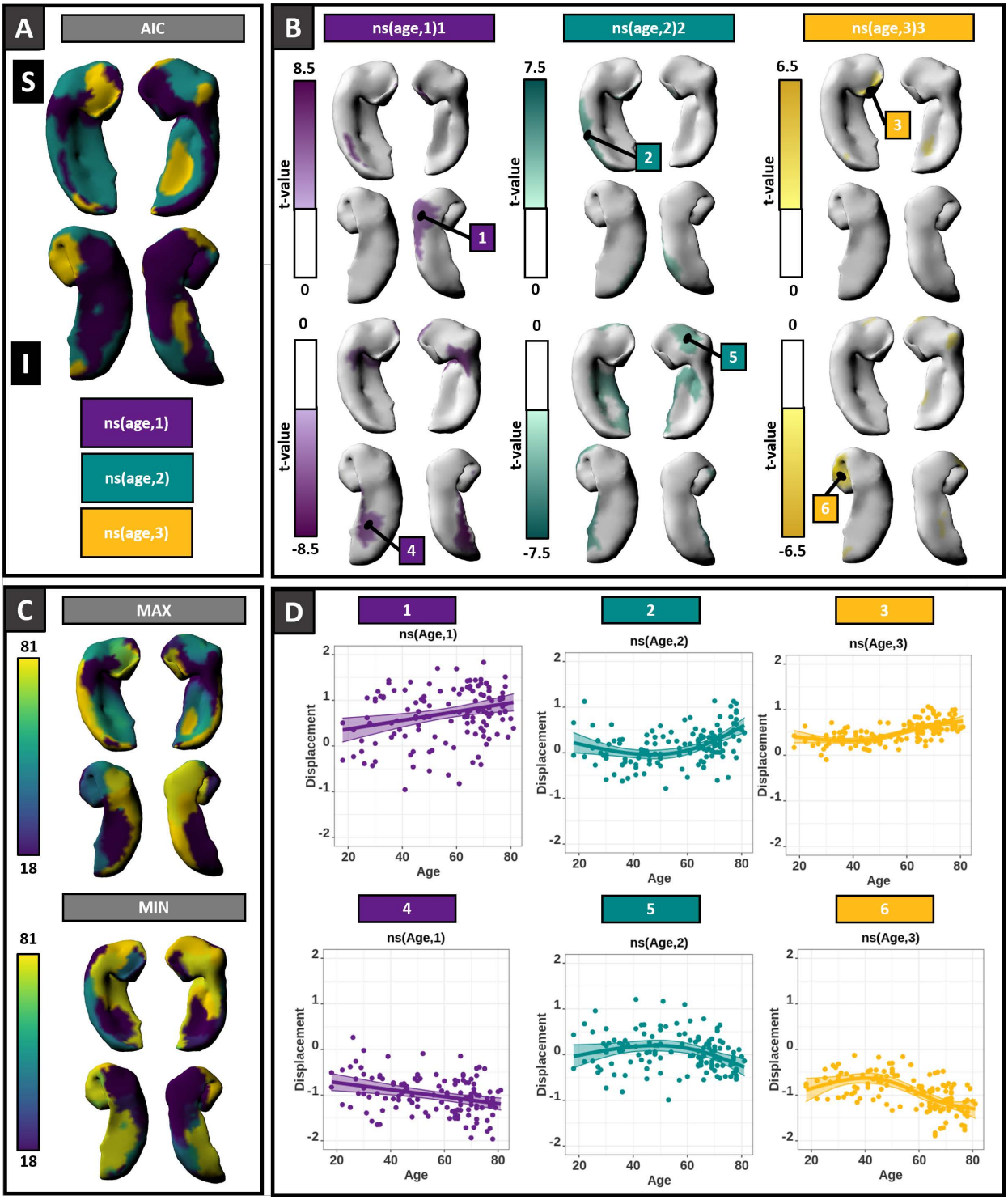

Figure 4.4: **A** Displacement vertex-wise best age-relationship models from AIC; purple for linear, cyan for second-order and yellow for third-order relationships with age; S: superior view; I: inferior view. **B** Representation of significant age effect using the best model at each vertex (only higher order predictor shown) and the location of 6 significant peak vertices. t-value maps correspond to significant p-values (corrected at FDR 5%). **C** Using the best model at each vertex, representation of the age for which displacement was at its maximum or minimum. **D** Plots of the displacement of 6 peak vertices with age.

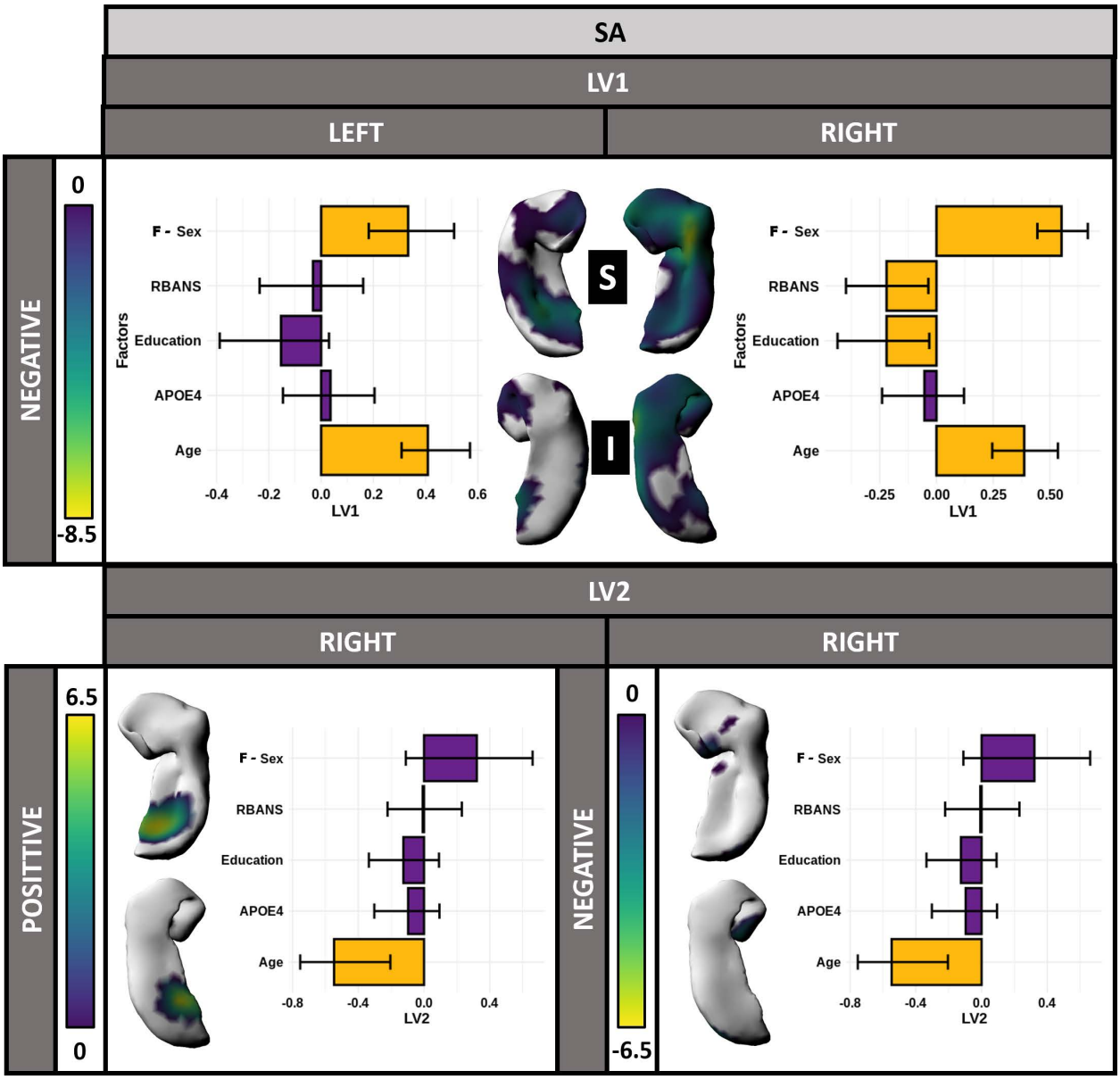

Figure 4.5: PLS analysis between the left/right SA and the demographic information identified two significant LVs on the right and one on the left ($p < 0.05$); S: superior view; I: inferior view. Right LV1 explained 79%, right LV2 explained 15% and left LV1 explained 68% of the covariance. Bar plots describe the correlation of each demographic variable with the LV, with error bars denoting the 95% confidence interval; yellow identifies variables contributing significantly to the LV. For each LV, vertex wise BSR is plotted on the hippocampal surface and thresholded at 2.58 ($p < 0.01$), describing the vertex wise SA patterns identified by each LV. BSR, bootstrap ratio; LV, latent variables; PLS, partial least square; SA, Surface area.

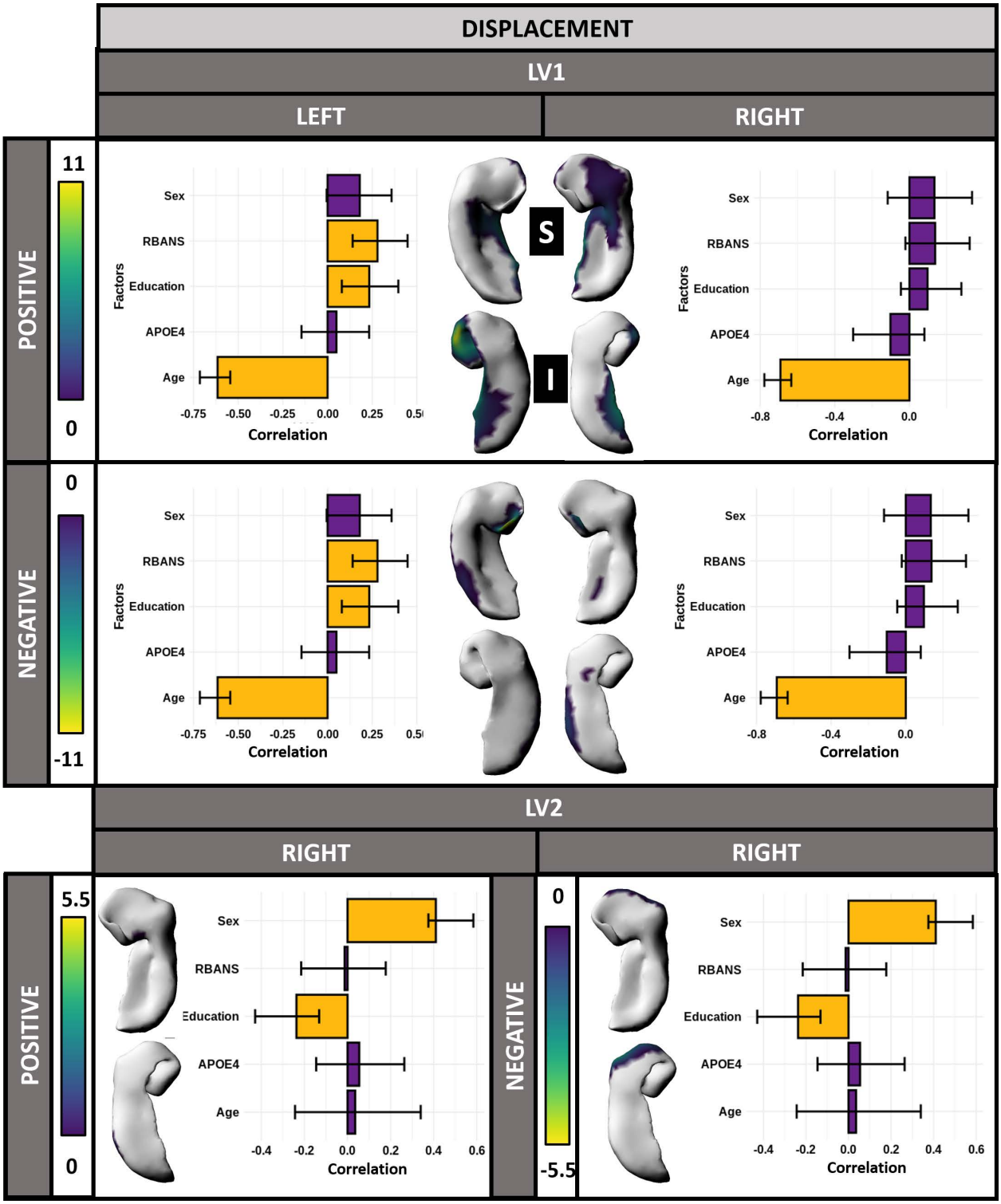

Figure 4.6: PLS analysis between the left/right displacement and the demographic information identified two significant LVs on the right and one on the left ($p < 0.05$); S: superior view; I: inferior view. Right LV1 explained 52%, right LV2 explained 29%, and left LV1 explained 77% of the covariance. Bar plots describe the correlation of each demographic variable with the LV, with error bars denoting the 95% confidence interval; yellow identifies variables contributing significantly to the LV. For each LV, vertex wise BSR is plotted on the hippocampal surface and thresholded at 2.58 ($p < 0.01$), describing the vertex wise displacement patterns identified by each LV. BSR, bootstrap ratio; LV, latent variables; PLS, partial least square; SA, Surface area.

4.7.3 Age relationship of the hippocampal subfield volume

	t-value ns(Age,3)1	t-value ns(Age,3)2	t-value ns(Age,3)3	p-value ns(Age,3)1	p-value ns(Age,3)2	p-value ns(Age,3)3
Left HIPGM	-1.49	-1.91	-5.88	0.14	0.06	***1.35e^{-7}***
Left CA1	-0.28	-1.72	-4.03	0.78	0.09	***1.95e^{-4}***
Left CA2CA3	-0.28	1.20	-3.54	0.78	0.23	***6.84e^{-4}***
Left CA4DG	-2.69	-2.65	-5.71	0.01	9.75e^{-3}	***2.64e^{-7}***
Left subiculum	-1.53	-1.99	-4.34	0.13	5.03e^{-2}	***4.55e^{-5}***
Left SRLM	-0.88	-1.15	-6.11	0.40	0.25	***3.34e^{-7}***
Right HIPGM	-1.62	-2.08	-4.53	0.12	0.04	***2.88e^{-5}***
Right CA1	0.44	-1.28	-2.90	0.66	0.21	4.89e^{-3}
Right CA2CA3	-1.84	-1.93	-3.70	0.08	0.06	***4.97e^{-4}***
Right CA4DG	-3.49	-3.49	-5.52	***9.66e^{-4}***	***8.15e^{-4}***	***5.20e^{-7}***
Right subiculum	-2.03	-1.17	-3.04	0.05	0.25	***3.55e^{-3}***
Right SRLM	-1.21	-1.60	-4.75	0.24	0.11	***1.95e^{-5}***

Table 4.3: T-values and p-values from linear mixed-effects models for the age relationship of the bilateral total hippocampus and each hippocampal subfield volume. Sex, intracranial volume, APOE-ϵ4 allele status, education, MMSE, and RBANS scores were included as fixed effects, while dataset was included as a random effect but only the age values were reported. Significant p-values after Bonferroni correction were italicized and in bold.

4.7.4 Model selection

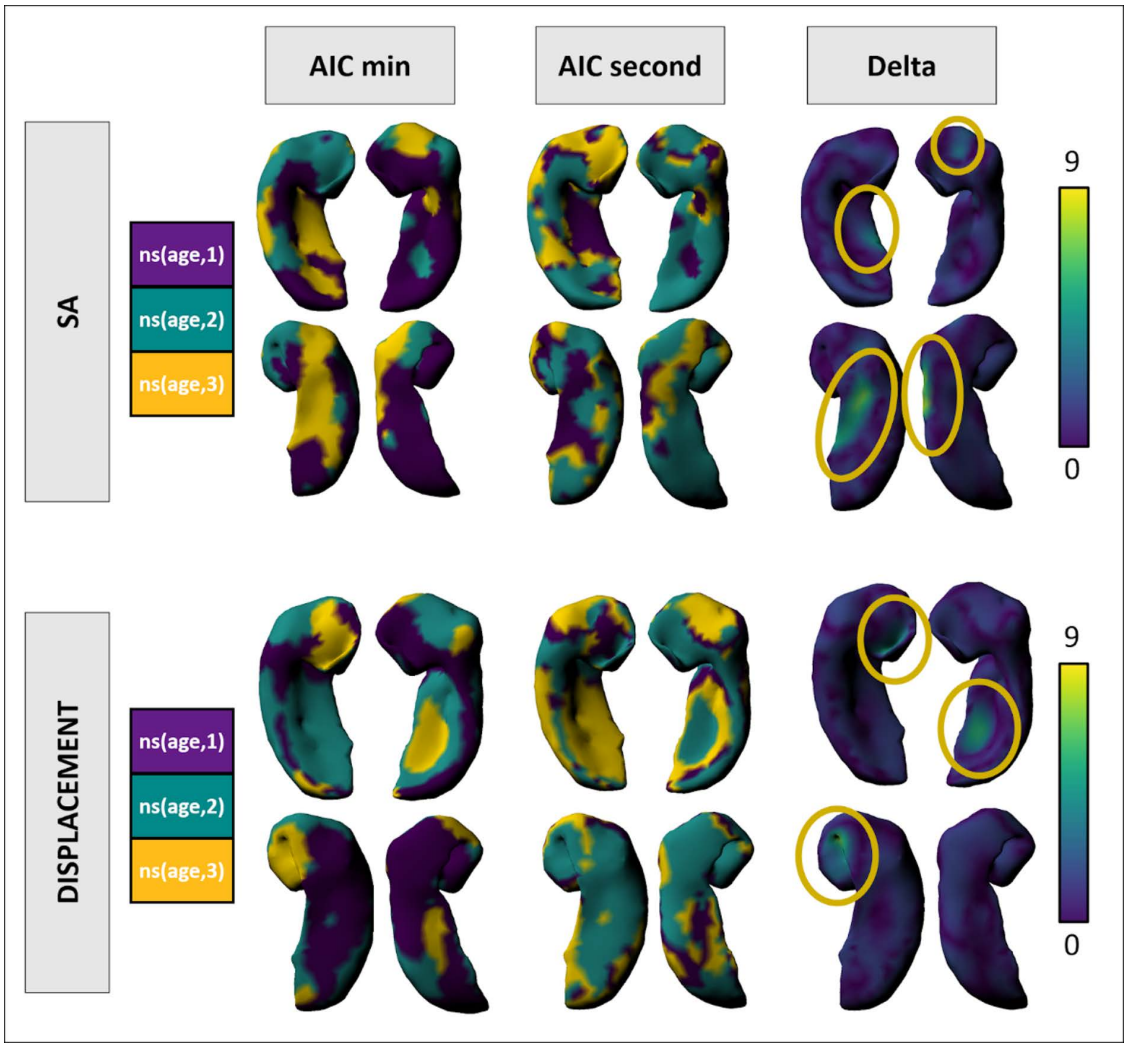

Figure 4.7: AICmin: Vertex-wise illustration of the best fit age-relationship models as determined by AIC; purple for linear, cyan for second order and yellow for third order relationships with age; AICsecond: Vertex-wise illustration of the second best fit age-relationship models as determined by AIC; Delta: Confidence map for the choice of model determined as the difference of AICmin value minus AICsecond value; Yellow circles surround the vertices with high delta, representing vertices where AICmin is strongly better than the AICsecond. Of note, these high deltas always coincide with a comparison between a third order relationship with age for the AICmin and a second order relationship with age for the AICsecond. However, in the vertices with delta close to 0 (purple verices), the data is similarly fitted with AICmin and AICsecond.

4.7.5 Replication dataset - SA

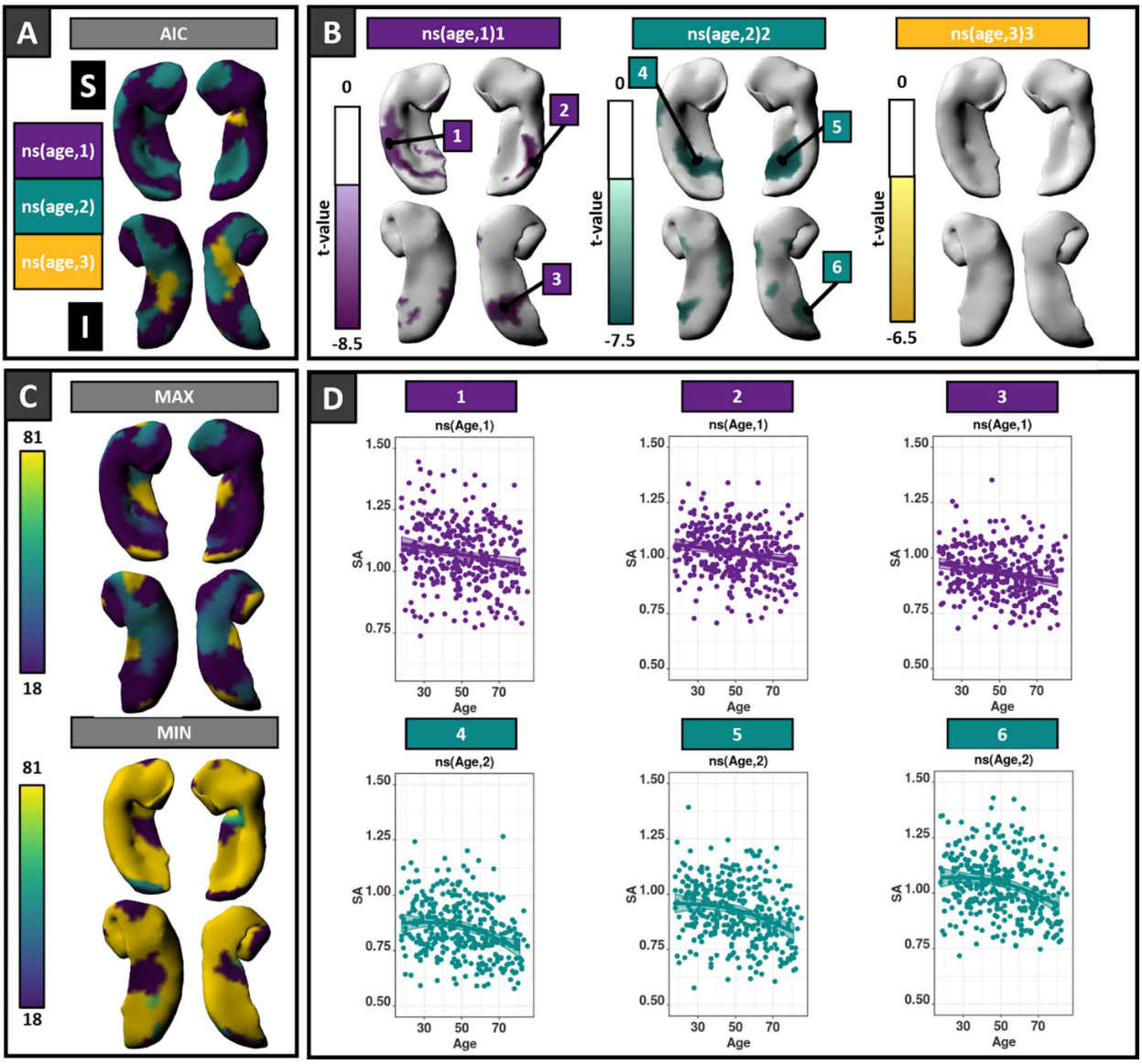

Figure 4.8: **A)** SA vertex-wise best fit age-relationship models as determined by AIC; purple for linear, cyan for second order and yellow for third order relationships with age; S: superior view; I: inferior view. **B)** Representation of significant age effects using the best model at each vertex (only higher order predictor shown) and the location of 6 significant peak vertices. t-value maps correspond to significant p-values (corrected at FDR 5%). **C)** Using the best model at each vertex, representation of the age for which SA was at its maximum or minimum. **D)** Plots of the SA of 6 peak vertices with age.

4.7.6 Replication dataset - Displacement

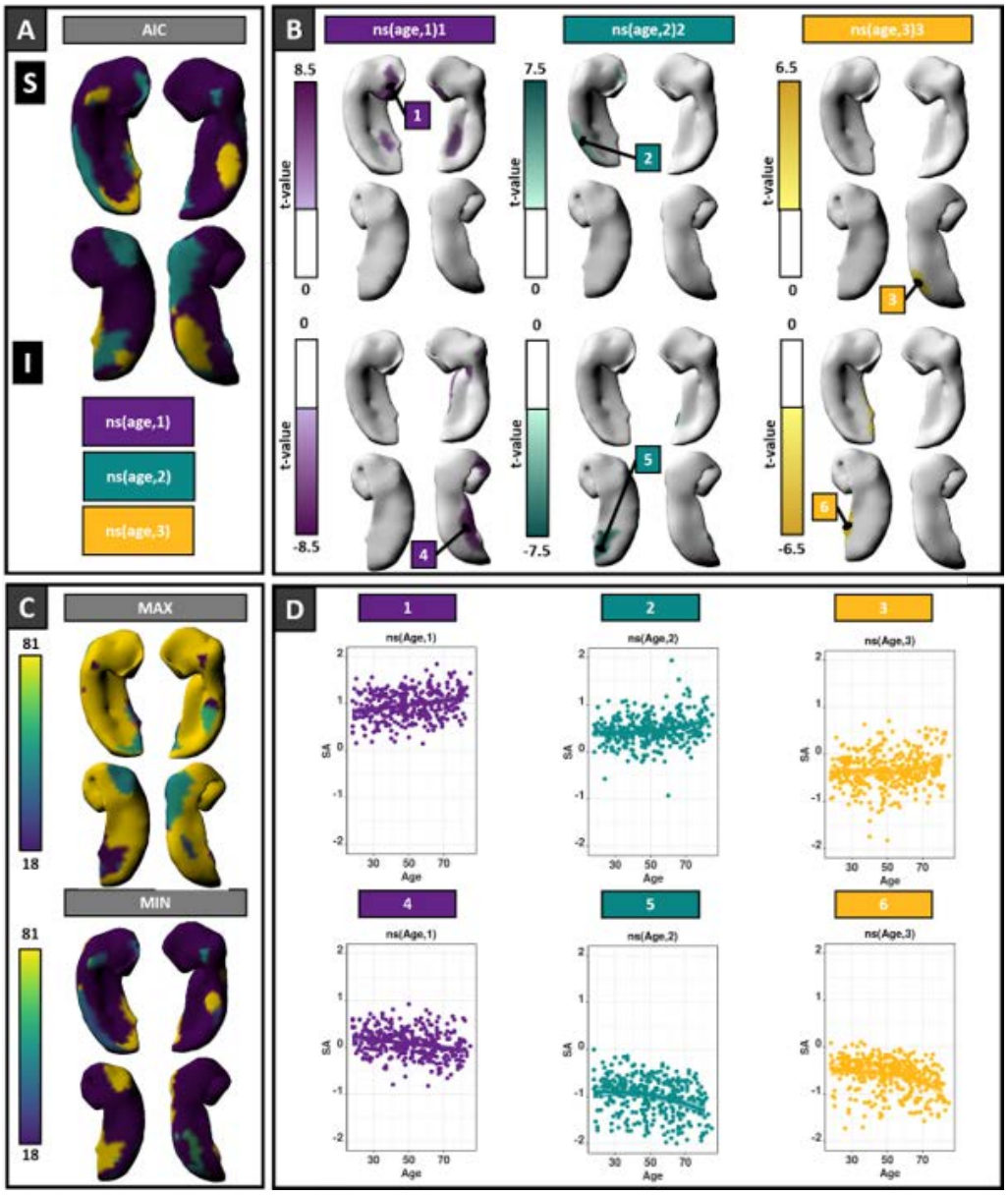

Figure 4.9: **A)** Displacement vertex-wise best fit age-relationship models as determined by AIC; purple for linear, cyan for second order and yellow for third order relationships with age; S: superior view; I: inferior view. **B)** Representation of significant age effects using the best model at each vertex (only higher order predictor shown) and the location of 6 significant peak vertices. t-value maps correspond to significant p-values (corrected at FDR 5%). **C)** Using the best model at each vertex, representation of the age for which displacement was at its maximum or minimum. **D)** Plots of the displacement of 6 peak vertices with age.

4.7.7 SA PLS using "age", "ns(age,2)" or "ns(age,3)"

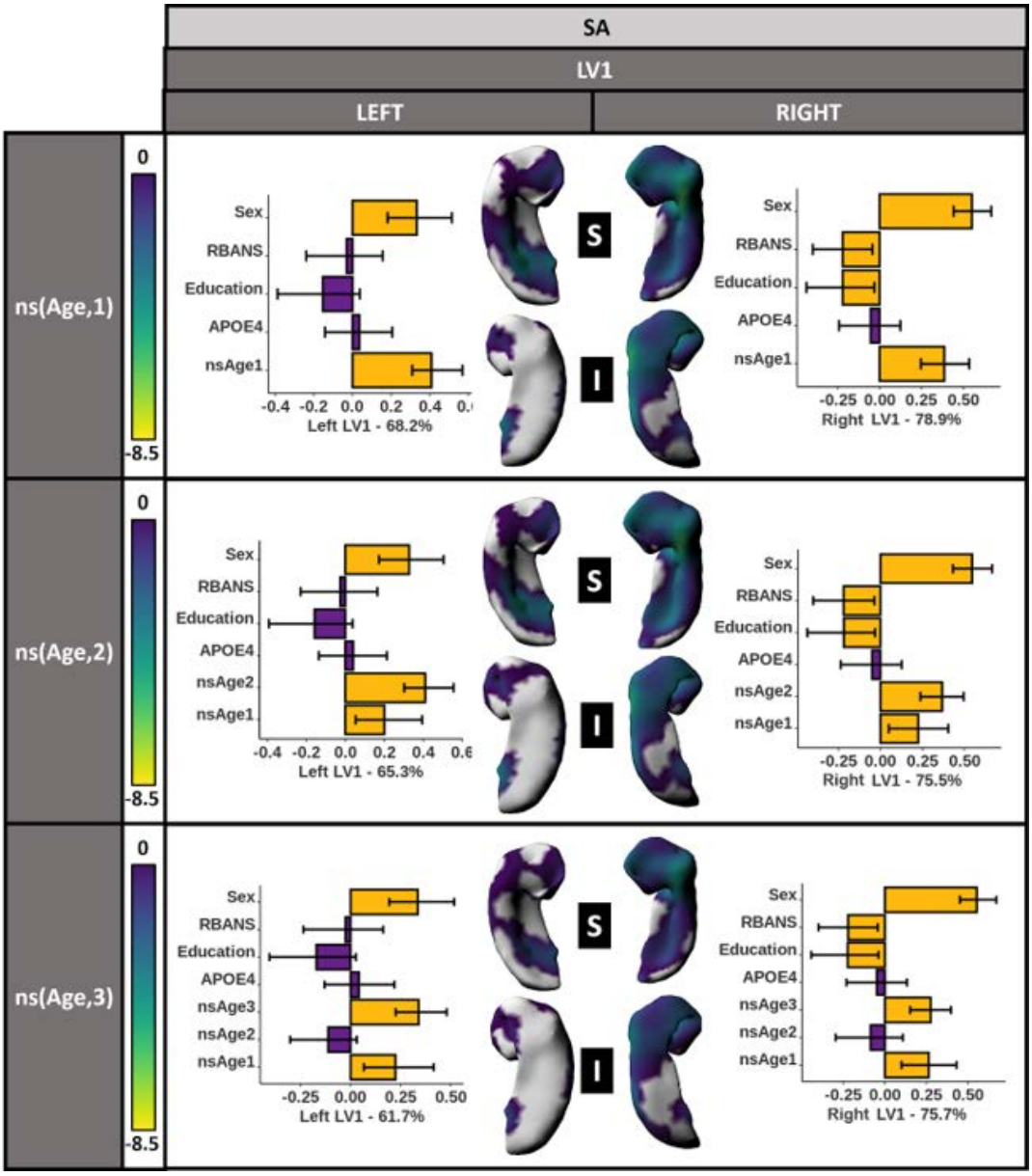

Figure 4.10: PLS significant first LV demonstrating association between the left/right SA and the demographic variables using either ns(age,1), ns(age,2) or ns(age,3). For each run, similar vertex-wise SA changes and similar associations with the demographic variables were found. S: superior view; I: inferior view. Bar plots describe the correlation of each demographic variable with the LV, with error bars denoting the 95% confidence interval; yellow identifies variables contributing significantly to the LV. Vertex wise BSR is plotted on the hippocampal surface and thresholded at 2.58 ($p<0.01$), describing the vertex wise SA patterns identified by each LV.

4.7.8 Displacement PLS using "age", "ns(age,2)" or "ns(age,3)"

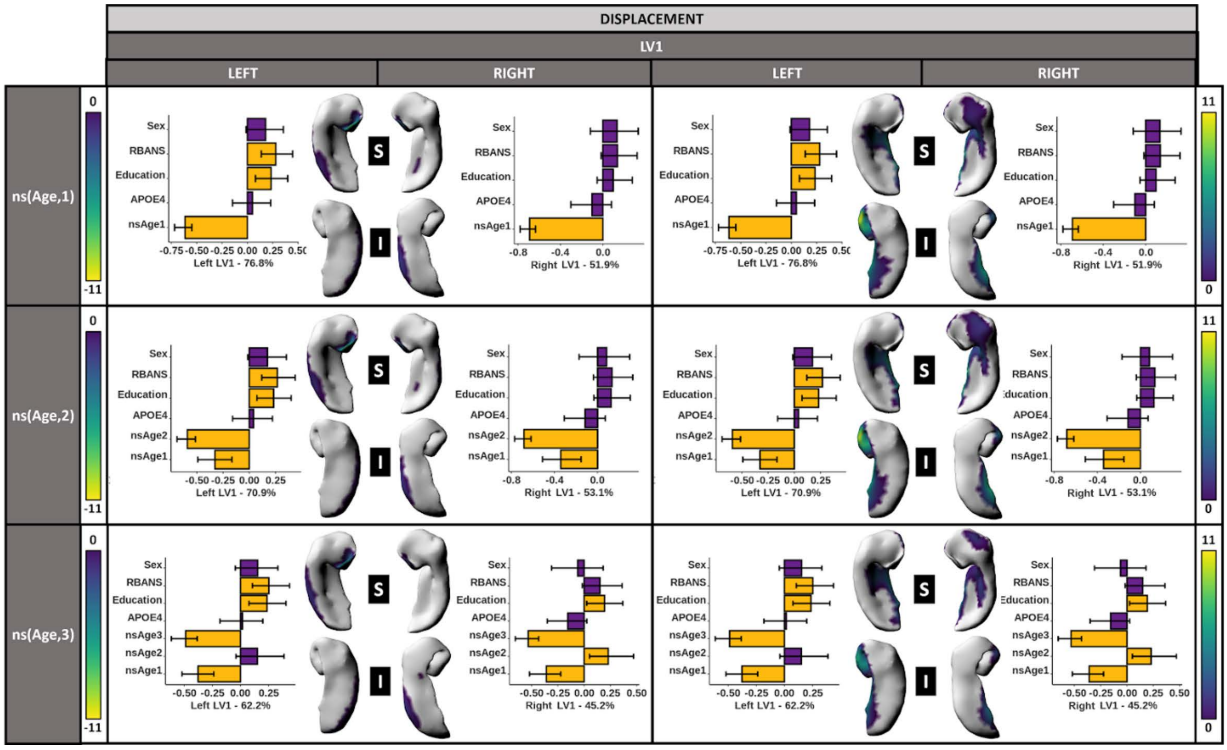

Figure 4.11: PLS significant first LV demonstrating association between the left/right displacement and the demographic variables using either ns(age,1), ns(age,2) or ns(age,3). For each run, similar vertex-wise displacement changes and similar associations with the demographic variables were found. S: superior view; I: inferior view. Bar plots describe the correlation of each demographic variable with the LV, with error bars denoting the 95% confidence interval; yellow identifies variables contributing significantly to the LV. Vertex wise BSR is plotted on the hippocampal surface and thresholded at 2.58 ($p<0.01$), describing the vertex wise displacement patterns identified by each LV.

References Chapter 4

Akaike, Hirotugu (1974). "A New Look at the Statistical Model Identification". In: *Springer Ser. Statist.*, pp. 215–222.

Alexander-Bloch, Aaron et al. (2016). "Subtle in-scanner motion biases automated measurement of brain anatomy from in vivo MRI". In: *Hum. Brain Mapp.* 37.7, pp. 2385–2397.

Amaral, Robert S C et al. (Apr. 2018). "Manual segmentation of the fornix, fimbria, and alveus on high-resolution 3T MRI: Application via fully-automated mapping of the human memory circuit white and grey matter in healthy and pathological aging". en. In: *Neuroimage* 170, pp. 132–150.

Apfel, Brigitte A et al. (Mar. 2011). "Hippocampal volume differences in Gulf War veterans with current versus lifetime posttraumatic stress disorder symptoms". en. In: *Biol. Psychiatry* 69.6, pp. 541–548.

Avants, B B et al. (Feb. 2008). "Symmetric diffeomorphic image registration with cross-correlation: evaluating automated labeling of elderly and neurodegenerative brain". en. In: *Med. Image Anal.* 12.1, pp. 26–41.

Beam, Christopher R et al. (2018). "Differences Between Women and Men in Incidence Rates of Dementia and Alzheimer's Disease". In: *J. Alzheimers. Dis.* 64.4, pp. 1077–1083.

Bedford, Saashi A et al. (Mar. 2020). "Large-scale analyses of the relationship between sex, age and intelligence quotient heterogeneity and cortical morphometry in autism spectrum disorder". en. In: *Mol. Psychiatry* 25.3, pp. 614–628.

Bellon, E M et al. (Dec. 1986). "MR artifacts: a review". en. In: *AJR Am. J. Roentgenol.* 147.6, pp. 1271–1281.

Benjamini, Y et al. (Nov. 2001). "Controlling the false discovery rate in behavior genetics research". en. In: *Behav. Brain Res.* 125.1-2, pp. 279–284.

Benjamini, Yoav and Yosef Hochberg (Jan. 1995). "Controlling the False Discovery Rate: A Practical and Powerful Approach to Multiple Testing". In: *J. R. Stat. Soc. Series B Stat. Methodol.* 57.1, pp. 289–300.

Bhagwat, Nikhil, Jon Pipitone, et al. (July 2016). "Manual-Protocol Inspired Technique for Improving Automated MR Image Segmentation during Label Fusion". en. In: *Front. Neurosci.* 10, p. 325.

Boldrini, Maura et al. (Apr. 2018). "Human Hippocampal Neurogenesis Persists throughout Aging". en. In: *Cell Stem Cell* 22.4, 589–599.e5.

Bremner, J D et al. (Jan. 2000). "Hippocampal volume reduction in major depression". en. In: *Am. J. Psychiatry* 157.1, pp. 115–118.

Bremner, J Douglas et al. (May 2003). "MRI and PET study of deficits in hippocampal structure and function in women with childhood sexual abuse and posttraumatic stress disorder". en. In: *Am. J. Psychiatry* 160.5, pp. 924–932.

Burnham, Kenneth P and David R Anderson (Nov. 2004). "Multimodel Inference: Understanding AIC and BIC in Model Selection". In: *Sociol. Methods Res.* 33.2, pp. 261–304.

Bussy, Aurélie, Raihaan Patel, et al. (Oct. 2021). "Hippocampal shape across the healthy lifespan and its relationship with cognition". en. In: *Neurobiol. Aging* 106, pp. 153–168.

Bussy, Aurélie, Eric Plitman, et al. (June 2021). "Hippocampal subfield volumes across the healthy lifespan and the effects of MR sequence on estimates". en. In: *Neuroimage* 233, p. 117931.

Bussy, Aurélie, B Joy Snider, et al. (Mar. 2019). "Effect of apolipoprotein E4 on clinical, neuroimaging, and biomarker measures in noncarrier participants in the Dominantly Inherited Alzheimer Network". en. In: *Neurobiol. Aging* 75, pp. 42–50.

Chakravarty, M Mallar, M Mallar Chakravarty, et al. (2009). "Comparison of piece-wise linear, linear, and nonlinear atlas-to-patient warping techniques: Analysis of the labeling of subcortical nuclei for functional neurosurgical applications". In: *Hum. Brain Mapp.* 30.11, pp. 3574–3595.

Chakravarty, M Mallar, Abbas F Sadikot, et al. (Dec. 2008). "Towards a validation of atlas warping techniques". en. In: *Med. Image Anal.* 12.6, pp. 713–726.

Chakravarty, M Mallar, Patrick Steadman, et al. (Oct. 2013). "Performing label-fusion-based segmentation using multiple automatically generated templates". en. In: *Hum. Brain Mapp.* 34.10, pp. 2635–2654.

Chapleau, Marianne et al. (June 2020). "Deformation-based shape analysis of the hippocampus in the semantic variant of primary progressive aphasia and Alzheimer's disease". en. In: *Neuroimage Clin* 27, p. 102305.

Collins, D L et al. (Mar. 1994). "Automatic 3D intersubject registration of MR volumetric data in standardized Talairach space". en. In: *J. Comput. Assist. Tomogr.* 18.2, pp. 192–205.

Convit, A et al. (1997). "Specific Hippocampal Volume Reductions in Individuals at Risk for Alzheimer's Disease". In: *Neurobiol. Aging* 18.2, pp. 131–138.

Coupé, Pierrick, Gwenaelle Catheline, et al. (Nov. 2017). "Towards a unified analysis of brain maturation and aging across the entire lifespan: A MRI analysis". en. In: *Hum. Brain Mapp.* 38.11, pp. 5501–5518.

Dadar, Mahsa et al. (July 2018). "A comparison of publicly available linear MRI stereotaxic registration techniques". en. In: *Neuroimage* 174, pp. 191–200.

Daugherty, Ana M et al. (Feb. 2016). "Age differences in hippocampal subfield volumes from childhood to late adulthood". en. In: *Hippocampus* 26.2, pp. 220–228.

DeKraker, Jordan et al. (Feb. 2018). "Unfolding the hippocampus: An intrinsic coordinate system for subfield segmentations and quantitative mapping". en. In: *Neuroimage* 167, pp. 408–418.

Dong, Qunxi et al. (Mar. 2019). "Applying surface-based hippocampal morphometry to study APOE-E4 allele dose effects in cognitively unimpaired subjects". en. In: *Neuroimage Clin* 22, p. 101744.

Driscoll, Ira et al. (Dec. 2003). "The aging hippocampus: cognitive, biochemical and structural findings". en. In: *Cereb. Cortex* 13.12, pp. 1344–1351.

Duvernoy, Henri M, Francoise Cattin, and Pierre-Yves Risold (June 2013). *The Human Hippocampus: Functional Anatomy, Vascularization and Serial Sections with MRI*. en. Springer Science & Business Media.

Eichenbaum, Howard (Sept. 2004). "Hippocampus: cognitive processes and neural representations that underlie declarative memory". en. In: *Neuron* 44.1, pp. 109–120.

Eskildsen, Simon F et al. (Feb. 2012). "BEaST: brain extraction based on nonlocal segmentation technique". en. In: *Neuroimage* 59.3, pp. 2362–2373.

Fanselow, Michael S and Hong-Wei Dong (Jan. 2010). "Are the dorsal and ventral hippocampus functionally distinct structures?" en. In: *Neuron* 65.1, pp. 7–19.

Fisher, Daniel W, David A Bennett, and Hongxin Dong (Oct. 2018). "Sexual dimorphism in predisposition to Alzheimer's disease". en. In: *Neurobiol. Aging* 70, pp. 308–324.

Fleisher, Adam et al. (June 2005). "Sex, apolipoprotein E epsilon 4 status, and hippocampal volume in mild cognitive impairment". en. In: *Arch. Neurol.* 62.6, pp. 953–957.

Flores, Robin de, Renaud La Joie, and Gaël Chételat (Nov. 2015). "Structural imaging of hippocampal subfields in healthy aging and Alzheimer's disease". en. In: *Neuroscience* 309, pp. 29–50.

Flores, Robin de, Renaud La Joie, Brigitte Landeau, et al. (Feb. 2015). "Effects of age and Alzheimer's disease on hippocampal subfields: comparison between manual and FreeSurfer volumetry". en. In: *Hum. Brain Mapp.* 36.2, pp. 463–474.

Folstein, Marshal F, Susan E Folstein, and Paul R McHugh (1975). ""Mini-mental state": a practical method for grading the cognitive state of patients for the clinician". In: *J. Psychiatr. Res.* 12.3, pp. 189–198.

Frisoni, Giovanni B, Rossana Ganzola, et al. (Dec. 2008). "Mapping local hippocampal changes in Alzheimer's disease and normal ageing with MRI at 3 Tesla". en. In: *Brain* 131.Pt 12, pp. 3266–3276.

Gómez-Isla, Teresa et al. (1996). "Profound Loss of Layer II Entorhinal Cortex Neurons Occurs in Very Mild Alzheimer's Disease". In: *J. Neurosci.* 16.14, pp. 4491–4500.

Gonneaud, Julie et al. (Oct. 2016). "Relative effect of APOE ϵ4 on neuroimaging biomarker changes across the lifespan". en. In: *Neurology* 87.16, pp. 1696–1703.

Gordon, Brian A et al. (2013). "Effects of aging and Alzheimer's disease along the longitudinal axis of the hippocampus". en. In: *J. Alzheimers. Dis.* 37.1, pp. 41–50.

Groot, Colin et al. (Jan. 2018). "Differential effects of cognitive reserve and brain reserve on cognition in Alzheimer disease". en. In: *Neurology* 90.2, e149–e156.

Jack Jr, Clifford R, Matt A Bernstein, et al. (2008). "The Alzheimer's disease neuroimaging initiative (ADNI): MRI methods". In: *Journal of Magnetic Resonance Imaging: An Official Journal of the International Society for Magnetic Resonance in Medicine* 27.4, pp. 685–691.

Jack Jr, Clifford R, Heather J Wiste, et al. (May 2015). "Age, Sex, and APOE ϵ4 Effects on Memory, Brain Structure, and β-Amyloid Across the Adult Life Span". en. In: *JAMA Neurol.* 72.5, pp. 511–519.

Janes, Amy C et al. (Jan. 2015). "Striatal morphology is associated with tobacco cigarette craving". en. In: *Neuropsychopharmacology* 40.2, pp. 406–411.

Kalpouzos, Grégoria et al. (Jan. 2009). "Voxel-based mapping of brain gray matter volume and glucose metabolism profiles in normal aging". en. In: *Neurobiol. Aging* 30.1, pp. 112–124.

Kordower, J H et al. (Feb. 2001). "Loss and atrophy of layer II entorhinal cortex neurons in elderly people with mild cognitive impairment". en. In: *Ann. Neurol.* 49.2, pp. 202–213.

Kornack, D R and P Rakic (May 1999). "Continuation of neurogenesis in the hippocampus of the adult macaque monkey". en. In: *Proc. Natl. Acad. Sci. U. S. A.* 96.10, pp. 5768–5773.

Krishnan, Anjali et al. (May 2011). "Partial Least Squares (PLS) methods for neuroimaging: a tutorial and review". en. In: *Neuroimage* 56.2, pp. 455–475.

La Joie, Renaud, Marine Fouquet, et al. (Nov. 2010). "Differential effect of age on hippocampal subfields assessed using a new high-resolution 3T MR sequence". en. In: *Neuroimage* 53.2, pp. 506–514.

Laakso, M P, G B Frisoni, et al. (June 2000). "Hippocampus and entorhinal cortex in frontotemporal dementia and Alzheimer's disease: a morphometric MRI study". en. In: *Biol. Psychiatry* 47.12, pp. 1056–1063.

Lancaster, Jack L et al. (Dec. 2011). "Automated analysis of fundamental features of brain structures". en. In: *Neuroinformatics* 9.4, pp. 371–380.

Langnes, Espen et al. (2020). "Anterior and posterior hippocampus macro- and microstructure across the lifespan in relation to memory—A longitudinal study". In: *Hippocampus* 30.7, pp. 678–692.

Lerch, Jason P, Jeffrey B Carroll, et al. (Jan. 2008). "Automated deformation analysis in the YAC128 Huntington disease mouse model". en. In: *Neuroimage* 39.1, pp. 32–39.

Li, Bolun et al. (Apr. 2016). "Influence of APOE Genotype on Hippocampal Atrophy over Time - An N=1925 Surface-Based ADNI Study". en. In: *PLoS One* 11.4, e0152901.

Makowski, Carolina et al. (Apr. 2018). "Evaluating accuracy of striatal, pallidal, and thalamic segmentation methods: Comparing automated approaches to manual delineation". en. In: *Neuroimage* 170, pp. 182–198.

Malykhin, Nikolai V, Yushan Huang, et al. (Nov. 2017). "Differential vulnerability of hippocampal subfields and anteroposterior hippocampal subregions in healthy cognitive aging". en. In: *Neurobiol. Aging* 59, pp. 121–134.

Mazerolle, Marc (Jan. 2006). "Improving data analysis in herpetology: using Akaike's Information Criterion (AIC) to assess the strength of biological hypotheses". en. In: *Amphib-reptil.* 27.2, pp. 169–180.

McIntosh, Anthony R and Bratislav Mišić (2013). "Multivariate statistical analyses for neuroimaging data". en. In: *Annu. Rev. Psychol.* 64, pp. 499–525.

McIntosh, Anthony Randal and Nancy J Lobaugh (2004). "Partial least squares analysis of neuroimaging data: applications and advances". en. In: *Neuroimage* 23 Suppl 1, S250–63.

Meng, Xiangfei and Carl D'Arcy (June 2012). "Education and dementia in the context of the cognitive reserve hypothesis: a systematic review with meta-analyses and qualitative analyses". en. In: *PLoS One* 7.6, e38268.

Mountcastle, V B (Apr. 1997). "The columnar organization of the neocortex". en. In: *Brain* 120 (Pt 4), pp. 701–722.

Mueller, S G et al. (May 2007). "Measurement of hippocampal subfields and age-related changes with high resolution MRI at 4T". en. In: *Neurobiol. Aging* 28.5, pp. 719–726.

Muñoz-Ruiz, Miguel Ángel et al. (Dec. 2012). "Structural MRI in frontotemporal dementia: comparisons between hippocampal volumetry, tensor-based morphometry and voxel-based morphometry". en. In: *PLoS One* 7.12, e52531.

Nelson, Michael D et al. (1997). "Hippocampal volume reduction in schizophrenia as assessed by magnetic resonance imaging: A meta-analytic study". In: *Schizophr. Res.* 24.1-2, p. 153.

Nobis, Lisa et al. (June 2019). "Hippocampal volume across age: Nomograms derived from over 19,700 people in UK Biobank". en. In: *Neuroimage Clin* 23, p. 101904.

Noble, Kimberly G et al. (Nov. 2012). "Hippocampal volume varies with educational attainment across the life-span". en. In: *Front. Hum. Neurosci.* 6, p. 307.

Nordin, Kristin et al. (2018). "Structural whole-brain covariance of the anterior and posterior hippocampus: Associations with age and memory". In: *Hippocampus* 28.2, pp. 151–163.

Nowakowski, R S and P Rakic (Feb. 1981). "The site of origin and route and rate of migration of neurons to the hippocampal region of the rhesus monkey". en. In: *J. Comp. Neurol.* 196.1, pp. 129–154.

O'Dwyer, Laurence et al. (Nov. 2012). "Reduced hippocampal volume in healthy young ApoE4 carriers: an MRI study". en. In: *PLoS One* 7.11, e48895.

O'Shea, Andrew et al. (Dec. 2016). "Cognitive Aging and the Hippocampus in Older Adults". en. In: *Front. Aging Neurosci.* 8, p. 298.

Panizzon, Matthew S et al. (Nov. 2009). "Distinct genetic influences on cortical surface area and cortical thickness". en. In: *Cereb. Cortex* 19.11, pp. 2728–2735.

Patel, Raihaan, Christopher J Steele, et al. (Feb. 2020). "Investigating microstructural variation in the human hippocampus using non-negative matrix factorization". en. In: *Neuroimage* 207, p. 116348.

Permanyer, Iñaki and Diederik Boertien (Feb. 2019). "A century of change in global education variability and gender differences in education". en. In: *PLoS One* 14.2, e0212692.

Pievani, Michela et al. (Apr. 2011). "APOE4 is associated with greater atrophy of the hippocampal formation in Alzheimer's disease". en. In: *Neuroimage* 55.3, pp. 909–919.

Pipitone, Jon et al. (Nov. 2014). "Multi-atlas segmentation of the whole hippocampus and subfields using multiple automatically generated templates". en. In: *Neuroimage* 101, pp. 494–512.

Piras, Fabrizio et al. (Feb. 2011). "Education mediates microstructural changes in bilateral hippocampus". en. In: *Hum. Brain Mapp.* 32.2, pp. 282–289.

Pruessner, J C et al. (Jan. 2001). "Age and gender predict volume decline in the anterior and posterior hippocampus in early adulthood". en. In: *J. Neurosci.* 21.1, pp. 194–200.

Przeździk, Izabela et al. (Oct. 2019). "The functional organisation of the hippocampus along its long axis is gradual and predicts recollection". en. In: *Cortex* 119, pp. 324–335.

Rakic, P (July 1988). "Specification of cerebral cortical areas". en. In: *Science* 241.4862, pp. 170–176.

— (Sept. 1995). "A small step for the cell, a giant leap for mankind: a hypothesis of neocortical expansion during evolution". en. In: *Trends Neurosci.* 18.9, pp. 383–388.

Rakic, Pasko (Oct. 2007). "The radial edifice of cortical architecture: From neuronal silhouettes to genetic engineering". In: *Brain Res. Rev.* 55.2, pp. 204–219.

Randolph, Christopher et al. (1998). "The Repeatable Battery for the Assessment of Neuropsychological Status (RBANS): Preliminary Clinical Validity". In: *J. Clin. Exp. Neuropsychol.* 20.3, pp. 310–319.

Raznahan, Armin et al. (Jan. 2014). "Longitudinal four-dimensional mapping of subcortical anatomy in human development". en. In: *Proc. Natl. Acad. Sci. U. S. A.* 111.4, pp. 1592–1597.

Reuter, Martin, M Dylan Tisdall, et al. (Feb. 2015). "Head motion during MRI acquisition reduces gray matter volume and thickness estimates". en. In: *Neuroimage* 107, pp. 107–115.

Sabuncu, Mert R et al. (Aug. 2011). "The dynamics of cortical and hippocampal atrophy in Alzheimer disease". en. In: *Arch. Neurol.* 68.8, pp. 1040–1048.

Sankar, Tejas et al. (June 2017). "Your algorithm might think the hippocampus grows in Alzheimer's disease: Caveats of longitudinal automated hippocampal volumetry". en. In: *Hum. Brain Mapp.* 38.6, pp. 2875–2896.

Schoemaker, Dorothee et al. (Apr. 2016). "Hippocampus and amygdala volumes from magnetic resonance images in children: Assessing accuracy of FreeSurfer and FSL against manual segmentation". en. In: *Neuroimage* 129, pp. 1–14.

Scoville, W B and B Milner (Feb. 1957). "Loss of recent memory after bilateral hippocampal lesions". en. In: *J. Neurol. Neurosurg. Psychiatry* 20.1, pp. 11–21.

Seeley, William W et al. (2009). "Neurodegenerative Diseases Target Large-Scale Human Brain Networks". In: *Neuron* 62.1, pp. 42–52.

Shafiei, Golia et al. (Apr. 2020). "Spatial Patterning of Tissue Volume Loss in Schizophrenia Reflects Brain Network Architecture". en. In: *Biol. Psychiatry* 87.8, pp. 727–735.

Shafto, Meredith A et al. (Oct. 2014). "The Cambridge Centre for Ageing and Neuroscience (Cam-CAN) study protocol: a cross-sectional, lifespan, multidisciplinary examination of healthy cognitive ageing". en. In: *BMC Neurol.* 14, p. 204.

Shaw, Philip et al. (July 2014). "Mapping the development of the basal ganglia in children with attention-deficit/hyperactivity disorder". en. In: *J. Am. Acad. Child Adolesc. Psychiatry* 53.7, 780–9.e11.

Shi, Jie et al. (2014). "Genetic influence of apolipoprotein E4 genotype on hippocampal morphometry: An N= 725 surface-based Alzheimer's disease neuroimaging initiative study". In: *Hum. Brain Mapp.* 35.8, pp. 3903–3918.

Shing, Yee Lee et al. (Feb. 2011). "Hippocampal subfield volumes: age, vascular risk, and correlation with associative memory". en. In: *Front. Aging Neurosci.* 3, p. 2.

Small, Scott A et al. (Sept. 2011). "A pathophysiological framework of hippocampal dysfunction in ageing and disease". en. In: *Nat. Rev. Neurosci.* 12.10, pp. 585–601.

Smith, T B and K S Nayak (2010). "MRI artifacts and correction strategies". In: *Imaging Med.*

Stranahan, Alexis M and Mark P Mattson (Dec. 2010). "Selective vulnerability of neurons in layer II of the entorhinal cortex during aging and Alzheimer's disease". en. In: *Neural Plast.* 2010, p. 108190.

Strange, B A et al. (Mar. 1999). "Segregating the functions of human hippocampus". en. In: *Proc. Natl. Acad. Sci. U. S. A.* 96.7, pp. 4034–4039.

Strange, Bryan A et al. (Oct. 2014). "Functional organization of the hippocampal longitudinal axis". en. In: *Nat. Rev. Neurosci.* 15.10, pp. 655–669.

Strien, N M van, N L M Cappaert, and M P Witter (Apr. 2009). "The anatomy of memory: an interactive overview of the parahippocampal–hippocampal network". In: *Nat. Rev. Neurosci.* 10.4, pp. 272–282.

Ta, Anh Tuan et al. (2012). "Age-related vulnerabilities along the hippocampal longitudinal axis". In: *Hum. Brain Mapp.* 33.10, pp. 2415–2427.

Tang, Lingfei et al. (June 2020). "Differential Functional Connectivity in Anterior and Posterior Hippocampus Supporting the Development of Memory Formation". en. In: *Front. Hum. Neurosci.* 14, p. 204.

Taylor, Jason R et al. (2017). "The Cambridge Centre for Ageing and Neuroscience (Cam-CAN) data repository: Structural and functional MRI, MEG, and cognitive data from a cross-sectional adult lifespan sample". In: *Neuroimage* 144, pp. 262–269.

Taylor, Joy L et al. (Nov. 2014). "APOE-epsilon4 and aging of medial temporal lobe gray matter in healthy adults older than 50 years". en. In: *Neurobiol. Aging* 35.11, pp. 2479–2485.

Thompson, Deanne K et al. (Aug. 2014). "Longitudinal growth and morphology of the hippocampus through childhood: Impact of prematurity and implications for memory and learning". en. In: *Hum. Brain Mapp.* 35.8, pp. 4129–4139.

Treadway, Michael T et al. (Feb. 2015). "Illness progression, recent stress, and morphometry of hippocampal subfields and medial prefrontal cortex in major depression". en. In: *Biol. Psychiatry* 77.3, pp. 285–294.

Tullo, Stephanie et al. (2019). "MR-based age-related effects on the striatum, globus pallidus, and thalamus in healthy individuals across the adult lifespan". In: *Hum. Brain Mapp.* 40.18, pp. 5269–5288.

Tustison, Nicholas J et al. (June 2010). "N4ITK: improved N3 bias correction". en. In: *IEEE Trans. Med. Imaging* 29.6, pp. 1310–1320.

Videbech, Poul and Barbara Ravnkilde (Nov. 2004). "Hippocampal volume and depression: a meta-analysis of MRI studies". en. In: *Am. J. Psychiatry* 161.11, pp. 1957–1966.

Vogel, Jacob W et al. (Feb. 2020). "A molecular gradient along the longitudinal axis of the human hippocampus informs large-scale behavioral systems". en. In: *Nat. Commun.* 11.1, p. 960.

Voineskos, Aristotle N et al. (Aug. 2015). "Hippocampal (subfield) volume and shape in relation to cognitive performance across the adult lifespan". en. In: *Hum. Brain Mapp.* 36.8, pp. 3020–3037.

Vos de Wael, Reinder et al. (Oct. 2018). "Anatomical and microstructural determinants of hippocampal subfield functional connectome embedding". en. In: *Proc. Natl. Acad. Sci. U. S. A.* 115.40, pp. 10154–10159.

Vuoksimaa, Eero et al. (May 2013). "Cognitive reserve moderates the association between hippocampal volume and episodic memory in middle age". en. In: *Neuropsychologia* 51.6, pp. 1124–1131.

Wada, Masataka et al. (2018). "Effect of Education on Alzheimer's Disease-Related Neuroimaging Biomarkers in Healthy Controls, and Participants with Mild Cognitive Impairment and Alzheimer's Disease: A Cross-Sectional Study". In: *J. Alzheimers. Dis.* 63.2, pp. 861–869.

Wang, Lei et al. (Oct. 2003). "Changes in hippocampal volume and shape across time distinguish dementia of the Alzheimer type from healthy aging". In: *Neuroimage* 20.2, pp. 667–682.

Winterburn, Julie L et al. (July 2013). "A novel in vivo atlas of human hippocampal subfields using high-resolution 3 T magnetic resonance imaging". en. In: *Neuroimage* 74, pp. 254–265.

Wisse, Laura E M, Geert Jan Biessels, et al. (Sept. 2014). "Hippocampal subfield volumes at 7T in early Alzheimer's disease and normal aging". en. In: *Neurobiol. Aging* 35.9, pp. 2039–2045.

Wisse, Laura E M, Ana M Daugherty, et al. (Jan. 2017). "A harmonized segmentation protocol for hippocampal and parahippocampal subregions: Why do we need one and what are the key goals?" en. In: *Hippocampus* 27.1, pp. 3–11.

Witter, Menno P et al. (June 2017). "Architecture of the Entorhinal Cortex A Review of Entorhinal Anatomy in Rodents with Some Comparative Notes". en. In: *Front. Syst. Neurosci.* 11, p. 46.

Wolf, Dominik et al. (Oct. 2015). "Differential associations of age with volume and microstructure of hippocampal subfields in healthy older adults". en. In: *Hum. Brain Mapp.* 36.10, pp. 3819–3831.

Yang, Xianfeng et al. (Nov. 2013). "Evolution of hippocampal shapes across the human lifespan". en. In: *Hum. Brain Mapp.* 34.11, pp. 3075–3085.

Yushkevich, Paul A, Robert S C Amaral, et al. (May 2015). "Quantitative comparison of 21 protocols for labeling hippocampal subfields and parahippocampal subregions in in vivo MRI: towards a harmonized segmentation protocol". en. In: *Neuroimage* 111, pp. 526–541.

Zeighami, Yashar et al. (Apr. 2019). "A clinical-anatomical signature of Parkinson's disease identified with partial least squares and magnetic resonance imaging". en. In: *Neuroimage* 190, pp. 69–78.

Zheng, Fenglian et al. (Oct. 2018). "The Volume of Hippocampal Subfields in Relation to Decline of Memory Recall Across the Adult Lifespan". en. In: *Front. Aging Neurosci.* 10, p. 320.

Zheng, Zhiwei et al. (Mar. 2017). "Sex Matters: Hippocampal Volume Predicts Individual Differences in Associative Memory in Cognitively Normal Older Women but Not Men". en. In: *Front. Hum. Neurosci.* 11, p. 93.

Zhou, Juan et al. (Mar. 2012). "Predicting regional neurodegeneration from the healthy brain functional connectome". en. In: *Neuron* 73.6, pp. 1216–1227.

Chapter 5

Combined structural and quantitative MRI reveal alterations in the hippocampus and cortex across the Alzheimer's disease spectrum.

Aurélie Bussy[1], Raihaan Patel[2], Olivier Parent[1], Alyssa Salaciak[3], Saashi A. Bedford[4], Sarah Farzin[3], Stephanie Tullo[1], Sylvia Villeneuve[4], Judes Poirier[4], John CS Breitner[4], Gabriel A. Devenyi[4], PREVENT-AD Research Group, Christine L. Tardif[5], M. Mallar Chakravarty[6]

1 - Computational Brain Anatomy (CoBrA) Laboratory, Cerebral Imaging Centre, Douglas Mental Health University Institute, Montreal, QC, Canada, Integrated Program in Neuroscience, McGill University, Montreal, Canada.

2 - Computational Brain Anatomy (CoBrA) Laboratory, Cerebral Imaging Centre, Douglas Mental Health University Institute, Montreal, QC, Canada, Department of Biological and Biomedical Engineering, McGill University, Montreal, QC, Canada.

3 - Computational Brain Anatomy (CoBrA) Laboratory, Cerebral Imaging Centre, Dou-

glas Mental Health University Institute, Montreal, QC, Canada.

4 - Computational Brain Anatomy (CoBrA) Laboratory, Cerebral Imaging Centre, Douglas Mental Health University Institute, Montreal, QC, Canada; Department of Psychiatry, McGill University, Montreal, QC, Canada.

5 - Department of Biological and Biomedical Engineering, McGill University, Montreal, QC, Canada; McConnell Brain Imaging Centre, Montreal Neurological Institute, Montreal, QC, Canada; Department of Neurology and Neurosurgery, McGill University, Montreal, QC, Canada.

6 - Computational Brain Anatomy (CoBrA) Laboratory, Cerebral Imaging Centre, Douglas Mental Health University Institute, Montreal, QC, Canada; Integrated Program in Neuroscience, McGill University, Montreal, Canada; Department of Psychiatry, McGill University, Montreal, QC, Canada; Department of Biological and Biomedical Engineering, McGill University, Montreal, QC, Canada.

5.1 Preface

In **Chapter 5**, we examined the variations in hippocampal microstructure, particularly iron and myelin, across the healthy lifespan and throughout the spectrum of AD. The study of AD has primarily focused on amyloid and tau pathology, recent research suggests that other microstructural changes may also contribute to disease progression. In this study, we examined the potential of hippocampal and cortical microstructural changes as indices of AD progression through different stages of the disease. By using advanced neuroimaging techniques such as qMRI we measured MRI-based signals related to myelin and iron content in the hippocampus, and using structural MRI we measured standard morphometric information. We identified joint signatures of covariance across MRI-based measures in the cortex and hippocampus and investigated the relationship between microstructural metrics and medical, lifestyle, and cognitive information relevant to AD progression.

Our research revealed a consistent pattern of decreased CT in the cortex and higher T1 and T2* values in the hippocampus, which were associated with various lifestyle risk factors. These risk factors included past smoking consumption, high blood pressure, high cholesterol levels, and increased anxiety. Moreover, these patterns were significantly linked to higher age and AD progression, as well as being female and carrying the APOE-ϵ4 gene.

This Chapter 5 indicated that hippocampal qMRI metrics could serve as valuable non-invasive tools for investigating the progression of AD. Additionally, it identifies specific lifestyle and medical risk factors that could be targeted by public health initiatives to potentially slow down the advancement of AD. This research is going to be submitted shortly.

5.2 Abstract

Although AD is primarily characterized by amyloid and tau pathology, other microstructural changes, such as myelin deterioration and inflammation-induced iron increases, are also involved early in the disease progression. Here, we aimed to explore whether hippocampal and cortical microstructural changes could serve as indices of AD progression through the different stages of the disease. We measured atrophy using structural MRI and estimated myelin and iron content using qMRI metrics, T1 and T2* relaxation times respectively. By employing non-negative matrix factorization, we identified joint signatures of covariance across MRI-based measures in the cortex and hippocampus. To understand the relationship between microstructural metrics and medical, lifestyle, and cognitive information relevant to the AD-spectrum, we used partial least squares. Our findings indicate a consistent pattern of decreased cortical thickness in the cortex and higher T1 and T2* in the hippocampus associated with key lifestyle risk factors, such as past smoking consumption, high blood pressure and cholesterol, and increased anxiety. These patterns were also significantly related to higher age, associated with AD progression, being female and APOE-ϵ4 carrier. Our study suggests that hippocampal qMRI metrics could be useful non-invasive tools for investigating

AD progression and identifies lifestyle and medical risk factors that could be specifically targeted by public health initiatives to slow the progression of AD.

5.3 Introduction

As the global population ages, the proportion of older individuals is increasing at an unprecedented rate. Advanced age is the most important risk factor for neurodegenerative diseases, such as AD (Rajan et al. 2021). AD is associated with memory loss, confusion, and difficulty in tasks related to daily living, and can place a significant burden on caregivers and the healthcare system. Recent data suggests that 1.6% of the US population suffered from AD and related dementias in 2014, and this burden is expected to more than double in 2060 (K. A. Matthews et al. 2019). Although some therapies have shown slight improvement in reducing cognitive decline (Tan et al. 2014), only a few have demonstrated some efficiency against AD pathophysiology, characterized by the extracellular deposition of Aβ and intracellular accumulation of ptau (Ito et al. 2010; Dyck et al. 2023). However, while Aβ and ptau are the main pathological hallmarks of AD, the disease is multifactorial and involves other microstructural changes such as myelin deterioration and inflammation-mediated increases in iron (Leng et al. 2023).

AD results from a complex interplay between genetic and environmental factors (Eid, Mhatre, and Richardson 2019). Certain genetic factors such as APOE-ϵ4 allele can contribute to an individual's risk of developing AD, while specific environmental factors such as education can protect the brain from the disease (Livingston et al. 2017). Further, AD presentation is highly heterogeneous due to the common presence of comorbid neuropathological diagnoses (such as Lewy body disease, hippocampal sclerosis, cerebral amyloid angiopathy, and vascular brain injury) (Spina et al. 2021). Therefore, understanding the sources of inter-individual variability in AD is critical for developing personalized approaches to diagnosis, treatment, and prevention. Our study aims to investigate the inter-individual variability

of participants along the progression of the AD-spectrum using advanced non-invasive neuroimaging techniques that leverage markers of atrophy, myelin and iron. Structural MRI studies have repeatedly identified hippocampal volume loss as a reliable indicator of AD pathology (Schuff et al. 2009; Clifford R Jack Jr, Barkhof, et al. 2011). Progressive degeneration of the cortex in AD, with significant atrophy particularly in the medial temporal lobes has been considered a reliable disease signature (C R Jack Jr, Petersen, Y. Xu, P. C. O'Brien, G E Smith, Ivnik, Tangalos, et al. 1998; Duara et al. 2008; Visser et al. 2002).

In addition to being sensitive to gross-morphometric variability, structural MRI metrics are sensitive to confounding factors unrelated to the underlying biology. These factors include MRI varying acquisition parameters, inhomogeneities of the RF pulses and RF coil sensitivities, and post-processing protocols (Christine Lucas Tardif et al. 2016a). Further, similar morphometric alterations are generally not disease specific as hippocampal atrophy has been linked to AD, multiple sclerosis, major depressive disorder, frontotemporal lobar degeneration, schizophrenia, and psychosis (Du et al. 2001; Sicotte et al. 2008; Arnone et al. 2013; L. A. v. d. Pol et al. 2006; L. A. v. d. Pol et al. 2006; Sasabayashi et al. 2021). Therefore, more specific and sensitive imaging markers may allow us to better understand microstructural relevant to the AD spectrum.

In this study, we seek to improve the characterization across different neuroanatomical dimensions of the AD spectrum through the use of qMRI (Christine Lucas Tardif et al. 2016a). These more advanced imaging techniques measure the biophysical properties of the underlying tissue sample (i.e amount of myelin, axons, glia and iron) through the use of relaxation times or magnetic susceptibility as a means of inferring the tissue microstructure composition. While qMRI has been increasingly used in some clinical research related to multiple sclerosis (Granziera et al. 2021) or musculoskeletal diseases (Eck et al. 2023), it has been under-explored in the context of the AD spectrum. Nonetheless, it has been demonstrated that myelin breakdown and inflammation-induced iron accumulation may promote amyloid accumulation (George Bartzokis, P. H. Lu, and Jim Mintz 2007; George Bartzokis

2011; J.-L. Liu et al. 2018; Papuć and Rejdak 2020; Depp et al. 2023). Furthermore, research has shown that the brain expresses higher iron load in the early stages of AD compared to healthy individuals (Bartzokis, Sultzer, et al. 1994; Raven et al. 2013; R. J. Ward et al. 2014). As such, myelin and iron are two pathologically-relevant microstructural properties in the context of AD, and their *in-vivo* measurement could add neurobiological insights regarding disease processes and severity.

Here, we used two qMRI methods sensitive to these important neurobiological compartments; namely T1 maps and T2* relaxation time. T1 maps provide information on the longitudinal relaxation time constant T1 at each voxel, which vary based on several factors, such as the concentration and properties of macromolecules like myelin (Lutti et al. 2014; Harkins, J. Xu, et al. 2016), but also iron (Vymazal, Brooks, et al. 1996) and proton density (Gelman et al. 2001). Notably, increased myelin and iron content lead to a T1 reduction while increased water content induces a T1 lengthening. In the subcortical GM, T1 variation has been primarily attributed to myelin content, as demonstrated in recent studies (Miletić et al. 2022). In complement to T1 mapping methods, T2* relaxation time reflects the dephasing caused by molecular interactions and local magnetic field inhomogeneities (Brown et al. 2014). These inhomogeneities may originate from differences in magnetic susceptibility from various tissues (J. Duyn 2013). Both myelin and iron decrease T2*, but *postmortem* analyses have shown that iron is the dominant source of contrast in T2* maps (Langkammer et al. 2010; Stüber et al. 2014). In aging, T2* has been shown to decrease in regions such as in the hippocampus (Naftali Raz, Rodrigue, and Haacke 2007) and basal ganglia (Cherubini et al. 2009). In individuals with dementia, T2* alterations were also seen in the hippocampus, insula, putamen, posterior and middle cingulate cortex, and parietal cortex (Rombouts et al. 2007). While these two methods have overlapping neurobiological sensitivities, their simultaneous application could have significant implications in identifying distinct microstructural mechanisms relevant to AD-related pathophysiology.

Our study aims to investigate the cortex and the hippocampus in relation to AD. A

combination of structural MRI techniques is used to characterize morphometry and qMRI metrics T1 and T2* to examine potential sources of contrast, specifically myelin and iron. We applied a matrix decomposition technique to derive joint signatures of covariance across these MRI-based measures in both the cortex and the hippocampus. Component-wise metrics were tested to investigate their sensitivity to AD progression. Then, to better understand the link between these derived brain components and relevant factors in the AD-spectrum, we examined their relationship to demographics, medical, cognitive information and lifestyle risk factors.

5.4 Methods

5.4.1 Participants

Individuals from two datasets collected at the Douglas Research Center were included in this study. This study was approved by McGill Institutional Review Board and Douglas Mental Health University Institute Research Ethics Board. 219 participants were originally included : 168 individuals were part of the ADB dataset (Tullo et al. 2019; Bussy, Plitman, et al. 2021; Bussy, Patel, et al. 2021; Parent et al. 2023) and 51 were part of the PREVENT-AD cohort (Tremblay-Mercier et al. 2021). Inclusion and exclusion criteria are described in previous work (Tullo et al. 2019; Tremblay-Mercier et al. 2021). Data acquisition was similar across the two studies. Demographics of our participants are reported in Table 5.1. After QC of the image processing (described in sections 5.4.2, 5.4.4 and 5.4.6), we included 158 individuals across the AD spectrum: 38 HC, 58 cognitively healthy individuals with a parental AD-history (FAMHX), 41 MCI and 21 AD participants.

5.4.2 Cognitive, psychological, medical and lifestyle information

Trained research assistants used semi-structured questionnaires to gather information in four broad categories: cognitive, psychological, medical, and lifestyle.

	HC (n=38)	**FAMHX** (n=58)	**MCI** (n=41)	**AD** (n=21)	**ALL** (n=158)
Age - Median [Min,Max]	68.6 [53,78]	63.1 [55,83]	69.1 [58,84]	70.2 [58,84]	66.9 [53,84]
Sex F - n (%)	22 (57.9%)	35 (60.3%)	30 (73.2%)	11 (52.4%)	98 (62.0%)
Education - Median (SD)	13.7 (6.1)	11.3 (4.9)	8.46 (6.1)	14.7 (9.7)	11.6 (6.6)
MOCA – Median (SD)	25.3 (2.65)	27.2 (2.30)	23.7 (3.65)	19.9 (6.26)	24.8 (4.25)
APOE4 - n (%)	9 (23.7%)	23 (39.7%)	18 (43.9%)	11 (52.4%)	61 (38.6%)
High BP - n (%)	14 (36.8%)	8 (13.8%)	19 (46.3%)	9 (42.9%)	50 (31.6%)
High Chol - n (%)	13 (34.2%)	11 (19.0%)	21 (51.2%)	10 (47.6%)	55 (34.8%)
Diabetes - n (%)	3 (7.9%)	3 (5.2%)	1 (2.4%)	2 (9.5%)	9 (5.7%)
Smoking current - n (%)	0 (0%)	1 (1.7%)	1 (2.4%)	0 (0%)	2 (1.3%)
Smoking past - n (%)	33 (86.8%)	57 (98.3%)	40 (97.6%)	20 (95.2%)	150 (94.9%)
Alcohol - n (%)	32 (84.2%)	53 (91.4%)	41 (100%)	14 (66.7%)	140 (88.6%)
Depression - n (%)	3 (7.9%)	14 (24.1%)	10 (24.4%)	8 (38.1%)	35 (22.2%)
Anxiety - n (%)	3 (7.9%)	11 (19.0%)	9 (22.0%)	7 (33.3%)	30 (19.0%)

Table 5.1: Demographic information of the 158 participants who passed QC and were therefore included in the study

- For cognitive assessment, the researchers used two standardized tests: the MoCA and the RBANS. The MoCA test has a score range of 0-30: a score of 26-30 is considered normal, 18-25 is indicative of mild cognitive impairment, 10-17 is indicative of moderate cognitive impairment, and a score below 10 is indicative of severe cognitive impairment. The RBANS test assesses multiple cognitive domains, including total score, immediate memory, delayed memory, attention, language, and visuospatial ability.

- For psychological variables, the researchers used binary variables for depression and anxiety. A value of 1 indicates that an individual admitted ever having an anxiety or depressive episode, while a value of 0 indicates that they never had such an episode.

- For medical information, the researchers used binary variables to indicate whether an individual had ever had a particular condition or not. The conditions included hearing problems, concussion, transient ischemic attack, brain injury, headaches, seizures, heart disease, liver disease, kidney disease, thyroid disease, cancer, arthritis, neck/back problems, and allergies.

- For lifestyle information, the researchers used binary variables to indicate whether an individual engaged in certain behaviors or had certain conditions; these included: alcohol use, current smoking, past smoking, drug use, high blood pressure, high cholesterol, and diabetes.

Because some values were missing for some variables (see supplementary table 5.2), we imputed missing values with Random Forest imputation using the missForest package (version 1.4) on R (version 3.5.1) for the 158 individuals which passed MRI QC.

5.4.3 Imaging acquisition

Participants of the two datasets were scanned on the same 3T Siemens Tim Trio MRI scanner at the Douglas Research Center using a 32-channel head coil.

- We acquired a whole brain magnetization prepared 2 rapid acquisition by gradient echo (MP2RAGE) sequence at 1 mm isotropic resolution (Marques, Kober, et al. 2010). The MP2RAGE sequence acquires two images at different inversion times, resulting in two different T1w contrasts. The images can be combined to generate an enhanced T1w uniform image (UNI), unbiased from B1 inhomogeneity, T2* and proton density, as well as a T1 map. The latter is a quantitative index of tissue microstructure, in particular related to myelin content, that can be directly compared across scans. The MP2RAGE acquisition parameters are: TI1/TI2 = 700/2500 ms, TE/TR = 2.91/5000 ms, α1/α2 = 4/5 deg, FOV =256 x 256 mm2, 176 slices, 1 mm isotropic voxel dimensions. The image acquisition is accelerated in the phase encode direction by a factor GRAPPA of 3, for a total scan time of 8 min 22 sec.

- A 3D multi-echo gradient echo scan was acquired with the following parameters: 12 TE = [2.84, 6.2, 9.56, 12.92, 16.28, 19.64, 23, 26.36, 29.72, 33.08, 36.44, 39.8] ms, TR= 44 ms, bandwidth=500 Hz/Px, α = 15 deg, FOV = 180 x 192, 144 slices, 1 mm isotropic resolution, phase partial Fourier 6/8, GRAPPA acceleration factor= 2, for a total scan time of 9 min 44 sec. T2* calculation is explained in Section 5.4.6.

5.4.4 Manual quality control

QC of the T1w raw images were performed using the QC procedure previously developed in our laboratory (Bedford et al. 2020) `https://github.com/CoBrALab/documentation/wiki/Motion-Quality-Control-Manual`. QC is an essential step of the image processing that prevents motion artifacts due to involuntary movements (cardiac or respiratory) which could systematically bias MRI-derived measurements (Bellon et al. 1986; T. B. Smith and Nayak 2010).

5.4.5 Preprocessing

The minc-bpipe-library pipeline https://github.com/CobraLab/minc-bpipe-library was employed to preprocess T1w images using N4 bias field correction (Tustison et al. 2010), to standardize the FOV, rotate the brain, extract the brain and create brain masks using BEaST (Eskildsen et al. 2012). QC at every step of the pipeline was performed.

5.4.6 T2* map extraction

A denoising algorithm (adaptive non-local means denoising) (Manjón, Coupé, et al. 2010) was used on each T2* echo to improve the quality of the scans (before/after example in Supplementary Figure 5.6). An exponential fit was used to extract T2* maps from the 12 echoes https://github.com/CoBrALab/minc-toolkit-extras/blob/master/t2star_fit_simpleitk.py. The Levenberg-Marquardt $curvefit$ function was used to obtain the T2* parameter from which the magnetization M was determined using the equation 5.1:

$$M = S_0 * e^{\frac{-t}{T2*}} \tag{5.1}$$

Here, S_0 represents the maximum signal amplitude that relies on PD and acquisition parameters like the flip angle, while t represents the TE and $T2*$ denotes the time constant. QC of the T2* maps was performed to rate the scan quality based on motion artifacts but also to remove scans with signal drop off (mostly in the temporal lobe) or spurious signal intensity variation throughout the map.

5.4.7 Cortical feature extraction

CIVET pipeline (version 2.1.1) was used on the T1w UNI preprocessed images to extract vertex-wise CT, SA and to generate pial surfaces ("0% surface"), mid-cortex surface ("50% surface) and GM/WM ("100% surface"). Additional cortical surfaces were created at several depths (12.5%, 25%, 37.5%, 62.5%, 75%, 87.5%) by averaging the vertex coordinates of

two surfaces (surface depth 25% averaged from surfaces depth 0% and 50% for example). T1w images were registered to the first echo of the T2* magnitude images. The same transformations were applied to the cortical surfaces (originally in T1w space) to extract and average vertex-wise T2* values across the different depths (0% and 100% depths not included to avoid partial volume effect) (Paquola et al. 2019). Vertex-wise extraction was performed in native space on T1 maps (same space as T1w images). Cortical measurements were performed at each vertex of the 40,962 vertices per hemisphere and were followed by a spatial smoothing with a 30 mm surface-based heat diffusion kernel (Moo K Chung, Adluru, and Vorperian 2020). The medial wall was masked and therefore only 38,561 vertices per hemisphere were considered in the rest of the analyses.

To correct for the T2* dependence on myelinated fiber orientation relative to B0, T2* values were residualized from the angle θ between the vertex normal and B0 (Cohen-Adad et al. 2012). Finally, the values were spatially smoothed using a 30 mm surface-based heat diffusion kernel (Moo K Chung, Adluru, and Vorperian 2020). Stepwise processing is illustrated in Figure 5.1.

5.4.8 Hippocampal feature extraction

To derive voxel-wise volumetric measurements of the hippocampus, we used a python pipeline for two-level DBM, which was developed by the CoBrA Lab `https://github.com/CoBrALab/twolevel_ants_dbm`. Our aim was to investigate voxel-wise morphometry by warping each individual image through affine and non-linear registration, resulting in an unbiased average via ANTs tools, which used a group-wise registration strategy (Brian B Avants et al. 2011). We calculated relative voxel volume changes by estimating the relative Jacobian (J) determinant at each voxel (M K Chung et al. 2001) from the individual non-linear displacement fields. The log J was calculated to have values between $\pm\infty$ to allow for more straightforward statistical analyses and interpretation: positive values indicate that the voxel in template space must be expanded to match the subject space, whereas negative

values indicate that the voxel in template space must be reduced.

To make sure that the DBM outputs, T2* and T1 maps have the same voxel-wise correspondence across all participants, we applied the transforms to T2* and T1 maps, which resulted in all measurements being in the same template space.

An hippocampal mask was created manually on the average T1w brain to extract voxel-wise hippocampal information : J, T1 and T2* values.

5.4.9 Non-negative matrix factorization

Non-negative matrix factorization (NMF) is a powerful method for analyzing high-dimensional data in various fields including neuroimaging. Its ability to extract underlying patterns and features from complex data while promoting sparsity in the solution makes it a valuable tool for exploring large datasets in neuroscience research (Sotiras, Resnick, and Davatzikos 2015). Here, we used orthogonal projective NMF to analyze cortical data (CT, SA, T1, T2*) and hippocampal data (J, T1, T2*) (Patel, Steele, et al. 2020). Concretely, NMF decomposes a $m \times n$ input matrix into a component matrix $W(m \times k)$, and weight matrix $H(k \times n)$, constructed such that their multiplication minimizes the reconstruction error between the original and reconstructed data. The number of components, k, is user defined. W describes component location, while H contains subject-wise weightings describing individual variability of measures in each component. In the specific implementation used in this work, each column of the input matrix contains hemispheric cortical vertex-wise metrics ($m = 38,561$) or bilateral hippocampal voxel-wise ($m = 6,222$) and each row represents subject metrics ($numberofrows = \#metrics \times 158subjects$).

For the cortex, each hemispheric metric ($38,561 \times 158$) was initially concatenated to obtain one whole brain matrix ($77,122 \times 158$). This whole brain matrix was z-scored across vertices for the cortex (or voxels for the hippocampus) and participants (Supplementary Figure 5.7). For example, for CT, values were z-scored across $77,122 \times 158$ measurements while J values were z-scored across $6,222 \times 158$ measurements.

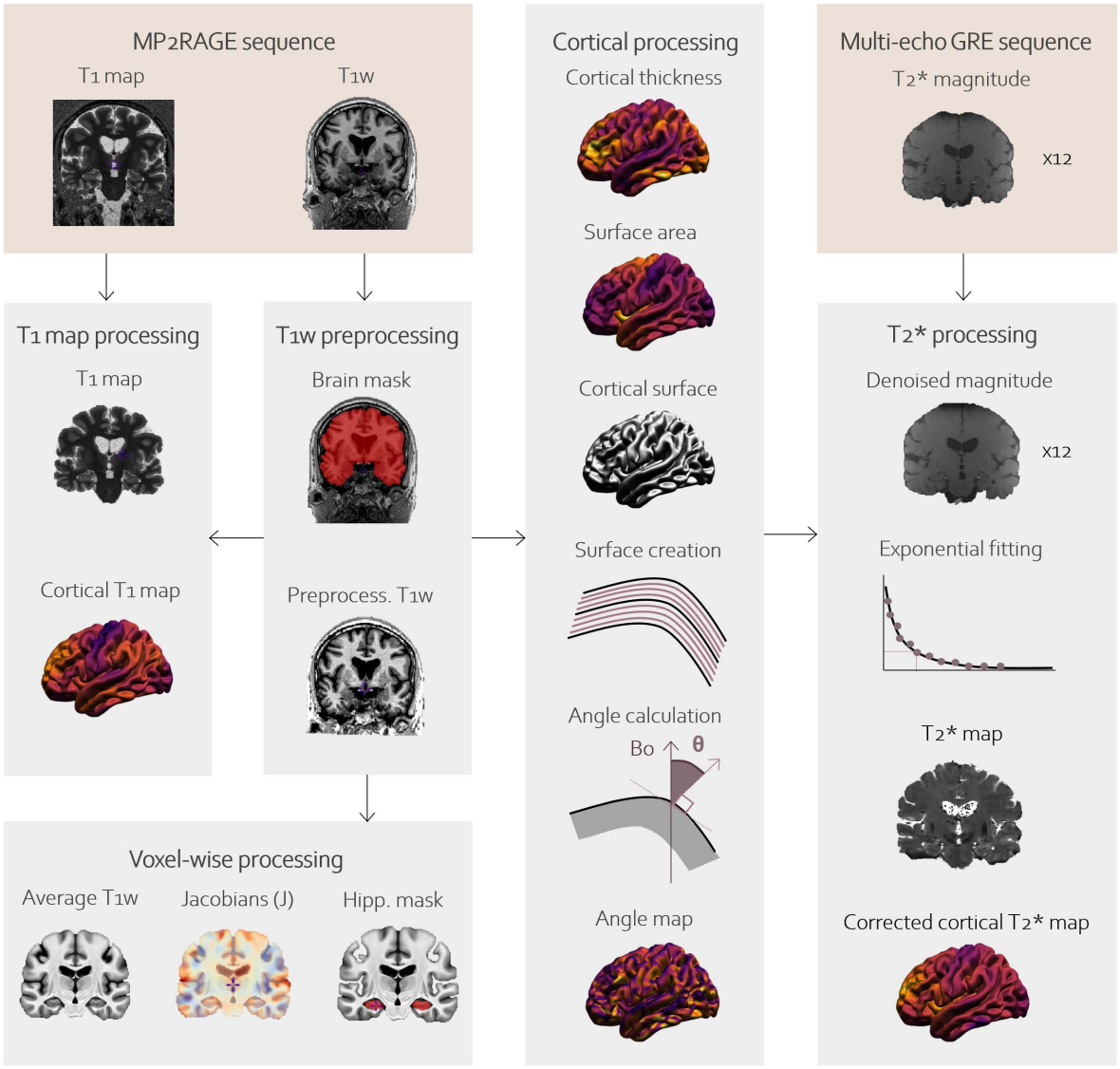

Figure 5.1: Schematic representation of the image processing steps. The MP2RAGE sequence provides a T1w image and a quantitative T1 map. The minc-bpipe-library is used to preprocess the T1w images and obtain a brain mask. CIVET is used to extract CT, SA and cortical surfaces. Additional surfaces were created to sample the maps at different cortical depths (12.5%, 25%, 37.5%, 50%, 62.5%, 75% and 87.5%). θ is defined as the angle between B_0 and the cortical normal at each vertex. The multi-echo gradient echo sequence provides 12 magnitude images. A denoising using adaptive non-local means denoising (Manjón, Coupé, et al. 2010) is applied on each echo. An exponential fit was used to extract T2* maps from the 12 echoes and the angle θ was used to residualized the cortical T2* values. Deformation based morphometry was used to calculate J using the T1w scans. Using the average template, we manually defined a hippocampal mask to extract hippocampal voxel-wise metrics.

NMF was run separately for the cortex and the hippocampus because of the difference in matrix size. For each NMF run, the z-scored matrices (CT, SA, T1 and T2* for the cortex or J, T1 and T2* for the hippocampus) were concatenated and the values were shifted by adding the minimal z-scored value across the 4 (or 3) matrices to have the minimum value equal to 0 (More details in Supplementary Figure 5.7).

To select the optimal number of components, we performed a split half analysis from $k = 2$ to $k = 20$ to assess stability and accuracy of decompositions across different granularities (Patel, Steele, et al. 2020). Results of the stability analyses are in Supplementary Figure 5.8.

5.4.10 Partial least squares

PLS analysis is a multivariate statistical technique that is commonly used to investigate the relationships between brain measures and behavioral or clinical measures. This technique identifies patterns of covariance between two matrices: one matrix represents brain measures and the other matrix includes cognitive, medical or lifestyle information. By decomposing these matrices into a set of orthogonal LV, PLS analysis identifies the most significant patterns of covariance between the two matrices. Each LV in PLS analysis represents a linear combination of the brain and behavior matrices, allowing researchers to investigate the specific brain regions and behavioral or clinical measures that are most closely related. The goal was to avoid using a mass-univariate approach, which may inflate the false-positive findings (Marek et al. 2022).

Here, our brain matrix included NMF weights and the other matrix included cognitive, psychological, medical and lifestyle information described in section 5.4.2. Of note, it did not include any information about group, APOE-ϵ4 allele status, age, sex and education level of the individuals because the goal was to identify in a data-driven approach, a set of cognitive, psychological, medical and lifestyle risk factors associated with our brain variables. After PLS analyses, we examined if these identified brain/behaviour patterns were sensitive to age

and disease progression.

Our brain data included the NMF weights from the cortex (10 components x 4 metrics) and the hippocampus (4 components x 3 metrics) combined i.e. 52 metrics for 158 participants. The values in the behaviour matrices were z-scored along each column prior to performing PLS (i.e. z-score the values of each medical/lifestyle information across all subjects). Each LV was tested statistically using permutation testing, bootstrap resampling and split half analyses following a similar protocol as in previous studies (Anthony Randal McIntosh and Lobaugh 2004; Kovacevic et al. 2013; Zeighami et al. 2019; Patel, Steele, et al. 2020; Bussy, Patel, et al. 2021; Bussy, Levy, et al. 2023).

5.4.11 Post-Hoc analyses

Brain and behaviour scores obtained from PLS analyses were further analyzed to determine if they were associated with key demographic and clinical variables not included in the PLS analysis. The relationship between group, age, sex, APOE-ϵ4 allele and education and PLS brain and behaviour scores of each LV were performed using ANCOVAs (2 models x 3 LVs). Post-hoc Tukey HSD tests were performed to examine pairwise group differences. FDR corrected p-values can be found in Supplementary table 5.3. The goal of these analyses was to determine if PLS successfully captured, using a data-driven approach, patterns of brain and behaviour specific to individual's demographics. Indeed, PLS was blind to the group, APOE-ϵ4 allele status, age, sex and education level of the individuals.

5.5 Results

5.5.1 Data

The final sample after quality control included 158 participants, with a mean age of 66.9 years, an age range between 53 and 84 years and 62% of females (Table 5.1). FAMHX group was significantly younger than the other groups ($p < 0.001$) and education was lower for the

MCI group compared to HC and AD ($p < 0.01$).

5.5.2 NMF decomposition

5.5.2.1 Cortical decomposition

The outputs of the cortical stability analyses are shown in Figure 5.2 A. Although we initially considered including 4 components because of its high stability score, we found that its spatial outputs were confined to the primary lobar regions (see Supplementary Figure 5.9). Because this did not offer a comprehensive cortical pattern, we opted to investigate more components. Since NMF was still able to maintain a reasonable correlation and reconstruction error, we made the decision to proceed with 10 components. Each component qualitatively demonstrated bilateral patterns in distinct cortical regions. Component 1 is located in the dorsomedial and superior temporal regions, component 2 in the occipital lobe, component 3 in the superior frontal cortex, component 4 in the auditory/motor cortices, component 5 in the inferior/medial temporal lobe, component 6 in the frontal lobe, component 7 in the cingulate/somatosensory regions, component 8 in the precuneus, component 9 is the premotor cortex and component 10 in the temporo-parietal junction.

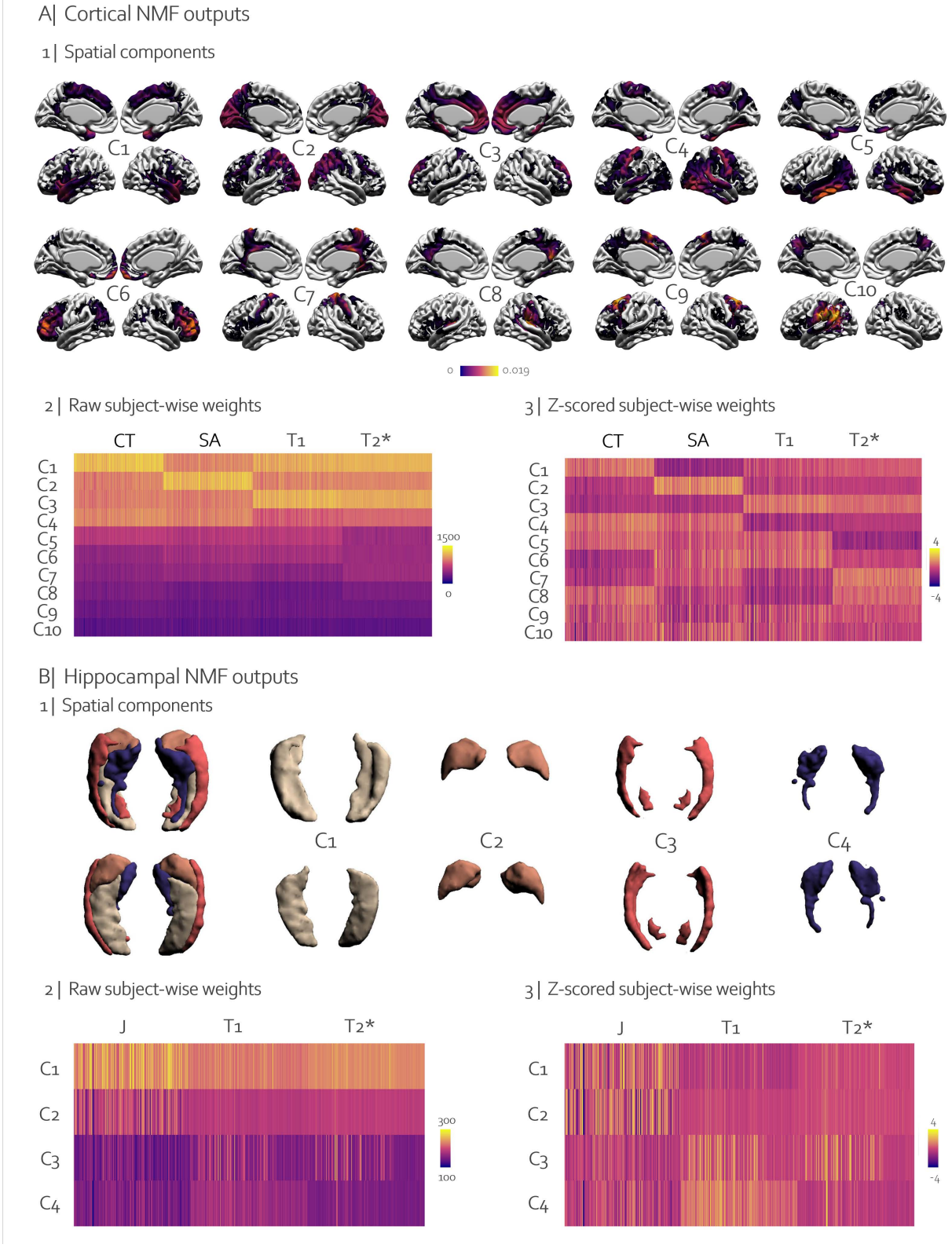
A| Cortical NMF outputs
1| Spatial components
C1
C2
C3
C4
C5
C6
C7
C8
C9
C10
0
0.019
2| Raw subject-wise weights
CT
SA
T1
T2*
1500
0
3| Z-scored subject-wise weights
4
-4
B| Hippocampal NMF outputs
1| Spatial components
J
300
100

Figure 5.2: **A — 1** Visualization of the 10 spatial components where each component is specific to a brain region. Component 1 is located in the dorsomedial and superior temporal regions, component 2 in the occipital lobe, component 3 in the superior frontal cortex, component 4 in the auditory/motor cortices, component 5 in the inferior/medial temporal lobe, component 6 in the frontal lobe, component 7 in the cingulate/somatosensory regions, component 8 in the precuneus, component 9 is the premotor cortex and component 10 in the temporo-parietal junction. **A — 2** Raw subject-metric weights matrix, where each line corresponds to a spatial component, and each column represents a subject-metric weight. **A — 3** Standardized subject-metric matrix by z-scoring across rows (i.e per component) to better visualize which metric contributes the most to each component. For example, across our individuals, CT contributes the most to component 1 while SA contributes the most to component 2. **B — 1** Visualization of the 4 hippocampal components, where each component is specific to a hippocampal region. Component 1 is in the body and tail, component 2 in the head, component 3 in the lateral regions, and component 4 in the medial regions of the hippocampus. **B — 2** Raw subject-metric weights matrix and **B — 3** standardized subject-metric matrix by z-scoring across rows.

5.5.2.2 Hippocampal decomposition

The outputs of the hippocampal stability analyses are shown in Figure 5.2 B. To ensure a high correlation and adequately-sized components, we chose 4 components given that the hippocampus is already a small structure. Additionally, prior research in our lab has shown that 4 components were appropriate for studying the hippocampus using a similar approach (Patel, Steele, et al. 2020). We identified distinct regions of the hippocampus for each of the 4 components: component 1 in the body and tail, component 2 in the head, component 3 in the lateral regions, and component 4 in the medial regions.

5.5.3 NMF components

5.5.3.1 Cortical components

Each component can be described spatially and based on their subject-metric weights. For instance, we can identify population-level global patterns by examining the weights assigned to each metric in a given component. In component 1 which corresponds to the dorsomedial and superior temporal regions, the high weights of CT, low weights of SA, and medium

weights of T1 and T2* can be observed in both the raw subject-weight matrix (Figure 5.2 A— 2) and the standardized subject-weight matrix (Figure 5.2 A— 3). This suggests that CT plays a greater contribution than SA in the spatial component 1.

However, comparing the contribution of a metric across different components is not possible in Figure 5.2 because the subject-wise weights are standardized per component. Nevertheless, we can compare the NMF weights of individuals within the same component and interpret the values as raw values. For example, if individual A has a higher CT weight than individual B in component 1, it means that individual A has a higher raw CT than individual B in component 1. To compare each metric across components, refer to Supplementary method 5.7.6 and Supplementary figure 5.10.

5.5.3.2 Hippocampal components

In the same way, each hippocampal component can be described with the subject-metric weights. J mostly contributed in component 1 and 2 patterns (hippocampal body and head) while T1 contributed the most to component 4 (medial hippocampus) and both T1 and T2* contributed more than J in component 3 (lateral hippocampus).

5.5.4 Pairwise group differences

We assessed whether our NMF components could differentiate our groups by using cortical and hippocampal metrics. The NMF weights were compared between groups using various metrics, as shown in Figure 5.3. In comparing AD individuals to FAMHX individuals, we observed lower CT throughout the brain, reduced SA in component 5 and 10 (which correspond to the temporal lobe and the temporo-parietal junction), and higher T1 and T2* in components 2, 3, and 4 of the hippocampus (which correspond to the head, lateral, and medial regions). A similar but more widespread pattern was observed when comparing AD and HC, with reductions in SA observed in more regions of the cortex and increases in T1 and T2* seen throughout the entire hippocampus. Additionally, T2* was higher in the

occipital regions of individuals with AD vs HC. Comparing AD and MCI, we observed fewer significant differences, but we still found lower CT in the occipital, temporal, and temporo-parietal junction, as well as higher T2* in the lateral region of the hippocampus. Comparing MCI and HC, we found lower CT in the dorsomedial and superior temporal regions, in the auditory/motor cortices, and in the precuneus, as well as higher T1 and T2* in the lateral and medial regions of the hippocampus. When comparing MCI and FAMHX, we only observed lower CT in the precuneus, and no significant differences were found between FAMHX and HC. Our results suggest that cortical morphometry and hippocampal microstructure are sensitive to AD progression. Individuals with AD showed greater brain changes compared to those with MCI, who in turn demonstrated significant differences from the control group.

5.5.5 Brain/behaviour relationships

5.5.5.1 Latent variable

Our PLS results demonstrated three significant LVs, explaining 76.9%, 7.5% and 5.2% of the covariance respectively. The results of the first LV are shown in Figure 5.4 (LV2 and LV3 in Supplementary Figure 5.11 and 5.13). Figure 5.4 A shows the brain pattern, describing a lower CT, SA in the entire brain, lower T2* in the dorsomedial and superior temporal regions, superior frontal cortex and in the premotor cortex and higher T2* in the occipital lobe. We found a decrease J in the body and tail, an increase J in the most lateral region as well as an increase of T1 and T2* values in all regions of the hippocampus. We discovered that cortical morphometry and hippocampal microstructure were linked to a pattern of past smoking consumption, high blood pressure (BP) and cholesterol, lower scores in all cognitive domains, and higher anxiety levels (Figure 5.4 B). This indicates that not only have we identified a consistent pattern of changes in the brain, but also suggests that these specific risk factors may contribute to their development.

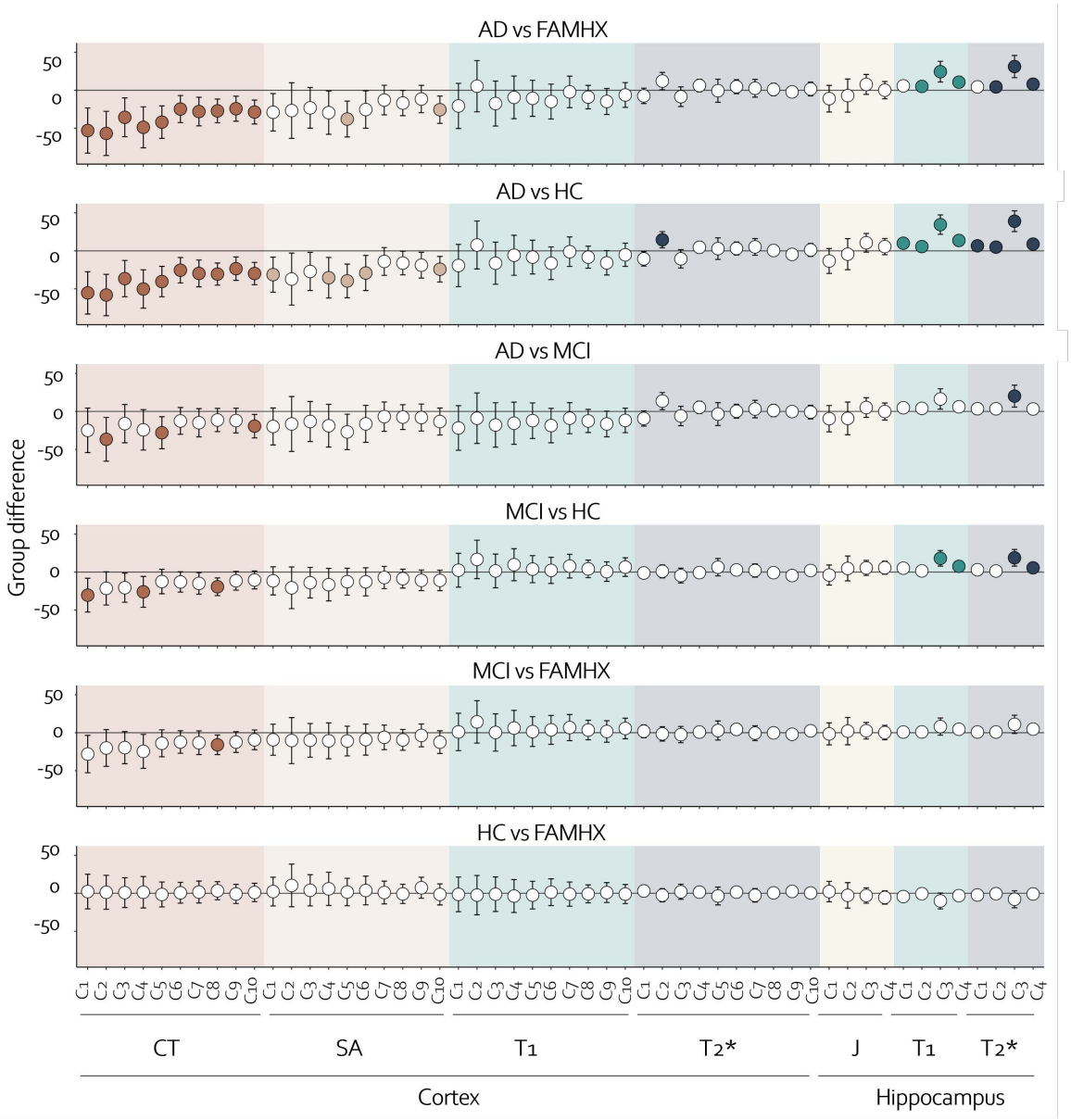

Figure 5.3: The NMF weights were compared pairwise across all the metrics for different groups, including AD vs FAMHX, AD vs HC, AD vs MCI, MCI vs HC, MCI vs FAMHX, and FAMHX vs HC individuals. The metrics included cortical CT, SA, T1, T2*, and hippocampal J, T1, and T2*. The mean group difference was indicated by circles, with gray circles representing non-significant differences, and colored circles representing significant differences (after FDR correction across all p-values). The plots are color coded by metric and the 95% confidence interval of the group difference was represented by vertical bars.

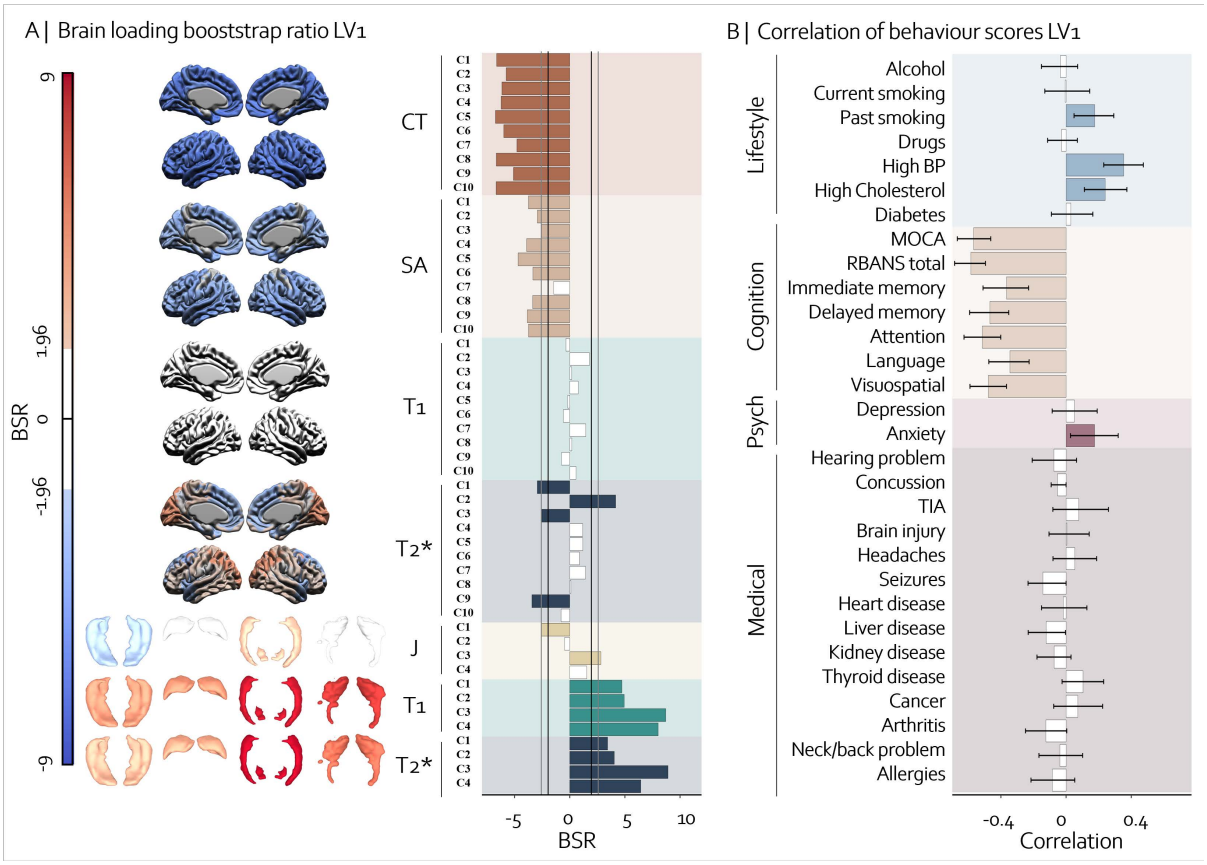

Figure 5.4: The first LV explained 76.9% of the covariance between brain and cognitive, psychological, medical, and lifestyle information. The brain pattern on the left **(A)** illustrates spatially the contribution of each metric to the pattern with BSR values on each brain structure. Blue color indicates negative BSR values and red indicates positive BSR values. Components with absolute BSR values higher than 1.96 are colored to show significant contribution. The bar plot in the middle of the figure shows more precisely the BSR values for each component, with black vertical lines representing a BSR of 1.96 (equivalent to p=0.05) and gray lines representing a BSR of 2.58 (equivalent to p=0.01). On the right-hand side **(B)**, we can see the cognitive, psychological, medical, and lifestyle patterns associated with the brain pattern on the left. Bars are colored if they are significant (when error bars do not cross zero), and are white if non-significant. The brain pattern is associated with past smoking consumption, high BP and cholesterol, lower cognitive scores, and higher anxiety.

5.5.5.2 Brain/behaviour pattern sensitive of disease progression, age and genetic risk

Lastly, we explored how age, group, APOE-ϵ4 allele status, sex, and education related to the brain and cognitive, psychological, medical, and lifestyle patterns of the LV1. Similar

analyses were performed for the LV2 and LV3 pattern (Supplementary Figure 5.12 and 5.14). We discovered significant group differences between each pair of groups, except for HC vs FAMHX in the brain and HC vs FAMHX and HC vs MCI in the cognitive, psychological, medical, and lifestyle scores. Our findings indicated that both brain and behavior were positively correlated with age and female sex. Additionally, APOE-ϵ4 allele carriers demonstrated a stronger association with the pattern than non-carriers. No significant effect of education was found in regards to this pattern.

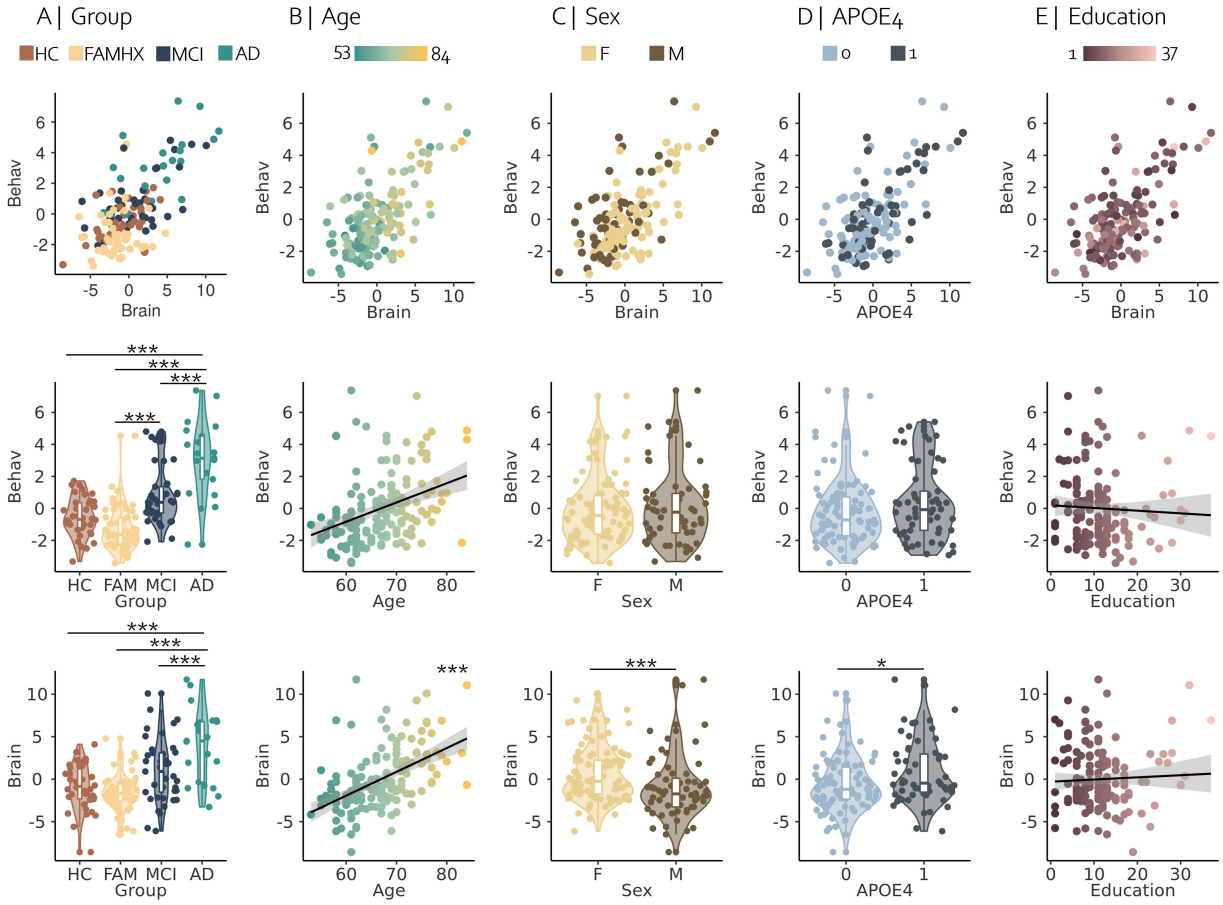

Figure 5.5: Post-hoc analyses of the PLS brain and behaviour scores of LV1. **(A)** is showing the pairwise group comparisons of the brain and behaviour scores. Results of the linear models illustrating the brain and behaviour relationships with age **(B)**, sex **(C)**, APOE-ϵ4 allele status **(D)** and education **(E)**. * $p < 0.05$, ** $p < 0.01$, *** $p < 0.001$ after FDR correction across all p-values.

5.6 Discussion

5.6.1 Brain pattern associated with AD

In this study, we aimed to examine if qMRI markers of iron and myelin could be sensitive to AD progression and AD-related risk factors. First, we took a data-driven approach to parcellate the cortex and the hippocampus. Ten cortical and four hippocampal regions were defined by integrating multimodal MRI data to take advantage of the complementary information conveyed by these indices. The radial unit hypothesis postulates that the cerebral cortex consists of cortical columns (Rakic 1988) and that CT reflects the quantity of cells within each column. On the other hand, SA is thought to reflect the number of columns in a particular area, which could be attributed to the pace of cell proliferation at birth (Rakic 1988; Rakic 2000). It has been shown that T1 and T2* are highly sensitive to myelin and iron respectively (Stüber et al. 2014; Lutti et al. 2014). Thus, an increase of T1 is commonly interpreted as a myelin reduction while a decrease of T2* as a higher iron content. Combining multimodal MRI metrics can therefore help researchers gain a more comprehensive understanding of the properties of the brain, and identify their differential susceptibility to aging and AD.

Next, we conducted pairwise group comparisons to determine which cortical and hippocampal metrics would be the most sensitive to AD progression. Cortical thinning was apparent throughout the brain when we compared AD vs FAMHX or AD vs HC. However, although we expected to see larger CT reduction in the temporal and frontal regions (Dickerson et al. 2009; V. Singh et al. 2006), these components did not necessarily show stronger effects. A previous study from our laboratory using similar methodologies demonstrated a widespread association between SA and performance across cognitive abilities in midlife individuals (Patel, Mackay, et al. 2022). Here, our results demonstrated sparse SA reduction in the temporal/parietal lobe in AD individuals compared to cognitively normal individuals (Iannopollo, Garcia, and Alzheimer' Disease Neuroimaging Initiative 2021). Given the findings in the

current and our previous study regarding SA and cognition in mid-life (Patel, Mackay, et al. 2022), there is strong rationale to include this measure in future studies related to AD progression and to better understand its biological relevance. Further, our results demonstrated that CT is more sensitive to the disease progression compared to SA (Xiong et al. 2022). Overall, despite harbouring a higher genetic risk load for AD due to familial history, FAMHX individuals appeared to show similar neurobiological patterns as the HC group. This is likely explained by the age difference between groups (Tremblay-Mercier et al. 2021).

Surprisingly, contrary to our cortical morphometry findings, no hippocampal volume differences were found between groups in our univariate analyses. However, a volume reduction of the hippocampal body and tail, and an increase in volume in the hippocampal lateral region were found when we used a multivariate analysis. These results suggest that while hippocampal volume did not show a specific relationship to the individual's diagnosis, it was more specific to the cognitive, psychological, lifestyle or medical pattern that we found (discussed in Section 5.6.2). Interestingly, those hippocampal alterations were similar to previous results from our group reporting SA reductions in the body and tail, as well as an outward lateral displacement associated with aging (Bussy, Patel, et al. 2021). Interestingly, the hippocampal parcellation obtained in this study was similar to a previous one (Patel, Steele, et al. 2020), suggesting that these hippocampal regions are indicative of a combined morphometry and microstructural pattern in the human hippocampus.

For the microstructure, cortical T1 and T2* did not differ between our groups, while hippocampal T1 and T2* did. Therefore, we hypothesize that the cortical thinning might not be driven by intra-cortical demyelination or iron accumulation but rather by neuronal death (Telegina et al. 2019). This further suggests that lower myelin content associated with AD may initiate in the hippocampus prior to manifesting in the cortex. This is in line with a previous study showing a specific myelin decrease in the hippocampus using magnetization transfer ratio (MTR) measurements in MCI individuals (Carmeli et al. 2013). Using T1w/T2w ratio to estimate intracortical myelin, another study demonstrated that

hippocampal demyelination was consistently associated with AD progression (X. Luo et al. 2019). Previous research showed that T2* decreased in the hippocampus of those with AD, indicating an increase in iron levels (Z. Zhao et al. 2021). However, our study revealed the opposite pattern, with disease progression associated with an increase in hippocampal T2*. Further discussion on these findings can be found in Section 5.6.3.

5.6.2 Cognitive, psychological, cognitive and medical alterations associated with AD

Our results demonstrated that the cognitive, psychological, lifestyle and medical pattern associated with our brain alterations were sensitive to AD progression. Interestingly lower cognitive scores, higher anxiety, BP, cholesterol and smoking are well characterised risk factors of AD (Livingston et al. 2017).

About 70% of AD patients present anxiety symptoms (Teri et al. 1999) which have been linked to a higher risk ratio of converting to MCI or dementia (Liew 2020), worse MMSE scores and younger age at onset (Porter et al. 2003; Kaiser et al. 2014). Interestingly, in a healthy aging population, anxiety disorders have been previously related to an increase of T1 values in the hippocampus (Trofimova et al. 2021). This is in line with our results showing an increased hippocampal T1 associated with higher anxiety and AD progression. We also found that the pattern of increased anxiety was significantly related to cortical thinning across the cortex. Similarly, previous research reported a relationship between higher levels of anxiety symptoms and reduced thickness in several cortical regions (Pink et al. 2017).

A negative correlation between arterial hypertension and myelin content has been observed in the WM (Trofimova et al. 2021). Systolic late-life cortical and WM atrophy were found to be linked with hypertension during early adulthood (George et al. 2023). In line with these findings, our study showed a similar effect, where higher BP was correlated with myelin reduction and cortical thinning (Gonzalez et al. 2015). Additionally, the brain pattern was significantly associated with the disease progression, which is consistent with hypertension

being linked to increased amyloid load and AD progression (Fungwe et al. 2023; Skoog and Gustafson 2006).

Elevated blood cholesterol levels have been reported to increase Aβ production in the brain (Sparks et al. 1994; Refolo, Malester, et al. 2000; Umeda et al. 2012). Conversely, drugs that reduce blood cholesterol have been shown to lower the risks of developing AD (Refolo, Pappolla, et al. 2001; Olmastroni et al. 2022). It's worth noting that the BBB typically prevents any exchange between the brain and the cholesterol, which means that most brain cholesterol comes from local synthesis. Further, it has been shown that the hippocampus is a brain region particularly susceptible to BBB breakdown (Montagne et al. 2015), and as a result, there may be early alterations in the level of hippocampal cholesterol in AD progression. However, while most studies report brain cholesterol increases related to aging and AD (Yanagisawa 2005; Umeda et al. 2012; Popugaeva, Pchitskaya, and Bezprozvanny 2018), others found the opposite effect (Thelen et al. 2006).

The identification of the APOE-ϵ4 allele gene as a crucial genetic risk factor for AD is in accordance with the involvement of cholesterol in AD's pathogenesis (Puglielli, Rudolph E Tanzi, and D. M. Kovacs 2003; Blanchard et al. 2022). Notably, in APOE-ϵ4 allele carriers, ApoE exhibits reduced binding capacity and transport affinity for lipids (Vance 2012; Hatters, Peters-Libeu, and Weisgraber 2006), which may decrease the transfer of cholesterol from astrocytes to neurons, eventually leading to neuronal apoptosis. This aligns with our findings, which demonstrated that APOE-ϵ4 allele carriers were more heavily loaded in the pattern of brain and lifestyle risk factor association that we observed. While there is a need to clarify the exact relationship between brain cholesterol levels and AD, altered hippocampal cholesterol could explain the hippocampal demyelination pattern related to being APOE-ϵ4 allele carriers.

Finally, research has shown that smoking was associated with an increased risk of dementia and AD (R. Chen 2012; Cataldo, Prochaska, and Glantz 2010). Smoking has also been linked to reduced brain volume and atrophy in specific cortical regions, including the frontal,

occipital, and temporal lobes (Kühn, Schubert, and Gallinat 2010; Brody et al. 2004). Even when taking into account the amount of tobacco smoked over their lifetime, individuals who currently smoke had greater hippocampal atrophy than those who never smoked or had quit smoking in the past (Duriez, Crivello, and Mazoyer 2014). Smokers have also been found to have a greater rate of atrophy in regions that are affected in the early stages of AD compared to non-smokers (Almeida et al. 2008). Furthermore, cigarette smoke is known to trigger the production of endogenous oxidants by affecting the immune response pathway associated with inflammation (Tappia, Troughton, et al. 1995; Bloomer 2007). Significant positive relationships between R2* and smoking were found in certain brain regions such as the basal ganglia, but not in the hippocampus (Trofimova et al. 2021). Here, we found an increase hippocampal T2* being associated with past smoking consumption. This difference of findings could be explained by the fact that our pattern was found in the context of AD progression while Trofimova (Trofimova et al. 2021) included healthy participants. Although R2* is commonly interpreted as being solely related to iron content, in Section 5.6.3, we discuss how other mechanisms linked to AD pathology can influence these metrics.

5.6.3 Specificity of qMRI metrics

While most studies are often careful to not assume one-to-one relationships between qMRI metrics and myelin or iron, they rarely discuss whether those metrics have been validated in the context of neuropsychiatric disorders. For example, T1 has been almost only validated compared to myelin in multiple sclerosis brains (Weijden et al. 2021; Christine L Tardif, Bedell, et al. 2012; Schmierer, Scaravilli, et al. 2004; Schmierer, Wheeler-Kingshott, et al. 2008; Mottershead et al. 2003) or in animal models with experimentally induced demyelination (Odrobina et al. 2005; Thiessen et al. 2013). T2* (or R2*) has been validated against iron in a larger range of applications, from cardiac studies (J. C. Wood and Ghugre 2008), hepatic studies (Hernando et al. 2014), to neurological studies in both multiple sclerosis (Walsh et al. 2013; Bagnato et al. 2018) and in healthy individuals (Langkammer et al. 2010;

Birkl et al. 2020). However, it is currently unclear what T1 and T2* metrics reflect in an AD brain where other microstructural changes, such as neuronal loss and increased amyloid and tau accumulation, occur simultaneously.

Interpretation of T2* is complex as it combines the effects of transverse relaxation T2 and magnetic susceptibility T2', where increased water content increases T2 and increased iron content decreases T2' ($\frac{1}{T2*} = \frac{1}{T2} + \frac{1}{T2'}$). While several studies have reported an extended T2 in the hippocampus of individuals with AD (Kirsch et al. 1992; Laakso, Partanen, Soininen, et al. 1996; Huali Wang et al. 2004), others have observed the opposite effect (Z. Luo et al. 2013) or no change at all (Campeau et al. 1997). Higher hippocampal T2 in the AD group has been postulated to be linked to increased MR visible water reflecting tissue damage (Raven et al. 2013). Indeed, in neurodegenerative disorders, the increased water content in degenerating tissue can also affect MRI relaxation times and reduce R2, which opposes the effect of iron (Kirsch et al. 1992). Therefore, in AD, the increased water content may make it difficult to detect increased iron levels with T2* (Wearn et al. 2020).

Our results demonstrated a significant increase in both T1 and T2* in the hippocampus of individuals with AD compared to HC. T1 is primarily linked to myelin content, where an increase in T1 generally indicates lower myelin content (Lutti et al. 2014). Therefore, we postulate that our findings principally captures a reduction in hippocampal tissue integrity, decreased myelin, and increased water content.

5.6.4 Role of myelin in AD progression

The myelin deterioration has been suggested as being an important factor in the progression of AD, with Bartzokis's pioneer work (George Bartzokis, P. H. Lu, and Jim Mintz 2007; George Bartzokis 2011). Several arguments highlight the link between myelin and AD. First, humans are the only animal susceptible to AD pathology. Indeed, even if some nonhuman primates and dogs develop amyloid, they do not present tau or dementia-like symptoms (Walker and Jucker 2017). Interestingly, the pattern of myelination is also different in humans

compared to other animals. For example, compared to chimpanzees, humans are born with a lower number of myelinated axons, and their myelin growth persists beyond adolescence (D. J. Miller et al. 2012). Furthermore, throughout the course of brain evolution, the number of glial cells has increased significantly more than that of neurons, with the proportion of glial cells rising from 10-20% in nematodes to 25% in flies, 65% in rodents, and 90% in humans (Pfrieger and Barres 1995). This has led to a higher percentage of brain dry weight being attributed to myelin in humans, accounting for 30% of the total weight, which is disproportionately greater than in rodents (Norton 1976).

Supporting the fact that amyloid might not be the main molecule triggering cognitive decline, combined data from multiple trials has demonstrated that reducing amyloid levels do not significantly enhance cognitive function (Ackley et al. 2021). Another important criticism is that both neuropathological and PET data reveal substantial evidence of Aβ pathology in older individuals who do not necessarily exhibit cognitive impairment (D A Bennett et al. 2006). Altogether, the presence of Aβ deposition without any cognitive impairment, along with the reduction of Aβ levels without any cognitive improvement, raises significant concerns regarding the validity of Aβ as a causal factor of AD (Herrup 2015; Kametani and Hasegawa 2018).

Interestingly, there is a noticeable similarity between the pattern of NFT changes observed in AD and the reverse order of cortical myelination (Braak and E. Braak 1996). Indeed, certain brain regions, such as the prefrontal cortex and association areas such as the parietal and temporal lobes, which are characterized by late myelination, are particularly susceptible to the development of amyloid and NFT. Late myelinated regions which have thinner sheath (George Bartzokis 2004) are more susceptible to degeneration (Pakkenberg et al. 2003). Conversely, heavily and early myelinated regions of the brain, such as the primary motor and sensory areas, appear to be more resistant to the disease (George Bartzokis 2004). In our results, while we did not find significant cortical T1 variation related to the disease progression, we found high sensitivity of hippocampal demyelination to the disease progression.

This could be explained by the fact that the hippocampus is one of the first regions to be impacted by AD pathology.

Studies have shown that higher amyloid deposition assessed by PET is associated with decreased T2* in the cortex (Z. Zhao et al. 2021). Therefore, our findings indicating a reduction in T2* in the dorsomedial and superior temporal regions, superior frontal cortex, and premotor cortex are consistent with an increased pathological burden in those areas. Notably, these regions correspond to late myelinated regions, which aligns with the theory that late myelinated regions are at higher risk of developing AD pathology. In contrast, we observed an opposite pattern in early myelinated regions such as the occipital lobe, which demonstrated an increased T2* value associated with our brain pattern. The cause of this increase of T2* is unclear, since it could be related to the tissue water content, a myelin reduction, death of glial cells or potentially a methodological limitation.

5.6.5 Methodological limitations

In a conventional MPRAGE sequence, the signal depends on T1 contrast, as well as M0 and T2$*$. However, if two MPRAGE images are acquired at different inversion times, they can be combined to eliminate the effects of radio frequency receive field ($B1^-$), M0, and T2$*$. Although radio frequency transmit field ($B1^+$) inhomogeneity correction is a more complicated process, studies have shown that the MP2RAGE sequence, which uses a small flip angle, can significantly reduce the impact of $B1^+$ on the resulting T1 maps (Marques, Kober, et al. 2010). However, some residual biases related to the $B1^+$ may persist. For example, $B1^+$ field inhomogeneity effects have been found near inferior temporal and frontal lobes, affecting the accuracy of automatic cortical thickness (Haast, Ivanov, and Uludağ 2018). Moreover, residual $B1^+$ effects on MP2RAGE signal intensities can also impact hippocampal analyses, potentially altering volume and shape measurements (Haast, Lau, et al. 2021). Acquiring additional $B1^+$ maps to correct for those inhomogeneities have been proposed to improve quantitative T1 mapping (Boudreau et al. 2017). Unfortunately, our

study did not have a $B1^+$ map acquisition, therefore while we cannot test it, it is possible that our results might be slightly influenced by the presence of $B1^+$ inhomogeneity residuals. The direction of fibers in relation to the main magnetic field B0 influences T2* relaxation times in the WM (B. Bender and Klose 2010). To reduce the angle dependency between B0 and myelinated fibers in cortical T2*, we used a previously proposed method (Cohen-Adad et al. 2012). However, the orientation of myelinated fibers in the hippocampus is difficult to estimate due to its complex shape, making this correction unfeasible. Although advanced metrics such as diffusion tensor imaging could be used to estimate fiber orientation, those were unavailable to us (Melhem et al. 2002; Tax et al. 2021). However, while it is not optimal, most papers using T2* in clinical applications do not correct for this effect due to its complexity.

5.6.6 Future research

This work has several potential avenues for future investigation. First, to further validate our interpretation, additional qMRI markers, such as PD and magnetization transfer (MT) metrics, could be used alongside T2* and T1. PD, in particular, could provide valuable information about the water content in the tissue. Second, the relationship between qMRI and amyloid deposition is not yet well characterized, and thus, including amyloid and tau PET scans alongside qMRI protocols would shed light on the impact of these pathological molecules on qMRI metrics. Finally, a longitudinal dataset with both PET and qMRI measurements in preclinical AD individuals would be ideal to determine whether myelin alterations can be detected before the appearance of amyloid and tau.

5.6.7 Conclusion

In conclusion, by using qMRI to investigate the underlying biological processes that could drive morphological changes, our study suggests that hippocampal T1 and T2* could serve as potential biomarkers for AD. Further, significant associations between certain risk factors

and AD-related brain pattern alterations demonstrate that public health initiatives aimed at reducing smoking, cholesterol levels, blood pressure, and anxiety in the population should be continued to slow the progression of AD.

5.7 Supplementary materials

5.7.1 Data imputation

	HC (n=38)	FAMHX (n=58)	MCI (n=41)	AD (n=21)
hearing problem	0	**1**	0	0
concussion	0	**1**	0	0
high BP	0	0	**6**	0
high chol	0	0	**6**	0
diabetes	0	0	**6**	0
heart disease	0	**3**	**6**	0
arthritis	0	0	**4**	0
neck back problem	0	0	**3**	0
liver disease	0	0	**6**	0
kindney disease	0	0	**6**	0
thyroid disease	0	0	**6**	0
drugs	0	0	**6**	0
MOCA	0	0	**1**	0
RBANS total	**2**	**2**	**4**	**8**
imm mem	**2**	**2**	**4**	**8**
attention	**2**	**2**	**4**	**8**
language	**2**	**2**	**4**	**6**
visuospatial	**2**	**2**	**4**	**8**
del mem	**3**	**2**	**4**	**8**

Table 5.2: Table of the number of missing values for each of the variable per group

5.7.2 T2* denoising

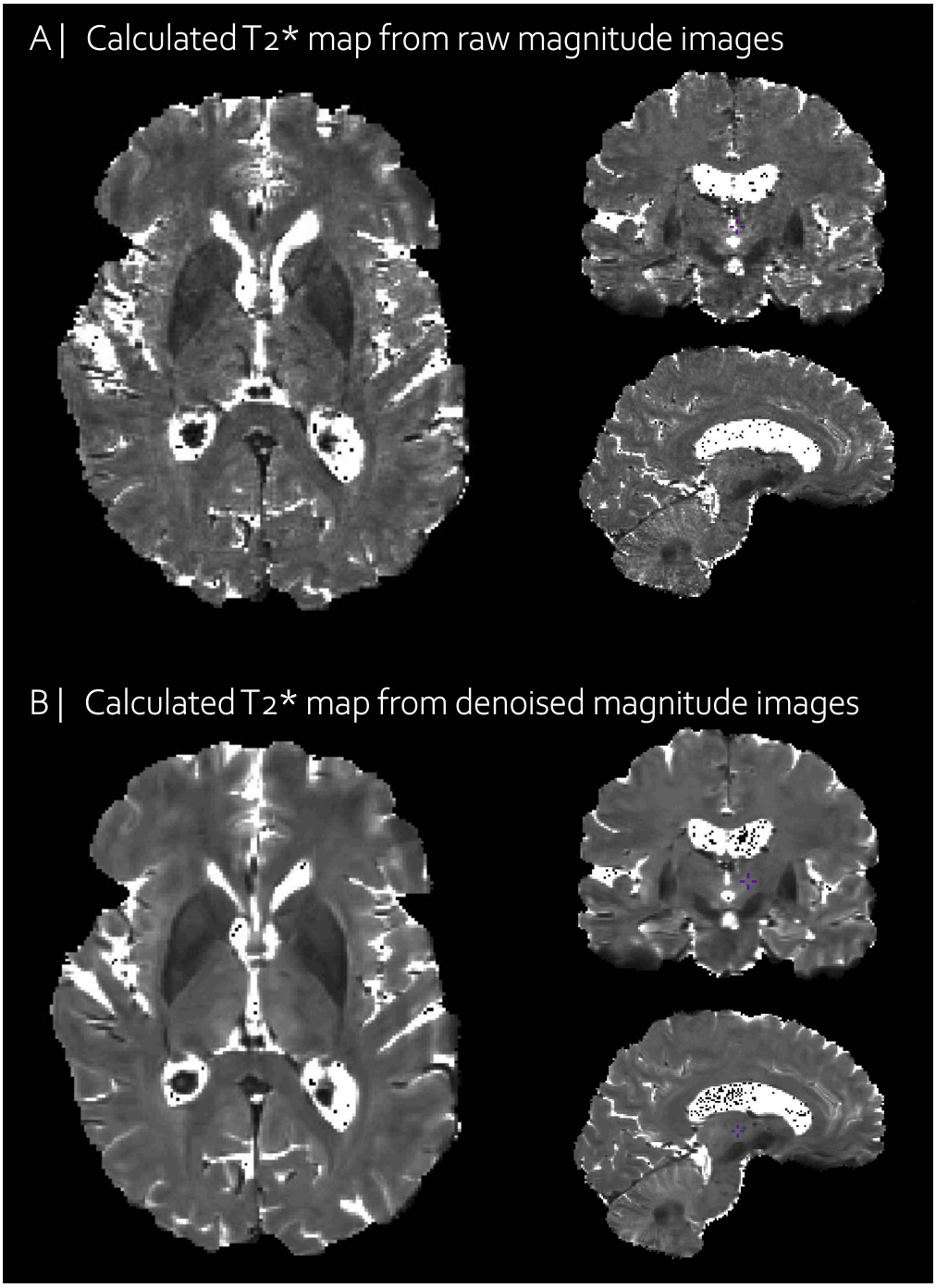

Figure 5.6: T2* map example with or without denoising.

5.7.3 Description of NMF

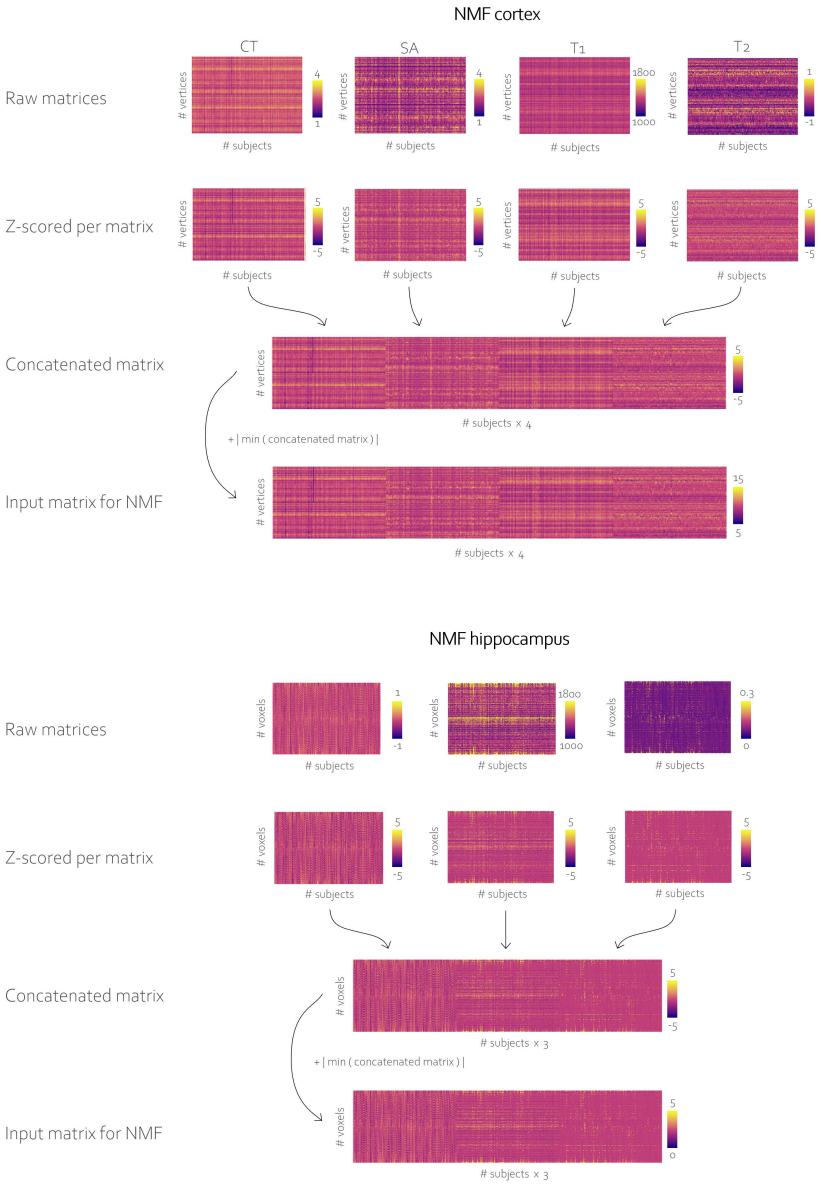

Figure 5.7: Input matrices of the (**A** —) vertex-wise cortical metrics and (**B** —) voxel-wise hippocampal metrics. First, we performed a z-scoring across each input matrix (for example, across participants and vertices for CT). Then, the z-scored matrices were concatenated to create a large matrix (*number of columns = number of participants x number of metrics*). Finally, the absolute value of the minimum z-scored value across the large input matrix was added to all values to obtain a non-negative matrix (Patel, Steele, et al. 2020).

5.7.4 NMF stability analyses

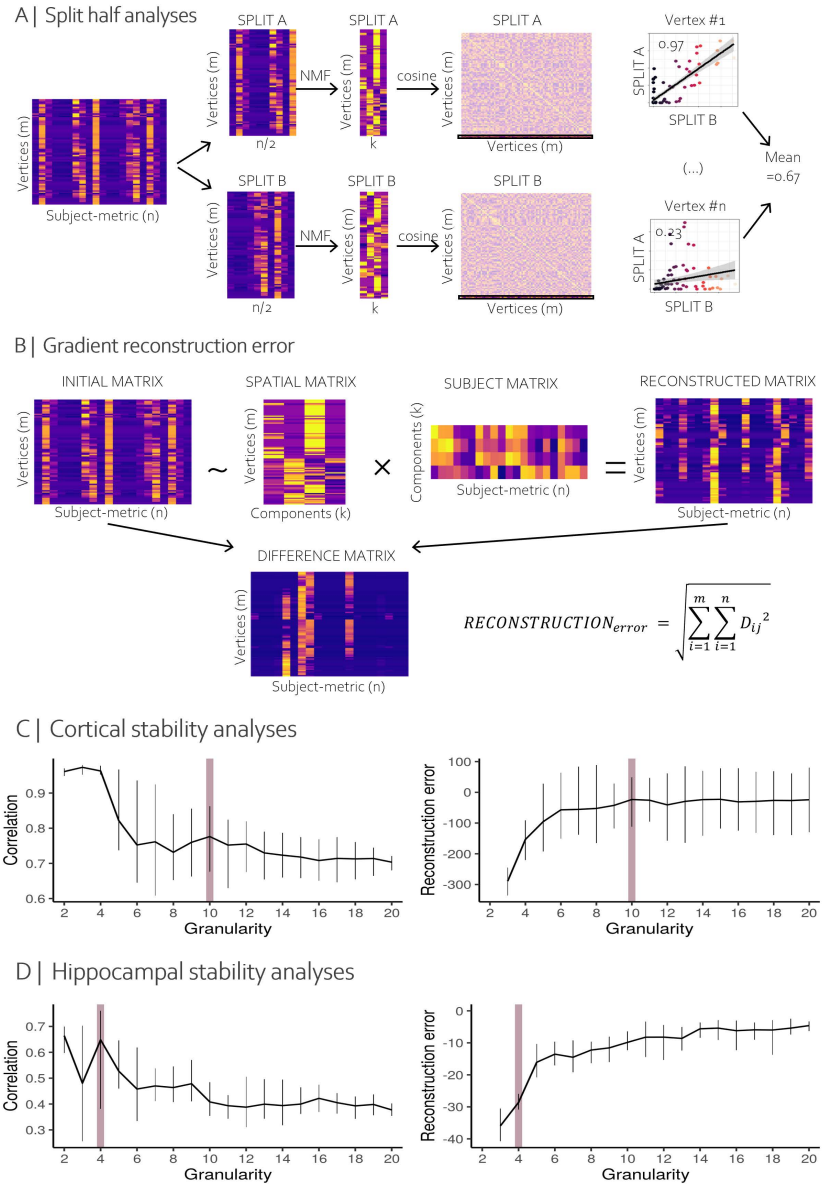

Figure 5.8: Stability analyses results. (**A** —) Representation of the calculation of the correlation calculation between split A and split B. (**B** —) Representation of the calculation of the gradient reconstruction error. (**C** — For the cortex, we decided to select 10 components to have a detailed enough parcellation, with reasonable correlation and reconstruction error. (**D**—) For the hippocampus, we selected 4 components to have a high correlation and components of a decent size (also, previous work from our lab already selected 4 hippocampal components with a similar approach

.

5.7.5 Cortical NMF k4

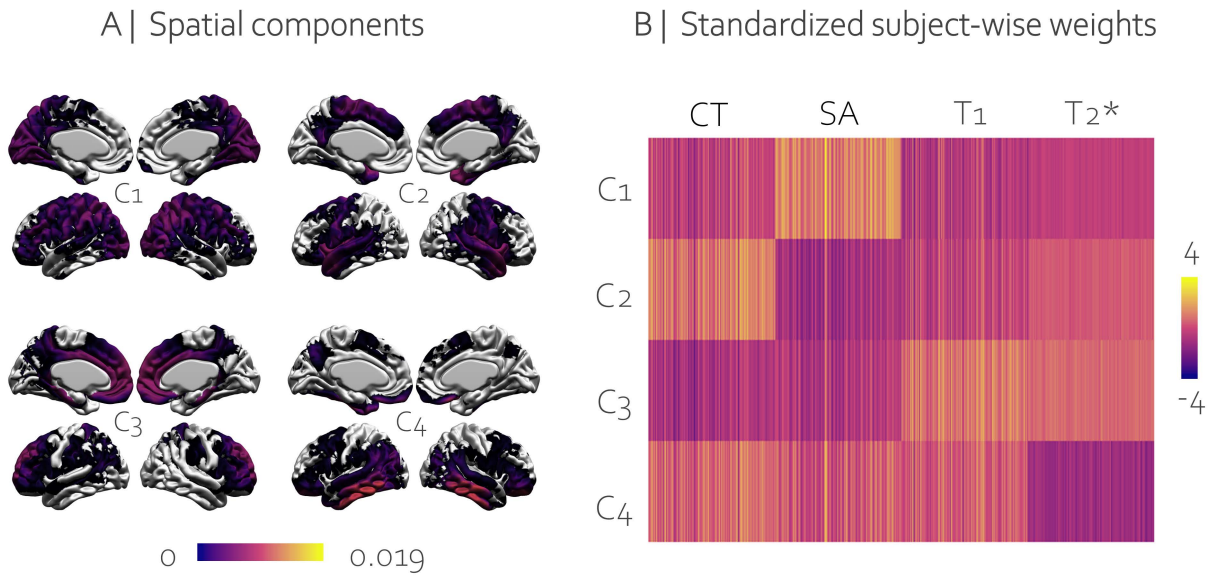

Figure 5.9: Outputs for 4 components cortical NMF run. (**A** —) Spatial maps and (**B** —) Standardized subject-wise weights matrix.

5.7.6 Component characteristics

Because the NMF output matrices are normalized per component, direct comparison of across components is not possible. Therefore, we used the NMF parcellation to extract the mean raw values to describe the components (Supplementary Figure 5.10). The properties of orthogonal projection NMF enable us to assign each vertex (or voxel), via a winner takes all approach, such that each vertex (or voxel) was assigned to a single component for which it had the highest component score. Mean vertex-wise (or voxel-wise) values were calculated for each component and for each individual to visualize the raw value variation across the structures of interest and individuals to better characterize the variation captured by the components (Figure 5.10). By doing so, we can appreciate the spatial variation of our metrics across our structures of interest, and we can visualize how variable the metrics are per component.

5.7.6.1 Cortical components

CT is higher in component 1, 4 and 5 which mostly corresponds to regions of the frontal, temporal and dorsomedial regions, while lower CT is seen in the occipital and sensorimotor regions. SA is mainly higher in the occipital lobe compared to the rest of the brain. T1 is higher in the frontal and temporal regions while T2* shows a gradient from high values in the occipital lobe to lower values in the occipital regions.

5.7.6.2 Hippocampal components

The distribution of J across participants is consistent in the four hippocampal components. However, higher T1 values were observed in the most lateral and the most medial regions of the hippocampus. T2* was higher in the lateral regions of the hippocampus.

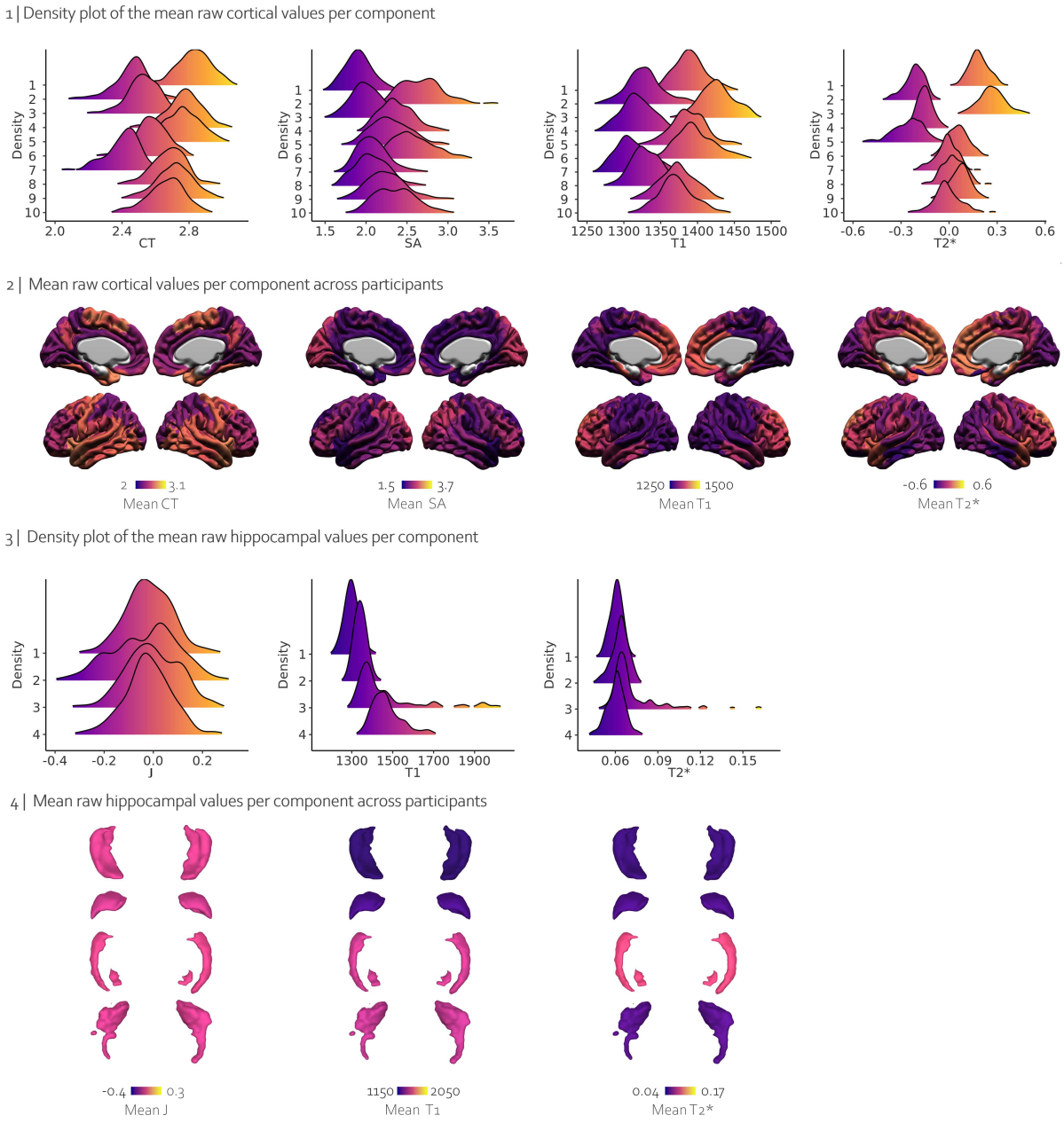

Figure 5.10: **1** — Density plot of the mean raw cortical values per component. **2**— Mean raw cortical values per component across participants. **3** — Density plot of the mean raw hippocampal values per component. **4** — Mean raw hippocampal values per component across participants

5.7.7 Statistical results of post-hoc analyses

	Variables	Behav LV1	Brain LV1	Behav LV2	Brain LV2	Behav LV3	Brain LV3
ANOVA	FAMHX-HC	0,262	0,971	1,000	1,000	1,000	1,000
	MCI-HC	**6,912E-03**	0,0938	1,000	1,000	1,000	1,000
	AD-HC	**1,017E-11**	**1,269E-06**	1,000	1,000	1,000	0,812
	MCI-FAMHX	**8,100E-08**	**1,106E-03**	1,000	0,968	0,922	1,000
	AD-FAMHX	**9,526E-14**	**1,807E-09**	1,000	1,000	1,000	0,792
	AD-MCI	**1,774E-05**	**7,811E-03**	1,000	0,922	1,000	0,825
Linear model	Age	**1,973E-05**	**5,180E-11**	0,300	0,568	0,589	0,069
	Sex - M	0,825	**2,874E-03**	0,262	**1,014E-03**	**5,050E-04**	**4,963E-05**
	APOE4 - 1	0,309	**2,971E-03**	1,000	1,000	0,485	0,891
	Years school	0,816	0,541	0,425	0,971	0,541	0,948

Table 5.3: Table of the p-values after FDR correction across all variables and LVs. Pairwise group differences were tested using ANOVA and post-hoc Tukey HSD, while age, sex, APOE-ϵ4 allele and education were tested using linear models.

5.7.8 LV2 results

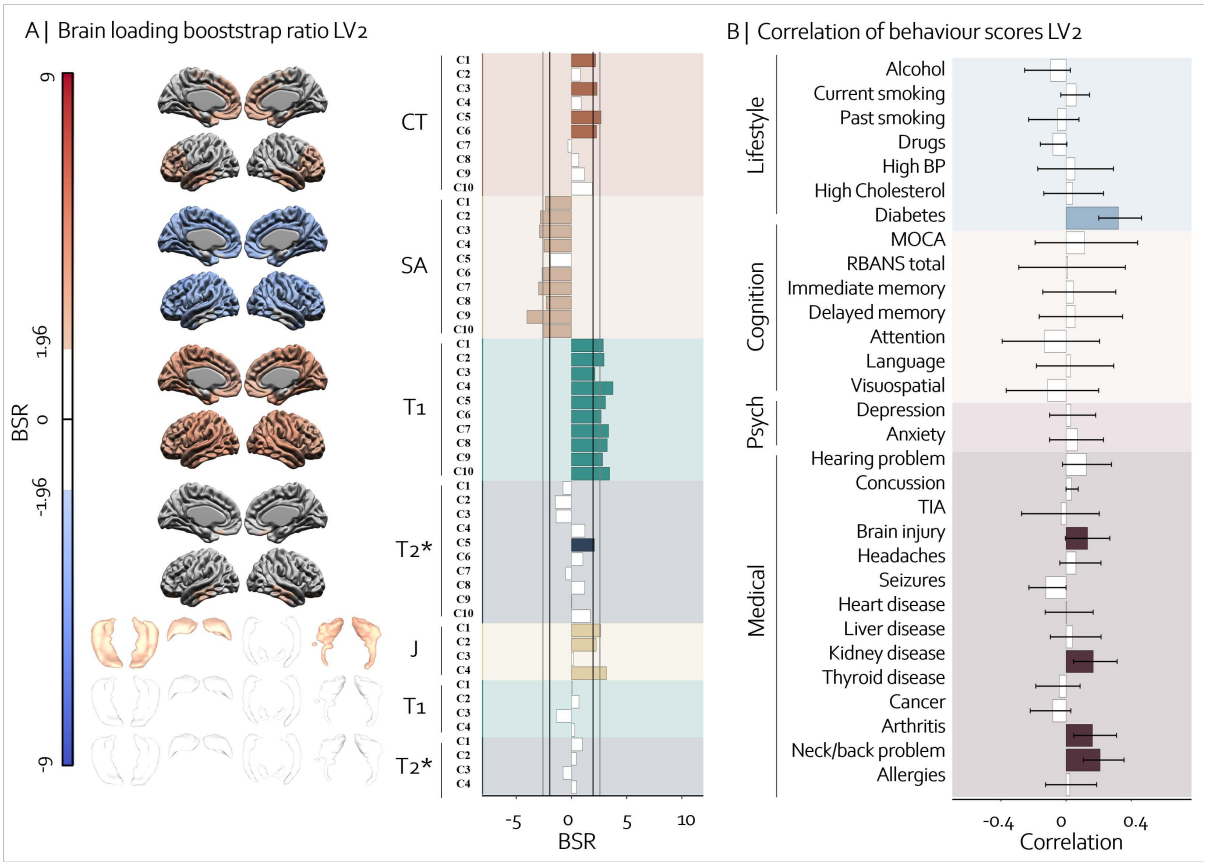

Figure 5.11: The second LV explained 7.5% of the covariance between brain and cognitive, psychological, medical, and lifestyle information. The brain pattern on the left **(A)** illustrates spatially the contribution of each metric to the pattern with BSR values on each brain structure. Blue color indicates negative BSR values and red indicates positive BSR values. Components with absolute BSR values higher than 1.96 are colored to show significant contribution. The bar plot in the middle of the figure shows more precisely the BSR values for each component, with black vertical lines representing a BSR of 1.96 (equivalent to p=0.05) and gray lines representing a BSR of 2.58 (equivalent to p=0.01). On the right-hand side **(B)**, we can see the cognitive, psychological, medical, and lifestyle patterns associated with the brain pattern on the left. Bars are colored if they are significant (when error bars do not cross zero), and are white if non-significant. The brain pattern is associated with having diabetes, brain injury, kidney disease, arthritis and neck/back problems.

5.7.9 Post-hoc analyses of LV2

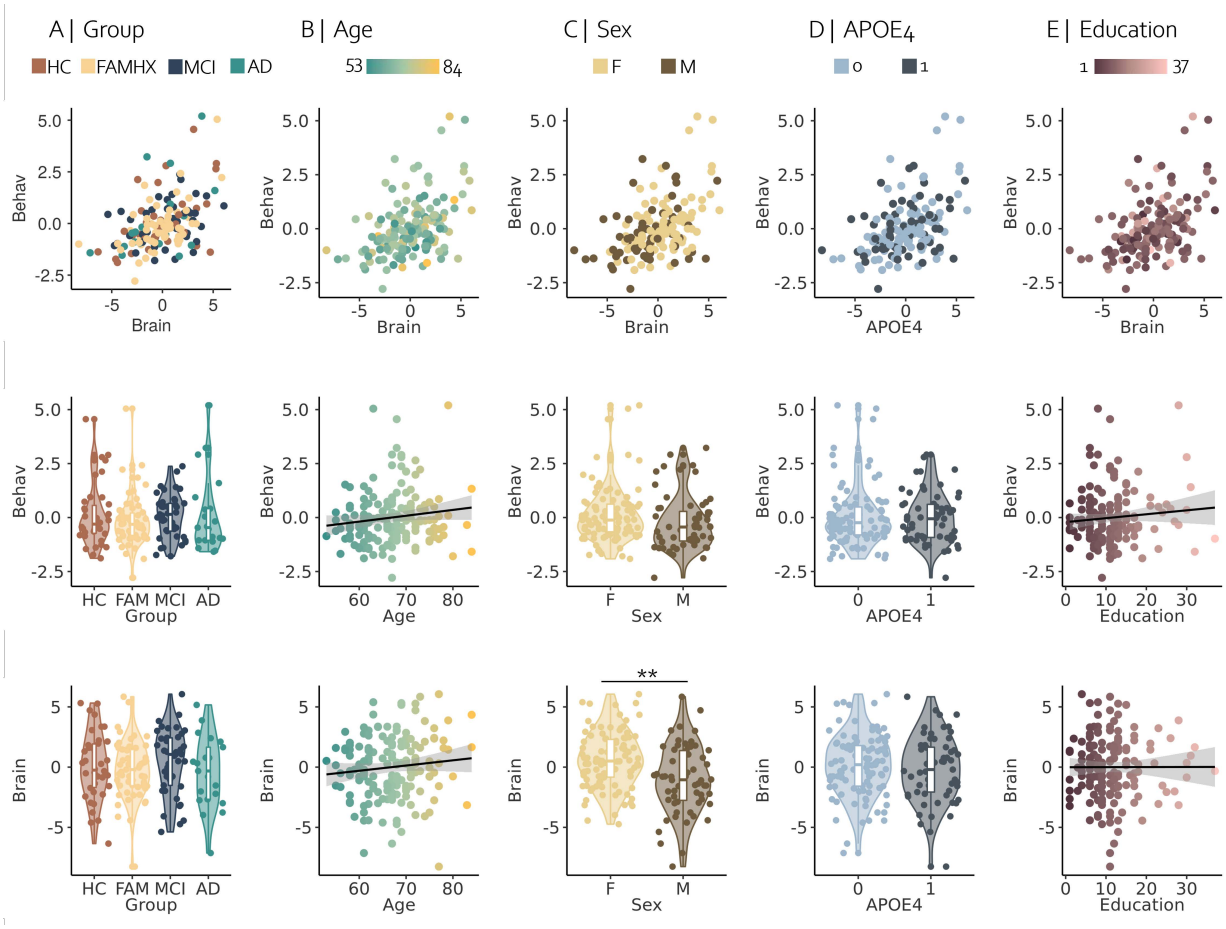

Figure 5.12: Post-hoc analyses of the PLS brain and behaviour scores of LV2. **(A)** is showing the pairwise group comparisons of the brain and behaviour scores. Results of the linear models illustrating the brain and behaviour relationships with age **(B)**, sex **(C)**, APOE-ϵ4 allele status **(D)** and education **(E)**. * $p < 0.05$, ** $p < 0.01$, *** $p < 0.001$ after FDR correction across all p-values.

5.7.10 LV3 results

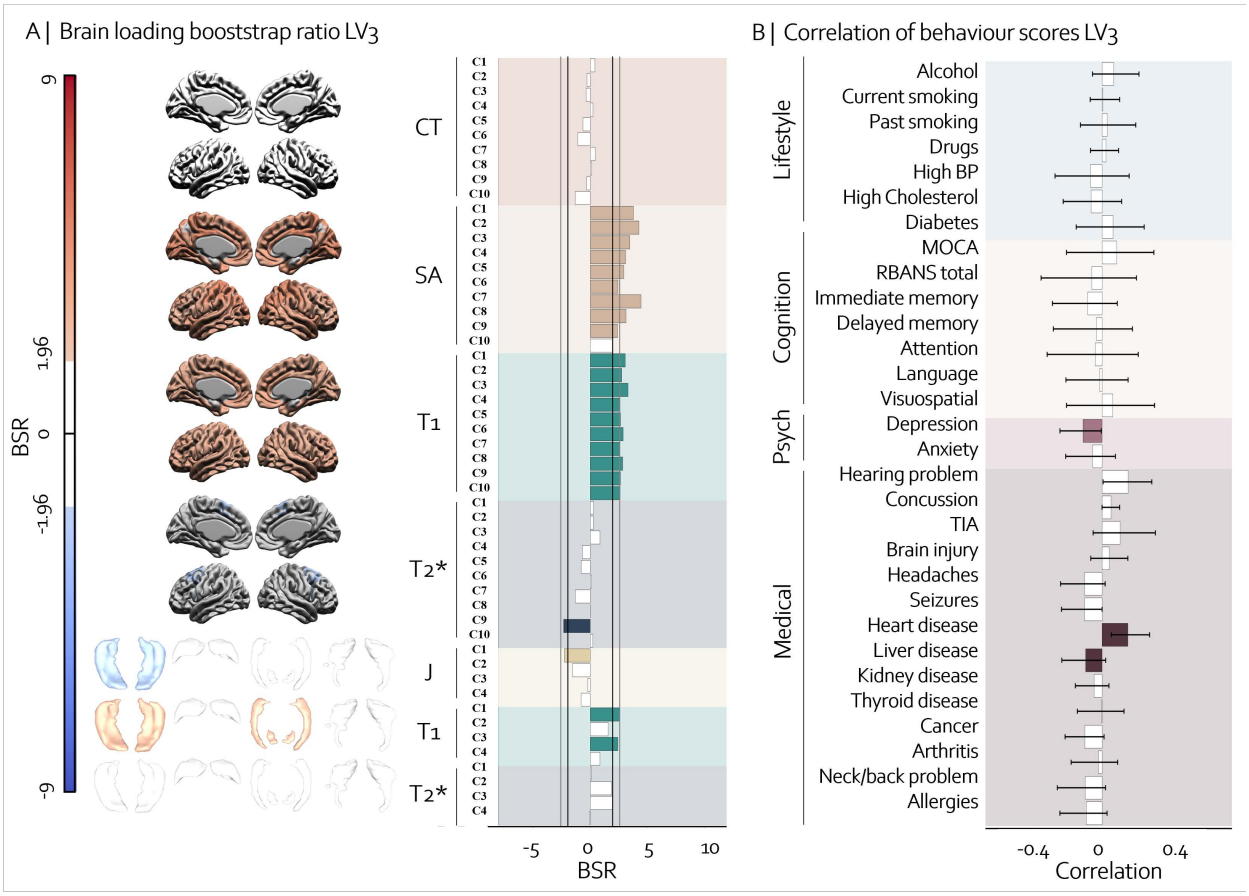

Figure 5.13: The third LV explained 5.2% of the covariance between brain and cognitive, psychological, medical, and lifestyle information. The brain pattern on the left **(A)** illustrates spatially the contribution of each metric to the pattern with BSR values on each brain structure. Blue color indicates negative BSR values and red indicates positive BSR values. Components with absolute BSR values higher than 1.96 are colored to show significant contribution. The bar plot in the middle of the figure shows more precisely the BSR values for each component, with black vertical lines representing a BSR of 1.96 (equivalent to p=0.05) and gray lines representing a BSR of 2.58 (equivalent to p=0.01). On the right-hand side **(B)**, we can see the cognitive, psychological, medical, and lifestyle patterns associated with the brain pattern on the left. Bars are colored if they are significant (when error bars do not cross zero), and are white if non-significant. The brain pattern is associated with having diabetes, brain injury, kidney disease, arthritis and neck/back problems.

5.7.11 Post-hoc analyses of LV3

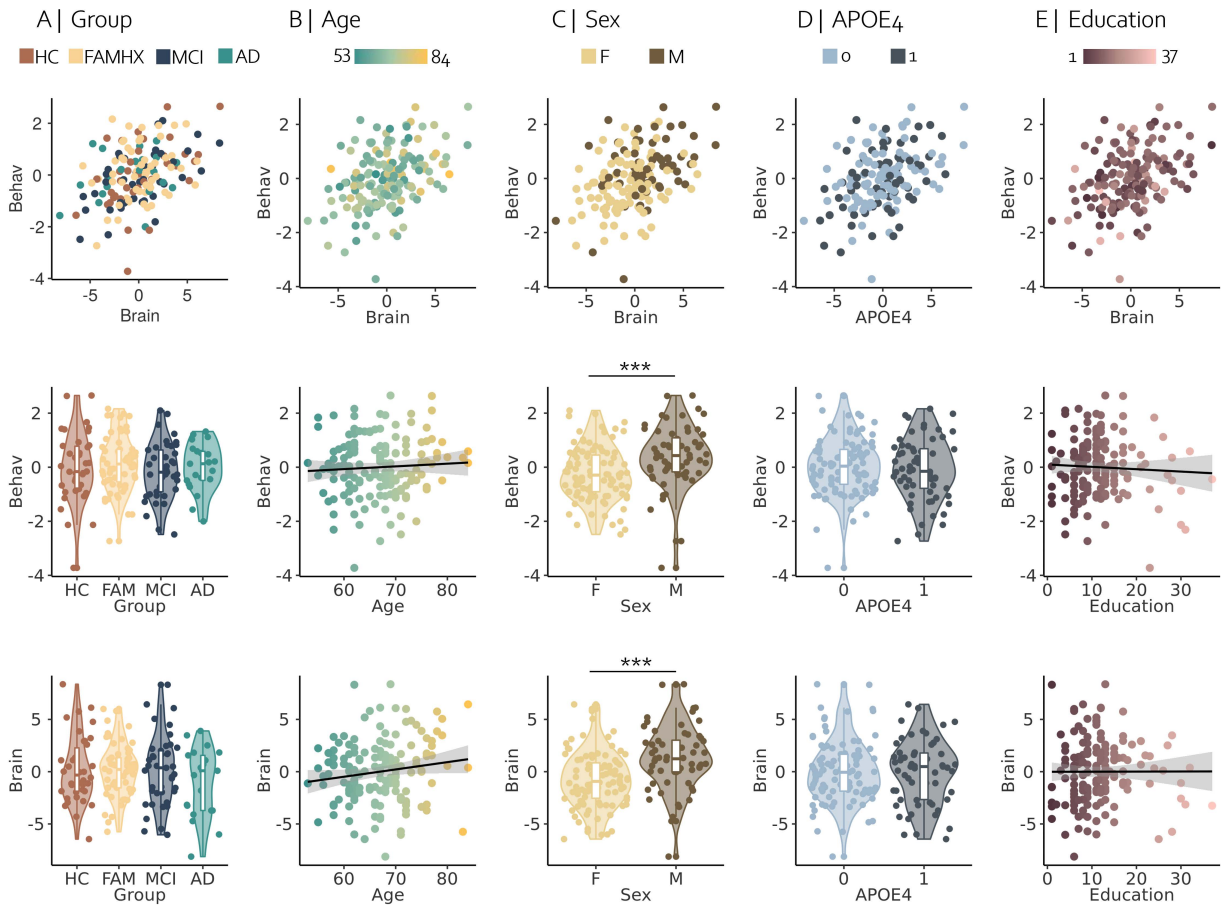

Figure 5.14: Post-hoc analyses of the PLS brain and behaviour scores of LV3. **(A)** is showing the pairwise group comparisons of the brain and behaviour scores. Results of the linear models illustrating the brain and behaviour relationships with age **(B)**, sex **(C)**, APOE-ϵ4 allele status **(D)** and education **(E)**. * $p < 0.05$, ** $p < 0.01$, *** $p < 0.001$ after FDR correction across all p-values.

References Chapter 5

Ackley, Sarah F et al. (Feb. 2021). "Effect of reductions in amyloid levels on cognitive change in randomized trials: instrumental variable meta-analysis". en. In: *BMJ* 372, n156.

Almeida, Osvaldo P et al. (Jan. 2008). "Smoking is associated with reduced cortical regional gray matter density in brain regions associated with incipient Alzheimer disease". en. In: *Am. J. Geriatr. Psychiatry* 16.1, pp. 92–98.

Arnone, D et al. (Dec. 2013). "State-dependent changes in hippocampal grey matter in depression". en. In: *Mol. Psychiatry* 18.12, pp. 1265–1272.

Avants, Brian B et al. (Feb. 2011). "A reproducible evaluation of ANTs similarity metric performance in brain image registration". en. In: *Neuroimage* 54.3, pp. 2033–2044.

Bagnato, Francesca et al. (Mar. 2018). "Untangling the R2* contrast in multiple sclerosis: A combined MRI-histology study at 7.0 Tesla". en. In: *PLoS One* 13.3, e0193839.

Bartzokis, G, D Sultzer, et al. (Apr. 1994). "In vivo evaluation of brain iron in Alzheimer's disease and normal subjects using MRI". en. In: *Biol. Psychiatry* 35.7, pp. 480–487.

Bartzokis, George (Jan. 2004). "Age-related myelin breakdown: a developmental model of cognitive decline and Alzheimer's disease". en. In: *Neurobiol. Aging* 25.1, 5–18, author reply 49–62.

— (2011). "Alzheimer's disease as homeostatic responses to age-related myelin breakdown". In: *Neurobiol. Aging* 32.8, pp. 1341–1371.

Bartzokis, George, Po H Lu, and Jim Mintz (Apr. 2007). "Human brain myelination and amyloid beta deposition in Alzheimer's disease". en. In: *Alzheimers. Dement.* 3.2, pp. 122–125.

Bedford, Saashi A et al. (Mar. 2020). "Large-scale analyses of the relationship between sex, age and intelligence quotient heterogeneity and cortical morphometry in autism spectrum disorder". en. In: *Mol. Psychiatry* 25.3, pp. 614–628.

Bellon, E M et al. (Dec. 1986). "MR artifacts: a review". en. In: *AJR Am. J. Roentgenol.* 147.6, pp. 1271–1281.

Bender, B and U Klose (Nov. 2010). "The in vivo influence of white matter fiber orientation towards B(0) on T2* in the human brain". en. In: *NMR Biomed.* 23.9, pp. 1071–1076.

Bennett, D A et al. (June 2006). "Neuropathology of older persons without cognitive impairment from two community-based studies". en. In: *Neurology* 66.12, pp. 1837–1844.

Birkl, Christoph et al. (Oct. 2020). "The influence of iron oxidation state on quantitative MRI parameters in post mortem human brain". en. In: *Neuroimage* 220, p. 117080.

Blanchard, Joel W et al. (Nov. 2022). "APOE4 impairs myelination via cholesterol dysregulation in oligodendrocytes". en. In: *Nature* 611.7937, pp. 769–779.

Bloomer, R J (2007). "Decreased blood antioxidant capacity and increased lipid peroxidation in young cigarette smokers compared to nonsmokers: impact of dietary intake". In: *Nutr. J.*

Boudreau, Mathieu et al. (Dec. 2017). "B1 mapping for bias-correction in quantitative T 1 imaging of the brain at 3T using standard pulse sequences". en. In: *J. Magn. Reson. Imaging* 46.6, pp. 1673–1682.

Braak, H and E Braak (Aug. 1996). "Development of Alzheimer-related neurofibrillary changes in the neocortex inversely recapitulates cortical myelogenesis". en. In: *Acta Neuropathol.* 92.2, pp. 197–201.

Brody, Arthur L et al. (Jan. 2004). "Differences between smokers and nonsmokers in regional gray matter volumes and densities". en. In: *Biol. Psychiatry* 55.1, pp. 77–84.

Brown, Robert W et al. (June 2014). *Magnetic Resonance Imaging: Physical Principles and Sequence Design*. en. John Wiley & Sons.

Bussy, Aurélie, Jake P Levy, et al. (Mar. 2023). "Cerebellar and subcortical atrophy contribute to psychiatric symptoms in frontotemporal dementia". en. In: *Hum. Brain Mapp.* 44.7, pp. 2684–2700.

Bussy, Aurélie, Raihaan Patel, et al. (Oct. 2021). "Hippocampal shape across the healthy lifespan and its relationship with cognition". en. In: *Neurobiol. Aging* 106, pp. 153–168.

Bussy, Aurélie, Eric Plitman, et al. (June 2021). "Hippocampal subfield volumes across the healthy lifespan and the effects of MR sequence on estimates". en. In: *Neuroimage* 233, p. 117931.

Campeau, N G et al. (Oct. 1997). "Hippocampal transverse relaxation times in patients with Alzheimer disease". en. In: *Radiology* 205.1, pp. 197–201.

Carmeli, Cristian et al. (Aug. 2013). "Demyelination in mild cognitive impairment suggests progression path to Alzheimer's disease". en. In: *PLoS One* 8.8, e72759.

Cataldo, Janine K, Judith J Prochaska, and Stanton A Glantz (2010). "Cigarette smoking is a risk factor for Alzheimer's Disease: an analysis controlling for tobacco industry affiliation". en. In: *J. Alzheimers. Dis.* 19.2, pp. 465–480.

Chen, Ruoling (Nov. 2012). "Association of environmental tobacco smoke with dementia and Alzheimer's disease among never smokers". en. In: *Alzheimers. Dement.* 8.6, pp. 590–595.

Cherubini, Andrea et al. (Oct. 2009). "Aging of subcortical nuclei: microstructural, mineralization and atrophy modifications measured in vivo using MRI". en. In: *Neuroimage* 48.1, pp. 29–36.

Chung, M K et al. (Sept. 2001). "A unified statistical approach to deformation-based morphometry". en. In: *Neuroimage* 14.3, pp. 595–606.

Chung, Moo K, Nagesh Adluru, and Houri K Vorperian (2020). "Heat Kernel Smoothing on Manifolds and Its Application to Hyoid Bone Growth Modeling". In: *Statistical Modeling in Biomedical Research: Contemporary Topics and Voices in the Field*. Ed. by Yichuan Zhao and Ding-Geng (din) Chen. Cham: Springer International Publishing, pp. 235–261.

Cohen-Adad, J et al. (Apr. 2012). "T* mapping and B orientation-dependence at 7 T reveal cyto- and myeloarchitecture organization of the human cortex". en. In: *Neuroimage* 60.2, pp. 1006–1014.

Depp, Constanze et al. (June 2023). "Myelin dysfunction drives amyloid-β deposition in models of Alzheimer's disease". en. In: *Nature* 618.7964, pp. 349–357.

Dickerson, Bradford C et al. (2009). "The cortical signature of Alzheimer's disease: regionally specific cortical thinning relates to symptom severity in very mild to mild AD dementia and is detectable in asymptomatic amyloid-positive individuals". In: *Cereb. Cortex* 19.3, pp. 497–510.

Du, A T et al. (Oct. 2001). "Magnetic resonance imaging of the entorhinal cortex and hippocampus in mild cognitive impairment and Alzheimer's disease". en. In: *J. Neurol. Neurosurg. Psychiatry* 71.4, pp. 441–447.

Duara, R et al. (Dec. 2008). "Medial temporal lobe atrophy on MRI scans and the diagnosis of Alzheimer disease". en. In: *Neurology* 71.24, pp. 1986–1992.

Duriez, Quentin, Fabrice Crivello, and Bernard Mazoyer (Nov. 2014). "Sex-related and tissue-specific effects of tobacco smoking on brain atrophy: assessment in a large longitudinal cohort of healthy elderly". en. In: *Front. Aging Neurosci.* 6, p. 299.

Duyn, Jeff (Apr. 2013). "MR susceptibility imaging". en. In: *J. Magn. Reson.* 229, pp. 198–207.

Dyck, Christopher H van et al. (Jan. 2023). "Lecanemab in Early Alzheimer's Disease". en. In: *N. Engl. J. Med.* 388.1, pp. 9–21.

Eck, Brendan L et al. (Jan. 2023). "Quantitative MRI for Evaluation of Musculoskeletal Disease: Cartilage and Muscle Composition, Joint Inflammation, and Biomechanics in Osteoarthritis". en. In: *Invest. Radiol.* 58.1, pp. 60–75.

Eid, Aseel, Isha Mhatre, and Jason R Richardson (July 2019). "Gene-environment interactions in Alzheimer's disease: A potential path to precision medicine". en. In: *Pharmacol. Ther.* 199, pp. 173–187.

Eskildsen, Simon F et al. (Feb. 2012). "BEaST: brain extraction based on nonlocal segmentation technique". en. In: *Neuroimage* 59.3, pp. 2362–2373.

Fungwe, Thomas V et al. (Feb. 2023). "Systolic Blood Pressure Is Associated with Increased Brain Amyloid Load in Mild Cognitively Impaired Participants: Alzheimer's Disease Neuroimaging Initiatives Study". en. In: *Dement. Geriatr. Cogn. Disord.*, pp. 1–8.

Gelman, N et al. (Jan. 2001). "Interregional variation of longitudinal relaxation rates in human brain at 3.0 T: relation to estimated iron and water contents". en. In: *Magn. Reson. Med.* 45.1, pp. 71–79.

George, Kristen M et al. (Apr. 2023). "Association of Early Adulthood Hypertension and Blood Pressure Change With Late-Life Neuroimaging Biomarkers". en. In: *JAMA Netw Open* 6.4, e236431.

Gonzalez, Christopher E et al. (June 2015). "Longitudinal changes in cortical thinning associated with hypertension". en. In: *J. Hypertens.* 33.6, pp. 1242–1248.

Granziera, Cristina et al. (June 2021). "Quantitative magnetic resonance imaging towards clinical application in multiple sclerosis". en. In: *Brain* 144.5, pp. 1296–1311.

Haast, Roy A M, Dimo Ivanov, and Kâmil Uludağ (June 2018). "The impact of correction on MP2RAGE cortical T 1 and apparent cortical thickness at 7 T". en. In: *Hum. Brain Mapp.* 39.6, pp. 2412–2425.

Haast, Roy A M, Jonathan C Lau, et al. (Jan. 2021). "Effects of MP2RAGE B1+ sensitivity on inter-site T1 reproducibility and hippocampal morphometry at 7T". en. In: *Neuroimage* 224, p. 117373.

Harkins, Kevin D, Junzhong Xu, et al. (Mar. 2016). "The microstructural correlates of T1 in white matter". en. In: *Magn. Reson. Med.* 75.3, pp. 1341–1345.

Hatters, Danny M, Clare A Peters-Libeu, and Karl H Weisgraber (Aug. 2006). "Apolipoprotein E structure: insights into function". en. In: *Trends Biochem. Sci.* 31.8, pp. 445–454.

Hernando, Diego et al. (Nov. 2014). "Quantification of liver iron with MRI: state of the art and remaining challenges". en. In: *J. Magn. Reson. Imaging* 40.5, pp. 1003–1021.

Herrup, Karl (June 2015). "The case for rejecting the amyloid cascade hypothesis". en. In: *Nat. Neurosci.* 18.6, pp. 794–799.

Iannopollo, Emily, Kara Garcia, and Alzheimer' Disease Neuroimaging Initiative (Aug. 2021). "Enhanced detection of cortical atrophy in Alzheimer's disease using structural

MRI with anatomically constrained longitudinal registration". en. In: *Hum. Brain Mapp.* 42.11, pp. 3576–3592.

Ito, Kaori et al. (Jan. 2010). "Disease progression meta-analysis model in Alzheimer's disease". en. In: *Alzheimers. Dement.* 6.1, pp. 39–53.

Jack Jr, C R, R C Petersen, Y Xu, P C O'Brien, G E Smith, R J Ivnik, E G Tangalos, et al. (Oct. 1998). "Rate of medial temporal lobe atrophy in typical aging and Alzheimer's disease". en. In: *Neurology* 51.4, pp. 993–999.

Jack Jr, Clifford R, Frederik Barkhof, et al. (July 2011). "Steps to standardization and validation of hippocampal volumetry as a biomarker in clinical trials and diagnostic criterion for Alzheimer's disease". en. In: *Alzheimers. Dement.* 7.4, 474–485.e4.

Kaiser, Natalie C et al. (2014). "Differences in anxiety among patients with early- versus late-onset Alzheimer's disease". en. In: *J. Neuropsychiatry Clin. Neurosci.* 26.1, pp. 73–80.

Kametani, Fuyuki and Masato Hasegawa (Jan. 2018). "Reconsideration of Amyloid Hypothesis and Tau Hypothesis in Alzheimer's Disease". en. In: *Front. Neurosci.* 12, p. 25.

Kirsch, S J et al. (Jan. 1992). "Prolongation of magnetic resonance T2 time in hippocampus of human patients marks the presence and severity of Alzheimer's disease". en. In: *Neurosci. Lett.* 134.2, pp. 187–190.

Kovacevic, Natasa et al. (2013). "Revisiting PLS Resampling: Comparing Significance Versus Reliability Across Range of Simulations". In: *New Perspectives in Partial Least Squares and Related Methods*. Springer New York, pp. 159–170.

Kühn, Simone, Florian Schubert, and Jürgen Gallinat (Dec. 2010). "Reduced thickness of medial orbitofrontal cortex in smokers". en. In: *Biol. Psychiatry* 68.11, pp. 1061–1065.

Laakso, M P, K Partanen, H Soininen, et al. (1996). "MR T2 relaxometry in Alzheimer's disease and age-associated memory impairment". en. In: *Neurobiol. Aging* 17.4, pp. 535–540.

Langkammer, Christian et al. (Nov. 2010). "Quantitative MR imaging of brain iron: a post-mortem validation study". en. In: *Radiology* 257.2, pp. 455–462.

Leng, Fangda et al. (Mar. 2023). "Neuroinflammation is independently associated with brain network dysfunction in Alzheimer's disease". en. In: *Mol. Psychiatry* 28.3, pp. 1303–1311.

Liew, Tau Ming (Sept. 2020). "Subjective cognitive decline, anxiety symptoms, and the risk of mild cognitive impairment and dementia". en. In: *Alzheimers. Res. Ther.* 12.1, p. 107.

Liu, Jun-Lin et al. (2018). "Iron and Alzheimer's Disease: From Pathogenesis to Therapeutic Implications". In: *Front. Neurosci.* 12.

Livingston, Gill et al. (Dec. 2017). "Dementia prevention, intervention, and care". en. In: *Lancet* 390.10113, pp. 2673–2734.

Luo, Xiao et al. (Sept. 2019). "Application of T1-/T2-Weighted Ratio Mapping to Elucidate Intracortical Demyelination Process in the Alzheimer's Disease Continuum". en. In: *Front. Neurosci.* 13, p. 904.

Luo, Zhuren et al. (Sept. 2013). "The correlation of hippocampal T2-mapping with neuropsychology test in patients with Alzheimer's disease". en. In: *PLoS One* 8.9, e76203.

Lutti, Antoine et al. (2014). "Using high-resolution quantitative mapping of R1 as an index of cortical myelination". In: *Neuroimage* 93, pp. 176–188.

Manjón, José V, Pierrick Coupé, et al. (Jan. 2010). "Adaptive non-local means denoising of MR images with spatially varying noise levels". en. In: *J. Magn. Reson. Imaging* 31.1, pp. 192–203.

Marek, Scott et al. (May 2022). "Publisher Correction: Reproducible brain-wide association studies require thousands of individuals". en. In: *Nature* 605.7911, E11.

Marques, José P, Tobias Kober, et al. (Jan. 2010). "MP2RAGE, a self bias-field corrected sequence for improved segmentation and T1-mapping at high field". en. In: *Neuroimage* 49.2, pp. 1271–1281.

Matthews, Kevin A et al. (2019). "Racial and ethnic estimates of Alzheimer's disease and related dementias in the United States (2015–2060) in adults aged ≥65 years". In: *Alzheimers. Dement.* 15.1, pp. 17–24.

McIntosh, Anthony Randal and Nancy J Lobaugh (2004). "Partial least squares analysis of neuroimaging data: applications and advances". en. In: *Neuroimage* 23 Suppl 1, S250–63.

Melhem, Elias R et al. (Jan. 2002). "Diffusion tensor MR imaging of the brain and white matter tractography". en. In: *AJR Am. J. Roentgenol.* 178.1, pp. 3–16.

Miletić, Steven et al. (Apr. 2022). "Charting human subcortical maturation across the adult lifespan with in vivo 7 T MRI". en. In: *Neuroimage* 249, p. 118872.

Miller, Daniel J et al. (Oct. 2012). "Prolonged myelination in human neocortical evolution". en. In: *Proc. Natl. Acad. Sci. U. S. A.* 109.41, pp. 16480–16485.

Montagne, Axel et al. (Jan. 2015). "Blood-brain barrier breakdown in the aging human hippocampus". en. In: *Neuron* 85.2, pp. 296–302.

Mottershead, J P et al. (Nov. 2003). "High field MRI correlates of myelin content and axonal density in multiple sclerosis–a post-mortem study of the spinal cord". en. In: *J. Neurol.* 250.11, pp. 1293–1301.

Norton, W (1976). "Formation, structure and biochemistry of myelin". In: *Basic neurochemistry.*

Odrobina, Ewa E et al. (Aug. 2005). "MR properties of excised neural tissue following experimentally induced demyelination". en. In: *NMR Biomed.* 18.5, pp. 277–284.

Olmastroni, Elena et al. (May 2022). "Statin use and risk of dementia or Alzheimer's disease: a systematic review and meta-analysis of observational studies". en. In: *Eur. J. Prev. Cardiol.* 29.5, pp. 804–814.

Pakkenberg, Bente et al. (2003). "Aging and the human neocortex". en. In: *Exp. Gerontol.* 38.1-2, pp. 95–99.

Papuć, Ewa and Konrad Rejdak (2020). "The role of myelin damage in Alzheimer's disease pathology". en. In: *Arch. Med. Sci.* 16.2, pp. 345–351.

Paquola, Casey et al. (May 2019). "Microstructural and functional gradients are increasingly dissociated in transmodal cortices". en. In: *PLoS Biol.* 17.5, e3000284.

Parent, Olivier et al. (Mar. 2023). "High spatial overlap but diverging age-related trajectories of cortical magnetic resonance imaging markers aiming to represent intracortical myelin and microstructure". en. In: *Hum. Brain Mapp.*

Patel, Raihaan, Clare E Mackay, et al. (Aug. 2022). "Inter- and intra-individual variation in brain structural-cognition relationships in aging". en. In: *Neuroimage* 257, p. 119254.

Patel, Raihaan, Christopher J Steele, et al. (Feb. 2020). "Investigating microstructural variation in the human hippocampus using non-negative matrix factorization". en. In: *Neuroimage* 207, p. 116348.

Pfrieger, F W and B A Barres (Dec. 1995). "What the fly's glia tell the fly's brain". en. In: *Cell* 83.5, pp. 671–674.

Pink, Anna et al. (2017). "Cortical Thickness and Anxiety Symptoms Among Cognitively Normal Elderly Persons: The Mayo Clinic Study of Aging". en. In: *J. Neuropsychiatry Clin. Neurosci.* 29.1, pp. 60–66.

Pol, L A van de et al. (Apr. 2006). "Hippocampal atrophy on MRI in frontotemporal lobar degeneration and Alzheimer's disease". en. In: *J. Neurol. Neurosurg. Psychiatry* 77.4, pp. 439–442.

Pol, L A van de et al. (2006). "Hippocampal atrophy in Alzheimer disease: Age matters". In: *Neurology* 66.2, pp. 236–238.

Popugaeva, Elena, Ekaterina Pchitskaya, and Ilya Bezprozvanny (Oct. 2018). "Dysregulation of Intracellular Calcium Signaling in Alzheimer's Disease". en. In: *Antioxid. Redox Signal.* 29.12, pp. 1176–1188.

Porter, Verna R et al. (2003). "Frequency and characteristics of anxiety among patients with Alzheimer's disease and related dementias". en. In: *J. Neuropsychiatry Clin. Neurosci.* 15.2, pp. 180–186.

Puglielli, Luigi, Rudolph E Tanzi, and Dora M Kovacs (Apr. 2003). "Alzheimer's disease: the cholesterol connection". en. In: *Nat. Neurosci.* 6.4, pp. 345–351.

Rajan, Kumar B et al. (Dec. 2021). "Population estimate of people with clinical Alzheimer's disease and mild cognitive impairment in the United States (2020-2060)". en. In: *Alzheimers. Dement.* 17.12, pp. 1966–1975.

Rakic, P (July 1988). "Specification of cerebral cortical areas". en. In: *Science* 241.4862, pp. 170–176.

— (2000). "Radial unit hypothesis of neocortical expansion". en. In: *Novartis Found. Symp.* 228, 30–42, discussion 42–52.

Raven, Erika P et al. (2013). "Increased iron levels and decreased tissue integrity in hippocampus of Alzheimer's disease detected in vivo with magnetic resonance imaging". en. In: *J. Alzheimers. Dis.* 37.1, pp. 127–136.

Raz, Naftali, Karen M Rodrigue, and E Mark Haacke (Feb. 2007). "Brain aging and its modifiers: insights from in vivo neuromorphometry and susceptibility weighted imaging". en. In: *Ann. N. Y. Acad. Sci.* 1097, pp. 84–93.

Refolo, L M, B Malester, et al. (Aug. 2000). "Hypercholesterolemia accelerates the Alzheimer's amyloid pathology in a transgenic mouse model". en. In: *Neurobiol. Dis.* 7.4, pp. 321–331.

Refolo, L M, M A Pappolla, et al. (Oct. 2001). "A cholesterol-lowering drug reduces beta-amyloid pathology in a transgenic mouse model of Alzheimer's disease". en. In: *Neurobiol. Dis.* 8.5, pp. 890–899.

Rombouts, Serge A R B et al. (Dec. 2007). "Whole brain analysis of T2* weighted baseline FMRI signal in dementia". en. In: *Hum. Brain Mapp.* 28.12, pp. 1313–1317.

Sasabayashi, Daiki et al. (Mar. 2021). "Reduced Hippocampal Subfield Volume in Schizophrenia and Clinical High-Risk State for Psychosis". en. In: *Front. Psychiatry* 12, p. 642048.

Schmierer, Klaus, Francesco Scaravilli, et al. (Sept. 2004). "Magnetization transfer ratio and myelin in postmortem multiple sclerosis brain". en. In: *Ann. Neurol.* 56.3, pp. 407–415.

Schmierer, Klaus, Claudia A M Wheeler-Kingshott, et al. (Feb. 2008). "Quantitative magnetic resonance of postmortem multiple sclerosis brain before and after fixation". en. In: *Magn. Reson. Med.* 59.2, pp. 268–277.

Schuff, N et al. (Apr. 2009). "MRI of hippocampal volume loss in early Alzheimer's disease in relation to ApoE genotype and biomarkers". en. In: *Brain* 132.Pt 4, pp. 1067–1077.

Sicotte, N L et al. (Apr. 2008). "Regional hippocampal atrophy in multiple sclerosis". en. In: *Brain* 131.Pt 4, pp. 1134–1141.

Singh, Vivek et al. (Nov. 2006). "Spatial patterns of cortical thinning in mild cognitive impairment and Alzheimer's disease". en. In: *Brain* 129.Pt 11, pp. 2885–2893.

Skoog, Ingmar and Deborah Gustafson (Sept. 2006). "Update on hypertension and Alzheimer's disease". en. In: *Neurol. Res.* 28.6, pp. 605–611.

Smith, T B and K S Nayak (2010). "MRI artifacts and correction strategies". In: *Imaging Med.*

Sotiras, Aristeidis, Susan M Resnick, and Christos Davatzikos (Mar. 2015). "Finding imaging patterns of structural covariance via Non-Negative Matrix Factorization". en. In: *Neuroimage* 108, pp. 1–16.

Sparks, D L et al. (Mar. 1994). "Induction of Alzheimer-like beta-amyloid immunoreactivity in the brains of rabbits with dietary cholesterol". en. In: *Exp. Neurol.* 126.1, pp. 88–94.

Spina, Salvatore et al. (Aug. 2021). "Comorbid neuropathological diagnoses in early versus late-onset Alzheimer's disease". en. In: *Brain* 144.7, pp. 2186–2198.

Stüber, Carsten et al. (2014). "Myelin and iron concentration in the human brain: A quantitative study of MRI contrast". In: *Neuroimage* 93, pp. 95–106.

Tan, Chen-Chen et al. (2014). "Efficacy and safety of donepezil, galantamine, rivastigmine, and memantine for the treatment of Alzheimer's disease: a systematic review and meta-analysis". en. In: *J. Alzheimers. Dis.* 41.2, pp. 615–631.

Tappia, P S, K L Troughton, et al. (1995). "Cigarette smoking influences cytokine production and antioxidant defences". In: *Clin. Sci.*

Tardif, Christine L, Barry J Bedell, et al. (Nov. 2012). "Quantitative magnetic resonance imaging of cortical multiple sclerosis pathology". en. In: *Mult. Scler. Int.* 2012, p. 742018.

Tardif, Christine Lucas et al. (May 2016a). "Advanced MRI techniques to improve our understanding of experience-induced neuroplasticity". en. In: *Neuroimage* 131, pp. 55–72.

Tax, Chantal M W et al. (Aug. 2021). "Measuring compartmental T2-orientational dependence in human brain white matter using a tiltable RF coil and diffusion-T2 correlation MRI". en. In: *Neuroimage* 236, p. 117967.

Telegina, Darya V et al. (Nov. 2019). "Mechanisms of Neuronal Death in the Cerebral Cortex during Aging and Development of Alzheimer's Disease-Like Pathology in Rats". en. In: *Int. J. Mol. Sci.* 20.22.

Teri, L et al. (July 1999). "Anxiety of Alzheimer's disease: prevalence, and comorbidity". en. In: *J. Gerontol. A Biol. Sci. Med. Sci.* 54.7, pp. M348–52.

Thelen, K M et al. (July 2006). "Cholesterol synthesis rate in human hippocampus declines with aging". en. In: *Neurosci. Lett.* 403.1-2, pp. 15–19.

Thiessen, Jonathan D et al. (Nov. 2013). "Quantitative MRI and ultrastructural examination of the cuprizone mouse model of demyelination". en. In: *NMR Biomed.* 26.11, pp. 1562–1581.

Tremblay-Mercier, Jennifer et al. (June 2021). "Open science datasets from PREVENT-AD, a longitudinal cohort of pre-symptomatic Alzheimer's disease". en. In: *NeuroImage Clin.* 31.102733, p. 102733.

Trofimova, Olga et al. (June 2021). "Brain tissue properties link cardio-vascular risk factors, mood and cognitive performance in the CoLaus—PsyCoLaus epidemiological cohort". en. In: *Neurobiol. Aging* 102, pp. 50–63.

Tullo, Stephanie et al. (2019). "MR-based age-related effects on the striatum, globus pallidus, and thalamus in healthy individuals across the adult lifespan". In: *Hum. Brain Mapp.* 40.18, pp. 5269–5288.

Tustison, Nicholas J et al. (June 2010). "N4ITK: improved N3 bias correction". en. In: *IEEE Trans. Med. Imaging* 29.6, pp. 1310–1320.

Umeda, Tomohiro et al. (Dec. 2012). "Hypercholesterolemia accelerates intraneuronal accumulation of Aβ oligomers resulting in memory impairment in Alzheimer's disease model mice". en. In: *Life Sci.* 91.23-24, pp. 1169–1176.

Vance, Jean E (Nov. 2012). "Dysregulation of cholesterol balance in the brain: contribution to neurodegenerative diseases". en. In: *Dis. Model. Mech.* 5.6, pp. 746–755.

Visser, P J et al. (Apr. 2002). "Medial temporal lobe atrophy predicts Alzheimer's disease in patients with minor cognitive impairment". en. In: *J. Neurol. Neurosurg. Psychiatry* 72.4, pp. 491–497.

Vymazal, J, R A Brooks, et al. (Jan. 1996). "The relation between brain iron and NMR relaxation times: an in vitro study". en. In: *Magn. Reson. Med.* 35.1, pp. 56–61.

Walker, Lary C and Mathias Jucker (June 2017). "The Exceptional Vulnerability of Humans to Alzheimer's Disease". en. In: *Trends Mol. Med.* 23.6, pp. 534–545.

Walsh, Andrew J et al. (May 2013). "Multiple sclerosis: validation of MR imaging for quantification and detection of iron". en. In: *Radiology* 267.2, pp. 531–542.

Wang, Huali et al. (June 2004). "Prolongation of T(2) relaxation times of hippocampus and amygdala in Alzheimer's disease". en. In: *Neurosci. Lett.* 363.2, pp. 150–153.

Ward, Roberta J et al. (Oct. 2014). "The role of iron in brain ageing and neurodegenerative disorders". en. In: *Lancet Neurol.* 13.10, pp. 1045–1060.

Wearn, Alfie R et al. (Sept. 2020). "T2 heterogeneity: a novel marker of microstructural integrity associated with cognitive decline in people with mild cognitive impairment". en. In: *Alzheimers. Res. Ther.* 12.1, p. 105.

Weijden, Chris W J van der et al. (Feb. 2021). "Myelin quantification with MRI: A systematic review of accuracy and reproducibility". en. In: *Neuroimage* 226, p. 117561.

Wood, John C and Nilesh Ghugre (2008). "Magnetic resonance imaging assessment of excess iron in thalassemia, sickle cell disease and other iron overload diseases". en. In: *Hemoglobin* 32.1-2, pp. 85–96.

Xiong, Raymond M et al. (Nov. 2022). "The pattern of cortical thickness underlying disruptive behaviors in Alzheimer's disease". en. In: *psychoradiology* 2.3, pp. 113–120.

Yanagisawa, Katsuhiko (2005). "Cholesterol and amyloid beta fibrillogenesis". en. In: *Subcell. Biochem.* 38, pp. 179–202.

Zeighami, Yashar et al. (Apr. 2019). "A clinical-anatomical signature of Parkinson's disease identified with partial least squares and magnetic resonance imaging". en. In: *Neuroimage* 190, pp. 69–78.

Zhao, Zhiyong et al. (Dec. 2021). "The effect of beta-amyloid and tau protein aggregations on magnetic susceptibility of anterior hippocampal laminae in Alzheimer's diseases". en. In: *Neuroimage* 244, p. 118584.

Chapter 6

Discussion

6.1 Summary of results

While the implication of the hippocampus in various diseases has been extensively studied, the relationship between multiple dimensions of hippocampal structure, such as its morphometry and microstructure, across the adult lifespan has been less examined. Further, while some individuals age with intact cognitive faculties, others experience accelerated decline; further increasing risk for neurodegenerative diseases. Therefore, a refined understanding of the normative variation of the hippocampus architecture across the adult lifespan may be critical in the identification of biomarkers of normal and pathological aging such as AD. In this context, multi-contrast MRI strategies can be used to refine our understanding of the hippocampus across multiple dimensions of the brain's architecture.

In **Chapter 3**, we investigated how different types of MR image acquisition techniques impact the study of hippocampal subfield volumes in aging. We used multiple datasets to combine images with different contrast and resolution, and individuals from various age-range. Our study compared the age trajectory obtained from three types of scans: T1w images, slab scans, and a new high-resolution isotropic T2w scans developed in our laboratory. We demonstrated that using different types of scans resulted in significantly different volume

estimates within the same participants, with slab volume estimates consistently lower than those from T1w and T2w isotropic scans. We also found that the age-relationships varied depending on the type of scan used, with slab images demonstrating important age trajectory differences compared to the other two scans. When we combined all our datasets and accounted for differences in scan type and age-range, we observed that CA1 showed the highest volume preservation in aging while CA2CA3 was the most impacted. Finally, we compared our findings using MAGeT to two other segmentation techniques and found consistent age-relationships which demonstrated that our results were not biased by our segmentation technique.

In **Chapter 4**, we expanded our research on the hippocampus and its age-related relationships by examining its shape. We employed a data-driven approach, using vertex-wise hippocampal metrics to measure SA and displacement at each vertex to avoid *a priori* definition of the hippocampus. We demonstrated an antero-posterior effect for SA, indicating that the posterior hippocampus is more affected by age than the hippocampal head. Meanwhile, displacement showed a medial-lateral effect, with inward displacement in the medial regions and outward displacement in the lateral regions. Taken together, these findings suggested an increase in curvature with age. Furthermore, we found that these patterns were consistent with lower cognitive scores and being female. Our findings were also replicated in an independent dataset, demonstrating the feasibility of our data-driven approach on other datasets. Overall, our study supported the hypothesis that the differences observed in subfield volumetric estimates between slab images and T1w and T2w scans in **Chapter 3** might be due, in part, to age-related changes in hippocampal shape. Our results also highlighted the potential limitations of using anisotropic scans, such as slab images, for capturing these shape changes compared to isotropic scans.

In **Chapter 5**, we aimed to investigate microstructural changes in individuals ranging from healthy aging to those with frank onset of AD. Specifically, we explored whether hippocam-

pal and cortical morphometric and microstructural changes could serve as an index of AD progression. First, we measured atrophy using structural MRI to derive CT and SA across the cortex and J in the hippocampus. Secondly, we derived joint signatures of covariance across MRI-based measures in the cortex and hippocampus. Our results revealed a consistent pattern of reduced CT in the cortex and elevated T1 and T2* in the hippocampus associated with certain lifestyle risk factors, such as past smoking, high BP and cholesterol, and increased anxiety. Additionally, these patterns were significantly associated with advanced age, being female, and carrying APOE-ϵ4 allele, all of which are linked to AD progression. Our findings suggest that hippocampal qMRI metrics can serve as valuable non-invasive tools for examining AD progression and identifying the specific lifestyle and medical risk factors that need to be addressed by public health initiatives to slow the onset of AD.

6.2 Interpretation of results

Our results demonstrated that anisotropic images led to variable volume estimation and altered age-relationships (Bussy, Plitman, et al. 2021). In light of these findings, we strongly recommend that future efforts should prioritize the use of isotropic high-resolution segmentation methods to minimize the inaccuracies introduced by the use of large and/or anisotropic voxels. Further, this would enable more accurate and reliable measurement of brain structures, particularly those that are smaller in size such as the hippocampus. Indeed, while we recognize that slab sequences have been the gold standard since their introduction in the field for the study hippocampal subfield anatomy (Hasboun et al. 1996), anisotropic images have significant limitations. Previous results indicated that using larger voxels and increasing anisotropy leads to greater deviations in both volume and shape measures, especially in small brain structures (Mulder et al. 2019).

Importantly, while there has been a growing interest in using MRI to measure the subfields of the human hippocampal formation, the advancement of this field has been hindered by

the substantial disagreement among groups. Indeed, controversy regarding the anatomical definition of subfields, the approaches used to group smaller subfields into larger anatomical labels, and the criteria used to establish subfield boundaries in MRI data have led to diverging protocols (Yushkevich, R. S. C. Amaral, et al. 2015). Therefore, there is a need for harmonizing the hippocampal segmentation protocols (Laura E M Wisse, Daugherty, et al. 2017). Hippocampal experts started to work towards a harmonized protocol by creating the Hippocampus Subfields Group. While their work include histology to define the anatomy, to our knowledge, most of their work to translate it into MRI atlases have been mostly performed on T2w $0.4 \times 0.4 \times 2mm$ images (Olsen et al. 2019). In light of our findings, the use of anisotropic images to define the ground truth for the community is disputable. Therefore, we recommend that future efforts should prioritize the use of isotropic high-resolution segmentation methods to minimize the inaccuracies introduced by the use of large and/or anisotropic voxels. Further, this would enable more accurate and reliable measurement of brain structures, particularly those that are smaller in size such as the hippocampus.

Further, despite the existence of several automated segmentation approaches (Patenaude et al. 2011; Van Leemput et al. 2009; Tzourio-Mazoyer et al. 2002; Pipitone et al. 2014; Coupé, Manjón, et al. 2011; Rousseau, Habas, and Studholme 2011; Jordan DeKraker et al. 2018; L.-C. Chen et al. 2018; Manjón, Romero, and Coupe 2022), there is still a lack of consensus on which technique is optimal. This is because each method uses different features, including MR intensity, shape, and coordinates, and has its own set of limitations, such as high computational demands or required coding expertise. Consequently, new users may have difficulty deciding which approach to use. While some papers have compared segmentation methods (Susanne G Mueller, Yushkevich, et al. 2018; Hurtz et al. 2019), most only evaluate a newly developed technique against a few older techniques. Therefore, further research is needed to build upon previous work (Yushkevich, Hongzhi Wang, et al. 2010) by comparing hippocampal subfield segmentation using different image protocols, resolutions, atlases, and segmentation methods, in order to better understand the impact of these factors

and help users to decide on which technique to select.

The anterior-posterior hippocampal curvature and the number of its digitations vary between individuals (S. Cai et al. 2019; DeKraker et al. 2020; Bussy, Patel, et al. 2021). This variability creates major challenges for cross-participant alignment and segmentation. Therefore, to capture such inter-individual variations, we suggest that using data-driven approaches to study the hippocampus would be beneficial. Two approaches were employed in this thesis. First, we used a data-driven vertex-wise linear models which provided reliable findings about the differential impact of aging across the hippocampal shape (Bussy, Patel, et al. 2021). This allowed us to find two dimensions of age-related changes across the antero-posterior and medial-lateral axis without using a priori anatomical definitions. Alternatively, we used NMF technique to take advantage of the complementary information conveyed by different indices (Christine Lucas Tardif et al. 2016b). We found a stable parcellation which described spatial components and subject-wise loadings for each of these components (Patel, Steele, et al. 2020). There are various multivariate techniques that researchers can use to identify patterns of covariation across multiple input modalities in neuroimaging studies (Adali, Levin-Schwartz, and Calhoun 2015; Groves et al. 2011). However, some of these techniques can be more challenging to interpret when negative weights are involved. In contrast, NMF allows for easier interpretation of the output components because of the non-negativity constraint, which allows for additive interpretation of the components (Patel, Steele, et al. 2020; Patel, Mackay, et al. 2022).

In this thesis, we also used a multivariate approach to identify covariance patterns between brain and some specific risk factors. Indeed, susceptibility to accelerated cognitive decline or AD progression is highly dependant on genetic and environmental risk factors. While some cognitive changes associated with aging are expected, individuals may either experience a fast rate of decline or maintain their cognitive abilities relatively well in old age (Tucker-Drob and Salthouse 2011; Wilson et al. 2002; Bhagwat, Viviano, et al. 2018). Further, certain genetic mutations, such as those in the APOE-ϵ4 allele gene, are known to increase an individual's

risk of developing AD. Factors such as diet, physical activity, and social engagement, may also influence an individual's risk of developing the disease (Livingston et al. 2017). Here, we demonstrated that public health strategies targeting smoking, hyper-cholesterol, high BP and anxiety could be the best targets to reduce the incidence of the disease. Interestingly, these factors are all modifiable risk factors which could be reduced with more prevention, highlighting the need for strong tobacco regulation, cholesterol and BP control (through diet, physical activity or medication), and strategies to reduce anxiety (through social activities, therapy or medication).

6.3 Limitations

6.3.1 Segmentation accuracy

Throughout the thesis, various methodological approaches were used to extract biological information from MRI scans. However, it is important to acknowledge that these techniques are not perfect.

In **Chapter 3**, MAGeT brain algorithm was used to extract hippocampal subfield volumes, and while this method has been validated with ground truth manual segmentation (Pipitone et al. 2014), there is still a possibility of biased segmentation due to the use of different datasets, image resolution and contrasts. Indeed, MAGeT was essentially used on T1w scans before (J. L. Winterburn et al. 2013; Pipitone et al. 2014; R. S. C. Amaral et al. 2018; Tullo et al. 2019). To investigate this potential bias with the available data, age-relationships obtained from MAGeT were compared to those from other segmentation techniques (ASHS and HIPS). However, it should be noted that this comparison can not be perfect due to differences in the atlases and segmentation methods used. ASHS used a different hippocampal subfield definition and HIPS used the same atlas but a different segmentation method. Ideally, comparison with a manually segmented output would have been preferred, but was not available. In addition, the spatial resolution of MRI may also impact the QC of seg-

mentation, particularly for small hippocampal subfields. For instance, our T1w scans had relatively low resolution and contrast to accurately identify these subfields. However, our T2w isotropic scans provided greater confidence in the quality control of segmentation due to the good contrast and resolution in all directions of the hippocampus.

In **Chapter 4** of the thesis, we investigated the shape measurements of the hippocampus, specifically SA and displacement, which were derived from MAGeT brain algorithm. While these metrics provide valuable information, it is worth noting that there are other shape metrics available to quantify differences in brain structure, such as thickness (Fischl and A M Dale 2000; Jordan DeKraker et al. 2018) and curvature (Pienaar et al. 2008; Schaer et al. 2012). The selection of metrics depends on the research question, the sensitivity of the metric to structural changes or disease processes and the method employed. In our case, displacement was used to capture age-related curvature, but there may be more specific metrics that can measure this effect precisely. While we made the best use of the available metrics, additional analyses using other metrics may provide a more comprehensive understanding of our findings and their generalizability. Furthermore, although there exist alternative metrics for analyzing hippocampal shape, it remains uncertain to what extent these measurements are contingent upon the accuracy of the initial hippocampal segmentation. Thus, conducting a proper validation with a ground truth manual segmentation may be necessary in ensuring the reliability of the results.

6.3.2 Lack of longitudinal datasets

Longitudinal studies are ideal for studying brain changes in the same individuals repeatedly over time. However longitudinal studies are rare, complicated to carry out and expensive (Farrington 1991). Therefore, cross-sectional data are often used to compare older and younger individuals to infer probable age trajectories (Rindfleisch et al. 2008). However, while informative, cross-sectional datasets only provide a snapshot of a particular point in time, which may not reflect the true trajectory of individual participants. This is particularly

relevant in the context of aging and AD, where mid-life environmental and lifestyle factors can influence brain changes later in life.

Further, by using cross-sectional datasets, we assume a certain common trajectory to all our participants. Individual variability has been demonstrated in anatomy, cognitive impairment and in the brain susceptibility. For example, differences in cortical folding patterns have been linked to differences in brain function and cognition, as well as various neurological and psychiatric disorders (Cash et al. 2012; Nordahl et al. 2007; Drobinin et al. 2020). In aging, individuals may exhibit exceptional cognitive abilities, such as "super-agers" who maintain high cognitive performance even beyond the age of 80 (Gefen et al. 2014). The symptoms of AD can vary widely from one individual to another, with some individuals experiencing rapid cognitive decline and others exhibiting a more gradual decline over several years (G. G. Kovacs 2012; Stanley et al. 2019). However, there is also variation in the distribution and extent of brain pathology. The most common presentation of AD is the progressive amnestic syndrome related to the impairment of the hippocampal formation, the EC and the limbic system (Arriagada, Marzloff, and Hyman 1992; C R Jack Jr, Petersen, Y. C. Xu, et al. 1997) while progressive aphasia individuals have significant atrophy in brain area involved in language and speech (Weintraub, Rubin, and M. M. Mesulam 1990; M.-M. Mesulam and Weintraub 1992). Finally, there is also variability in the genetic and environmental risk factors that contribute to the development of AD. Indeed, certain genetic mutations, such as those in the APOE-ϵ4 allele gene, are known to increase an individual's risk of developing AD, but not all carriers will be susceptible to the disease.

Overall, even though they may be expensive, conducting longitudinal studies that cover several decades of a person's life can have a significant impact on understanding the aging brain and the specific lifestyle and environmental risk factors associated with it.

6.3.3 Reliability and specificity of MRI metrics

To better understand the reliability of structural scan analysis, various factors have been investigated. For example, effects of software version, workstation type and operating system have been shown to impact the reproducibility of analysis (Jovicich et al. 2009).

Reliability studies on structural scan analysis to examine the effect of those factors on multiple outcomes has demonstrated conflicting results. Morphometry metrics extracted from FreeSurfer across manufacturers and field strengths have demonstrated good test-retest reliability (Han et al. 2006; Reuter, Schmansky, et al. 2012). The impact of the sequence protocol impact has been tested on the cortical surface (Fujimoto et al. 2014), subcortical (Okubo et al. 2016; Yan et al. 2020) and on CT and volume estimates (Knussmann et al. 2022). Head tilt also demonstrated a large adverse impact on outcome estimates, specifically for CT (Hedges et al. 2022). Studies have also investigated the effect of scanner upgrades. Measurements demonstrated high reliability, but significant differences in volumes (Medawar et al. 2021) and in CT (Plitman et al. 2021), suggesting that scanner upgrades during a longitudinal study might introduce biases.

In comparison to structural MRI reliability, fewer qMRI test-retest reliability studies have been performed. Intra- and inter-site reliability of the MPM protocol demonstrated a low inter-site bias of less than 5% in the quantitative maps. The higher inter-site CoV was observed for R2* maps which the authors partly attribute to the poor reproducibility and performance of shimming routines (Leutritz et al. 2020). A spine qMRI protocol demonstrated less than 5% inter-site coefficient of variation (Julien Cohen-Adad et al. 2021). For each qMRI metric, multiple mapping methods are used in the literature. For example, many T1 mapping methods are available, with inversion-recovery spin-echo (Hahn 1949), variable flip angle (Gupta 1977), Look-Locker inversion-recovery (Look and Locker 1970), and MP2RAGE (Marques, Kober, et al. 2010). In the same scan session for a given participant, these methods have demonstrated a range of up to 30% variability between sequences (Stikov et al. 2015). However, a recent study using the MP2RAGE sequence showed very

high repeatability across sites and subjects in a multi-center study (Voelker et al. 2021). Importantly, an innovative approach has recently been proposed to enhance the inter-vendor reproducibility of qMRI metrics, which involves using a vendor-neutral sequence (Karakuzu et al. 2022). This approach has demonstrated significant potential for developing more reproducible qMRI protocols and measurements in the future.

Additionally, MRI signal intensity or derived metrics are biologically ambiguous and difficult to interpret at a microscopic level, as they can be associated with several different cellular and molecular mechanisms (Christine Lucas Tardif et al. 2016b). In normal brain aging, there is a general reduction in brain size, which is attributed to shrinkage in both GM and WM volumes. However, rather than a direct loss of neurons, the underlying histological changes responsible for these macroscopic alterations have been shown to be more likely due to a decrease in dendrites and synapses, and a loss of nerve fibers (Huttenlocher 1979; Huttenlocher and Dabholkar 1997). For instance, a study has demonstrated that the number of neurons was constant while cortical thinning was found in the aging brain (Freeman et al. 2008; Pakkenberg et al. 2003). Comparing morphometry measurements sensitivity, CT was found to be a more sensitive metric compared to SA to age-related changed (Rettmann et al. 2006; Lemaitre et al. 2012). Further CT measurements extracted from FreeSurfer were validated against histologic measurements of the cortex (Cardinale et al. 2014). However, research in childhood demonstrated that apparent thinning of human visual cortex was associated with myelination (Natu et al. 2019), demonstrating a need to carefully interpretation of the results.

Different protocols of qMRI can provide various quantitative metrics, with each being differently related to underlying biological mechanisms. The correlation between histological myelin measurements and various qMRI metrics varied in strength, with myelin water fraction (MWF), MTR, quantitative MT, R2*, T1, T2, and quantitative susceptibility mapping (QSM) showing the strongest to weakest correlations, respectively (Weijden et al. 2021). As highlighted in another meta-analysis of MRI biomarkers of myelin, most popular imaging

techniques are indirect measurements of myelin (Mancini et al. 2020). For example, diffusion acquisitions are the most popular techniques to study myelin while it is not directly sensitive to myelin measurement, but rather rely on the interaction between intracellular and extracellular water compartments (Beaulieu 2002). MT is the second most popular technique and estimates myelin by acquiring data with and without saturation of the macromolecular proton pool. However, these methods also includes non-myelin contributions in the final measurement (Duhamel et al. 2019). T2 relaxometry experiments allow for direct observation of water trapped between myelin bilayers and can therefore estimate the MWF (Prasloski et al. 2012). Nonetheless, these techniques require longer acquisitions, and the multi-compartment model used in multi-exponential T2 relaxometry generally assumes slow water exchange between compartments, which may not be accurate (Harkins, Dula, and Does 2012). Finally, T1 is sensitive to the water content and macromolecular composition of brain tissue, as well as the interaction between the two. In healthy human brains, T1 is mainly influenced by variations in myelin content, with a smaller contribution from iron (Stüber et al. 2014). T1 maps of cortical surfaces have been shown to reflect the distribution of myelin (Dick et al. 2012; Christine Lucas Tardif et al. 2016a). Despite their limitations, all these methods have been widely used for estimating myelin content in the brain.

6.4 Future directions

In this thesis, we combined multiple measurements of morphometry and microstructure to better understand the biological mechanisms happening in the aging or AD brain. However, most MRI-derived metrics are indirectly related to a biological process making the interpretation of our findings difficult.

MRI sequence development is a very active field of research and newer techniques are constantly developed. In future studies, it would be interesting to use MRI techniques that could allow the differentiation of the signal between iron and myelin. Indeed, while these

molecules have opposite magnetic susceptibility characteristics, measuring their individual concentrations is challenging due to their co-existence in most brain regions (J. H. Duyn and Schenck 2017). Iron has a higher magnetic susceptibility compared to water, making it paramagnetic ($\chi > 0$), while myelin has a negative magnetic susceptibility, making it diamagnetic ($\chi < 0$). Researchers have attempted to separate their contributions by using QSM and R2* methods (Stüber et al. 2014). However, the magnetic susceptibility anisotropy of myelin and its orientation to the main magnetic field have been shown to influence the T2* and phase maps in both the WM and cortex (Cohen-Adad et al. 2012). Further, changes in cerebral blood flow and cerebral blood volume can also impact T2* and QSM due to local increases in deoxyhemoglobin concentration. To overcome some of these challenges, a recent approach called χ separation has been proposed (Shin et al. 2021). This technique uses biophysical model to describes the individual contribution of paramagnetic (e.g., iron) and diamagnetic (e.g., myelin) susceptibility sources to the frequency shift and transverse relaxation of MRI signals. When compared to histological features of iron and myelin, the proposed approach showed high accuracy in detecting abnormalities in healthy volunteers and multiple sclerosis patients (Shin et al. 2021). This highlights its potential for future studies in understanding the underlying pathology of multiple disorders.

Another approach for future studies would be to combine qMRI with other markers of AD pathology. For example, a very interesting avenue of research would be to combine qMRI and PET imaging on the same individuals to see if qMRI markers could be sensitive to Aβ and ptau. Indeed, due to the known accumulation of iron around the Aβ plaques (Lovell et al. 1998; Bayer et al. 2003; Maynard et al. 2002), we would expect that T2*, QSM or χ separation to be sensitive techniques. On the other hand, we expect that ptau accumulation which leads to microtubule disorganisation and eventually neuronal death, might be capture by PD or MD due to an increase water content.

Further, longitudinal dataset would be critical for helping understand the temporal evolution of the disease. Indeed, as discussed in 5.6, there are evidence of myelin having a central

role in the AD progression (Bartzokis, Mintz, et al. 1994; Bartzokis, Beckson, et al. 2001; George Bartzokis, P. H. Lu, and Jim Mintz 2007). Therefore, following healthy participants for decades could help us understand what is the first abnormality in the brain. Indeed, while the famous study by Bateman (Bateman et al. 2012) used CSF, glucose metabolism, PET amyloid and tau and brain atrophy to characterise the progression of the disease, very little attention has been given to the WM. Further, the role of WMH in the disease should be investigated as well since it has been shown that WMH volume was elevated among individuals with autosomal dominant AD up to 20 years before the expected onset of symptoms (S. Lee et al. 2016). This demonstrates that WMH could be a crucial feature to investigate in AD. Specifically, a recent study from our laboratory demonstrated that T2* values of WMH regions were sensitive to the disease progression demonstrating the potential of combining qMRI and WM analyses (Parent et al. 2023).

6.5 Conclusion

Overall, this thesis aimed at better understanding how the hippocampal structure relate to aging and AD. More specifically, we employed a large range of techniques, from **Chapter 3** with atlas-based segmentation to derive subfield-wise volumes, to **Chapter 4** with surface-based analyses to analyse the hippocampal shape, to **Chapter 5** with qMRI to investigate the hippocampal microstructure. Additionally, we used a variety of statistical analyses to either characterise the non-linear volumetric relationship with age in **Chapter 3**, relate hippocampal shape to demographics and risk factor of interest in **Chapter 4**, to data-driven parcellation and multivariate analyses to relate multiple dimension of brain characteristics with known lifestyle and medical risk factors for AD in **Chapter 5**.

This thesis informed us that MRI sequence choice does impact the age-trajectories of the hippocampal subfield volumes and that isotropic scans should be preferred. The hippocampal shape demonstrated that the hippocampal curvature might increase in aging and that

the body and tail of the structure are the most impacted by aging. Lastly, our results demonstrated that cortical morphometry and hippocampal microstructure were sensitive to AD progression and that this relationship was associated with lifestyle risk factors such as past smoking consumption, anxiety, high BP and cholesterol.

References

Ackley, Sarah F et al. (Feb. 2021). "Effect of reductions in amyloid levels on cognitive change in randomized trials: instrumental variable meta-analysis". en. In: *BMJ* 372, n156.

Adali, Tülay, Yuri Levin-Schwartz, and Vince D Calhoun (Sept. 2015). "Multi-modal data fusion using source separation: Two effective models based on ICA and IVA and their properties". en. In: *Proc. IEEE Inst. Electr. Electron. Eng.* 103.9, pp. 1478–1493.

Adler, Daniel H, John Pluta, et al. (Jan. 2014). "Histology-derived volumetric annotation of the human hippocampal subfields in postmortem MRI". en. In: *Neuroimage* 84, pp. 505–523.

Adler, Daniel H, Laura E M Wisse, et al. (Apr. 2018). "Characterizing the human hippocampus in aging and Alzheimer's disease using a computational atlas derived from ex vivo MRI and histology". en. In: *Proc. Natl. Acad. Sci. U. S. A.* 115.16, pp. 4252–4257.

Agahi, Neda, Benjamin A Shaw, and Stefan Fors (Aug. 2014). "Social and economic conditions in childhood and the progression of functional health problems from midlife into old age". en. In: *J. Epidemiol. Community Health* 68.8, pp. 734–740.

Akaike, Hirotugu (1974). "A New Look at the Statistical Model Identification". In: *Springer Ser. Statist.*, pp. 215–222.

Akiyoshi, Ryohei et al. (Oct. 2018). "Microglia Enhance Synapse Activity to Promote Local Network Synchronization". en. In: *eNeuro* 5.5.

Alexander-Bloch, Aaron et al. (2016). "Subtle in-scanner motion biases automated measurement of brain anatomy from in vivo MRI". In: *Hum. Brain Mapp.* 37.7, pp. 2385–2397.

Almeida, Osvaldo P et al. (Jan. 2008). "Smoking is associated with reduced cortical regional gray matter density in brain regions associated with incipient Alzheimer disease". en. In: *Am. J. Geriatr. Psychiatry* 16.1, pp. 92–98.

Amaral, D G (Apr. 1993). "Emerging principles of intrinsic hippocampal organization". en. In: *Curr. Opin. Neurobiol.* 3.2, pp. 225–229.

Amaral, D G and M P Witter (1989). "The three-dimensional organization of the hippocampal formation: a review of anatomical data". en. In: *Neuroscience* 31.3, pp. 571–591.

Amaral, Robert S C et al. (Apr. 2018). "Manual segmentation of the fornix, fimbria, and alveus on high-resolution 3T MRI: Application via fully-automated mapping of the human memory circuit white and grey matter in healthy and pathological aging". en. In: *Neuroimage* 170, pp. 132–150.

Amunts, Katrin, Claude Lepage, et al. (June 2013). "BigBrain: an ultrahigh-resolution 3D human brain model". en. In: *Science* 340.6139, pp. 1472–1475.

Amunts, Katrin and Karl Zilles (Dec. 2015). "Architectonic Mapping of the Human Brain beyond Brodmann". en. In: *Neuron* 88.6, pp. 1086–1107.

Anblagan, Devasuda et al. (Feb. 2018). "Coupled changes in hippocampal structure and cognitive ability in later life". en. In: *Brain Behav.* 8.2, e00838.

Anderson, Peter (June 2002). "Assessment and development of executive function (EF) during childhood". en. In: *Child Neuropsychol.* 8.2, pp. 71–82.

Anderson, V A et al. (2001). "Development of executive functions through late childhood and adolescence in an Australian sample". en. In: *Dev. Neuropsychol.* 20.1, pp. 385–406.

Apfel, Brigitte A et al. (Mar. 2011). "Hippocampal volume differences in Gulf War veterans with current versus lifetime posttraumatic stress disorder symptoms". en. In: *Biol. Psychiatry* 69.6, pp. 541–548.

Apostolova, Liana G et al. (Jan. 2008). "3D mapping of language networks in clinical and pre-clinical Alzheimer's disease". en. In: *Brain Lang.* 104.1, pp. 33–41.

Arain, Mariam et al. (Apr. 2013). "Maturation of the adolescent brain". en. In: *Neuropsychiatr. Dis. Treat.* 9, pp. 449–461.

Arata, L K et al. (Nov. 1995). "Three-dimensional anatomical model-based segmentation of MR brain images through Principal Axes Registration". en. In: *IEEE Trans. Biomed. Eng.* 42.11, pp. 1069–1078.

Arbel, Tal et al. (2004). "Automatic non-linear MRI-ultrasound registration for the correction of intra-operative brain deformations". en. In: *Comput. Aided Surg.* 9.4, pp. 123–136.

Arnone, D et al. (Dec. 2013). "State-dependent changes in hippocampal grey matter in depression". en. In: *Mol. Psychiatry* 18.12, pp. 1265–1272.

Arriagada, Paulina V, K Marzloff, and Bradley T Hyman (Sept. 1992). "Distribution of Alzheimer-type pathologic changes in nondemented elderly individuals matches the pattern in Alzheimer's disease". en. In: *Neurology* 42.9, pp. 1681–1681.

Ashburner, J et al. (1998). "Identifying global anatomical differences: deformation-based morphometry". en. In: *Hum. Brain Mapp.* 6.5-6, pp. 348–357.

Ashburner, John and Karl J Friston (June 2000). "Voxel-Based Morphometry—The Methods". In: *Neuroimage* 11.6, pp. 805–821.

Avants, B B et al. (Feb. 2008). "Symmetric diffeomorphic image registration with cross-correlation: evaluating automated labeling of elderly and neurodegenerative brain". en. In: *Med. Image Anal.* 12.1, pp. 26–41.

Avants, Brian B et al. (Feb. 2011). "A reproducible evaluation of ANTs similarity metric performance in brain image registration". en. In: *Neuroimage* 54.3, pp. 2033–2044.

Ayton, Scott et al. (Nov. 2020). "Brain iron is associated with accelerated cognitive decline in people with Alzheimer pathology". en. In: *Mol. Psychiatry* 25.11, pp. 2932–2941.

Bagnato, Francesca et al. (Mar. 2018). "Untangling the R2* contrast in multiple sclerosis: A combined MRI-histology study at 7.0 Tesla". en. In: *PLoS One* 13.3, e0193839.

Baillarger, Jules Gabriel François (1840). *Recherches sur la structure de la couche corticale des circonvolutions du cerveau*. chez J.-B. Baillière.

Barnes, Josephine et al. (Nov. 2009). "A meta-analysis of hippocampal atrophy rates in Alzheimer's disease". en. In: *Neurobiol. Aging* 30.11, pp. 1711–1723.

Bartzokis, G, M Beckson, et al. (May 2001). "Age-related changes in frontal and temporal lobe volumes in men: a magnetic resonance imaging study". en. In: *Arch. Gen. Psychiatry* 58.5, pp. 461–465.

Bartzokis, G, J Mintz, et al. (June 1994). "In vivo MR evaluation of age-related increases in brain iron". en. In: *AJNR Am. J. Neuroradiol.* 15.6, pp. 1129–1138.

Bartzokis, G, D Sultzer, et al. (Apr. 1994). "In vivo evaluation of brain iron in Alzheimer's disease and normal subjects using MRI". en. In: *Biol. Psychiatry* 35.7, pp. 480–487.

Bartzokis, George (Jan. 2004). "Age-related myelin breakdown: a developmental model of cognitive decline and Alzheimer's disease". en. In: *Neurobiol. Aging* 25.1, 5–18, author reply 49–62.

— (2011). "Alzheimer's disease as homeostatic responses to age-related myelin breakdown". In: *Neurobiol. Aging* 32.8, pp. 1341–1371.

Bartzokis, George, Po H Lu, and Jim Mintz (Apr. 2007). "Human brain myelination and amyloid beta deposition in Alzheimer's disease". en. In: *Alzheimers. Dement.* 3.2, pp. 122–125.

Bartzokis, George, David Sultzer, et al. (Aug. 2004). "Heterogeneous age-related breakdown of white matter structural integrity: implications for cortical "disconnection" in aging and Alzheimer's disease". en. In: *Neurobiol. Aging* 25.7, pp. 843–851.

Basaiawmoit, Rajiv Vaid and Suresh I S Rattan (2010). "Cellular stress and protein misfolding during aging". en. In: *Methods Mol. Biol.* 648, pp. 107–117.

Bateman, Randall J et al. (Aug. 2012). "Clinical and biomarker changes in dominantly inherited Alzheimer's disease". en. In: *N. Engl. J. Med.* 367.9, pp. 795–804.

Bayer, Thomas A et al. (2003). "Dietary Cu stabilizes brain superoxide dismutase 1 activity and reduces amyloid Aβ production in APP23 transgenic mice". In: *Proceedings of the National Academy of Sciences* 100.24, pp. 14187–14192.

Beam, Christopher R et al. (2018). "Differences Between Women and Men in Incidence Rates of Dementia and Alzheimer's Disease". In: *J. Alzheimers. Dis.* 64.4, pp. 1077–1083.

Bear, M F and W C Abraham (1996). "Long-term depression in hippocampus". en. In: *Annu. Rev. Neurosci.* 19, pp. 437–462.

Beaulieu, Christian (2002). "The basis of anisotropic water diffusion in the nervous system - a technical review". en. In: *NMR Biomed.* 15.7-8, pp. 435–455.

Bedard, Anne-Claude et al. (2002). "The development of selective inhibitory control across the life span". en. In: *Dev. Neuropsychol.* 21.1, pp. 93–111.

Bedford, Saashi A et al. (Mar. 2020). "Large-scale analyses of the relationship between sex, age and intelligence quotient heterogeneity and cortical morphometry in autism spectrum disorder". en. In: *Mol. Psychiatry* 25.3, pp. 614–628.

Belaroussi, Boubakeur et al. (Apr. 2006). "Intensity non-uniformity correction in MRI: existing methods and their validation". en. In: *Med. Image Anal.* 10.2, pp. 234–246.

Bellon, E M et al. (Dec. 1986). "MR artifacts: a review". en. In: *AJR Am. J. Roentgenol.* 147.6, pp. 1271–1281.

Bender, Andrew R et al. (Feb. 2018). "Optimization and validation of automated hippocampal subfield segmentation across the lifespan". en. In: *Hum. Brain Mapp.* 39.2, pp. 916–931.

Bender, B and U Klose (Nov. 2010). "The in vivo influence of white matter fiber orientation towards B(0) on T2* in the human brain". en. In: *NMR Biomed.* 23.9, pp. 1071–1076.

Benjamini, Y et al. (Nov. 2001). "Controlling the false discovery rate in behavior genetics research". en. In: *Behav. Brain Res.* 125.1-2, pp. 279–284.

Benjamini, Yoav and Yosef Hochberg (Jan. 1995). "Controlling the False Discovery Rate: A Practical and Powerful Approach to Multiple Testing". In: *J. R. Stat. Soc. Series B Stat. Methodol.* 57.1, pp. 289–300.

Bennett, D A et al. (June 2006). "Neuropathology of older persons without cognitive impairment from two community-based studies". en. In: *Neurology* 66.12, pp. 1837–1844.

Bensaid, A M et al. (May 1996). "Validity-guided (re)clustering with applications to image segmentation". In: *IEEE Trans. Fuzzy Syst.* 4.2, pp. 112–123.

Benussi, Alberto et al. (Apr. 2019). "Clinical and biomarker changes in presymptomatic genetic frontotemporal dementia". en. In: *Neurobiol. Aging* 76, pp. 133–140.

Bernhard, D et al. (2007). "Cigarette smoke – an aging accelerator?" In: *Exp. Gerontol.* 42.3, pp. 160–165.

Bertram, Lars et al. (Jan. 2007). "Systematic meta-analyses of Alzheimer disease genetic association studies: the AlzGene database". en. In: *Nat. Genet.* 39.1, pp. 17–23.

Best, John R, Patricia H Miller, and Lara L Jones (Sept. 2009). "Executive Functions after Age 5: Changes and Correlates". en. In: *Dev. Rev.* 29.3, pp. 180–200.

Bethlehem, R A I et al. (Apr. 2022). "Brain charts for the human lifespan". en. In: *Nature* 604.7906, pp. 525–533.

Bhagwat, Nikhil, Jon Pipitone, et al. (July 2016). "Manual-Protocol Inspired Technique for Improving Automated MR Image Segmentation during Label Fusion". en. In: *Front. Neurosci.* 10, p. 325.

Bhagwat, Nikhil, Joseph D Viviano, et al. (Sept. 2018). "Modeling and prediction of clinical symptom trajectories in Alzheimer's disease using longitudinal data". en. In: *PLoS Comput. Biol.* 14.9, e1006376.

Birkl, Christoph et al. (Oct. 2020). "The influence of iron oxidation state on quantitative MRI parameters in post mortem human brain". en. In: *Neuroimage* 220, p. 117080.

Bishop, Nicholas A, Tao Lu, and Bruce A Yankner (Mar. 2010). "Neural mechanisms of ageing and cognitive decline". en. In: *Nature* 464.7288, pp. 529–535.

Blanchard, Joel W et al. (Nov. 2022). "APOE4 impairs myelination via cholesterol dysregulation in oligodendrocytes". en. In: *Nature* 611.7937, pp. 769–779.

Bloch, F (Oct. 1946). "Nuclear Induction". In: *Phys. Rev.* 70.7-8, pp. 460–474.

Bloomer, R J (2007). "Decreased blood antioxidant capacity and increased lipid peroxidation in young cigarette smokers compared to nonsmokers: impact of dietary intake". In: *Nutr. J.*

Bobinski, M et al. (2000). "The histological validation of post mortem magnetic resonance imaging-determined hippocampal volume in Alzheimer's disease". en. In: *Neuroscience* 95.3, pp. 721–725.

Boldrini, Maura et al. (Apr. 2018). "Human Hippocampal Neurogenesis Persists throughout Aging". en. In: *Cell Stem Cell* 22.4, 589–599.e5.

Borrell, Vıctor and Magdalena Götz (Aug. 2014). "Role of radial glial cells in cerebral cortex folding". en. In: *Curr. Opin. Neurobiol.* 27, pp. 39–46.

Boudreau, Mathieu et al. (Dec. 2017). "B1 mapping for bias-correction in quantitative T 1 imaging of the brain at 3T using standard pulse sequences". en. In: *J. Magn. Reson. Imaging* 46.6, pp. 1673–1682.

Bowley, Michael P et al. (Aug. 2010). "Age changes in myelinated nerve fibers of the cingulate bundle and corpus callosum in the rhesus monkey". en. In: *J. Comp. Neurol.* 518.15, pp. 3046–3064.

Braak, H and E Braak (1991a). "Alzheimer's disease affects limbic nuclei of the thalamus". en. In: *Acta Neuropathol.* 81.3, pp. 261–268.

— (1991b). "Neuropathological stageing of Alzheimer-related changes". In: *Acta Neuropathol.* 82.4, pp. 239–259.

— (Aug. 1996). "Development of Alzheimer-related neurofibrillary changes in the neocortex inversely recapitulates cortical myelogenesis". en. In: *Acta Neuropathol.* 92.2, pp. 197–201.

Braak, Heiko, Irina Alafuzoff, et al. (Oct. 2006). "Staging of Alzheimer disease-associated neurofibrillary pathology using paraffin sections and immunocytochemistry". en. In: *Acta Neuropathol.* 112.4, pp. 389–404.

Braak, Heiko and Kelly Del Tredici (Oct. 2015). "The preclinical phase of the pathological process underlying sporadic Alzheimer's disease". en. In: *Brain* 138.Pt 10, pp. 2814–2833.

Bremner, J D et al. (Jan. 2000). "Hippocampal volume reduction in major depression". en. In: *Am. J. Psychiatry* 157.1, pp. 115–118.

Bremner, J Douglas et al. (May 2003). "MRI and PET study of deficits in hippocampal structure and function in women with childhood sexual abuse and posttraumatic stress disorder". en. In: *Am. J. Psychiatry* 160.5, pp. 924–932.

Brodmann (1909). "Über Rindenmessungen. Centralbl. f. Nervenheilkunde u. Psychiatrie, Bd. 19. 1909 Vergleichende Lokalisationslehre der Grosshirnrinde. Leipzig. 1909 . . . " In: *Kaes. Über Rindenmessungen. Neurolog. Centralbl.*

Brody, Arthur L et al. (Jan. 2004). "Differences between smokers and nonsmokers in regional gray matter volumes and densities". en. In: *Biol. Psychiatry* 55.1, pp. 77–84.

Brown, Robert W et al. (June 2014). *Magnetic Resonance Imaging: Physical Principles and Sequence Design.* en. John Wiley & Sons.

Buades, A, B Coll, and J M Morel (Jan. 2005). "A Review of Image Denoising Algorithms, with a New One". In: *Multiscale Model. Simul.* 4.2, pp. 490–530.

Buckner, Randy L, Jessica R Andrews-Hanna, and Daniel L Schacter (Mar. 2008). "The brain's default network: anatomy, function, and relevance to disease". en. In: *Ann. N. Y. Acad. Sci.* 1124, pp. 1–38.

Buford, Thomas W (Mar. 2016). "Hypertension and aging". en. In: *Ageing Res. Rev.* 26, pp. 96–111.

Burnham, Kenneth P and David R Anderson (Nov. 2004). "Multimodel Inference: Understanding AIC and BIC in Model Selection". In: *Sociol. Methods Res.* 33.2, pp. 261–304.

Bussy, Aurélie, Jake P Levy, et al. (Mar. 2023). "Cerebellar and subcortical atrophy contribute to psychiatric symptoms in frontotemporal dementia". en. In: *Hum. Brain Mapp.* 44.7, pp. 2684–2700.

Bussy, Aurélie, Raihaan Patel, et al. (Oct. 2021). "Hippocampal shape across the healthy lifespan and its relationship with cognition". en. In: *Neurobiol. Aging* 106, pp. 153–168.

Bussy, Aurélie, Eric Plitman, et al. (June 2021). "Hippocampal subfield volumes across the healthy lifespan and the effects of MR sequence on estimates". en. In: *Neuroimage* 233, p. 117931.

Bussy, Aurélie, B Joy Snider, et al. (Mar. 2019). "Effect of apolipoprotein E4 on clinical, neuroimaging, and biomarker measures in noncarrier participants in the Dominantly Inherited Alzheimer Network". en. In: *Neurobiol. Aging* 75, pp. 42–50.

Butt, Arthur M, Irene Chacon De La Rocha, and Andrea Rivera (2019). "Oligodendroglial Cells in Alzheimer's Disease". en. In: *Adv. Exp. Med. Biol.* 1175, pp. 325–333.

Butters, N et al. (Oct. 1987). "Episodic and semantic memory: a comparison of amnesic and demented patients". en. In: *J. Clin. Exp. Neuropsychol.* 9.5, pp. 479–497.

Cai, Shuxiu et al. (Mar. 2019). "Is hippocampus getting bumpier with age: a quantitative analysis of fine-scale dentational feature under the hippocampus on 552 healthy subjects". en. In: *Medical Imaging 2019: Image Processing*. Vol. 10949. SPIE, pp. 807–812.

Cai, Zhiyou and Ming Xiao (2016). "Oligodendrocytes and Alzheimer's disease". en. In: *Int. J. Neurosci.* 126.2, pp. 97–104.

Callaghan, Martina F et al. (Aug. 2014). "Widespread age-related differences in the human brain microstructure revealed by quantitative magnetic resonance imaging". en. In: *Neurobiol. Aging* 35.8, pp. 1862–1872.

Campbell, Alfred W (1904). "Histological Studies on the Localisation of Cerebral Function". In: *J. Ment. Sci.* 50.211, pp. 651–662.

Campbell, Stephanie and Glenda MacQueen (2004). "The role of the hippocampus in the pathophysiology of major depression". In: *J. Psychiatry Neurosci.* 6.

Campeau, N G et al. (Oct. 1997). "Hippocampal transverse relaxation times in patients with Alzheimer disease". en. In: *Radiology* 205.1, pp. 197–201.

Caputo, Fabio et al. (June 2012). "Alcohol use disorders in the elderly: a brief overview from epidemiology to treatment options". en. In: *Exp. Gerontol.* 47.6, pp. 411–416.

Cardenas, V A et al. (May 2001). "Reliability of tissue volumes and their spatial distribution for segmented magnetic resonance images". en. In: *Psychiatry Res.* 106.3, pp. 193–205.

Cardinale, Francesco et al. (Oct. 2014). "Validation of FreeSurfer-estimated brain cortical thickness: comparison with histologic measurements". en. In: *Neuroinformatics* 12.4, pp. 535–542.

Carmeli, Cristian et al. (Aug. 2013). "Demyelination in mild cognitive impairment suggests progression path to Alzheimer's disease". en. In: *PLoS One* 8.8, e72759.

Cash, David M et al. (2012). "Cortical folding analysis on patients with Alzheimer's disease and mild cognitive impairment". en. In: *Med. Image Comput. Comput. Assist. Interv.* 15.Pt 3, pp. 289–296.

Castro, F Javier Sanchez et al. (Nov. 2006). "A cross validation study of deep brain stimulation targeting: from experts to atlas-based, segmentation-based and automatic registration algorithms". en. In: *IEEE Trans. Med. Imaging* 25.11, pp. 1440–1450.

Cataldo, Janine K, Judith J Prochaska, and Stanton A Glantz (2010). "Cigarette smoking is a risk factor for Alzheimer's Disease: an analysis controlling for tobacco industry affiliation". en. In: *J. Alzheimers. Dis.* 19.2, pp. 465–480.

Chakravarty, M Mallar, M Mallar Chakravarty, et al. (2009). "Comparison of piece-wise linear, linear, and nonlinear atlas-to-patient warping techniques: Analysis of the labeling of subcortical nuclei for functional neurosurgical applications". In: *Hum. Brain Mapp.* 30.11, pp. 3574–3595.

Chakravarty, M Mallar, Abbas F Sadikot, et al. (Dec. 2008). "Towards a validation of atlas warping techniques". en. In: *Med. Image Anal.* 12.6, pp. 713–726.

Chakravarty, M Mallar, Patrick Steadman, et al. (Oct. 2013). "Performing label-fusion-based segmentation using multiple automatically generated templates". en. In: *Hum. Brain Mapp.* 34.10, pp. 2635–2654.

Chapleau, Marianne et al. (June 2020). "Deformation-based shape analysis of the hippocampus in the semantic variant of primary progressive aphasia and Alzheimer's disease". en. In: *Neuroimage Clin* 27, p. 102305.

Chavhan, Govind B et al. (Sept. 2009). "Principles, techniques, and applications of T2*-based MR imaging and its special applications". en. In: *Radiographics* 29.5, pp. 1433–1449.

Chen, Guo-Fang et al. (Sept. 2017). "Amyloid beta: structure, biology and structure-based therapeutic development". en. In: *Acta Pharmacol. Sin.* 38.9, pp. 1205–1235.

Chen, Liang-Chieh et al. (Apr. 2018). "DeepLab: Semantic Image Segmentation with Deep Convolutional Nets, Atrous Convolution, and Fully Connected CRFs". en. In: *IEEE Trans. Pattern Anal. Mach. Intell.* 40.4, pp. 834–848.

Chen, Ruoling (Nov. 2012). "Association of environmental tobacco smoke with dementia and Alzheimer's disease among never smokers". en. In: *Alzheimers. Dement.* 8.6, pp. 590–595.

Cheng, Haoyue et al. (July 2022). "Global trends in total fertility rate and its relation to national wealth, life expectancy and female education". en. In: *BMC Public Health* 22.1, p. 1346.

Cherbuin, Nicolas et al. (Oct. 2007). "Neuroimaging and APOE genotype: a systematic qualitative review". en. In: *Dement. Geriatr. Cogn. Disord.* 24.5, pp. 348–362.

Cherubini, Andrea et al. (Oct. 2009). "Aging of subcortical nuclei: microstructural, mineralization and atrophy modifications measured in vivo using MRI". en. In: *Neuroimage* 48.1, pp. 29–36.

Chételat, G et al. (Jan. 2008). "Three-dimensional surface mapping of hippocampal atrophy progression from MCI to AD and over normal aging as assessed using voxel-based morphometry". en. In: *Neuropsychologia* 46.6, pp. 1721–1731.

Cho, Hanna et al. (Aug. 2016). "In vivo cortical spreading pattern of tau and amyloid in the Alzheimer disease spectrum". en. In: *Ann. Neurol.* 80.2, pp. 247–258.

Chung, M K et al. (Sept. 2001). "A unified statistical approach to deformation-based morphometry". en. In: *Neuroimage* 14.3, pp. 595–606.

Chung, Moo K, Nagesh Adluru, and Houri K Vorperian (2020). "Heat Kernel Smoothing on Manifolds and Its Application to Hyoid Bone Growth Modeling". In: *Statistical Modeling in Biomedical Research: Contemporary Topics and Voices in the Field*. Ed. by Yichuan Zhao and Ding-Geng (din) Chen. Cham: Springer International Publishing, pp. 235–261.

Cicchetti, Domenic V (1994). "Guidelines, criteria, and rules of thumb for evaluating normed and standardized assessment instruments in psychology". In: *Psychol. Assess.* 6.4, p. 284.

Cipriani, Sara et al. (July 2018). "Hippocampal Radial Glial Subtypes and Their Neurogenic Potential in Human Fetuses and Healthy and Alzheimer's Disease Adults". en. In: *Cereb. Cortex* 28.7, pp. 2458–2478.

Clavaguera, Florence et al. (July 2009). "Transmission and spreading of tauopathy in transgenic mouse brain". en. In: *Nat. Cell Biol.* 11.7, pp. 909–913.

Cohen-Adad, J et al. (Apr. 2012). "T* mapping and B orientation-dependence at 7 T reveal cyto- and myeloarchitecture organization of the human cortex". en. In: *Neuroimage* 60.2, pp. 1006–1014.

Cohen-Adad, Julien et al. (Aug. 2021). "Open-access quantitative MRI data of the spinal cord and reproducibility across participants, sites and manufacturers". en. In: *Sci Data* 8.1, p. 219.

Collier, Dawn C et al. (2003). "Assessment of consistency in contouring of normal-tissue anatomic structures". en. In: *J. Appl. Clin. Med. Phys.* 4.1, pp. 17–24.

Collins, D L et al. (Mar. 1994). "Automatic 3D intersubject registration of MR volumetric data in standardized Talairach space". en. In: *J. Comput. Assist. Tomogr.* 18.2, pp. 192–205.

Connor, J R, K L Boeshore, et al. (Mar. 1994). "Isoforms of ferritin have a specific cellular distribution in the brain". en. In: *J. Neurosci. Res.* 37.4, pp. 461–465.

Connor, J R, B S Snyder, et al. (Feb. 1992). "Regional distribution of iron and iron-regulatory proteins in the brain in aging and Alzheimer's disease". en. In: *J. Neurosci. Res.* 31.2, pp. 327–335.

Connor, James R and Sharon L Menzies (1996). "Relationship of iron to oligondendrocytes and myelination". In: *Glia* 17.2, pp. 83–93.

Convit, A et al. (1997). "Specific Hippocampal Volume Reductions in Individuals at Risk for Alzheimer's Disease". In: *Neurobiol. Aging* 18.2, pp. 131–138.

Corder, E H et al. (Aug. 1993). "Gene dose of apolipoprotein E type 4 allele and the risk of Alzheimer's disease in late onset families". en. In: *Science* 261.5123, pp. 921–923.

Coupé, Pierrick, Gwenaelle Catheline, et al. (Nov. 2017). "Towards a unified analysis of brain maturation and aging across the entire lifespan: A MRI analysis". en. In: *Hum. Brain Mapp.* 38.11, pp. 5501–5518.

Coupé, Pierrick, José V Manjón, et al. (Jan. 2011). "Patch-based segmentation using expert priors: application to hippocampus and ventricle segmentation". en. In: *Neuroimage* 54.2, pp. 940–954.

Cox, Simon R et al. (Dec. 2016). "Ageing and brain white matter structure in 3,513 UK Biobank participants". en. In: *Nat. Commun.* 7, p. 13629.

Cragg, Lucy and Kate Nation (2008). "Go or no-go? Developmental improvements in the efficiency of response inhibition in mid-childhood". In: *Dev. Sci.* 11.6, pp. 819–827.

Csernansky, J G et al. (Sept. 1998). "Hippocampal morphometry in schizophrenia by high dimensional brain mapping". en. In: *Proc. Natl. Acad. Sci. U. S. A.* 95.19, pp. 11406–11411.

Dadar, Mahsa et al. (July 2018). "A comparison of publicly available linear MRI stereotaxic registration techniques". en. In: *Neuroimage* 174, pp. 191–200.

Dam, A M (Dec. 1980). "Epilepsy and neuron loss in the hippocampus". en. In: *Epilepsia* 21.6, pp. 617–629.

Damadian, Raymond (1971). "Tumor Detection by Nuclear Magnetic Resonance". In: *Science* 171.3976, pp. 1151–1153.

Das, Sandhitsu R et al. (Apr. 2012). "Measuring longitudinal change in the hippocampal formation from in vivo high-resolution T2-weighted MRI". en. In: *Neuroimage* 60.2, pp. 1266–1279.

Daskalopoulou, C et al. (Sept. 2017). "Physical activity and healthy ageing: A systematic review and meta-analysis of longitudinal cohort studies". en. In: *Ageing Res. Rev.* 38, pp. 6–17.

Daugherty, Ana M et al. (Feb. 2016). "Age differences in hippocampal subfield volumes from childhood to late adulthood". en. In: *Hippocampus* 26.2, pp. 220–228.

DeKraker, J et al. (Feb. 2020). "Hippocampal subfields revealed through unfolding and unsupervised clustering of laminar and morphological features in 3D BigBrain". en. In: *Neuroimage* 206, p. 116328.

DeKraker, Jordan et al. (Feb. 2018). "Unfolding the hippocampus: An intrinsic coordinate system for subfield segmentations and quantitative mapping". en. In: *Neuroimage* 167, pp. 408–418.

Del Bigio, Marc R (Jan. 2010). "Ependymal cells: biology and pathology". en. In: *Acta Neuropathol.* 119.1, pp. 55–73.

Delis, Dean C et al. (1991). "Profiles of demented and amnesic patients on the California Verbal Learning Test: Implications for the assessment of memory disorders". In: *Psychological Assessment: A Journal of Consulting and Clinical Psychology* 3.1, p. 19.

Depp, Constanze et al. (June 2023). "Myelin dysfunction drives amyloid-β deposition in models of Alzheimer's disease". en. In: *Nature* 618.7964, pp. 349–357.

Derix, Johanna et al. (2014). "Visualization of the amygdalo-hippocampal border and its structural variability by 7T and 3T magnetic resonance imaging". In: *Hum. Brain Mapp.* 35.9, pp. 4316–4329.

Despotović, Ivana, Bart Goossens, and Wilfried Philips (Mar. 2015). "MRI segmentation of the human brain: challenges, methods, and applications". en. In: *Comput. Math. Methods Med.* 2015, p. 450341.

Diamond, Adele (2013). "Executive functions". en. In: *Annu. Rev. Psychol.* 64, pp. 135–168.

Dick, Frederic et al. (Nov. 2012). "In vivo functional and myeloarchitectonic mapping of human primary auditory areas". en. In: *J. Neurosci.* 32.46, pp. 16095–16105.

Dickerson, Bradford C et al. (2009). "The cortical signature of Alzheimer's disease: regionally specific cortical thinning relates to symptom severity in very mild to mild AD dementia and is detectable in asymptomatic amyloid-positive individuals". In: *Cereb. Cortex* 19.3, pp. 497–510.

Dickstein, D L et al. (Oct. 2013). "Dendritic spine changes associated with normal aging". en. In: *Neuroscience* 251, pp. 21–32.

Dimovasili, Christina et al. (Feb. 2023). "Aging compromises oligodendrocyte precursor cell maturation and efficient remyelination in the monkey brain". en. In: *Geroscience* 45.1, pp. 249–264.

Ding, Song-Lin (Dec. 2013). "Comparative anatomy of the prosubiculum, subiculum, presubiculum, postsubiculum, and parasubiculum in human, monkey, and rodent". en. In: *J. Comp. Neurol.* 521.18, pp. 4145–4162.

Ding, Song-Lin and Gary W Van Hoesen (2015). "Organization and detailed parcellation of human hippocampal head and body regions based on a combined analysis of Cyto- and chemoarchitecture". In: *J. Comp. Neurol.* 523.15, pp. 2233–2253.

Domingues, Helena S et al. (June 2016). "Oligodendrocyte, Astrocyte, and Microglia Crosstalk in Myelin Development, Damage, and Repair". en. In: *Front Cell Dev Biol* 4, p. 71.

Dong, Qunxi et al. (Mar. 2019). "Applying surface-based hippocampal morphometry to study APOE-E4 allele dose effects in cognitively unimpaired subjects". en. In: *Neuroimage Clin* 22, p. 101744.

Double, Kay L et al. (Aug. 2003). "Iron-binding characteristics of neuromelanin of the human substantia nigra". en. In: *Biochem. Pharmacol.* 66.3, pp. 489–494.

Dounavi, Maria-Eleni et al. (Mar. 2020). "Volumetric alterations in the hippocampal subfields of subjects at increased risk of dementia". In: *Neurobiol. Aging* 91, pp. 36–44.

Driscoll, Ira et al. (Dec. 2003). "The aging hippocampus: cognitive, biochemical and structural findings". en. In: *Cereb. Cortex* 13.12, pp. 1344–1351.

Drobinin, Vladislav et al. (Mar. 2020). "Psychotic symptoms are associated with lower cortical folding in youth at risk for mental illness". en. In: *J. Psychiatry Neurosci.* 45.2, pp. 125–133.

Du, A T et al. (Oct. 2001). "Magnetic resonance imaging of the entorhinal cortex and hippocampus in mild cognitive impairment and Alzheimer's disease". en. In: *J. Neurol. Neurosurg. Psychiatry* 71.4, pp. 441–447.

Duara, R et al. (Dec. 2008). "Medial temporal lobe atrophy on MRI scans and the diagnosis of Alzheimer disease". en. In: *Neurology* 71.24, pp. 1986–1992.

Duhamel, G et al. (Oct. 2019). "Validating the sensitivity of inhomogeneous magnetization transfer (ihMT) MRI to myelin with fluorescence microscopy". en. In: *Neuroimage* 199, pp. 289–303.

Dujardin, Simon and Bradley T Hyman (2019). "Tau Prion-Like Propagation: State of the Art and Current Challenges". en. In: *Adv. Exp. Med. Biol.* 1184, pp. 305–325.

Duriez, Quentin, Fabrice Crivello, and Bernard Mazoyer (Nov. 2014). "Sex-related and tissue-specific effects of tobacco smoking on brain atrophy: assessment in a large longitudinal cohort of healthy elderly". en. In: *Front. Aging Neurosci.* 6, p. 299.

Duvernoy, Henri M (June 2005). *The Human Hippocampus: Functional Anatomy, Vascularization and Serial Sections with MRI*. en. Springer Science & Business Media.

Duvernoy, Henri M, Francoise Cattin, and Pierre-Yves Risold (June 2013). *The Human Hippocampus: Functional Anatomy, Vascularization and Serial Sections with MRI*. en. Springer Science & Business Media.

Duyn, Jeff (Apr. 2013). "MR susceptibility imaging". en. In: *J. Magn. Reson.* 229, pp. 198–207.

Duyn, Jeff H and John Schenck (Apr. 2017). "Contributions to magnetic susceptibility of brain tissue". en. In: *NMR Biomed.* 30.4.

Dwork, A J (1997). "Postmortem Studies of the Hippocampal Formation in Schizophrenia". In: *Schizophr. Bull.* 23.3, pp. 385–402.

Dyck, Christopher H van et al. (Jan. 2023). "Lecanemab in Early Alzheimer's Disease". en. In: *N. Engl. J. Med.* 388.1, pp. 9–21.

Eck, Brendan L et al. (Jan. 2023). "Quantitative MRI for Evaluation of Musculoskeletal Disease: Cartilage and Muscle Composition, Joint Inflammation, and Biomechanics in Osteoarthritis". en. In: *Invest. Radiol.* 58.1, pp. 60–75.

Economo, Constantin von and Georg N Koskinas (1925). *Die Cytoarchitektonik der Hirnrinde des erwachsenen Menschen: Textband u. Atlas*. de. Berlin, Germany: Springer.

Edler, Melissa K et al. (Nov. 2020). "Neuron loss associated with age but not Alzheimer's disease pathology in the chimpanzee brain". en. In: *Philos. Trans. R. Soc. Lond. B Biol. Sci.* 375.1811, p. 20190619.

Eichenbaum, Howard (Sept. 2004). "Hippocampus: cognitive processes and neural representations that underlie declarative memory". en. In: *Neuron* 44.1, pp. 109–120.

Eid, Aseel, Isha Mhatre, and Jason R Richardson (July 2019). "Gene-environment interactions in Alzheimer's disease: A potential path to precision medicine". en. In: *Pharmacol. Ther.* 199, pp. 173–187.

Elder, Greg J et al. (Nov. 2017). "The influence of hippocampal atrophy on the cognitive phenotype of dementia with Lewy bodies". en. In: *Int. J. Geriatr. Psychiatry* 32.11, pp. 1182–1189.

Eldridge, Laura L et al. (Mar. 2005). "A dissociation of encoding and retrieval processes in the human hippocampus". en. In: *J. Neurosci.* 25.13, pp. 3280–3286.

Emery, Ben (Nov. 2010). "Regulation of oligodendrocyte differentiation and myelination". en. In: *Science* 330.6005, pp. 779–782.

Eriksson, P S et al. (Nov. 1998). "Neurogenesis in the adult human hippocampus". en. In: *Nat. Med.* 4.11, pp. 1313–1317.

Eriksson, Sofia H et al. (Jan. 2008). "PROPELLER MRI visualizes detailed pathology of hippocampal sclerosis". en. In: *Epilepsia* 49.1, pp. 33–39.

Eskildsen, Simon F et al. (Feb. 2012). "BEaST: brain extraction based on nonlocal segmentation technique". en. In: *Neuroimage* 59.3, pp. 2362–2373.

Evans, Alan C et al. (Aug. 2012). "Brain templates and atlases". en. In: *Neuroimage* 62.2, pp. 911–922.

Fanselow, Michael S and Hong-Wei Dong (Jan. 2010). "Are the dorsal and ventral hippocampus functionally distinct structures?" en. In: *Neuron* 65.1, pp. 7–19.

Farrington, D P (May 1991). "Longitudinal research strategies: advantages, problems, and prospects". en. In: *J. Am. Acad. Child Adolesc. Psychiatry* 30.3, pp. 369–374.

Ferguson, Heather J, Victoria E A Brunsdon, and Elisabeth E F Bradford (Jan. 2021). "The developmental trajectories of executive function from adolescence to old age". en. In: *Sci. Rep.* 11.1, p. 1382.

Ferraro, Kenneth F, Blakelee R Kemp, and Monica M Williams (Mar. 2017). "Diverse Aging and Health Inequality by Race and Ethnicity". en. In: *Innov Aging* 1.1, igx002.

Finch, C E and R E Tanzi (Oct. 1997). "Genetics of aging". en. In: *Science* 278.5337, pp. 407–411.

Fischl, B and A M Dale (Sept. 2000). "Measuring the thickness of the human cerebral cortex from magnetic resonance images". en. In: *Proc. Natl. Acad. Sci. U. S. A.* 97.20, pp. 11050–11055.

Fischl, Bruce, David H Salat, Evelina Busa, et al. (Jan. 2002). "Whole brain segmentation: automated labeling of neuroanatomical structures in the human brain". en. In: *Neuron* 33.3, pp. 341–355.

Fischl, Bruce, David H Salat, André J W van der Kouwe, et al. (2004). "Sequence-independent segmentation of magnetic resonance images". en. In: *Neuroimage* 23 Suppl 1, S69–84.

Fisher, Daniel W, David A Bennett, and Hongxin Dong (Oct. 2018). "Sexual dimorphism in predisposition to Alzheimer's disease". en. In: *Neurobiol. Aging* 70, pp. 308–324.

Fjell, Anders M, Markus H Sneve, et al. (Mar. 2017). "The Disconnected Brain and Executive Function Decline in Aging". en. In: *Cereb. Cortex* 27.3, pp. 2303–2317.

Fjell, Anders M and Kristine B Walhovd (2010). "Structural brain changes in aging: courses, causes and cognitive consequences". en. In: *Rev. Neurosci.* 21.3, pp. 187–221.

Fjell, Anders M, Kristine B Walhovd, Christine Fennema-Notestine, et al. (Dec. 2009). "One-year brain atrophy evident in healthy aging". en. In: *J. Neurosci.* 29.48, pp. 15223–15231.

Fjell, Anders M, Kristine B Walhovd, Ivar Reinvang, et al. (Feb. 2006). "Selective increase of cortical thickness in high-performing elderly—structural indices of optimal cognitive aging". In: *Neuroimage* 29.3, pp. 984–994.

Fjell, Anders M, Lars T Westlye, et al. (Apr. 2014). "Accelerating cortical thinning: unique to dementia or universal in aging?" en. In: *Cereb. Cortex* 24.4, pp. 919–934.

Fleisher, Adam et al. (June 2005). "Sex, apolipoprotein E epsilon 4 status, and hippocampal volume in mild cognitive impairment". en. In: *Arch. Neurol.* 62.6, pp. 953–957.

Flores, Robin de, Renaud La Joie, and Gaël Chételat (Nov. 2015). "Structural imaging of hippocampal subfields in healthy aging and Alzheimer's disease". en. In: *Neuroscience* 309, pp. 29–50.

Flores, Robin de, Renaud La Joie, Brigitte Landeau, et al. (Feb. 2015). "Effects of age and Alzheimer's disease on hippocampal subfields: comparison between manual and FreeSurfer volumetry". en. In: *Hum. Brain Mapp.* 36.2, pp. 463–474.

Folstein, Marshal F, Susan E Folstein, and Paul R McHugh (1975). ""Mini-mental state": a practical method for grading the cognitive state of patients for the clinician". In: *J. Psychiatr. Res.* 12.3, pp. 189–198.

Fonov, Vladimir S and D Louis Collins (Mar. 2018). "Comparison of different methods for average anatomical templates creation: do we really gain anything from a diffeomorphic framework?" en.

Fontana, Luigi and Frank B Hu (June 2014). "Optimal body weight for health and longevity: bridging basic, clinical, and population research". en. In: *Aging Cell* 13.3, pp. 391–400.

Freeman, Stefanie H et al. (Dec. 2008). "Preservation of neuronal number despite age-related cortical brain atrophy in elderly subjects without Alzheimer disease". en. In: *J. Neuropathol. Exp. Neurol.* 67.12, pp. 1205–1212.

Frisoni, Giovanni B, Rossana Ganzola, et al. (Dec. 2008). "Mapping local hippocampal changes in Alzheimer's disease and normal ageing with MRI at 3 Tesla". en. In: *Brain* 131.Pt 12, pp. 3266–3276.

Frisoni, Giovanni B and Clifford R Jack (Feb. 2015). "HarP: the EADC-ADNI Harmonized Protocol for manual hippocampal segmentation. A standard of reference from a global working group". en. In: *Alzheimers. Dement.* 11.2, pp. 107–110.

Frisoni, Giovanni B, Annapaola Prestia, et al. (June 2009). "In vivo mapping of incremental cortical atrophy from incipient to overt Alzheimer's disease". en. In: *J. Neurol.* 256.6, pp. 916–924.

Frost, Bess, Rachel L Jacks, and Marc I Diamond (2009). "Propagation of tau misfolding from the outside to the inside of a cell". In: *J. Biol. Chem.* 284.19, pp. 12845–12852.

Fujimoto, Kyoko et al. (Apr. 2014). "Quantitative comparison of cortical surface reconstructions from MP2RAGE and multi-echo MPRAGE data at 3 and 7 T". en. In: *Neuroimage* 90, pp. 60–73.

Fukunaga, Masaki et al. (Feb. 2010). "Layer-specific variation of iron content in cerebral cortex as a source of MRI contrast". en. In: *Proc. Natl. Acad. Sci. U. S. A.* 107.8, pp. 3834–3839.

Fungwe, Thomas V et al. (Feb. 2023). "Systolic Blood Pressure Is Associated with Increased Brain Amyloid Load in Mild Cognitively Impaired Participants: Alzheimer's Disease Neuroimaging Initiatives Study". en. In: *Dement. Geriatr. Cogn. Disord.*, pp. 1–8.

Gaig, Carles and Eduardo Tolosa (2009). "When does Parkinson's disease begin?" In: *Mov. Disord.* 24.S2, S656–S664.

Garon, Nancy, Susan E Bryson, and Isabel M Smith (Jan. 2008). "Executive function in preschoolers: a review using an integrative framework". en. In: *Psychol. Bull.* 134.1, pp. 31–60.

Gauthier, Serge et al. (Apr. 2006). "Mild cognitive impairment". en. In: *Lancet* 367.9518, pp. 1262–1270.

Gefen, Tamar et al. (Aug. 2014). "Longitudinal neuropsychological performance of cognitive SuperAgers". en. In: *J. Am. Geriatr. Soc.* 62.8, pp. 1598–1600.

Gelman, N et al. (Jan. 2001). "Interregional variation of longitudinal relaxation rates in human brain at 3.0 T: relation to estimated iron and water contents". en. In: *Magn. Reson. Med.* 45.1, pp. 71–79.

Gennari, Francesco (1782). *De peculiari structura cerebri nonnullisque ejus morbis*. la. Ex Regio Typographeo.

George, Kristen M et al. (Apr. 2023). "Association of Early Adulthood Hypertension and Blood Pressure Change With Late-Life Neuroimaging Biomarkers". en. In: *JAMA Netw Open* 6.4, e236431.

Giraud, Rémi et al. (Jan. 2016). "An Optimized PatchMatch for multi-scale and multi-feature label fusion". en. In: *Neuroimage* 124.Pt A, pp. 770–782.

Glasser, M F and D C Van Essen (2011). "Mapping Human Cortical Areas In Vivo Based on Myelin Content as Revealed by T1- and T2-Weighted MRI". In: *Journal of Neuroscience* 31.32, pp. 11597–11616.

Golgi, Camillo (1885). *Sulla fina anatomia degli organi centrali del sistema nervoso*. it. S. Calderini.

Golomb, J et al. (Sept. 1996). "Hippocampal formation size predicts declining memory performance in normal aging". en. In: *Neurology* 47.3, pp. 810–813.

Gómez-Isla, Teresa et al. (1996). "Profound Loss of Layer II Entorhinal Cortex Neurons Occurs in Very Mild Alzheimer's Disease". In: *J. Neurosci.* 16.14, pp. 4491–4500.

Gonneaud, Julie et al. (Oct. 2016). "Relative effect of APOE $\epsilon 4$ on neuroimaging biomarker changes across the lifespan". en. In: *Neurology* 87.16, pp. 1696–1703.

Gonzalez, Christopher E et al. (June 2015). "Longitudinal changes in cortical thinning associated with hypertension". en. In: *J. Hypertens.* 33.6, pp. 1242–1248.

Good, C D et al. (July 2001). "A voxel-based morphometric study of ageing in 465 normal adult human brains". en. In: *Neuroimage* 14.1 Pt 1, pp. 21–36.

Gordon, Brian A et al. (2013). "Effects of aging and Alzheimer's disease along the longitudinal axis of the hippocampus". en. In: *J. Alzheimers. Dis.* 37.1, pp. 41–50.

Götmark, Frank and Malte Andersson (Feb. 2020). "Human fertility in relation to education, economy, religion, contraception, and family planning programs". en. In: *BMC Public Health* 20.1, p. 265.

Graeber, Manuel B and Wolfgang J Streit (Jan. 2010). "Microglia: biology and pathology". en. In: *Acta Neuropathol.* 119.1, pp. 89–105.

Granziera, Cristina et al. (June 2021). "Quantitative magnetic resonance imaging towards clinical application in multiple sclerosis". en. In: *Brain* 144.5, pp. 1296–1311.

Griffin, C M et al. (May 2002). "T1 histograms of normal-appearing brain tissue are abnormal in early relapsing-remitting multiple sclerosis". en. In: *Mult. Scler.* 8.3, pp. 211–216.

Grimm, Amandine and Anne Eckert (Nov. 2017). "Brain aging and neurodegeneration: from a mitochondrial point of view". en. In: *J. Neurochem.* 143.4, pp. 418–431.

Groot, Colin et al. (Jan. 2018). "Differential effects of cognitive reserve and brain reserve on cognition in Alzheimer disease". en. In: *Neurology* 90.2, e149–e156.

Groves, Adrian R et al. (Feb. 2011). "Linked independent component analysis for multimodal data fusion". en. In: *Neuroimage* 54.3, pp. 2198–2217.

Gupta, Raj K (Jan. 1977). "A new look at the method of variable nutation angle for the measurement of spin-lattice relaxation times using fourier transform NMR". In: *J. Magn. Reson.* 25.1, pp. 231–235.

Haast, Roy A M, Dimo Ivanov, and Kâmil Uludağ (June 2018). "The impact of correction on MP2RAGE cortical T 1 and apparent cortical thickness at 7 T". en. In: *Hum. Brain Mapp.* 39.6, pp. 2412–2425.

Haast, Roy A M, Jonathan C Lau, et al. (Jan. 2021). "Effects of MP2RAGE B1+ sensitivity on inter-site T1 reproducibility and hippocampal morphometry at 7T". en. In: *Neuroimage* 224, p. 117373.

Habes, M et al. (Sept. 2016). "Relationship between APOE Genotype and Structural MRI Measures throughout Adulthood in the Study of Health in Pomerania Population-Based Cohort". en. In: *AJNR Am. J. Neuroradiol.* 37.9, pp. 1636–1642.

Hackert, V H et al. (Nov. 2002). "Hippocampal head size associated with verbal memory performance in nondemented elderly". en. In: *Neuroimage* 17.3, pp. 1365–1372.

Hägg, Sara and Juulia Jylhävä (May 2021). "Sex differences in biological aging with a focus on human studies". en. In: *Elife* 10.

Haglund, L, L W Swanson, and C Köhler (Oct. 1984). "The projection of the supramammillary nucleus to the hippocampal formation: an immunohistochemical and anterograde transport study with the lectin PHA-L in the rat". en. In: *J. Comp. Neurol.* 229.2, pp. 171–185.

Hahn, Erwin L (July 1949). "An Accurate Nuclear Magnetic Resonance Method for Measuring Spin-Lattice Relaxation Times". In: *Phys. Rev.* 76.1, pp. 145–146.

Han, Xiao et al. (Aug. 2006). "Reliability of MRI-derived measurements of human cerebral cortical thickness: the effects of field strength, scanner upgrade and manufacturer". en. In: *Neuroimage* 32.1, pp. 180–194.

Hänninen, T et al. (Jan. 1997). "Decline of frontal lobe functions in subjects with age-associated memory impairment". en. In: *Neurology* 48.1, pp. 148–153.

Harkins, Kevin D, Adrienne N Dula, and Mark D Does (Mar. 2012). "Effect of intercompartmental water exchange on the apparent myelin water fraction in multiexponential T2 measurements of rat spinal cord". en. In: *Magn. Reson. Med.* 67.3, pp. 793–800.

Harkins, Kevin D, Junzhong Xu, et al. (Mar. 2016). "The microstructural correlates of T1 in white matter". en. In: *Magn. Reson. Med.* 75.3, pp. 1341–1345.

Harrison, Paul J (June 2004). "The hippocampus in schizophrenia: a review of the neuropathological evidence and its pathophysiological implications". In: *Psychopharmacology* 174.1, pp. 151–162.

Hasboun, D et al. (1996). "MR determination of hippocampal volume: comparison of three methods". en. In: *AJNR Am. J. Neuroradiol.* 17.6, pp. 1091–1098.

Hatters, Danny M, Clare A Peters-Libeu, and Karl H Weisgraber (Aug. 2006). "Apolipoprotein E structure: insights into function". en. In: *Trends Biochem. Sci.* 31.8, pp. 445–454.

He, Wan, Daniel Goodkind, and Paul R Kowal (2016). *An Aging World : 2015*. en. United States Census Bureau.

Heckers, S (2001). "Neuroimaging studies of the hippocampus in schizophrenia". en. In: *Hippocampus* 11.5, pp. 520–528.

Hedges, Emily P et al. (Feb. 2022). "Reliability of structural MRI measurements: The effects of scan session, head tilt, inter-scan interval, acquisition sequence, FreeSurfer version and processing stream". en. In: *Neuroimage* 246, p. 118751.

Hedman, Anna M et al. (Aug. 2012). "Human brain changes across the life span: a review of 56 longitudinal magnetic resonance imaging studies". en. In: *Hum. Brain Mapp.* 33.8, pp. 1987–2002.

Hefendehl, Jasmin K et al. (2014). "Homeostatic and injury-induced microglia behavior in the aging brain". In: *Aging Cell* 13.1, pp. 60–69.

Hernando, Diego et al. (Nov. 2014). "Quantification of liver iron with MRI: state of the art and remaining challenges". en. In: *J. Magn. Reson. Imaging* 40.5, pp. 1003–1021.

Herrup, Karl (June 2015). "The case for rejecting the amyloid cascade hypothesis". en. In: *Nat. Neurosci.* 18.6, pp. 794–799.

Hodges, J R, D P Salmon, and N Butters (Aug. 1991). "The nature of the naming deficit in Alzheimer's and Huntington's disease". en. In: *Brain* 114 (Pt 4), pp. 1547–1558.

Hofer, Edith et al. (Sept. 2020). "Genetic correlations and genome-wide associations of cortical structure in general population samples of 22,824 adults". en. In: *Nat. Commun.* 11.1, p. 4796.

Hohman, Timothy J et al. (Oct. 2017). "Evaluating Alzheimer's disease biomarkers as mediators of age-related cognitive decline". en. In: *Neurobiol. Aging* 58, pp. 120–128.

Holmes, Brandon B and Marc I Diamond (July 2014). "Prion-like properties of Tau protein: the importance of extracellular Tau as a therapeutic target". en. In: *J. Biol. Chem.* 289.29, pp. 19855–19861.

House, M J et al. (Feb. 2006). "Quantitative MR imaging R2 relaxometry in elderly participants reporting memory loss". en. In: *AJNR Am. J. Neuroradiol.* 27.2, pp. 430–439.

Howard, Cortney M et al. (Feb. 2022). "Cortical iron mediates age-related decline in fluid cognition". en. In: *Hum. Brain Mapp.* 43.3, pp. 1047–1060.

Huang, Elbert S et al. (Feb. 2014). "Rates of complications and mortality in older patients with diabetes mellitus: the diabetes and aging study". en. In: *JAMA Intern. Med.* 174.2, pp. 251–258.

Huberfeld, G, T Blauwblomme, and R Miles (Mar. 2015). "Hippocampus and epilepsy: Findings from human tissues". en. In: *Rev. Neurol.* 171.3, pp. 236–251.

Hunsaker, Michael R, Jenna S Rosenberg, and Raymond P Kesner (2008). "The role of the dentate gyrus, CA3a,b, and CA3c for detecting spatial and environmental novelty". en. In: *Hippocampus* 18.10, pp. 1064–1073.

Hurtz, Sona et al. (2019). "Automated and manual hippocampal segmentation techniques: Comparison of results, reproducibility and clinical applicability". en. In: *Neuroimage Clin* 21, p. 101574.

Huttenlocher, P R (Mar. 1979). "Synaptic density in human frontal cortex - developmental changes and effects of aging". en. In: *Brain Res.* 163.2, pp. 195–205.

Huttenlocher, P R and A S Dabholkar (Oct. 1997). "Regional differences in synaptogenesis in human cerebral cortex". en. In: *J. Comp. Neurol.* 387.2, pp. 167–178.

Iannopollo, Emily, Kara Garcia, and Alzheimer' Disease Neuroimaging Initiative (Aug. 2021). "Enhanced detection of cortical atrophy in Alzheimer's disease using structural MRI with anatomically constrained longitudinal registration". en. In: *Hum. Brain Mapp.* 42.11, pp. 3576–3592.

Iglesias, Juan Eugenio, Jean C Augustinack, et al. (July 2015). "A computational atlas of the hippocampal formation using ex vivo, ultra-high resolution MRI: Application to adaptive segmentation of in vivo MRI". en. In: *Neuroimage* 115, pp. 117–137.

Iglesias, Juan Eugenio and Mert R Sabuncu (Aug. 2015). "Multi-atlas segmentation of biomedical images: A survey". en. In: *Med. Image Anal.* 24.1, pp. 205–219.

Iosifescu, D V et al. (July 1997). "An automated registration algorithm for measuring MRI subcortical brain structures". en. In: *Neuroimage* 6.1, pp. 13–25.

Ito, Kaori et al. (Jan. 2010). "Disease progression meta-analysis model in Alzheimer's disease". en. In: *Alzheimers. Dement.* 6.1, pp. 39–53.

Jack Jr, C R, D W Dickson, et al. (Mar. 2002). "Antemortem MRI findings correlate with hippocampal neuropathology in typical aging and dementia". en. In: *Neurology* 58.5, pp. 750–757.

Jack Jr, C R, R C Petersen, Y Xu, P C O'Brien, G E Smith, R J Ivnik, B F Boeve, et al. (Aug. 2000). "Rates of hippocampal atrophy correlate with change in clinical status in aging and AD". en. In: *Neurology* 55.4, pp. 484–489.

Jack Jr, C R, R C Petersen, Y Xu, P C O'Brien, G E Smith, R J Ivnik, E G Tangalos, et al. (Oct. 1998). "Rate of medial temporal lobe atrophy in typical aging and Alzheimer's disease". en. In: *Neurology* 51.4, pp. 993–999.

Jack Jr, C R, R C Petersen, Y C Xu, et al. (Sept. 1997). "Medial temporal atrophy on MRI in normal aging and very mild Alzheimer's disease". en. In: *Neurology* 49.3, pp. 786–794.

Jack Jr, Clifford R, Frederik Barkhof, et al. (July 2011). "Steps to standardization and validation of hippocampal volumetry as a biomarker in clinical trials and diagnostic criterion for Alzheimer's disease". en. In: *Alzheimers. Dement.* 7.4, 474–485.e4.

Jack Jr, Clifford R, Matt A Bernstein, et al. (2008). "The Alzheimer's disease neuroimaging initiative (ADNI): MRI methods". In: *Journal of Magnetic Resonance Imaging: An Official Journal of the International Society for Magnetic Resonance in Medicine* 27.4, pp. 685–691.

Jack Jr, Clifford R, Heather J Wiste, et al. (May 2015). "Age, Sex, and APOE $\epsilon 4$ Effects on Memory, Brain Structure, and β-Amyloid Across the Adult Life Span". en. In: *JAMA Neurol.* 72.5, pp. 511–519.

Jakovcevski, Igor et al. (June 2009). "Oligodendrocyte development and the onset of myelination in the human fetal brain". en. In: *Front. Neuroanat.* 3, p. 5.

Janes, Amy C et al. (Jan. 2015). "Striatal morphology is associated with tobacco cigarette craving". en. In: *Neuropsychopharmacology* 40.2, pp. 406–411.

Jaul, Efraim and Jeremy Barron (Dec. 2017). "Age-Related Diseases and Clinical and Public Health Implications for the 85 Years Old and Over Population". en. In: *Front Public Health* 5, p. 335.

Jessen, Frank et al. (Jan. 2014). "AD dementia risk in late MCI, in early MCI, and in subjective memory impairment". en. In: *Alzheimers. Dement.* 10.1, pp. 76–83.

Jessen, Nadia Aalling et al. (Dec. 2015). "The Glymphatic System: A Beginner's Guide". en. In: *Neurochem. Res.* 40.12, pp. 2583–2599.

Jiang, Tianyi and Enrique Cadenas (Dec. 2014). "Astrocytic metabolic and inflammatory changes as a function of age". en. In: *Aging Cell* 13.6, pp. 1059–1067.

Jovicich, Jorge et al. (May 2009). "MRI-derived measurements of human subcortical, ventricular and intracranial brain volumes: Reliability effects of scan sessions, acquisition sequences, data analyses, scanner upgrade, scanner vendors and field strengths". en. In: *Neuroimage* 46.1, pp. 177–192.

Kaiser, Natalie C et al. (2014). "Differences in anxiety among patients with early- versus late-onset Alzheimer's disease". en. In: *J. Neuropsychiatry Clin. Neurosci.* 26.1, pp. 73–80.

Kalpouzos, Grégoria et al. (Jan. 2009). "Voxel-based mapping of brain gray matter volume and glucose metabolism profiles in normal aging". en. In: *Neurobiol. Aging* 30.1, pp. 112–124.

Kametani, Fuyuki and Masato Hasegawa (Jan. 2018). "Reconsideration of Amyloid Hypothesis and Tau Hypothesis in Alzheimer's Disease". en. In: *Front. Neurosci.* 12, p. 25.

Karakuzu, Agah et al. (Sept. 2022). "Vendor-neutral sequences and fully transparent workflows improve inter-vendor reproducibility of quantitative MRI". en. In: *Magn. Reson. Med.* 88.3, pp. 1212–1228.

Katsuno, Masahisa et al. (Aug. 2018). "Preclinical progression of neurodegenerative diseases". en. In: *Nagoya J. Med. Sci.* 80.3, pp. 289–298.

Kaup, Allison R et al. (2011). "A review of the brain structure correlates of successful cognitive aging". en. In: *J. Neuropsychiatry Clin. Neurosci.* 23.1, pp. 6–15.

Kerchner, G A et al. (Oct. 2010). "Hippocampal CA1 apical neuropil atrophy in mild Alzheimer disease visualized with 7-T MRI". en. In: *Neurology* 75.15, pp. 1381–1387.

Kerchner, Geoffrey A et al. (Feb. 2014). "APOE ϵ4 worsens hippocampal CA1 apical neuropil atrophy and episodic memory". en. In: *Neurology* 82.8, pp. 691–697.

Kirsch, S J et al. (Jan. 1992). "Prolongation of magnetic resonance T2 time in hippocampus of human patients marks the presence and severity of Alzheimer's disease". en. In: *Neurosci. Lett.* 134.2, pp. 187–190.

Klein, Arno et al. (Oct. 2005). "Mindboggle: automated brain labeling with multiple atlases". en. In: *BMC Med. Imaging* 5, p. 7.

Knight, Michael J et al. (Dec. 2016). "Quantitative T1 and T2 MRI signal characteristics in the human brain: different patterns of MR contrasts in normal ageing". en. In: *MAGMA* 29.6, pp. 833–842.

Knussmann, Graham N et al. (June 2022). "Test-retest reliability of FreeSurfer-derived volume, area and cortical thickness from MPRAGE and MP2RAGE brain MRI images". en. In: *Neuroimage Rep* 2.2.

Kodiweera, Chandana et al. (Mar. 2016). "Age effects and sex differences in human brain white matter of young to middle-aged adults: A DTI, NODDI, and q-space study". en. In: *Neuroimage* 128, pp. 180–192.

Köhncke, Ylva et al. (May 2016). "Three-year changes in leisure activities are associated with concurrent changes in white matter microstructure and perceptual speed in individuals aged 80 years and older". In: *Neurobiol. Aging* 41, pp. 173–186.

Kono, Rena, Yuji Ikegaya, and Ryuta Koyama (May 2021). "Phagocytic Glial Cells in Brain Homeostasis". en. In: *Cells* 10.6.

Kordower, J H et al. (Feb. 2001). "Loss and atrophy of layer II entorhinal cortex neurons in elderly people with mild cognitive impairment". en. In: *Ann. Neurol.* 49.2, pp. 202–213.

Kornack, D R and P Rakic (May 1999). "Continuation of neurogenesis in the hippocampus of the adult macaque monkey". en. In: *Proc. Natl. Acad. Sci. U. S. A.* 96.10, pp. 5768–5773.

Kovacevic, Natasa et al. (2013). "Revisiting PLS Resampling: Comparing Significance Versus Reliability Across Range of Simulations". In: *New Perspectives in Partial Least Squares and Related Methods*. Springer New York, pp. 159–170.

Kovacs, Gabor G (Oct. 2012). "Clinical stratification of subtypes of Alzheimer's disease". en. In: *Lancet Neurol.* 11.10, pp. 839–841.

Krishnan, Anjali et al. (May 2011). "Partial Least Squares (PLS) methods for neuroimaging: a tutorial and review". en. In: *Neuroimage* 56.2, pp. 455–475.

Kühn, Simone, Florian Schubert, and Jürgen Gallinat (Dec. 2010). "Reduced thickness of medial orbitofrontal cortex in smokers". en. In: *Biol. Psychiatry* 68.11, pp. 1061–1065.

Kulaga-Yoskovitz, Jessie et al. (Nov. 2015). "Multi-contrast submillimetric 3 Tesla hippocampal subfield segmentation protocol and dataset". en. In: *Sci Data* 2, p. 150059.

Kumar, Rajesh et al. (Feb. 2012). "Age-related regional brain T2-relaxation changes in healthy adults". en. In: *J. Magn. Reson. Imaging* 35.2, pp. 300–308.

Kurth, Florian, Nicolas Cherbuin, and Eileen Luders (Dec. 2017). "The impact of aging on subregions of the hippocampal complex in healthy adults". en. In: *Neuroimage* 163, pp. 296–300.

La Joie, Renaud, Marine Fouquet, et al. (Nov. 2010). "Differential effect of age on hippocampal subfields assessed using a new high-resolution 3T MR sequence". en. In: *Neuroimage* 53.2, pp. 506–514.

La Joie, Renaud, Audrey Perrotin, et al. (Aug. 2013). "Hippocampal subfield volumetry in mild cognitive impairment, Alzheimer's disease and semantic dementia". en. In: *Neuroimage Clin* 3, pp. 155–162.

Laakso, M P, G B Frisoni, et al. (June 2000). "Hippocampus and entorhinal cortex in frontotemporal dementia and Alzheimer's disease: a morphometric MRI study". en. In: *Biol. Psychiatry* 47.12, pp. 1056–1063.

Laakso, M P, K Partanen, P Riekkinen, et al. (Mar. 1996). "Hippocampal volumes in Alzheimer's disease, Parkinson's disease with and without dementia, and in vascular dementia: An MRI study". en. In: *Neurology* 46.3, pp. 678–681.

Laakso, M P, K Partanen, H Soininen, et al. (1996). "MR T2 relaxometry in Alzheimer's disease and age-associated memory impairment". en. In: *Neurobiol. Aging* 17.4, pp. 535–540.

Laakso, M P, H Soininen, et al. (1998). "MRI of the Hippocampus in Alzheimer's Disease: Sensitivity, Specificity, and Analysis of the Incorrectly Classified Subjects". In: *Neurobiol. Aging* 19.1, pp. 23–31.

Lampe, Leonie et al. (Jan. 2019). "Lesion location matters: The relationships between white matter hyperintensities on cognition in the healthy elderly". en. In: *J. Cereb. Blood Flow Metab.* 39.1, pp. 36–43.

Lancaster, Jack L et al. (Dec. 2011). "Automated analysis of fundamental features of brain structures". en. In: *Neuroinformatics* 9.4, pp. 371–380.

Langkammer, Christian et al. (Nov. 2010). "Quantitative MR imaging of brain iron: a post-mortem validation study". en. In: *Radiology* 257.2, pp. 455–462.

Langnes, Espen et al. (2020). "Anterior and posterior hippocampus macro- and microstructure across the lifespan in relation to memory—A longitudinal study". In: *Hippocampus* 30.7, pp. 678–692.

Lasser, Micaela, Jessica Tiber, and Laura Anne Lowery (June 2018). "The Role of the Microtubule Cytoskeleton in Neurodevelopmental Disorders". en. In: *Front. Cell. Neurosci.* 12, p. 165.

Lauterbur, P C (1973). "Image Formation by Induced Local Interactions: Examples Employing Nuclear Magnetic Resonance". In: *Nature* 242.5394, pp. 190–191.

Le Duigou, Caroline et al. (Jan. 2014). "Recurrent synapses and circuits in the CA3 region of the hippocampus: an associative network". en. In: *Front. Cell. Neurosci.* 7, p. 262.

Ledergerber, Debora and Edvard Ingjald Moser (Nov. 2017). "Memory Retrieval: Taking the Route via Subiculum". en. In: *Curr. Biol.* 27.22, R1225–R1227.

Lee, Seonjoo et al. (June 2016). "White matter hyperintensities are a core feature of Alzheimer's disease: Evidence from the dominantly inherited Alzheimer network". en. In: *Ann. Neurol.* 79.6, pp. 929–939.

Lee, Yoojin et al. (Jan. 2019). "Establishing intra- and inter-vendor reproducibility of T1 relaxation time measurements with 3T MRI". en. In: *Magn. Reson. Med.* 81.1, pp. 454–465.

Lehéricy, Stéphane et al. (June 2012). "Magnetic resonance imaging of the substantia nigra in Parkinson's disease". en. In: *Mov. Disord.* 27.7, pp. 822–830.

Lemaitre, Herve et al. (Mar. 2012). "Normal age-related brain morphometric changes: nonuniformity across cortical thickness, surface area and gray matter volume?" en. In: *Neurobiol. Aging* 33.3, 617.e1–9.

Leng, Fangda et al. (Mar. 2023). "Neuroinflammation is independently associated with brain network dysfunction in Alzheimer's disease". en. In: *Mol. Psychiatry* 28.3, pp. 1303–1311.

Leong, Ruth L F et al. (Feb. 2017). "Longitudinal brain structure and cognitive changes over 8 years in an East Asian cohort". en. In: *Neuroimage* 147, pp. 852–860.

Lerch, Jason P, Jeffrey B Carroll, et al. (Jan. 2008). "Automated deformation analysis in the YAC128 Huntington disease mouse model". en. In: *Neuroimage* 39.1, pp. 32–39.

Lerch, Jason P, Jens C Pruessner, et al. (July 2005). "Focal decline of cortical thickness in Alzheimer's disease identified by computational neuroanatomy". en. In: *Cereb. Cortex* 15.7, pp. 995–1001.

Lescher, Stephanie et al. (Jan. 2015). "Quantitative T1 and T2 mapping in recurrent glioblastomas under bevacizumab: earlier detection of tumor progression compared to conventional MRI". en. In: *Neuroradiology* 57.1, pp. 11–20.

Leutritz, Tobias et al. (2020). "Multiparameter mapping of relaxation (R1, R2*), proton density and magnetization transfer saturation at 3 T: A multicenter dual-vendor reproducibility and repeatability study". In: *Hum. Brain Mapp.* 41.15, pp. 4232–4247.

Li, Bolun et al. (Apr. 2016). "Influence of APOE Genotype on Hippocampal Atrophy over Time - An N=1925 Surface-Based ADNI Study". en. In: *PLoS One* 11.4, e0152901.

Li, Yan et al. (2020). "Iron Content in Deep Gray Matter as a Function of Age Using Quantitative Susceptibility Mapping: A Multicenter Study". en. In: *Front. Neurosci.* 14, p. 607705.

Liew, Tau Ming (Sept. 2020). "Subjective cognitive decline, anxiety symptoms, and the risk of mild cognitive impairment and dementia". en. In: *Alzheimers. Res. Ther.* 12.1, p. 107.

Lightbourne R, S Singh, and C P Green (Mar. 1982). "The World Fertility Survey: charting global childbearing". en. In: *Popul. Bull.* 37.1, pp. 1–55.

Lindberg, Laura D et al. (June 2020). "Early impacts of the COVID-19 pandemic: Findings from the 2020 Guttmacher survey of reproductive health experiences". In.

Lindsey, Benjamin W et al. (Nov. 2018). "The role of neuro-epithelial-like and radial-glial stem and progenitor cells in development, plasticity, and repair". en. In: *Prog. Neurobiol.* 170, pp. 99–114.

Liu, Chia-Chen et al. (Feb. 2013). "Apolipoprotein E and Alzheimer disease: risk, mechanisms and therapy". en. In: *Nat. Rev. Neurol.* 9.2, pp. 106–118.

Liu, Jun-Lin et al. (2018). "Iron and Alzheimer's Disease: From Pathogenesis to Therapeutic Implications". In: *Front. Neurosci.* 12.

Livingston, Gill et al. (Dec. 2017). "Dementia prevention, intervention, and care". en. In: *Lancet* 390.10113, pp. 2673–2734.

Look, D C and D R Locker (Feb. 1970). "Time saving in measurement of NMR and EPR relaxation times". In: *Rev. Sci. Instrum.* 41.2, pp. 250–251.

Lovell, M A et al. (June 1998). "Copper, iron and zinc in Alzheimer's disease senile plaques". en. In: *J. Neurol. Sci.* 158.1, pp. 47–52.

Luo, Xiao et al. (Sept. 2019). "Application of T1-/T2-Weighted Ratio Mapping to Elucidate Intracortical Demyelination Process in the Alzheimer's Disease Continuum". en. In: *Front. Neurosci.* 13, p. 904.

Luo, Zhuren et al. (Sept. 2013). "The correlation of hippocampal T2-mapping with neuropsychology test in patients with Alzheimer's disease". en. In: *PLoS One* 8.9, e76203.

Lupien, S J et al. (May 1998). "Cortisol levels during human aging predict hippocampal atrophy and memory deficits". en. In: *Nat. Neurosci.* 1.1, pp. 69–73.

Lutti, Antoine et al. (2014). "Using high-resolution quantitative mapping of R1 as an index of cortical myelination". In: *Neuroimage* 93, pp. 176–188.

MacKay, Alex L and Cornelia Laule (Dec. 2016). "Magnetic Resonance of Myelin Water: An in vivo Marker for Myelin". en. In: *Brain Plast* 2.1, pp. 71–91.

MacQueen, J (1967). "Some methods for classification and analysis of multivariate observations". In: *Proc. 5th Berkeley Symp. on Math. Statist. and Prob* 5.1.

Madar, Antoine D, Laura A Ewell, and Mathew V Jones (Mar. 2019). "Pattern separation of spiketrains in hippocampal neurons". en. In: *Sci. Rep.* 9.1, p. 5282.

Maes, F et al. (Apr. 1997). "Multimodality image registration by maximization of mutual information". en. In: *IEEE Trans. Med. Imaging* 16.2, pp. 187–198.

Maintz, J B and M A Viergever (Mar. 1998). "A survey of medical image registration". en. In: *Med. Image Anal.* 2.1, pp. 1–36.

Makowski, Carolina et al. (Apr. 2018). "Evaluating accuracy of striatal, pallidal, and thalamic segmentation methods: Comparing automated approaches to manual delineation". en. In: *Neuroimage* 170, pp. 182–198.

Malykhin, N V et al. (Jan. 2010). "In vivo quantification of hippocampal subfields using 4.7 T fast spin echo imaging". en. In: *Neuroimage* 49.2, pp. 1224–1230.

Malykhin, Nikolai V, Rawle Carter, et al. (Sept. 2010). "Structural changes in the hippocampus in major depressive disorder: contributions of disease and treatment". en. In: *J. Psychiatry Neurosci.* 35.5, pp. 337–343.

Malykhin, Nikolai V, Yushan Huang, et al. (Nov. 2017). "Differential vulnerability of hippocampal subfields and anteroposterior hippocampal subregions in healthy cognitive aging". en. In: *Neurobiol. Aging* 59, pp. 121–134.

Mancini, Matteo et al. (Oct. 2020). "An interactive meta-analysis of MRI biomarkers of myelin". en. In: *Elife* 9.

Mandelkow, Eva-Maria and Eckhard Mandelkow (July 2012). "Biochemistry and cell biology of tau protein in neurofibrillary degeneration". en. In: *Cold Spring Harb. Perspect. Med.* 2.7, a006247.

Manjón, José V, Pierrick Coupé, et al. (Jan. 2010). "Adaptive non-local means denoising of MR images with spatially varying noise levels". en. In: *J. Magn. Reson. Imaging* 31.1, pp. 192–203.

Manjón, José V, José E Romero, and Pierrick Coupe (Jan. 2022). "A novel deep learning based hippocampus subfield segmentation method". en. In: *Sci. Rep.* 12.1, p. 1333.

Mansfield, P and A A Maudsley (1977). "Medical imaging by NMR". In: *Br. J. Radiol.* 50.591, pp. 188–194.

Marek, Scott et al. (May 2022). "Publisher Correction: Reproducible brain-wide association studies require thousands of individuals". en. In: *Nature* 605.7911, E11.

Marques, José P, Tobias Kober, et al. (Jan. 2010). "MP2RAGE, a self bias-field corrected sequence for improved segmentation and T1-mapping at high field". en. In: *Neuroimage* 49.2, pp. 1271–1281.

Marques, José P and David G Norris (2018). "How to choose the right MR sequence for your research question at 7 T and above?" In: *Neuroimage* 168, pp. 119–140.

Martin, A and P Fedio (May 1983). "Word production and comprehension in Alzheimer's disease: the breakdown of semantic knowledge". en. In: *Brain Lang.* 19.1, pp. 124–141.

Martins de Carvalho, Luana et al. (Nov. 2019). "Effect of alcohol use disorder on cellular aging". en. In: *Psychopharmacology* 236.11, pp. 3245–3255.

Matthews, Kevin A et al. (2019). "Racial and ethnic estimates of Alzheimer's disease and related dementias in the United States (2015–2060) in adults aged ≥65 years". In: *Alzheimers. Dement.* 15.1, pp. 17–24.

Maynard, Christa J et al. (Nov. 2002). "Overexpression of Alzheimer's disease amyloid-beta opposes the age-dependent elevations of brain copper and iron". en. In: *J. Biol. Chem.* 277.47, pp. 44670–44676.

Mazerolle, Marc (Jan. 2006). "Improving data analysis in herpetology: using Akaike's Information Criterion (AIC) to assess the strength of biological hypotheses". en. In: *Amphib-reptil.* 27.2, pp. 169–180.

McIntosh, Anthony R and Bratislav Mišić (2013). "Multivariate statistical analyses for neuroimaging data". en. In: *Annu. Rev. Psychol.* 64, pp. 499–525.

McIntosh, Anthony Randal and Nancy J Lobaugh (2004). "Partial least squares analysis of neuroimaging data: applications and advances". en. In: *Neuroimage* 23 Suppl 1, S250–63.

McRobbie, Donald W et al. (2017). *MRI from Picture to Proton*. Cambridge university press.

Medawar, Evelyn et al. (Oct. 2021). "Estimating the effect of a scanner upgrade on measures of grey matter structure for longitudinal designs". en. In: *PLoS One* 16.10, e0239021.

Meeks, S and S A Murrell (Feb. 2001). "Contribution of education to health and life satisfaction in older adults mediated by negative affect". en. In: *J. Aging Health* 13.1, pp. 92–119.

Melhem, Elias R et al. (Jan. 2002). "Diffusion tensor MR imaging of the brain and white matter tractography". en. In: *AJR Am. J. Roentgenol.* 178.1, pp. 3–16.

Meng, Xiangfei and Carl D'Arcy (June 2012). "Education and dementia in the context of the cognitive reserve hypothesis: a systematic review with meta-analyses and qualitative analyses". en. In: *PLoS One* 7.6, e38268.

Menkin, Josephine A et al. (Aug. 2017). "Racial/Ethnic Differences in Expectations Regarding Aging Among Older Adults". en. In: *Gerontologist* 57.suppl_2, S138–S148.

Mesulam, M-M and S Weintraub (1992). "Primary Progressive Aphasia: Sharpening the Focus on a Clinical Syndrome". In: *Heterogeneity of Alzheimer's Disease*. Springer Berlin Heidelberg, pp. 43–66.

Miletić, Steven et al. (Apr. 2022). "Charting human subcortical maturation across the adult lifespan with in vivo 7 T MRI". en. In: *Neuroimage* 249, p. 118872.

Miller, Daniel J et al. (Oct. 2012). "Prolonged myelination in human neocortical evolution". en. In: *Proc. Natl. Acad. Sci. U. S. A.* 109.41, pp. 16480–16485.

Mirzaei, Golrokh and Hojjat Adeli (Dec. 2018). "Segmentation and clustering in brain MRI imaging". en. In: *Rev. Neurosci.* 30.1, pp. 31–44.

Möller, Christiane et al. (Feb. 2016). "Different patterns of cortical gray matter loss over time in behavioral variant frontotemporal dementia and Alzheimer's disease". en. In: *Neurobiol. Aging* 38, pp. 21–31.

Montagne, Axel et al. (Jan. 2015). "Blood-brain barrier breakdown in the aging human hippocampus". en. In: *Neuron* 85.2, pp. 296–302.

Moon, So Young et al. (Aug. 2017). "Associations between white matter hyperintensities and cognitive decline over three years in non-dementia older adults with memory complaints". en. In: *J. Neurol. Sci.* 379, pp. 266–270.

Morelli, Alessandro et al. (June 2012). "Impairment of heme synthesis in myelin as potential trigger of multiple sclerosis". en. In: *Med. Hypotheses* 78.6, pp. 707–710.

Moreno-Jiménez, Elena P et al. (Mar. 2021). "Evidences for Adult Hippocampal Neurogenesis in Humans". en. In: *J. Neurosci.* 41.12, pp. 2541–2553.

Mottershead, J P et al. (Nov. 2003). "High field MRI correlates of myelin content and axonal density in multiple sclerosis–a post-mortem study of the spinal cord". en. In: *J. Neurol.* 250.11, pp. 1293–1301.

Mountcastle, V B (Apr. 1997). "The columnar organization of the neocortex". en. In: *Brain* 120 (Pt 4), pp. 701–722.

Mueller, S G et al. (May 2007). "Measurement of hippocampal subfields and age-related changes with high resolution MRI at 4T". en. In: *Neurobiol. Aging* 28.5, pp. 719–726.

Mueller, Susanne G and Michael W Weiner (June 2009). "Selective effect of age, Apo e4, and Alzheimer's disease on hippocampal subfields". en. In: *Hippocampus* 19.6, pp. 558–564.

Mueller, Susanne G, Paul A Yushkevich, et al. (2018). "Systematic comparison of different techniques to measure hippocampal subfield volumes in ADNI2". In: *NeuroImage: Clinical* 17, pp. 1006–1018.

Mugler III, John P and James R Brookeman (1990). "Three-dimensional magnetization-prepared rapid gradient-echo imaging (3D MP RAGE)". In: *Magn. Reson. Med.* 15.1, pp. 152–157.

Mulder, Martijn J et al. (Apr. 2019). "Size and shape matter: The impact of voxel geometry on the identification of small nuclei". en. In: *PLoS One* 14.4, e0215382.

Muñoz-Ruiz, Miguel Ángel et al. (Dec. 2012). "Structural MRI in frontotemporal dementia: comparisons between hippocampal volumetry, tensor-based morphometry and voxel-based morphometry". en. In: *PLoS One* 7.12, e52531.

Munro, H N and M C Linder (Apr. 1978). "Ferritin: structure, biosynthesis, and role in iron metabolism". en. In: *Physiol. Rev.* 58.2, pp. 317–396.

Murty, Vishnu P et al. (Oct. 2010). "fMRI studies of successful emotional memory encoding: A quantitative meta-analysis". en. In: *Neuropsychologia* 48.12, pp. 3459–3469.

Nasreddine, Ziad S et al. (Apr. 2005). "The Montreal Cognitive Assessment, MoCA: a brief screening tool for mild cognitive impairment". en. In: *J. Am. Geriatr. Soc.* 53.4, pp. 695–699.

Nations, United (2017). "World population prospects: the 2017 revision, key findings and advance tables". In: *Department of Economics and Social Affairs PD, editor. New York: United Nations* 46.

Natu, Vaidehi S et al. (Oct. 2019). "Apparent thinning of human visual cortex during childhood is associated with myelination". en. In: *Proc. Natl. Acad. Sci. U. S. A.* 116.41, pp. 20750–20759.

Neddens, Joerg et al. (June 2018). "Phosphorylation of different tau sites during progression of Alzheimer's disease". en. In: *Acta Neuropathol Commun* 6.1, p. 52.

Nelson, Michael D et al. (1997). "Hippocampal volume reduction in schizophrenia as assessed by magnetic resonance imaging: A meta-analytic study". In: *Schizophr. Res.* 24.1-2, p. 153.

Neunuebel, Joshua P and James J Knierim (Jan. 2014). "CA3 retrieves coherent representations from degraded input: direct evidence for CA3 pattern completion and dentate gyrus pattern separation". en. In: *Neuron* 81.2, pp. 416–427.

Nieuwenhuys, Rudolf (Mar. 2013). "The myeloarchitectonic studies on the human cerebral cortex of the Vogt-Vogt school, and their significance for the interpretation of functional neuroimaging data". en. In: *Brain Struct. Funct.* 218.2, pp. 303–352.

Nilsson, Lars-Göran (2003). "Memory function in normal aging". en. In: *Acta Neurol. Scand. Suppl.* 179, pp. 7–13.

Nobis, Lisa et al. (June 2019). "Hippocampal volume across age: Nomograms derived from over 19,700 people in UK Biobank". en. In: *Neuroimage Clin* 23, p. 101904.

Noble, Kimberly G et al. (Nov. 2012). "Hippocampal volume varies with educational attainment across the life-span". en. In: *Front. Hum. Neurosci.* 6, p. 307.

Noble, Wendy et al. (July 2013). "The importance of tau phosphorylation for neurodegenerative diseases". en. In: *Front. Neurol.* 4, p. 83.

Nordahl, Christine Wu et al. (Oct. 2007). "Cortical folding abnormalities in autism revealed by surface-based morphometry". en. In: *J. Neurosci.* 27.43, pp. 11725–11735.

Nordin, Kristin et al. (2018). "Structural whole-brain covariance of the anterior and posterior hippocampus: Associations with age and memory". In: *Hippocampus* 28.2, pp. 151–163.

Norton, W (1976). "Formation, structure and biochemistry of myelin". In: *Basic neurochemistry.*

Nowakowski, R S and P Rakic (Feb. 1981). "The site of origin and route and rate of migration of neurons to the hippocampal region of the rhesus monkey". en. In: *J. Comp. Neurol.* 196.1, pp. 129–154.

Núñez, Marco T et al. (Aug. 2012). "Iron toxicity in neurodegeneration". en. In: *Biometals* 25.4, pp. 761–776.

Nyo, Myat Thet et al. (Dec. 2022). "Otsu's thresholding technique for MRI image brain tumor segmentation". en. In: *Multimed. Tools Appl.* 81.30, pp. 43837–43849.

O'Brien, J T et al. (Mar. 1997). "Magnetic resonance imaging correlates of memory impairment in the healthy elderly: association with medial temporal lobe atrophy but not white matter lesions". en. In: *Int. J. Geriatr. Psychiatry* 12.3, pp. 369–374.

O'Brien, Richard J and Philip C Wong (2011). "Amyloid precursor protein processing and Alzheimer's disease". en. In: *Annu. Rev. Neurosci.* 34, pp. 185–204.

O'Dwyer, Laurence et al. (Nov. 2012). "Reduced hippocampal volume in healthy young ApoE4 carriers: an MRI study". en. In: *PLoS One* 7.11, e48895.

O'Mara, Shane M et al. (June 2001). "The subiculum: a review of form, physiology and function". In: *Prog. Neurobiol.* 64.2, pp. 129–155.

O'Shea, Andrew et al. (Dec. 2016). "Cognitive Aging and the Hippocampus in Older Adults". en. In: *Front. Aging Neurosci.* 8, p. 298.

Odrobina, Ewa E et al. (Aug. 2005). "MR properties of excised neural tissue following experimentally induced demyelination". en. In: *NMR Biomed.* 18.5, pp. 277–284.

Okubo, Gosuke et al. (Jan. 2016). "MP2RAGE for deep gray matter measurement of the brain: A comparative study with MPRAGE". en. In: *J. Magn. Reson. Imaging* 43.1, pp. 55–62.

Oliveira, Francisco P M and João Manuel R S Tavares (2014). "Medical image registration: a review". en. In: *Comput. Methods Biomech. Biomed. Engin.* 17.2, pp. 73–93.

Olmastroni, Elena et al. (May 2022). "Statin use and risk of dementia or Alzheimer's disease: a systematic review and meta-analysis of observational studies". en. In: *Eur. J. Prev. Cardiol.* 29.5, pp. 804–814.

Olsen, Rosanna K et al. (Dec. 2019). "Progress update from the hippocampal subfields group". en. In: *Alzheimers. Dement.* 11, pp. 439–449.

Ossenkoppele, Rik et al. (Nov. 2015). "Atrophy patterns in early clinical stages across distinct phenotypes of Alzheimer's disease". en. In: *Hum. Brain Mapp.* 36.11, pp. 4421–4437.

Pakkenberg, Bente et al. (2003). "Aging and the human neocortex". en. In: *Exp. Gerontol.* 38.1-2, pp. 95–99.

Palmqvist, Sebastian et al. (Apr. 2016). "Cerebrospinal fluid analysis detects cerebral amyloid-β accumulation earlier than positron emission tomography". en. In: *Brain* 139.Pt 4, pp. 1226–1236.

Panizzon, Matthew S et al. (Nov. 2009). "Distinct genetic influences on cortical surface area and cortical thickness". en. In: *Cereb. Cortex* 19.11, pp. 2728–2735.

Papez, James W (Oct. 1937). "A PROPOSED MECHANISM OF EMOTION". In: *Arch NeurPsych* 38.4, pp. 725–743.

Papuć, Ewa and Konrad Rejdak (2020). "The role of myelin damage in Alzheimer's disease pathology". en. In: *Arch. Med. Sci.* 16.2, pp. 345–351.

Paquola, Casey et al. (May 2019). "Microstructural and functional gradients are increasingly dissociated in transmodal cortices". en. In: *PLoS Biol.* 17.5, e3000284.

Paradiso, S et al. (Jan. 1997). "Cerebellar size and cognition: correlations with IQ, verbal memory and motor dexterity". en. In: *Neuropsychiatry Neuropsychol. Behav. Neurol.* 10.1, pp. 1–8.

Parekh, Mansi B et al. (May 2015). "Ultra-high resolution in-vivo 7.0T structural imaging of the human hippocampus reveals the endfolial pathway". en. In: *Neuroimage* 112, pp. 1–6.

Parent, Olivier et al. (Mar. 2023). "High spatial overlap but diverging age-related trajectories of cortical magnetic resonance imaging markers aiming to represent intracortical myelin and microstructure". en. In: *Hum. Brain Mapp.*

Park, Jong Geun and Chulhee Lee (Oct. 2009). "Skull stripping based on region growing for magnetic resonance brain images". en. In: *Neuroimage* 47.4, pp. 1394–1407.

Passat, Nicolas et al. (June 2005). "Region-growing segmentation of brain vessels: an atlas-based automatic approach". en. In: *J. Magn. Reson. Imaging* 21.6, pp. 715–725.

Patel, Raihaan, Clare E Mackay, et al. (Aug. 2022). "Inter- and intra-individual variation in brain structural-cognition relationships in aging". en. In: *Neuroimage* 257, p. 119254.

Patel, Raihaan, Christopher J Steele, et al. (Feb. 2020). "Investigating microstructural variation in the human hippocampus using non-negative matrix factorization". en. In: *Neuroimage* 207, p. 116348.

Patenaude, Brian et al. (June 2011). "A Bayesian model of shape and appearance for subcortical brain segmentation". en. In: *Neuroimage* 56.3, pp. 907–922.

Patzke, Nina et al. (Jan. 2015). "In contrast to many other mammals, cetaceans have relatively small hippocampi that appear to lack adult neurogenesis". en. In: *Brain Struct. Funct.* 220.1, pp. 361–383.

Pereira, Joana B et al. (Apr. 2014). "Regional vulnerability of hippocampal subfields to aging measured by structural and diffusion MRI". en. In: *Hippocampus* 24.4, pp. 403–414.

Periaswamy, Senthil and Hany Farid (July 2003). "Elastic registration in the presence of intensity variations". en. In: *IEEE Trans. Med. Imaging* 22.7, pp. 865–874.

Permanyer, Iñaki and Diederik Boertien (Feb. 2019). "A century of change in global education variability and gender differences in education". en. In: *PLoS One* 14.2, e0212692.

Perry, V Hugh, James A R Nicoll, and Clive Holmes (Apr. 2010). "Microglia in neurodegenerative disease". en. In: *Nat. Rev. Neurol.* 6.4, pp. 193–201.

Peters, A, K Josephson, and S L Vincent (Mar. 1991). "Effects of aging on the neuroglial cells and pericytes within area 17 of the rhesus monkey cerebral cortex". en. In: *Anat. Rec.* 229.3, pp. 384–398.

Peterson, Diana C, Vamsi Reddy, and Debra A Mayes (Aug. 2022). "Neuroanatomy, Mammillary Bodies". In: *StatPearls*. Treasure Island (FL): StatPearls Publishing.

Petralia, Ronald S, Mark P Mattson, and Pamela J Yao (Mar. 2014). "Communication breakdown: the impact of ageing on synapse structure". en. In: *Ageing Res. Rev.* 14, pp. 31–42.

Pfrieger, F W and B A Barres (Dec. 1995). "What the fly's glia tell the fly's brain". en. In: *Cell* 83.5, pp. 671–674.

Pienaar, R et al. (June 2008). "A METHODOLOGY FOR ANALYZING CURVATURE IN THE DEVELOPING BRAIN FROM PRETERM TO ADULT". en. In: *Int. J. Imaging Syst. Technol.* 18.1, pp. 42–68.

Pievani, Michela et al. (Apr. 2011). "APOE4 is associated with greater atrophy of the hippocampal formation in Alzheimer's disease". en. In: *Neuroimage* 55.3, pp. 909–919.

Pink, Anna et al. (2017). "Cortical Thickness and Anxiety Symptoms Among Cognitively Normal Elderly Persons: The Mayo Clinic Study of Aging". en. In: *J. Neuropsychiatry Clin. Neurosci.* 29.1, pp. 60–66.

Pipitone, Jon et al. (Nov. 2014). "Multi-atlas segmentation of the whole hippocampus and subfields using multiple automatically generated templates". en. In: *Neuroimage* 101, pp. 494–512.

Piras, Fabrizio et al. (Feb. 2011). "Education mediates microstructural changes in bilateral hippocampus". en. In: *Hum. Brain Mapp.* 32.2, pp. 282–289.

Plitman, Eric et al. (Sept. 2021). "The impact of the Siemens Tim Trio to Prisma upgrade and the addition of volumetric navigators on cortical thickness, structure volume, and 1H-MRS indices: An MRI reliability study with implications for longitudinal study designs". In: *Neuroimage* 238, p. 118172.

Pluta, John et al. (2012). "In vivo analysis of hippocampal subfield atrophy in mild cognitive impairment via semi-automatic segmentation of T2-weighted MRI". en. In: *J. Alzheimers. Dis.* 31.1, pp. 85–99.

Pol, L A van de et al. (Apr. 2006). "Hippocampal atrophy on MRI in frontotemporal lobar degeneration and Alzheimer's disease". en. In: *J. Neurol. Neurosurg. Psychiatry* 77.4, pp. 439–442.

Pol, L A van de et al. (2006). "Hippocampal atrophy in Alzheimer disease: Age matters". In: *Neurology* 66.2, pp. 236–238.

Popugaeva, Elena, Ekaterina Pchitskaya, and Ilya Bezprozvanny (Oct. 2018). "Dysregulation of Intracellular Calcium Signaling in Alzheimer's Disease". en. In: *Antioxid. Redox Signal.* 29.12, pp. 1176–1188.

Porter, Verna R et al. (2003). "Frequency and characteristics of anxiety among patients with Alzheimer's disease and related dementias". en. In: *J. Neuropsychiatry Clin. Neurosci.* 15.2, pp. 180–186.

Poulin, Stéphane P et al. (Oct. 2011). "Amygdala atrophy is prominent in early Alzheimer's disease and relates to symptom severity". en. In: *Psychiatry Res.* 194.1, pp. 7–13.

Prasloski, Thomas et al. (Oct. 2012). "Rapid whole cerebrum myelin water imaging using a 3D GRASE sequence". en. In: *Neuroimage* 63.1, pp. 533–539.

Pruessner, J C et al. (Jan. 2001). "Age and gender predict volume decline in the anterior and posterior hippocampus in early adulthood". en. In: *J. Neurosci.* 21.1, pp. 194–200.

Przeździk, Izabela et al. (Oct. 2019). "The functional organisation of the hippocampus along its long axis is gradual and predicts recollection". en. In: *Cortex* 119, pp. 324–335.

Puglielli, Luigi, Rudolph E Tanzi, and Dora M Kovacs (Apr. 2003). "Alzheimer's disease: the cholesterol connection". en. In: *Nat. Neurosci.* 6.4, pp. 345–351.

Puig, Sergi et al. (Nov. 2017). "The elemental role of iron in DNA synthesis and repair". en. In: *Metallomics* 9.11, pp. 1483–1500.

Purcell, E M, H C Torrey, and R V Pound (Jan. 1946). "Resonance Absorption by Nuclear Magnetic Moments in a Solid". In: *Phys. Rev.* 69.1-2, pp. 37–38.

Rajan, Kumar B et al. (Dec. 2021). "Population estimate of people with clinical Alzheimer's disease and mild cognitive impairment in the United States (2020-2060)". en. In: *Alzheimers. Dement.* 17.12, pp. 1966–1975.

Rajmohan, V and E Mohandas (Apr. 2007). "The limbic system". en. In: *Indian J. Psychiatry* 49.2, pp. 132–139.

Rakic, P (July 1988). "Specification of cerebral cortical areas". en. In: *Science* 241.4862, pp. 170–176.

— (Sept. 1995). "A small step for the cell, a giant leap for mankind: a hypothesis of neocortical expansion during evolution". en. In: *Trends Neurosci.* 18.9, pp. 383–388.

— (2000). "Radial unit hypothesis of neocortical expansion". en. In: *Novartis Found. Symp.* 228, 30–42, discussion 42–52.

Rakic, Pasko (Oct. 2007). "The radial edifice of cortical architecture: From neuronal silhouettes to genetic engineering". In: *Brain Res. Rev.* 55.2, pp. 204–219.

Ramon Cajal and Azoulay (1909). "Histologie du système nerveux de l'homme et des vertébrés". In: *Histologie du systeme nerveux.*

Ramón y Cajal, Santiago (1899). *Textura del sistema nervioso del hombre y de los vertebrados: estudios sobre el plan estructural y composición histológica de los centros nerviosos adicionados de consideraciones fisiológicas fundadas en los nuevos descubrimientos.* es. Moya.

Randolph, Christopher et al. (1998). "The Repeatable Battery for the Assessment of Neuropsychological Status (RBANS): Preliminary Clinical Validity". In: *J. Clin. Exp. Neuropsychol.* 20.3, pp. 310–319.

Raven, Erika P et al. (2013). "Increased iron levels and decreased tissue integrity in hippocampus of Alzheimer's disease detected in vivo with magnetic resonance imaging". en. In: *J. Alzheimers. Dis.* 37.1, pp. 127–136.

Rawle, Mark James et al. (2018). "Apolipoprotein-E (Apoe) $\epsilon 4$ and cognitive decline over the adult life course". In: *Transl. Psychiatry* 8.1.

Raz, N et al. (Feb. 2004). "Differential aging of the medial temporal lobe: a study of a five-year change". en. In: *Neurology* 62.3, pp. 433–438.

Raz, Naftali, Ana M Daugherty, et al. (Sept. 2015). "Volume of the hippocampal subfields in healthy adults: differential associations with age and a pro-inflammatory genetic variant". en. In: *Brain Struct. Funct.* 220.5, pp. 2663–2674.

Raz, Naftali, Karen M Rodrigue, and E Mark Haacke (Feb. 2007). "Brain aging and its modifiers: insights from in vivo neuromorphometry and susceptibility weighted imaging". en. In: *Ann. N. Y. Acad. Sci.* 1097, pp. 84–93.

Raznahan, Armin et al. (Jan. 2014). "Longitudinal four-dimensional mapping of subcortical anatomy in human development". en. In: *Proc. Natl. Acad. Sci. U. S. A.* 111.4, pp. 1592–1597.

Refolo, L M, B Malester, et al. (Aug. 2000). "Hypercholesterolemia accelerates the Alzheimer's amyloid pathology in a transgenic mouse model". en. In: *Neurobiol. Dis.* 7.4, pp. 321–331.

Refolo, L M, M A Pappolla, et al. (Oct. 2001). "A cholesterol-lowering drug reduces beta-amyloid pathology in a transgenic mouse model of Alzheimer's disease". en. In: *Neurobiol. Dis.* 8.5, pp. 890–899.

Reinert, Anja et al. (May 2019). "Iron concentrations in neurons and glial cells with estimates on ferritin concentrations". en. In: *BMC Neurosci.* 20.1, p. 25.

Reiss, Allison B et al. (Aug. 2018). "Amyloid toxicity in Alzheimer's disease". en. In: *Rev. Neurosci.* 29.6, pp. 613–627.

Resing, H A and H C Torrey (Aug. 1963). "Nuclear Spin Relaxation by Translational Diffusion. III. Spin-Spin Relaxation". In: *Phys. Rev.* 131.3, pp. 1102–1104.

Rettmann, Maryam E et al. (Nov. 2006). "Cross-sectional and longitudinal analyses of anatomical sulcal changes associated with aging". en. In: *Cereb. Cortex* 16.11, pp. 1584–1594.

Reuter, Martin, Nicholas J Schmansky, et al. (July 2012). "Within-subject template estimation for unbiased longitudinal image analysis". en. In: *Neuroimage* 61.4, pp. 1402–1418.

Reuter, Martin, M Dylan Tisdall, et al. (Feb. 2015). "Head motion during MRI acquisition reduces gray matter volume and thickness estimates". en. In: *Neuroimage* 107, pp. 107–115.

Rindfleisch, Aric et al. (June 2008). "Cross-Sectional versus Longitudinal Survey Research: Concepts, Findings, and Guidelines". In: *J. Mark. Res.* 45.3, pp. 261–279.

Ritchie, Stuart J et al. (Dec. 2015). "Brain volumetric changes and cognitive ageing during the eighth decade of life". en. In: *Hum. Brain Mapp.* 36.12, pp. 4910–4925.

Robert, Vincent et al. (May 2021). "Local circuit allowing hypothalamic control of hippocampal area CA2 activity and consequences for CA1". en. In: *Elife* 10.

Rombouts, Serge A R B et al. (Dec. 2007). "Whole brain analysis of T2* weighted baseline FMRI signal in dementia". en. In: *Hum. Brain Mapp.* 28.12, pp. 1313–1317.

Romero, José E, Pierrick Coupé, and José V Manjón (Dec. 2017). "HIPS: A new hippocampus subfield segmentation method". en. In: *Neuroimage* 163, pp. 286–295.

Roseborough, Austyn D et al. (Jan. 2023). "White matter hyperintensities and longitudinal cognitive decline in cognitively normal populations and across diagnostic categories: A meta-analysis, systematic review, and recommendations for future study harmonization". en. In: *Alzheimers. Dement.* 19.1, pp. 194–207.

Rousseau, Françcois, Piotr A Habas, and Colin Studholme (Oct. 2011). "A supervised patch-based approach for human brain labeling". en. In: *IEEE Trans. Med. Imaging* 30.10, pp. 1852–1862.

Rowe, J W and R L Kahn (July 1987). "Human aging: usual and successful". en. In: *Science* 237.4811, pp. 143–149.

Ruthotto, Lars, Erlend Hodneland, and Jan Modersitzki (2012). "Registration of Dynamic Contrast Enhanced MRI with Local Rigidity Constraint". In: *Biomedical Image Registration*. Springer Berlin Heidelberg, pp. 190–198.

Ruthotto, Lars and Jan Modersitzki (Jan. 2015). "Non-linear Image Registration". en. In: *Handbook of Mathematical Methods in Imaging*. New York, NY: Springer New York, pp. 2005–2051.

Saab, Aiman S and Klaus-Armin Nave (Dec. 2017). "Myelin dynamics: protecting and shaping neuronal functions". en. In: *Curr. Opin. Neurobiol.* 47, pp. 104–112.

Saab, Aiman S, Iva D Tzvetanova, and Klaus-Armin Nave (Dec. 2013). "The role of myelin and oligodendrocytes in axonal energy metabolism". en. In: *Curr. Opin. Neurobiol.* 23.6, pp. 1065–1072.

Sabuncu, Mert R et al. (Aug. 2011). "The dynamics of cortical and hippocampal atrophy in Alzheimer disease". en. In: *Arch. Neurol.* 68.8, pp. 1040–1048.

Salami, Alireza et al. (Apr. 2021). "Elevated neuroinflammation contributes to the deleterious impact of iron overload on brain function in aging". en. In: *Neuroimage* 230, p. 117792.

Salat, D H et al. (Oct. 2009). "Age-associated alterations in cortical gray and white matter signal intensity and gray to white matter contrast". en. In: *Neuroimage* 48.1, pp. 21–28.

Sankar, Tejas et al. (June 2017). "Your algorithm might think the hippocampus grows in Alzheimer's disease: Caveats of longitudinal automated hippocampal volumetry". en. In: *Hum. Brain Mapp.* 38.6, pp. 2875–2896.

Sasabayashi, Daiki et al. (Mar. 2021). "Reduced Hippocampal Subfield Volume in Schizophrenia and Clinical High-Risk State for Psychosis". en. In: *Front. Psychiatry* 12, p. 642048.

Sasaki, Takuya et al. (Feb. 2018). "Dentate network activity is necessary for spatial working memory by supporting CA3 sharp-wave ripple generation and prospective firing of CA3 neurons". en. In: *Nat. Neurosci.* 21.2, pp. 258–269.

Schaer, Marie et al. (Jan. 2012). "How to measure cortical folding from MR images: a step-by-step tutorial to compute local gyrification index". en. In: *J. Vis. Exp.* 59, e3417.

Schmierer, Klaus, Francesco Scaravilli, et al. (Sept. 2004). "Magnetization transfer ratio and myelin in postmortem multiple sclerosis brain". en. In: *Ann. Neurol.* 56.3, pp. 407–415.

Schmierer, Klaus, Claudia A M Wheeler-Kingshott, et al. (Feb. 2008). "Quantitative magnetic resonance of postmortem multiple sclerosis brain before and after fixation". en. In: *Magn. Reson. Med.* 59.2, pp. 268–277.

Schoemaker, Dorothee et al. (Apr. 2016). "Hippocampus and amygdala volumes from magnetic resonance images in children: Assessing accuracy of FreeSurfer and FSL against manual segmentation". en. In: *Neuroimage* 129, pp. 1–14.

Schuff, N et al. (Apr. 2009). "MRI of hippocampal volume loss in early Alzheimer's disease in relation to ApoE genotype and biomarkers". en. In: *Brain* 132.Pt 4, pp. 1067–1077.

Scott, S A et al. (Oct. 1992). "Amygdala cell loss and atrophy in Alzheimer's disease". en. In: *Ann. Neurol.* 32.4, pp. 555–563.

Scoville, W B and B Milner (Feb. 1957). "Loss of recent memory after bilateral hippocampal lesions". en. In: *J. Neurol. Neurosurg. Psychiatry* 20.1, pp. 11–21.

Seeley, William W et al. (2009). "Neurodegenerative Diseases Target Large-Scale Human Brain Networks". In: *Neuron* 62.1, pp. 42–52.

Sezgin, Mehmet and Bülent Sankur (Jan. 2004). "Survey over image thresholding techniques and quantitative performance evaluation". en. In: *JEI* 13.1, pp. 146–165.

Shafiei, Golia et al. (Apr. 2020). "Spatial Patterning of Tissue Volume Loss in Schizophrenia Reflects Brain Network Architecture". en. In: *Biol. Psychiatry* 87.8, pp. 727–735.

Shafto, Meredith A et al. (Oct. 2014). "The Cambridge Centre for Ageing and Neuroscience (Cam-CAN) study protocol: a cross-sectional, lifespan, multidisciplinary examination of healthy cognitive ageing". en. In: *BMC Neurol.* 14, p. 204.

Shams, Zahra, David G Norris, and José P Marques (July 2019). "A comparison of in vivo MRI based cortical myelin mapping using T1w/T2w and R1 mapping at 3T". en. In: *PLoS One* 14.7, e0218089.

Shaw, Philip et al. (July 2014). "Mapping the development of the basal ganglia in children with attention-deficit/hyperactivity disorder". en. In: *J. Am. Acad. Child Adolesc. Psychiatry* 53.7, 780–9.e11.

Shaw, Thomas B et al. (Dec. 2019). "Non-linear realignment improves hippocampus subfield segmentation reliability". en. In: *Neuroimage* 203, p. 116206.

Shi, Jie et al. (2014). "Genetic influence of apolipoprotein E4 genotype on hippocampal morphometry: An N= 725 surface-based Alzheimer's disease neuroimaging initiative study". In: *Hum. Brain Mapp.* 35.8, pp. 3903–3918.

Shin, Hyeong-Geol et al. (Oct. 2021). "X-separation: Magnetic susceptibility source separation toward iron and myelin mapping in the brain". en. In: *Neuroimage* 240, p. 118371.

Shing, Yee Lee et al. (Feb. 2011). "Hippocampal subfield volumes: age, vascular risk, and correlation with associative memory". en. In: *Front. Aging Neurosci.* 3, p. 2.

Sicotte, N L et al. (Apr. 2008). "Regional hippocampal atrophy in multiple sclerosis". en. In: *Brain* 131.Pt 4, pp. 1134–1141.

Singh, Amanjot and Jagroop Singh (2016). "Comparative analysis of gaussian filter with wavelet denoising for various noises present in images". In: *Indian J. Sci. Technol.* 9.47.

Singh, Vivek et al. (Nov. 2006). "Spatial patterns of cortical thinning in mild cognitive impairment and Alzheimer's disease". en. In: *Brain* 129.Pt 11, pp. 2885–2893.

Skoog, Ingmar and Deborah Gustafson (Sept. 2006). "Update on hypertension and Alzheimer's disease". en. In: *Neurol. Res.* 28.6, pp. 605–611.

Slater, David A et al. (May 2019). "Evolution of white matter tract microstructure across the life span". en. In: *Hum. Brain Mapp.* 40.7, pp. 2252–2268.

Sled, J G and G B Pike (Nov. 2001). "Quantitative imaging of magnetization transfer exchange and relaxation properties in vivo using MRI". en. In: *Magn. Reson. Med.* 46.5, pp. 923–931.

Sled, J G, A P Zijdenbos, and A C Evans (1998). "A nonparametric method for automatic correction of intensity nonuniformity in MRI data". In: *IEEE transactions on.*

Sled, John G (Nov. 2018). "Modelling and interpretation of magnetization transfer imaging in the brain". en. In: *Neuroimage* 182, pp. 128–135.

Sliwinski, M and H Buschke (Mar. 1999). "Cross-sectional and longitudinal relationships among age, cognition, and processing speed". en. In: *Psychol. Aging* 14.1, pp. 18–33.

Small, Scott A et al. (Sept. 2011). "A pathophysiological framework of hippocampal dysfunction in ageing and disease". en. In: *Nat. Rev. Neurosci.* 12.10, pp. 585–601.

Smith, Charles D et al. (June 2009). "MRI diffusion tensor tracking of a new amygdalofusiform and hippocampo-fusiform pathway system in humans". en. In: *J. Magn. Reson. Imaging* 29.6, pp. 1248–1261.

Smith, Grafton Elliot (1907). *Journal of Anatomy and Physiology: A new topographical survey of the human cerebral cortex, being an account of the distribution of the anatomically distinct cortical areas and their relationship to the cerebral sulci.* en.

Smith, Stephen M (Nov. 2002). "Fast robust automated brain extraction". en. In: *Hum. Brain Mapp.* 17.3, pp. 143–155.

Smith, T B and K S Nayak (2010). "MRI artifacts and correction strategies". In: *Imaging Med.*

Sorrells, Shawn F et al. (Mar. 2018). "Human hippocampal neurogenesis drops sharply in children to undetectable levels in adults". en. In: *Nature* 555.7696, pp. 377–381.

Sotiras, Aristeidis, Christos Davatzikos, and Nikos Paragios (July 2013). "Deformable medical image registration: a survey". en. In: *IEEE Trans. Med. Imaging* 32.7, pp. 1153–1190.

Sotiras, Aristeidis, Susan M Resnick, and Christos Davatzikos (Mar. 2015). "Finding imaging patterns of structural covariance via Non-Negative Matrix Factorization". en. In: *Neuroimage* 108, pp. 1–16.

Soto, Claudio (Jan. 2003). "Unfolding the role of protein misfolding in neurodegenerative diseases". en. In: *Nat. Rev. Neurosci.* 4.1, pp. 49–60.

Sowell, Elizabeth R et al. (Mar. 2003). "Mapping cortical change across the human life span". en. In: *Nat. Neurosci.* 6.3, pp. 309–315.

Spalding, Kirsty L et al. (June 2013). "Dynamics of hippocampal neurogenesis in adult humans". en. In: *Cell* 153.6, pp. 1219–1227.

Sparks, D L et al. (Mar. 1994). "Induction of Alzheimer-like beta-amyloid immunoreactivity in the brains of rabbits with dietary cholesterol". en. In: *Exp. Neurol.* 126.1, pp. 88–94.

Spencer, Robert J et al. (2013). "Psychometric limitations of the mini-mental state examination among nondemented older adults: an evaluation of neurocognitive and magnetic resonance imaging correlates". en. In: *Exp. Aging Res.* 39.4, pp. 382–397.

Sperling, Reisa A et al. (May 2011). "Toward defining the preclinical stages of Alzheimer's disease: recommendations from the National Institute on Aging-Alzheimer's Association workgroups on diagnostic guidelines for Alzheimer's disease". en. In: *Alzheimers. Dement.* 7.3, pp. 280–292.

Spina, Salvatore et al. (Aug. 2021). "Comorbid neuropathological diagnoses in early versus late-onset Alzheimer's disease". en. In: *Brain* 144.7, pp. 2186–2198.

Stadelmann, Christine et al. (July 2019). "Myelin in the Central Nervous System: Structure, Function, and Pathology". en. In: *Physiol. Rev.* 99.3, pp. 1381–1431.

Staff, Roger T et al. (May 2006). "Generality and specificity in cognitive aging: a volumetric brain analysis". en. In: *Neuroimage* 30.4, pp. 1433–1440.

Stanley, Karen et al. (2019). "Rate of Cognitive Decline in Alzheimer's Disease Stratified by Age". en. In: *J. Alzheimers. Dis.* 69.4, pp. 1153–1160.

Stern, Yaakov (Mar. 2002). "What is cognitive reserve? Theory and research application of the reserve concept". en. In: *J. Int. Neuropsychol. Soc.* 8.3, pp. 448–460.

— (Aug. 2009). "Cognitive reserve". en. In: *Neuropsychologia* 47.10, pp. 2015–2028.

Stikov, Nikola et al. (Feb. 2015). "On the accuracy of T1 mapping: searching for common ground". en. In: *Magn. Reson. Med.* 73.2, pp. 514–522.

Stockmeier, Craig A et al. (Nov. 2004). "Cellular changes in the postmortem hippocampus in major depression". en. In: *Biol. Psychiatry* 56.9, pp. 640–650.

Storsve, Andreas B et al. (June 2014). "Differential longitudinal changes in cortical thickness, surface area and volume across the adult life span: regions of accelerating and decelerating change". en. In: *J. Neurosci.* 34.25, pp. 8488–8498.

Stranahan, Alexis M and Mark P Mattson (Dec. 2010). "Selective vulnerability of neurons in layer II of the entorhinal cortex during aging and Alzheimer's disease". en. In: *Neural Plast.* 2010, p. 108190.

Strange, B A et al. (Mar. 1999). "Segregating the functions of human hippocampus". en. In: *Proc. Natl. Acad. Sci. U. S. A.* 96.7, pp. 4034–4039.

Strange, Bryan A et al. (Oct. 2014). "Functional organization of the hippocampal longitudinal axis". en. In: *Nat. Rev. Neurosci.* 15.10, pp. 655–669.

Strien, N M van, N L M Cappaert, and M P Witter (Apr. 2009). "The anatomy of memory: an interactive overview of the parahippocampal–hippocampal network". In: *Nat. Rev. Neurosci.* 10.4, pp. 272–282.

Stüber, Carsten et al. (2014). "Myelin and iron concentration in the human brain: A quantitative study of MRI contrast". In: *Neuroimage* 93, pp. 95–106.

Sullivan, E V et al. (July 1995). "Age-related decline in MRI volumes of temporal lobe gray matter but not hippocampus". en. In: *Neurobiol. Aging* 16.4, pp. 591–606.

Sullivan, Edith V, Laura Marsh, and Adolf Pfefferbaum (July 2005). "Preservation of hippocampal volume throughout adulthood in healthy men and women". en. In: *Neurobiol. Aging* 26.7, pp. 1093–1098.

Svarer, Claus et al. (Feb. 2005). "MR-based automatic delineation of volumes of interest in human brain PET images using probability maps". en. In: *Neuroimage* 24.4, pp. 969–979.

Swarbrick, S et al. (Sept. 2019). "Systematic Review of miRNA as Biomarkers in Alzheimer's Disease". en. In: *Mol. Neurobiol.* 56.9, pp. 6156–6167.

Ta, Anh Tuan et al. (2012). "Age-related vulnerabilities along the hippocampal longitudinal axis". In: *Hum. Brain Mapp.* 33.10, pp. 2415–2427.

Tamnes, Christian K et al. (Mar. 2013). "Brain development and aging: overlapping and unique patterns of change". en. In: *Neuroimage* 68, pp. 63–74.

Tan, Chen-Chen et al. (2014). "Efficacy and safety of donepezil, galantamine, rivastigmine, and memantine for the treatment of Alzheimer's disease: a systematic review and meta-analysis". en. In: *J. Alzheimers. Dis.* 41.2, pp. 615–631.

Tang, Lingfei et al. (June 2020). "Differential Functional Connectivity in Anterior and Posterior Hippocampus Supporting the Development of Memory Formation". en. In: *Front. Hum. Neurosci.* 14, p. 204.

Tappia, P S, K L Troughton, et al. (1995). "Cigarette smoking influences cytokine production and antioxidant defences". In: *Clin. Sci.*

Tardif, Christine L, Barry J Bedell, et al. (Nov. 2012). "Quantitative magnetic resonance imaging of cortical multiple sclerosis pathology". en. In: *Mult. Scler. Int.* 2012, p. 742018.

Tardif, Christine L, Gabriel A Devenyi, et al. (Feb. 2018). "Regionally specific changes in the hippocampal circuitry accompany progression of cerebrospinal fluid biomarkers in preclinical Alzheimer's disease". en. In: *Hum. Brain Mapp.* 39.2, pp. 971–984.

Tardif, Christine Lucas et al. (May 2016a). "Advanced MRI techniques to improve our understanding of experience-induced neuroplasticity". en. In: *Neuroimage* 131, pp. 55–72.

— (May 2016b). "Advanced MRI techniques to improve our understanding of experience-induced neuroplasticity". en. In: *Neuroimage* 131, pp. 55–72.

Tax, Chantal M W et al. (Aug. 2021). "Measuring compartmental T2-orientational dependence in human brain white matter using a tiltable RF coil and diffusion-T2 correlation MRI". en. In: *Neuroimage* 236, p. 117967.

Taylor, Jason R et al. (2017). "The Cambridge Centre for Ageing and Neuroscience (Cam-CAN) data repository: Structural and functional MRI, MEG, and cognitive data from a cross-sectional adult lifespan sample". In: *Neuroimage* 144, pp. 262–269.

Taylor, Joy L et al. (Nov. 2014). "APOE-epsilon4 and aging of medial temporal lobe gray matter in healthy adults older than 50 years". en. In: *Neurobiol. Aging* 35.11, pp. 2479–2485.

Telegina, Darya V et al. (Nov. 2019). "Mechanisms of Neuronal Death in the Cerebral Cortex during Aging and Development of Alzheimer's Disease-Like Pathology in Rats". en. In: *Int. J. Mol. Sci.* 20.22.

Teri, L et al. (July 1999). "Anxiety of Alzheimer's disease: prevalence, and comorbidity". en. In: *J. Gerontol. A Biol. Sci. Med. Sci.* 54.7, pp. M348–52.

Teyler, Timothy J and Pascal Discenna (June 1984). "The topological anatomy of the hippocampus: A clue to its function". In: *Brain Res. Bull.* 12.6, pp. 711–719.

Thelen, K M et al. (July 2006). "Cholesterol synthesis rate in human hippocampus declines with aging". en. In: *Neurosci. Lett.* 403.1-2, pp. 15–19.

Thiessen, Jonathan D et al. (Nov. 2013). "Quantitative MRI and ultrastructural examination of the cuprizone mouse model of demyelination". en. In: *NMR Biomed.* 26.11, pp. 1562–1581.

Thirupathi, Anand and Yan-Zhong Chang (2019). "Brain Iron Metabolism and CNS Diseases". In: *Brain Iron Metabolism and CNS Diseases*, pp. 1–19.

Thomas, David L et al. (June 2004). "High-resolution fast spin echo imaging of the human brain at 4.7 T: implementation and sequence characteristics". en. In: *Magn. Reson. Med.* 51.6, pp. 1254–1264.

Thompson, Deanne K et al. (Aug. 2014). "Longitudinal growth and morphology of the hippocampus through childhood: Impact of prematurity and implications for memory and learning". en. In: *Hum. Brain Mapp.* 35.8, pp. 4129–4139.

Tihonov, A N (1963). "Solution of incorrectly formulated problems and the regularization method". In: *Soviet Math.* 4, pp. 1035–1038.

Tisserand, Danielle J et al. (Sept. 2004). "A voxel-based morphometric study to determine individual differences in gray matter density associated with age and cognitive change over time". en. In: *Cereb. Cortex* 14.9, pp. 966–973.

Todorich, Bozho et al. (Apr. 2009). "Oligodendrocytes and myelination: the role of iron". en. In: *Glia* 57.5, pp. 467–478.

Toga, A W and P M Thompson (Jan. 2001). "The role of image registration in brain mapping". en. In: *Image Vis. Comput.* 19.1-2, pp. 3–24.

Toledo-Morrell, L de et al. (2000). "Hemispheric differences in hippocampal volume predict verbal and spatial memory performance in patients with Alzheimer's disease". en. In: *Hippocampus* 10.2, pp. 136–142.

Tombaugh, T N and N J McIntyre (Sept. 1992). "The mini-mental state examination: a comprehensive review". en. In: *J. Am. Geriatr. Soc.* 40.9, pp. 922–935.

Treadway, Michael T et al. (Feb. 2015). "Illness progression, recent stress, and morphometry of hippocampal subfields and medial prefrontal cortex in major depression". en. In: *Biol. Psychiatry* 77.3, pp. 285–294.

Tremblay-Mercier, Jennifer et al. (June 2021). "Open science datasets from PREVENT-AD, a longitudinal cohort of pre-symptomatic Alzheimer's disease". en. In: *NeuroImage Clin.* 31.102733, p. 102733.

Treves, A and E T Rolls (June 1994). "Computational analysis of the role of the hippocampus in memory". en. In: *Hippocampus* 4.3, pp. 374–391.

Trofimova, Olga et al. (June 2021). "Brain tissue properties link cardio-vascular risk factors, mood and cognitive performance in the CoLaus—PsyCoLaus epidemiological cohort". en. In: *Neurobiol. Aging* 102, pp. 50–63.

Truong, Trong-Kha et al. (Feb. 2006). "Effects of static and radiofrequency magnetic field inhomogeneity in ultra-high field magnetic resonance imaging". en. In: *Magn. Reson. Imaging* 24.2, pp. 103–112.

Trzepacz, Paula T et al. (Sept. 2015). "Relationship between the Montreal Cognitive Assessment and Mini-mental State Examination for assessment of mild cognitive impairment in older adults". en. In: *BMC Geriatr.* 15, p. 107.

Tsushima, Yoshito and Keigo Endo (July 2006). "Hypointensities in the brain on T2*-weighted gradient-echo magnetic resonance imaging". en. In: *Curr. Probl. Diagn. Radiol.* 35.4, pp. 140–150.

Tucker-Drob, Elliot M and Timothy A Salthouse (2011). "in Cognitive Aging". In: *The Wiley-Blackwell handbook of individual differences*, p. 242.

Tullberg, M et al. (July 2004). "White matter lesions impair frontal lobe function regardless of their location". en. In: *Neurology* 63.2, pp. 246–253.

Tullo, Stephanie et al. (2019). "MR-based age-related effects on the striatum, globus pallidus, and thalamus in healthy individuals across the adult lifespan". In: *Hum. Brain Mapp.* 40.18, pp. 5269–5288.

Tustison, Nicholas J et al. (June 2010). "N4ITK: improved N3 bias correction". en. In: *IEEE Trans. Med. Imaging* 29.6, pp. 1310–1320.

Tzourio-Mazoyer, N et al. (Jan. 2002). "Automated anatomical labeling of activations in SPM using a macroscopic anatomical parcellation of the MNI MRI single-subject brain". en. In: *Neuroimage* 15.1, pp. 273–289.

Umeda, Tomohiro et al. (Dec. 2012). "Hypercholesterolemia accelerates intraneuronal accumulation of Aβ oligomers resulting in memory impairment in Alzheimer's disease model mice". en. In: *Life Sci.* 91.23-24, pp. 1169–1176.

United Nations (Jan. 2020). *World Economic Situation and Prospects 2020*. en. United Nations.

Vaishali, S, K Kishan Rao, and G V Subba Rao (Jan. 2015). "A review on noise reduction methods for brain MRI images". In: *2015 International Conference on Signal Processing and Communication Engineering Systems*, pp. 363–365.

Van Leemput, Koen et al. (2009). "Automated segmentation of hippocampal subfields from ultra-high resolution in vivo MRI". In: *Hippocampus* 19.6, pp. 549–557.

Van Petten, Cyma et al. (2004). "Memory and executive function in older adults: relationships with temporal and prefrontal gray matter volumes and white matter hyperintensities". en. In: *Neuropsychologia* 42.10, pp. 1313–1335.

Vance, Jean E (Nov. 2012). "Dysregulation of cholesterol balance in the brain: contribution to neurodegenerative diseases". en. In: *Dis. Model. Mech.* 5.6, pp. 746–755.

Vasile, Flora, Elena Dossi, and Nathalie Rouach (July 2017). "Human astrocytes: structure and functions in the healthy brain". en. In: *Brain Struct. Funct.* 222.5, pp. 2017–2029.

Vereecken, T H, O J Vogels, and R Nieuwenhuys (1994). "Neuron loss and shrinkage in the amygdala in Alzheimer's disease". en. In: *Neurobiol. Aging* 15.1, pp. 45–54.

Videbech, Poul and Barbara Ravnkilde (Nov. 2004). "Hippocampal volume and depression: a meta-analysis of MRI studies". en. In: *Am. J. Psychiatry* 161.11, pp. 1957–1966.

Visser, P J et al. (Apr. 2002). "Medial temporal lobe atrophy predicts Alzheimer's disease in patients with minor cognitive impairment". en. In: *J. Neurol. Neurosurg. Psychiatry* 72.4, pp. 491–497.

Voelker, Maximilian N et al. (May 2021). "The traveling heads 2.0: Multicenter reproducibility of quantitative imaging methods at 7 Tesla". en. In: *Neuroimage* 232, p. 117910.

Vogel, Jacob W et al. (Feb. 2020). "A molecular gradient along the longitudinal axis of the human hippocampus informs large-scale behavioral systems". en. In: *Nat. Commun.* 11.1, p. 960.

Vogt and Vogt (1903). "Zur anatomischen Gliederung des Cortex cerebri". In: *J. Psychol. Neuropsychiatr. Disord. Brain Stimul.*

Voineskos, Aristotle N et al. (Aug. 2015). "Hippocampal (subfield) volume and shape in relation to cognitive performance across the adult lifespan". en. In: *Hum. Brain Mapp.* 36.8, pp. 3020–3037.

Vos de Wael, Reinder et al. (Oct. 2018). "Anatomical and microstructural determinants of hippocampal subfield functional connectome embedding". en. In: *Proc. Natl. Acad. Sci. U. S. A.* 115.40, pp. 10154–10159.

Vrenken, H et al. (Apr. 2006). "Voxel-based analysis of quantitative T1 maps demonstrates that multiple sclerosis acts throughout the normal-appearing white matter". en. In: *AJNR Am. J. Neuroradiol.* 27.4, pp. 868–874.

Vuoksimaa, Eero et al. (May 2013). "Cognitive reserve moderates the association between hippocampal volume and episodic memory in middle age". en. In: *Neuropsychologia* 51.6, pp. 1124–1131.

Vymazal, J, R A Brooks, et al. (Jan. 1996). "The relation between brain iron and NMR relaxation times: an in vitro study". en. In: *Magn. Reson. Med.* 35.1, pp. 56–61.

Vymazal, J, A Righini, et al. (May 1999). "T1 and T2 in the brain of healthy subjects, patients with Parkinson disease, and patients with multiple system atrophy: relation to iron content". en. In: *Radiology* 211.2, pp. 489–495.

Wada, Masataka et al. (2018). "Effect of Education on Alzheimer's Disease-Related Neuroimaging Biomarkers in Healthy Controls, and Participants with Mild Cognitive Impairment and Alzheimer's Disease: A Cross-Sectional Study". In: *J. Alzheimers. Dis.* 63.2, pp. 861–869.

Walker, Lary C and Mathias Jucker (June 2017). "The Exceptional Vulnerability of Humans to Alzheimer's Disease". en. In: *Trends Mol. Med.* 23.6, pp. 534–545.

Walsh, Andrew J et al. (May 2013). "Multiple sclerosis: validation of MR imaging for quantification and detection of iron". en. In: *Radiology* 267.2, pp. 531–542.

Wang, Fei et al. (Apr. 2020). "Myelin degeneration and diminished myelin renewal contribute to age-related deficits in memory". en. In: *Nat. Neurosci.* 23.4, pp. 481–486.

Wang, Hongzhi et al. (Mar. 2013). "Multi-Atlas Segmentation with Joint Label Fusion". en. In: *IEEE Trans. Pattern Anal. Mach. Intell.* 35.3, pp. 611–623.

Wang, Huali et al. (June 2004). "Prolongation of T(2) relaxation times of hippocampus and amygdala in Alzheimer's disease". en. In: *Neurosci. Lett.* 363.2, pp. 150–153.

Wang, Lei et al. (Oct. 2003). "Changes in hippocampal volume and shape across time distinguish dementia of the Alzheimer type from healthy aging". In: *Neuroimage* 20.2, pp. 667–682.

Ward, Roberta J et al. (Oct. 2014). "The role of iron in brain ageing and neurodegenerative disorders". en. In: *Lancet Neurol.* 13.10, pp. 1045–1060.

Wearn, Alfie R et al. (Sept. 2020). "T2 heterogeneity: a novel marker of microstructural integrity associated with cognitive decline in people with mild cognitive impairment". en. In: *Alzheimers. Res. Ther.* 12.1, p. 105.

Weijden, Chris W J van der et al. (Feb. 2021). "Myelin quantification with MRI: A systematic review of accuracy and reproducibility". en. In: *Neuroimage* 226, p. 117561.

Weiner, Michael W et al. (May 2017). "The Alzheimer's Disease Neuroimaging Initiative 3: Continued innovation for clinical trial improvement". en. In: *Alzheimers. Dement.* 13.5, pp. 561–571.

Weingarten, M D et al. (May 1975). "A protein factor essential for microtubule assembly". en. In: *Proc. Natl. Acad. Sci. U. S. A.* 72.5, pp. 1858–1862.

Weintraub, S, N P Rubin, and M M Mesulam (Dec. 1990). "Primary progressive aphasia. Longitudinal course, neuropsychological profile, and language features". en. In: *Arch. Neurol.* 47.12, pp. 1329–1335.

Weintraub, Sandra, Alissa H Wicklund, and David P Salmon (Apr. 2012). "The neuropsychological profile of Alzheimer disease". en. In: *Cold Spring Harb. Perspect. Med.* 2.4, a006171.

Weiskopf, Nikolaus et al. (June 2013). "Quantitative multi-parameter mapping of R1, PD(*), MT, and R2(*) at 3T: a multi-center validation". en. In: *Front. Neurosci.* 7, p. 95.

West, M J et al. (Sept. 1994). "Differences in the pattern of hippocampal neuronal loss in normal ageing and Alzheimer's disease". en. In: *Lancet* 344.8925, pp. 769–772.

Westlye, Lars T, Kristine B Walhovd, Anders M Dale, Atle Bjørnerud, et al. (Sept. 2010). "Life-span changes of the human brain white matter: diffusion tensor imaging (DTI) and volumetry". en. In: *Cereb. Cortex* 20.9, pp. 2055–2068.

Westlye, Lars T, Kristine B Walhovd, Anders M Dale, Thomas Espeseth, et al. (Oct. 2009). "Increased sensitivity to effects of normal aging and Alzheimer's disease on cortical thickness by adjustment for local variability in gray/white contrast: a multi-sample MRI study". en. In: *Neuroimage* 47.4, pp. 1545–1557.

Williams, B R et al. (Jan. 1999). "Development of inhibitory control across the life span". en. In: *Dev. Psychol.* 35.1, pp. 205–213.

Wilson, Robert S et al. (June 2002). "Individual differences in rates of change in cognitive abilities of older persons". en. In: *Psychol. Aging* 17.2, pp. 179–193.

Winterburn, Julie et al. (Nov. 2015). "High-resolution In Vivo Manual Segmentation Protocol for Human Hippocampal Subfields Using 3T Magnetic Resonance Imaging". en. In: *J. Vis. Exp.* 105, e51861.

Winterburn, Julie L et al. (July 2013). "A novel in vivo atlas of human hippocampal subfields using high-resolution 3 T magnetic resonance imaging". en. In: *Neuroimage* 74, pp. 254–265.

Wisse, L E M et al. (July 2012). "Subfields of the hippocampal formation at 7 T MRI: in vivo volumetric assessment". en. In: *Neuroimage* 61.4, pp. 1043–1049.

Wisse, Laura E M, Geert Jan Biessels, et al. (Sept. 2014). "Hippocampal subfield volumes at 7T in early Alzheimer's disease and normal aging". en. In: *Neurobiol. Aging* 35.9, pp. 2039–2045.

Wisse, Laura E M, Gaël Chételat, et al. (2020). "Hippocampal subfield volumetry from structural isotropic 1 mm 3 MRI scans: A note of caution". In: *Hum. Brain Mapp.* 42.2, pp. 539–550.

Wisse, Laura E M, Ana M Daugherty, et al. (Jan. 2017). "A harmonized segmentation protocol for hippocampal and parahippocampal subregions: Why do we need one and what are the key goals?" en. In: *Hippocampus* 27.1, pp. 3–11.

Witter, Menno P et al. (June 2017). "Architecture of the Entorhinal Cortex A Review of Entorhinal Anatomy in Rodents with Some Comparative Notes". en. In: *Front. Syst. Neurosci.* 11, p. 46.

Wittner, Lucia and Richard Miles (Nov. 2007). "Factors defining a pacemaker region for synchrony in the hippocampus". en. In: *J. Physiol.* 584.Pt 3, pp. 867–883.

Wolf, Dominik et al. (Oct. 2015). "Differential associations of age with volume and microstructure of hippocampal subfields in healthy older adults". en. In: *Hum. Brain Mapp.* 36.10, pp. 3819–3831.

Won, Junyeon et al. (Feb. 2022). "Differential associations of regional cerebellar volume with gait speed and working memory". en. In: *Sci. Rep.* 12.1, p. 2355.

Wood, Bryony et al. (2015). "Magnetic resonance scanning and image segmentation procedure at 3 T for volumetry of human hippocampal subfields". In: *Biomed. Spectrosc. Imaging* 4.2, pp. 197–208.

Wood, John C and Nilesh Ghugre (2008). "Magnetic resonance imaging assessment of excess iron in thalassemia, sickle cell disease and other iron overload diseases". en. In: *Hemoglobin* 32.1-2, pp. 85–96.

Woollett, Katherine and Eleanor A Maguire (Dec. 2011). "Acquiring "the Knowledge" of London's layout drives structural brain changes". en. In: *Curr. Biol.* 21.24, pp. 2109–2114.

World Health Organization (June 2016). *World Health Statistics 2016: Monitoring Health for the SDGs Sustainable Development Goals*. en. World Health Organization.

Wycoco, Victor et al. (May 2013). "White matter anatomy: what the radiologist needs to know". en. In: *Neuroimaging Clin. N. Am.* 23.2, pp. 197–216.

Xiong, Raymond M et al. (Nov. 2022). "The pattern of cortical thickness underlying disruptive behaviors in Alzheimer's disease". en. In: *psychoradiology* 2.3, pp. 113–120.

Xuereb, J H et al. (June 1991). "NERVE CELL LOSS IN THE THALAMUS IN ALZEHEIMER'S DISEASE AND PARKINSON'S DISEASE". en. In: *Brain* 114.3, pp. 1363–1379.

Yan, Shuang et al. (Jan. 2020). "Test-retest variability of brain morphometry analysis: an investigation of sequence and coil effects". en. In: *Ann Transl Med* 8.1, p. 12.

Yanagisawa, Katsuhiko (2005). "Cholesterol and amyloid beta fibrillogenesis". en. In: *Subcell. Biochem.* 38, pp. 179–202.

Yang, Xianfeng et al. (Nov. 2013). "Evolution of hippocampal shapes across the human lifespan". en. In: *Hum. Brain Mapp.* 34.11, pp. 3075–3085.

Yates, Jennifer A, Linda Clare, Robert T Woods, Fiona E Matthews, et al. (Sept. 2015). "Subjective Memory Complaints are Involved in the Relationship between Mood and Mild Cognitive Impairment". en. In: *J. Alzheimers. Dis.* 48 Suppl 1, S115–23.

Yates, Jennifer A, Linda Clare, Robert T Woods, and MRC CFAS (Mar. 2017). "Subjective memory complaints, mood and MCI: a follow-up study". en. In: *Aging Ment. Health* 21.3, pp. 313–321.

Yeatman, Jason D, Brian A Wandell, and Aviv A Mezer (Sept. 2014). "Lifespan maturation and degeneration of human brain white matter". en. In: *Nat. Commun.* 5, p. 4932.

Yoon, Sang-Sun and Sang-Mee AhnJo (2012). "Mechanisms of Amyloid-β Peptide Clearance: Potential Therapeutic Targets for Alzheimer's Disease". In: *Biomolecules and Therapeutics* 20.3, pp. 245–255.

Youdim, M B and A R Green (Sept. 1978). "Iron deficiency and neurotransmitter synthesis and function". en. In: *Proc. Nutr. Soc.* 37.2, pp. 173–179.

Yuan, Peng and Naftali Raz (May 2014). "Prefrontal cortex and executive functions in healthy adults: a meta-analysis of structural neuroimaging studies". en. In: *Neurosci. Biobehav. Rev.* 42, pp. 180–192.

Yushkevich, Paul A, Robert S C Amaral, et al. (May 2015). "Quantitative comparison of 21 protocols for labeling hippocampal subfields and parahippocampal subregions in in vivo MRI: towards a harmonized segmentation protocol". en. In: *Neuroimage* 111, pp. 526–541.

Yushkevich, Paul A, John B Pluta, et al. (Jan. 2015). "Automated volumetry and regional thickness analysis of hippocampal subfields and medial temporal cortical structures in mild cognitive impairment". en. In: *Hum. Brain Mapp.* 36.1, pp. 258–287.

Yushkevich, Paul A, Hongzhi Wang, et al. (Dec. 2010). "Nearly automatic segmentation of hippocampal subfields in in vivo focal T2-weighted MRI". en. In: *Neuroimage* 53.4, pp. 1208–1224.

Zecca, L et al. (Mar. 2001). "Iron, neuromelanin and ferritin content in the substantia nigra of normal subjects at different ages: consequences for iron storage and neurodegenerative processes". en. In: *J. Neurochem.* 76.6, pp. 1766–1773.

Zeighami, Yashar et al. (Apr. 2019). "A clinical-anatomical signature of Parkinson's disease identified with partial least squares and magnetic resonance imaging". en. In: *Neuroimage* 190, pp. 69–78.

Zelazo, Philip David et al. (July 2014). "NIH Toolbox Cognition Battery (CB): validation of executive function measures in adults". en. In: *J. Int. Neuropsychol. Soc.* 20.6, pp. 620–629.

Zhang, Hui et al. (July 2012). "NODDI: practical in vivo neurite orientation dispersion and density imaging of the human brain". en. In: *Neuroimage* 61.4, pp. 1000–1016.

Zhang, Jingya et al. (Oct. 2015). "Physical Constraint Finite Element Model for Medical Image Registration". en. In: *PLoS One* 10.10, e0140567.

Zhang, Shuping et al. (2022). "Double-edge sword roles of iron in driving energy production versus instigating ferroptosis". In: *Cell Death Dis.* 13.1.

Zhao, Weina et al. (Mar. 2019). "Trajectories of the Hippocampal Subfields Atrophy in the Alzheimer's Disease: A Structural Imaging Study". en. In: *Front. Neuroinform.* 13, p. 13.

Zhao, Zhiyong et al. (Dec. 2021). "The effect of beta-amyloid and tau protein aggregations on magnetic susceptibility of anterior hippocampal laminae in Alzheimer's diseases". en. In: *Neuroimage* 244, p. 118584.

Zheng, Fenglian et al. (Oct. 2018). "The Volume of Hippocampal Subfields in Relation to Decline of Memory Recall Across the Adult Lifespan". en. In: *Front. Aging Neurosci.* 10, p. 320.

Zheng, Hui and Edward H Koo (Apr. 2011). "Biology and pathophysiology of the amyloid precursor protein". en. In: *Mol. Neurodegener.* 6.1, p. 27.

Zheng, Zhiwei et al. (Mar. 2017). "Sex Matters: Hippocampal Volume Predicts Individual Differences in Associative Memory in Cognitively Normal Older Women but Not Men". en. In: *Front. Hum. Neurosci.* 11, p. 93.

Zhou, Juan et al. (Mar. 2012). "Predicting regional neurodegeneration from the healthy brain functional connectome". en. In: *Neuron* 73.6, pp. 1216–1227.

Ziegler, Gabriel et al. (Oct. 2012). "Brain structural trajectories over the adult lifespan". en. In: *Hum. Brain Mapp.* 33.10, pp. 2377–2389.

Zimmerman, Molly E et al. (Oct. 2006). "The relationship between frontal gray matter volume and cognition varies across the healthy adult lifespan". en. In: *Am. J. Geriatr. Psychiatry* 14.10, pp. 823–833.